

Multiphasic Flow Processes in Deformable Porous Media under Consideration of Fluid Phase Transitions

Von der Fakultät Bau- und Umweltingenieurwissenschaften
der Universität Stuttgart zur Erlangung der Würde
eines Doktor-Ingenieurs (Dr.-Ing.)
genehmigte Abhandlung

vorgelegt von

Dipl.-Ing. Tobias Graf

aus

Nagold

Hauptberichter: Prof. Dr.-Ing. Wolfgang Ehlers

1. Mitberichter: Prof. Dr.-Ing. Rainer Helmig

2. Mitberichter: Prof. Dr.-Ing. Stefan Diebels

Tag der mündlichen Prüfung: 12. Juni 2008

Institut für Mechanik (Bauwesen) der Universität Stuttgart

Lehrstuhl II, Prof. Dr.-Ing. W. Ehlers

2008

Report No. II-17
Institut für Mechanik (Bauwesen), Lehrstuhl II
Universität Stuttgart, Germany, 2008

Editor:

Prof. Dr.-Ing. W. Ehlers

© Tobias Graf
Institut für Mechanik (Bauwesen)
Lehrstuhl II
Universität Stuttgart
Pfaffenwaldring 7
70569 Stuttgart, Germany

All rights reserved. No part of this publication may be reproduced, stored in a retrieval system, or transmitted, in any form or by any means, electronic, mechanical, photocopying, recording, scanning or otherwise, without the permission in writing of the author.



Produced by Verlag Glückauf GmbH, Essen, Germany
Printed by DPI – Digital Print, Witten, Germany, 2008

ISBN 978-3-937399-17-8
(D 93 – Dissertation, Universität Stuttgart)

Acknowledgments

The work presented in this thesis was carried out in the years between 2001 and 2007, when I was a research associate at the Institute of Applied Mechanics (Civil Engineering) at the Universität Stuttgart. Numerous people contributed in many ways to the realization of this work - all their support is most gratefully acknowledged.

First of all, I want to thank my supervisor Professor Wolfgang Ehlers for giving me the opportunity to prepare my thesis at the institute, for his scientific support and for the many interesting discussions we had. His research in the field of continuum mechanics built the important foundation for this work.

I am also very grateful to Professor Rainer Helmig for taking the first co-chair in my promotion procedure. He and the members of his institute always gave me willingly support concerning the numerical treatment of multiphasic flow processes in porous materials.

Furthermore, I want to thank Professor Stefan Diebels for taking the second co-chair in my promotion procedure. He was my supervisor during the diploma thesis and had a great influence sparking my interest in computational mechanics.

Next, I want to thank all my fellow workers at the institute and all colleagues of the DFG-research group *Mechanik teilgesättigter Böden* for creating a pleasant and friendly working atmosphere. Especially, I would like to express my gratitude to my room mates Martin Ammann and Okan Avcı for the many discussions we had on continuum mechanical fundamentals and the design of boundary-value problems. Moreover, very important and time-consuming work was done by Ayhan Acartürk, Martin Ammann, Okan Avcı and Holger Steeb at the proof-reading stage.

Finally, I would like to thank my wife Katja and my children Anna and Lena. They have always been there supporting me, often only with smile, understood the importance of my work and are the most important part of my life.

Stuttgart, June 2008

Tobias Graf

By perseverance the snail reached the ark.
(*Charles Haddon Spurgeon*)

Deutsche Zusammenfassung

In den unterschiedlichsten Bereichen des Ingenieurwesens werden Materialien betrachtet, die als poröse Medien aufgefaßt werden können, wie z. B. Metall- oder Polyurethanschäume, biologische Gewebe wie die Bandscheibe oder natürliche Böden. Dabei zählt der natürliche Boden zu den interessantesten aber auch am schwierigsten zu beschreibenden porösen Materialien, die unser tägliches Leben in vielen Fällen beeinflussen. Das Versagen einer Böschung nach einem starken Regenereignis kann zur Zerstörung von Straßen oder Eisenbahnlinien führen, während ein Schadstoffeintrag nach einem Verkehrsunfall eines Tanklastzugs zur Verschmutzung des Grundwassers führen kann. Die Vorhersage des Materialverhaltens von natürlichen Böden mittels numerischen Simulationen ist daher ein äußerst wichtiger Punkt, um solche katastrophalen Zwischenfälle zu verhindern bzw. ihre Auswirkungen abzuschätzen. Die dabei benötigten mechanischen Modelle können basierend auf einem kontinuumsmechanischen Ansatz im Rahmen der Theorie Poröser Medien (TPM) entwickelt werden. Dabei müssen für eine möglichst genaue Abbildung der Realität in dem zugrunde liegenden mechanischen Modell neben einer deformierbaren Bodenmatrix (Festkörperskelett) mindestens zwei Porenfluide, z. B. Porenluft und Porenwasser, berücksichtigt werden.

Bei einer genaueren Untersuchung von Böschungsbrüchen läßt sich feststellen, daß das Verhalten der Festkörpermatrix durch ein plötzliches Versagen charakterisiert ist, wobei sich die auftretenden plastischen Deformationen in dünnen Bändern oder Flächen konzentrieren, den sogenannten Scherbändern bzw. Scherflächen. Das Versagen selbst wird durch das Einwirken von internen oder externen Belastungen auf die Bodenmatrix ausgelöst. Externe Belastungen resultieren zum Beispiel von Gebäuden oder Brückenpfeilern, während interne Belastungen aus einer Interaktion mit den vorherrschenden Porenfluiden folgen. Eines der dabei zu untersuchenden Phänomene ist die Destabilisierung einer natürlichen Böschung auf Grund eines anwachsenden Porenfluidrucks, was in Folge eines ansteigenden Wasserspiegels, z. B. nach einem starken Regenereignis, geschehen kann. Dies bedeutet, daß für eine numerische Simulation solcher Anfangs-Randwertprobleme das zugrunde liegende mechanische Modell nicht nur das Lokalisierungsverhalten der Festkörperdeformation und die komplexen Mehrphasenströmungsprozesse zwischen Porenluft und Porenwasser, sondern auch das gekoppelte Materialverhalten zwischen der Festkörper- und den Fluidphasen in geeigneter Weise beschreiben können muß.

Ein für die Lösung dieser geotechnischen Fragestellungen entwickeltes kontinuumsmechanisches Modell kann auch als Grundlage für die Beschreibung der Speicherung von Kohlendioxid (CO_2) im Untergrund verwendet werden. Dabei werden zur Reduktion der CO_2 -Konzentration in der Atmosphäre große Mengen dieses Treibhausgases in tiefen geologischen Formationen durch Injektion von flüssigem CO_2 gespeichert. Dies kann in wassergesättigte Schichten geschehen, wobei die Aufwärtsbewegung des Kohlendioxids durch eine darüberliegende, undurchlässigere Schicht verhindert wird. Die Nachhaltigkeit der Lagerung muß anhand von numerischen Simulationen abgeschätzt werden, bei denen die Änderung der Durchlässigkeit in Abhängigkeit der Deformation der Bodenmatrix berücksichtigt werden muß. Da die Temperatur bei diesen Fragestellungen als nicht

konstant angenommen werden kann, muß das mechanische Modell für nicht-isotherme Bedingungen erweitert werden. Dabei können in dem betrachteten Temperaturbereich Phasenübergangsprozesse der Fluidkomponenten auftreten, die in geeigneter Weise innerhalb des mechanischen Modells berücksichtigt werden müssen.

Ein Dreiphasenmodell im Rahmen der Theorie Poröser Medien bestehend aus einer elastoviskoplastischen Festkörpermatrix und zwei Porenfluiden, einer materiell inkompressiblen Flüssigphase (Porenwasser) und einer materiell kompressiblen Gasphase (Porenluft) wurde in den Arbeiten von *Blome* [10], *Ehlers & Blome* [50] und *Ehlers et al.* [56] vorgestellt und auf diverse praxisrelevante, geotechnische Problemstellungen angewandt. Dieses Dreiphasenmodell basiert allerdings auf einem isothermen Ansatz und es wurden dort auch keine Massenaustauschprozesse (Phasenübergänge) berücksichtigt. Auf der anderen Seite präsentierte *Ghadiani* [77] ein im Rahmen der TPM entwickeltes, nicht-isothermes Zweiphasenmodell bestehend aus einem elastischen Festkörpermaterial und einer materiell kompressiblen Gasphase, in dem die beiden Phasen durch zwei unabhängige Temperaturen regiert werden. Auch werden hier keine Masseninteraktionen berücksichtigt.

Bei all diesen Modellen wird jeweils die Bodenmatrix als deformierbares Festkörperskelett beschrieben. In vielen Bereichen, z. B. in der Simulation von Schadstofftransportprozessen im Untergrund, kann allerdings von der Annahme ausgegangen werden, daß die Porenfluidströmung zu keinen Deformationen der Bodenmatrix führt. Arbeiten, die auf dieser Annahme aufbauen, legen den Fokus auf die Beschreibung der Mehrphasenströmungsprozesse. *Helmig* [90] befaßt sich intensiv mit der mechanische Beschreibung und der numerischen Behandlung solcher Strömungsphänomene, wobei eine Erweiterung auf nicht-isotherme Bedingungen unter Berücksichtigung von Phasenübergängen in *Class* [26] und *Class & Helmig* [27] vorgestellt wurde.

Basierend auf diesen Überlegungen ist es das Ziel dieser Arbeit, ein thermodynamisch konsistentes, kontinuumsmechanisches Modell im Rahmen der Theorie Poröser Medien zu entwickeln, das als Grundlage für die numerische Simulation der oben genannten Problemstellungen dient. Dabei werden innerhalb eines nicht-isothermen Ansatzes ein deformierbares Festkörperskelett sowie mehrere Porenfluide unter Berücksichtigung von Phasenübergängen zwischen flüssigem und gasförmigem Porenwasser berücksichtigt. Die numerische Umsetzung erfolgt mit Hilfe der Finite-Elemente-Methode (FEM) mit einem speziellen Fokus auf der numerischen Behandlung von Mehrphasenströmungsprozessen. Abschließend werden anhand von mehreren numerischen Beispielen die Fähigkeiten des entwickelten Modells zur Simulation von praxisrelevanten zwei- und dreidimensionalen Anfangs-Randwertproblemen aufgezeigt.

Die Grundlagen der Theorie Poröser Medien (TPM) werden in **Kapitel 2** vorgestellt, wobei nach Einführung der kinematischen Beziehungen die mechanischen und thermischen Bilanzgleichungen diskutiert werden. Die Ursprünge der Theorie Poröser Medien gehen zurück auf Arbeiten von *Truesdell & Toupin* [136], *Bowen* [15] und *Truesdell* [135], während die TPM in ihrer heutigen Form auf Arbeiten von *Bowen* [16, 17], *de Boer & Ehlers* [13] und *Ehlers* [40, 41, 43, 46] basiert. Der Grundgedanke dieser makroskopischen Theorie besteht darin, die einzelnen Konstituierenden des Modells im Rahmen der Kontinuumsmechanik von Einphasenmaterialien zu beschreiben und ihre Interaktionen mit den übrigen Konstituierenden durch geeignete Produktionsterme für die mechanischen,

d. h. Masse, Impuls und Drall, und thermischen, d. h. Energie und Entropie, Größen zu berücksichtigen.

In **Kapitel 3** werden thermodynamisch konsistente Konstitutivgleichungen für ein nicht-isothermes Mehrphasenmodell bestehend aus einem deformierbaren, elasto-viskoplastischen Festkörperskelett und einer beliebigen Anzahl von inkompressiblen und kompressiblen Fluidkonstituierenden basierend auf einer Auswertung der Entropieungleichung hergeleitet. Dabei wird jede Phase von ihrer jeweils eigenen Temperatur regiert und Phasenübergänge zwischen flüssigem und gasförmigem Porenwasser berücksichtigt. Abschließend werden die bestimmenden Bilanzgleichungen sowie die zugehörigen Konstitutivgleichungen für ein nicht-isothermes Dreiphasenmodell bestehend aus einem elasto-viskoplastischen Festkörperskelett, einer inkompressiblen, flüssigen Porenwasserphase und einer kompressiblen Porengasphase konkretisiert. Die Gasphase wird dabei von zwei kompressiblen Gaskomponenten, Porenluft und gasförmigem Porenwasser, gebildet.

Innerhalb dieses Modells wird die effektive Dichte des Festkörperskeletts sowie der flüssigen Porenfluide als eine Funktion der jeweiligen Temperatur angenommen, so daß diese Konstituierenden nur im mechanischen Sinne als materiell inkompressibel aufgefaßt werden können. Die gasförmigen Fluidkonstituierenden werden als ideale Gase beschrieben und bilden in der Summe die globale Gasphase. Dabei wird durch die Auswertung der Entropieungleichung gezeigt, daß das Verhältnis zwischen dem Partialdruck einer Gaskomponente innerhalb der globalen Gasphase und dem effektiven Gasdruck der globalen Gasphase durch den Molenbruch gegeben ist. Des weiteren ergibt sich der effektive Gasdruck der globalen Gasphase aus der Summe der einzelnen Partialdrücke der Gaskomponenten innerhalb der globalen Gasphase.

Da jede Phase von ihrer eigenen Temperatur beherrscht wird und Phasenübergänge zwischen flüssigem und gasförmigem Porenwasser berücksichtigt werden, werden nicht nur Konstitutivgleichungen für die freien *Helmholtz*-Energien der einzelnen Konstituierenden und die Impulsproduktionsterme der Porenfluide benötigt, sondern auch für den Massenproduktionsterm des Porenwassers sowie die direkten Energieproduktionsterme der Fluidkonstituierenden. Mit Hilfe einer Auswertung der Entropieungleichung können geeignete Konstitutivgleichungen für die Impuls- und direkte Energieproduktionsterme formuliert werden. Diese führen auf erweiterte *Darcy*-Beziehungen für die Sickergeschwindigkeiten der Porenfluidphasen, während die Diffusionsgeschwindigkeiten der Gaskomponenten innerhalb der Gasphase direkt vom Gradienten der Molenbrüche abhängen. Die direkte Energieproduktion ist eine Funktion der Temperaturdifferenzen zwischen den Phasen und wird als Wärmeübergang identifiziert. Da der Phasenübergang zwischen flüssigem und gasförmigem Porenwasser ein reversibler Prozess ist, folgt aus der Auswertung der Entropieungleichung keine Restriktion für die Formulierung einer Konstitutivgleichung für den Massenproduktionsterm des Porenwassers. Es folgt vielmehr eine zusätzliche Beziehung zwischen den Prozeßvariablen, die eingehalten werden muß so lange Phasenübergangsprozesse stattfinden. Basierend auf dieser Beziehung kann der Partialdruck von Wasserdampf innerhalb der Gasphase während des Phasenübergangs bestimmt werden. Unter der Annahme einer globalen Temperatur für das gesamte poröse Material und gleichzeitiger Vernachlässigung der kinetischen Energien folgt aus der gefundenen Beziehung die Gleichheit der freien *Gibbs*chen Enthalpien von flüssigem und gasförmigem Wasser

solange Phasenübergangsprozesse stattfinden. In diesem Fall kann direkt eine Beziehung zwischen dem Partialdruck des Wasserdampfs innerhalb der Gasphase, dem sogenannten Sättigungsdampfdruck, und der regierenden Temperatur hergeleitet werden. Dadurch verliert die Massenbilanz des Wasserdampfs die Eigenschaft einer Bestimmungsgleichung für die Partialdichte des Wasserdampfs innerhalb der globalen Gasphase und kann für die Berechnung der Massenproduktion verwendet werden.

Die numerische Umsetzung des entwickelten Mehrphasenmodells mit Hilfe der Finite-Elemente-Methode (FEM) wird in **Kapitel 4** behandelt. Dabei werden zuerst die schwachen Formulierungen der benötigten Bilanzgleichungen, d. h. der Massenbilanzen der Porenfluide, die Impulsbilanz des gesamten porösen Materials sowie die Energiebilanzen aller Phasen, für den quasi-statischen Fall hergeleitet. Ihre räumliche Diskretisierung basiert auf erweiterten *Taylor-Hood*-Elementen mit quadratischen Ansatzfunktionen für die Festkörperverschiebung und linearen Ansatzfunktionen für die Porenfluiddrücke bzw. Sättigungen und Temperaturen. Für die Zeitdiskretisierung wird das implizite *Euler*-Verfahren verwendet. Das vollständig diskretisierte System liefert ein nichtlineares Gleichungssystem, daß mit dem *Newton-Raphson*-Verfahren gelöst werden muß. Auf Grund auftretender numerischer Probleme bei der Simulation von Mehrphasenströmungsprozessen unter Verwendung der Porenfluiddrücke als Freiheitsgrade für die Porenfluide, wird die Sättigung als alternativer Freiheitsgrad eingeführt. Dies kann allerdings zu Oszillationen in der Lösung führen, die aber durch die Anwendung eines geeigneten Stabilisierungsverfahrens [91] verhindert werden können.

In **Kapitel 5** werden verschiedene numerische Beispiele vorgestellt, die die Möglichkeiten des entwickelten nicht-isothermen Dreiphasenmodells aufzeigen. Dafür wurde das entwickelte Modell in das FE-Programmpaket PANDAS/M++ [2, 140, 142] implementiert. Im einzelnen werden die Simulationsergebnisse von Schadstofftransportproblemen in heterogenen porösen Materialien, Stabilitätsuntersuchungen von natürlichen Böschungen, nicht-isotherme Injektionsprozesse in wassergesättigte Böden sowie Verdampfungs- und Kondensationsvorgänge von Porenwasser diskutiert.

Bei der numerischen Simulation von Schadstoffinfiltrationsprozessen in wassergesättigte, heterogene Sandboxen zeigt das Dreiphasenmodell, daß es in der Lage ist, den Verdrängungsprozeß von Porenwasser durch einen einsickernden Schadstoff sowohl für den zwei- als auch für den dreidimensionalen Fall zu beschreiben. Die Beispiele zeigen des weiteren die Effektivität der implementierten Stabilisierungsmethode bei der Beschreibung von Mehrphasenströmungsprozessen an der Grenze von zwei porösen Materialien mit unterschiedlichen Permeabilitäten.

Ob das entwickelte Modell in der Lage ist, die Interaktion zwischen der deformierbaren Bodenmatrix und den Porenfluiden in geeigneter Weise zu beschreiben, läßt sich am besten durch numerische Simulationen von Böschungbrüchen zeigen, die durch einen Anstieg des Wasserspiegels ausgelöst werden. Dabei wirkt der Porenfluiddruck als innere Last auf das Festkörperskelett. Da die Dichte von Wasser um den Faktor tausend höher ist als die Dichte der Porenluft, steigt der Porenfluiddruck im selben Maße mit steigendem Wasserspiegel. Somit kann bei einer anfänglich stabilen Böschung ein Anstieg des Wasserspiegels ein Versagen hervorrufen. Anhand der beiden numerischen Beispiele wird gezeigt, daß das Modell in der Lage ist, nicht nur das Lokalisierungsverhalten des Festkörperskeletts und

den Verdrängungsvorgang der Porenluft durch eindringendes Porenwasser, sondern auch die Interaktion zwischen den einzelnen Phasen in geeigneter Weise abzubilden. Dabei wird auf Grund der hohen Anzahl an Unbekannten bei der Berechnung des dreidimensionalen Anfangs-Randwertproblems auf parallele Programmstrukturen zurückgegriffen.

Um die Fähigkeiten des Dreiphasenmodells zur Beschreibung von nicht-isothermen Anfangs-Randwertproblemen zu untersuchen, wird in einem weiteren Beispiel heißes Porengas in ein wassergesättigtes poröses Material injiziert. Dabei wird die Aufwärtsbewegung des Porengases durch eine horizontale Schicht mit einer geringeren Durchlässigkeit behindert. Dieses Beispiel zeigt die Fähigkeiten des Modells, nicht nur die mechanischen Strömungsprozesse, sondern auch die thermischen Effekte wie Wärmeübergang oder Wärmetransport zu beschreiben. Schließlich werden an einem letzten numerischen Beispiel Verdampfungs- und Kondensationsprozesse von Porenwasser untersucht, wobei gezeigt werden kann, daß der Phasenübergang zwischen flüssigem und gasförmigem Porenwasser korrekt beschrieben wird.

Contents

1	Introduction and overview	1
1.1	Motivation	1
1.2	Scope, aims and state of the art	2
1.3	Outline of the thesis	4
2	Theoretical fundamentals of the Theory of Porous Media	5
2.1	Kinematical relations	5
2.1.1	Mixture and Concept of Volume Fractions	5
2.1.2	Motion functions	8
2.1.3	Deformation and strain measures	11
2.1.4	Deformation and strain rates	12
2.1.5	Stress measures	13
2.2	Balance relations	14
2.2.1	General structure of the balance relations	15
2.2.2	Mechanical balance laws	17
2.2.3	Thermodynamical balance laws	22
3	Constitutive settings	27
3.1	Evaluation of the entropy inequality	28
3.1.1	Preliminaries	28
3.1.2	Saturation constraint and effective stress principle	30
3.1.3	Constitutive variables	34
3.1.4	Restrictions	36
3.2	The pore fluid constituents	45
3.2.1	Free <i>Helmholtz</i> energies	45
3.2.2	Mass interactions	47
3.2.3	Momentum productions	56
3.2.4	Direct energy productions	62
3.2.5	Heat influx vectors and mechanical fluid extra stresses	66

3.3	The solid constituent	68
3.3.1	Free <i>Helmholtz</i> energy, entropy and effective stress	69
3.3.2	Plastic material behavior	71
3.4	A triphasic porous material model	77
4	Numerical Treatment	85
4.1	Weak formulations of the governing equations	85
4.2	Spatial and temporal discretization	90
4.2.1	Finite element method	90
4.2.2	Time integration	94
4.2.3	Solution of the nonlinear system of equations	95
4.3	Multiphase flow processes	98
5	Numerical Examples	107
5.1	Pollutant infiltration problems in inhomogeneous porous materials	108
5.2	Slope failure problems	113
5.3	Heat transport problems	118
6	Summary and outlook	129
6.1	Summary	129
6.2	Outlook	130
A	Tensor calculus	133
A.1	Tensor algebra	133
A.1.1	Basic tensor products	133
A.1.2	Symmetric and skew-symmetric part of a tensor	134
A.1.3	Fundamental tensors	134
A.1.4	Spherical and deviatoric part of a tensor	135
A.1.5	Incomplete mapping	135
A.1.6	Outer tensor product of a vector and a tensor	135
A.2	Invariants of a 2-nd order tensor	136
	Bibliography	137

Chapter 1: Introduction and overview

1.1 Motivation

A variety of materials used in different engineering fields can be regarded as porous materials, e. g., metal or polyurethane foams, biological soft tissues or natural soils. Thereby, one of the most interesting and difficult porous material to describe is natural soil, which affects our daily life in many cases. The failure of natural slopes after heavy rainfall events can lead to a destruction of highways or railroads, cf. Figure 1.1, whereas the pollutant infiltration after an accident of a road tanker can lead to a contamination of the groundwater. The estimation of the material behavior of natural soils based on numerical simulations is a very important issue to avoid such catastrophic incidents or appraise the effects, whereby adequate mechanical models are required. Based on a continuum mechanical approach, natural soils can be described within the well-founded framework of the Theory of Porous Media (TPM), where the underlying mechanical model has to consist beside of a deformable solid constituent of at least two pore fluid constituents, e. g., pore water and pore air.

In particular, failure problems of natural slopes are characterized by a sudden failure of the soil matrix, where the plastic deformation is concentrated in the localization zone. They are initiated by internal or external loads acting on the soil matrix. External loads result, e. g., from buildings or bridge piers, whereas internal loads result from an interaction with the pore fluids. One of the crucial phenomena is the destabilization of a natural



Figure 1.1: Canadian Landscapes: Cecil Lake Road landslide, British Columbia, July 2001, http://gsc.nrcan.gc.ca/landslides/photos_high/cecil_lake_rd_bc.2001.jpg

slope due to an increasing water content after, e. g., a heavy rainfall event. Thus, for a numerical simulation of such kind of initial boundary-value problems, the underlying mechanical model must be able to describe correctly not only the localization behavior and the complex multiphasic flow processes, but also the coupled material behavior between the solid and fluid constituents.

A continuum mechanical model for the solution of the above mentioned geotechnical problems can be used as basis for the description of carbon dioxide (CO_2) storage processes in the subsurface as well. For a reduction of the carbon dioxide concentration in the atmosphere, large volumes of this greenhouse gas may be stored in deep geological formations by injection of fluidized CO_2 . This may be done in water-saturated aquifers, where the upward migration of carbon dioxide is limited by a low permeable cap layer. To estimate the durability of such storages, numerical simulations have to be carried out, where porosity-driven permeability changes of both the aquifer and the cap layer have to be considered as a result of soil deformations. Due to the fact that in this case the temperature can not be assumed as constant within the considered time and space domain, the mechanical model has to be based on a non-isothermal approach. Furthermore, as temperature ranges are considered, wherein phase transition processes of the respective components may occur, mass interactions between the liquid and gaseous fluid phases have to be included in the continuum mechanical approach as well.

1.2 Scope, aims and state of the art

It is the aim of this contribution, to derive a multiphasic, thermodynamically consistent porous media model, in which beside of a deformable solid skeleton several fluid constituents under non-isothermal conditions are considered and phase transition processes between liquid and gaseous pore water are taken in account. Furthermore, its numerical realization within the finite element method (FEM) with a special focus on the numerical treatment of multiphasic flow processes is discussed. Finally, several numerical examples are presented, where the model is applied to two- and three-dimensional initial boundary-value problems of practical relevance.

The presented continuum mechanical model is embedded in the well-founded frame of the Theory of Porous Media (TPM), which traces back to the works by *Truesdell & Toupin* [136], *Bowen* [15] and *Truesdell* [135] and is based in its present form on the publications by *Bowen* [16, 17], *de Boer & Ehlers* [13] and *Ehlers* [40, 41, 43, 46]. An excellent historical overview of the development of the TPM is given in *de Boer* [12]. Focusing on publications based on the TPM and dealing additionally with more than one pore fluid, a triphasic porous media model consisting of a deformable, elasto-viscoplastic solid skeleton and two fluid phases, a materially incompressible liquid and a materially compressible gas phase, is presented in the works of *Ehlers & Blome* [50], *Blome* [10] and *Ehlers et al.* [56]. However, isothermal conditions are assumed and no mass interactions are considered. On the other hand, *Ghadiani* [77] presented a biphasic porous media model consisting of an elastic solid skeleton and one pore fluid, i. e., a materially compressible gas phase. Each phase is governed by its respective temperature and it could be shown

that the heat exchange between the two phases depends directly on the temperature difference between them. Further publications dealing with more than one pore fluid and a deformable solid skeleton are given by *Klubertanz* [96] and *Klubertanz et al.* [97] or *Schrefler* and coworkers, e. g., [105, 115, 118–120].

Taking a closer look on the description of a solid skeleton within an elastoplastic theory under consideration of hardening and softening effects as well as a non-linear elasticity law, *Müllerschön* [110] and *Scholz* [117] identified the resulting material parameters using results of biaxial and triaxial experiments, cf. [65, 110, 117]. Furthermore, taking into account the special material behavior of partially saturated soils, *Bolzano et al.* [14] or *Laloui & Nuth* [102] postulated that the yield surface within the elastoplastic theory is a function of the stress state as well as of the pore water saturation. Additionally, *Laloui et al.* [101] have extended this set of variables by the temperature to include the non-isothermal material behavior of the solid skeleton.

An excellent overview on the mechanical modeling as well as the numerical realization of multiphasic flow processes can be found in *Helmig* [90] and citations therein, whereas an extension towards non-isothermal conditions under consideration of mass interactions between the pore fluids are given in *Class* [26] and *Class & Helmig* [27]. Nevertheless, the main focus of these models is set on the pore fluid flow and as a result, it is assumed in all these publications that the pore fluid flow has no influence on the deformation of the soil matrix, which is, therefore, described as a rigid material.

Concerning the numerical treatment of porous media models, where the solid skeleton is described within an elasto-viscoplastic theory, the reader is referred to the work of *Ellsiepen* [68]. Therein, different time- and space adaptive methods are additionally discussed and applied to a biphasic porous media model. The numerical treatment of triphasic porous media models under consideration of an elasto-viscoplastic solid skeleton and using parallel solution strategies is discussed in the works of *Ammann* [2], *Wieners* [139] and *Wieners et al.* [140–142]. Furthermore, the reader is referred to the works of the research group of *Ehlers* [46, 48, 49, 53, 54, 56, 108] as well as *Schrefler* and coworkers, e. g., [105, 118–120], where a deformable solid behavior is taken into account as well.

Besides the numerical treatment of the applied elasto-viscoplastic theory, a special attention has to be taken on the numerical treatment of the relations concerning the modeling of multiphasic flow processes. Thereby, certain stabilization techniques have to be applied to overcome the occurring numerical problems. A detailed discussion of this topic is given in *Class et al.* [28], *Forsyth* [71], *Knabner & Angermann* [98], *Helmig* [90], *Helmig & Huber* [91], *Niessner et al.* [111] and *Paul* [113].

The application of the above mentioned multiphasic porous media models to geotechnical problems, gas saturated polyurethane foams, biological soft tissues and rocket thrust chambers under isothermal as well as non-isothermal conditions can be found in, e. g., *Blome* [10], *Ellsiepen* [68], *Ghadiani* [77], *Markert* [108] and *Ehlers* and coworkers [4, 45, 48–50, 53, 54, 56–64]. A discussion of numerical simulations concerning multiphasic flow processes in rigid porous materials, is given in *Helmig* [90], *Helmig & Huber* [91], *Class & Helmig* [27] or *Bielinski* [8] and citations therein.

1.3 Outline of the thesis

This thesis is divided into five main chapters, whereby the respective topic and its state of the art are particularly discussed at the beginning of each chapter.

The fundamentals of the Theory of Porous Media (TPM) are briefly introduced in **Chapter 2**, where the kinematical relations are presented firstly, before the governing balance laws of multiphasic materials are discussed. Thereby, the basic idea is to describe the particular constituents of a porous medium within the well-known continuum mechanical frame of single-phasic materials and to consider the thermomechanical interactions with the other constituents by so-called production terms.

Chapter 3 is concentrated on the formulation of constitutive relations to close the resulting system of equations of a general porous media model, which consists of a deformable, elasto-viscoplastic solid skeleton and an arbitrary number of materially incompressible and compressible fluid constituents. Each phase is governed by its individual temperature and phase transition processes between liquid and gaseous pore water are additionally considered. Finally, the governing equations of a triphasic material model consisting of a solid and two pore fluid phases as well as the belonging constitutive relations are presented.

In **Chapter 4**, the numerical realization of the presented multiphasic model is given. After the derivation of the required weak formulations of the governing equations, the spatial and temporal discretization as well as the solution of the resulting nonlinear system of equations are discussed. Furthermore, a special regard is taken on the numerical treatment of multiphasic flow processes in porous materials.

The porous media model presented in the previous chapters is applied to several two- and three-dimensional initial boundary-value problems within **Chapter 5**. In particular, the triphasic model is used for the simulation of typical pollutant infiltration problems, which show the capability of the model and the applied stabilization method to describe the correct physical behavior of multiphasic flow processes in inhomogeneous porous materials. Furthermore, the coupled failure mechanism of natural slopes is investigated, whereby the strong interaction between the pore fluids and the solid skeleton has to be described in a proper way. Finally, two numerical examples are presented, where the triphasic model is discussed under non-isothermal conditions and phase transition processes between liquid and gaseous pore water are taken into account.

Finally, the whole thesis is summarized in **Chapter 6**, where some further, possible extensions and developments of the presented porous media model are given as well.

Chapter 2:

Theoretical fundamentals of the Theory of Porous Media

The fundamentals of the Theory of Porous Media (TPM) are briefly introduced within this chapter. Thereby, the kinematical relations are presented firstly before the governing balance laws of multiphasic materials are discussed. The basic idea is to describe the particular constituents of a porous medium within the well-known continuum mechanical frame of single-phasic materials and to consider the thermomechanical interactions with the other constituents by so-called production terms.

The Theory of Porous Media is based on the Theory of Mixtures (TM) extended by the Concept of Volume Fractions. Thereby, the Theory of Mixtures traces back to the works by *Truesdell & Toupin* [136], *Bowen* [15] and *Truesdell* [135], whereas the idea of the Concept of Volume Fractions was firstly applied to geotechnical problems by *Biot* [9] and *Heinrich & Desoyer* [87–89]. The TPM in its present form is based on the publications by *Bowen* [16,17], *de Boer & Ehlers* [13] and *Ehlers* [40,41,43]. For a historical overview of the development of the TPM, the interested reader is referred to *de Boer* [12].

2.1 Kinematical relations

2.1.1 Mixture and Concept of Volume Fractions

Porous materials with k individual constituents φ^α can be described in general by a macroscopic model φ consisting of one immiscible solid phase ($\alpha = S$), several immiscible pore liquid phases ($\alpha = \xi$) and multiple gas components ($\alpha = \gamma$) building together one overall gas phase ($\alpha = G$), which is immiscible with respect to the solid and the pore liquid phases, cf. Table 2.1. Such a multiphasic body can be described very well within the macroscopic Theory of Porous Media. Therefore, after a real or a virtual averaging process over a representative elementary volume (REV), the single aggregates of the multiphasic body are assumed to be in a state of ideal disarrangement and smeared out over the considered domain. This leads to a macroscopic model of superimposed and interconnecting continua,

$$\varphi = \bigcup_{\alpha} \varphi^{\alpha}, \quad (2.1)$$

where φ is the set union of φ^α . After a homogenization procedure, all macroscopic quantities are understood as local averages of their microscopic counterparts, cf. Figure 2.1. Consequently, each spatial point \mathbf{x} is occupied by material points P^α of all individual constituents. Thus, the mathematical functions describing the geometrical and physical properties of the multiphasic material are field functions defined over the whole aggregate.

φ^α : all constituents of the porous material		
φ^S : solid constituent	φ^ξ : liquid constituents	φ^γ : gaseous constituents
$\varphi^L = \bigcup_{\xi} \varphi^\alpha$: overall liquid constituent		$\varphi^G = \bigcup_{\gamma} \varphi^\alpha$: overall gas constituent
$\varphi^F = \varphi^L \cup \varphi^G$: overall fluid constituent		
further indices: $\beta = \xi, G$: fluid phases, $\zeta = \xi, \gamma$: fluid constituents		

Table 2.1: Overview of the introduced indices and constituents.

In contrast to the classical Theory of Mixtures, where miscible constituents are considered and no information about the inner structure of the multiphasic body is provided, immiscible phases can be differentiated in the frame of the TPM by their partial volumes V^S and V^β ($\beta = \xi, G$) within the overall medium. Therefore, the overall volume V of a multiphasic body \mathcal{B} is given by the sum of the partial volumes of the constituents:

$$V = \int_{\mathcal{B}} dv, \quad V^\alpha = \int_{\mathcal{B}} dv^\alpha \quad \text{and} \quad V = V^S + \sum_{\beta} V^\beta. \quad (2.2)$$

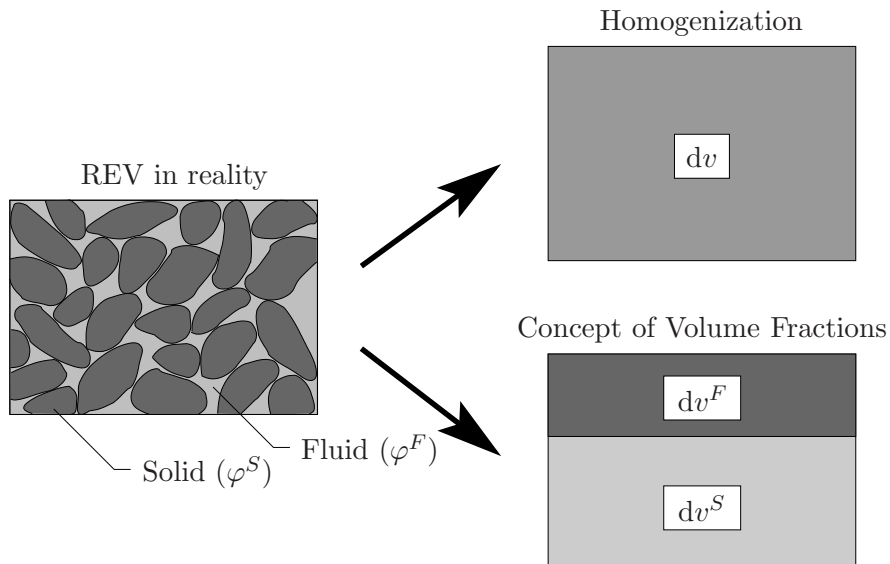


Figure 2.1: Homogenization and Concept of Volume Fractions.

By an introduction of the volume fraction n^α via

$$V^\alpha =: \int_{\mathcal{B}} n^\alpha dv, \quad (2.3)$$

informations about the local volume distribution of the single constituents and, therefore, about the inner structure of the multiphasic material are provided. One finds directly that the volume fraction relates the volume element dv^α of a constituent φ^α to the volume element dv of the whole medium φ and that, furthermore, the so-called saturation condition holds:

$$n^\alpha = \frac{dv^\alpha}{dv} \quad \text{and} \quad n^S + \sum_{\beta} n^\beta = 1. \quad (2.4)$$

Considering more than one fluid phase, it is convenient to introduce so-called saturation functions s^β , which relate the volumes of the liquid and gas phases to the volume fraction (porosity) n^F of the overall pore fluid:

$$s^\beta = \frac{n^\beta}{n^F} \quad \text{and} \quad n^F = \sum_{\beta} n^\beta = 1 - n^S. \quad (2.5)$$

Furthermore, one easily concludes that

$$\sum_{\beta} s^\beta = 1 \quad (2.6)$$

and, therefore, one can recognize that (2.6) relates the saturation condition to the pore content, whereas (2.4)₂ relates the saturation condition to the overall aggregate.

By the assumption that the individual phases are immiscible and, thus, occupy their own partial volume within the porous material, two different densities can be introduced:

$$\rho^{\alpha R} = \frac{dm^\alpha}{dv^\alpha} \quad \text{and} \quad \rho^\alpha = \frac{dm^\alpha}{dv}, \quad \text{where} \quad \alpha = S, \xi, G. \quad (2.7)$$

Therein, the material (effective or realistic) density $\rho^{\alpha R}$ relates the local mass dm^α to the volume element dv^α of a single phase, whereas the partial (global or bulk) density ρ^α relates the local mass to the volume element dv of the overall porous medium. Using the definition of the volume fractions, one finds directly that the two densities are related to each other via

$$\rho^\alpha = n^\alpha \rho^{\alpha R}. \quad (2.8)$$

If constituents under isothermal conditions are assumed to behave materially incompressible, the material density $\rho^{\alpha R}$ is constant ($\rho^{\alpha R} = \text{const.}$). Nevertheless, it can be recognized from (2.8) that the partial density ρ^α can indeed change due to a change of the volume fraction n^α .

The materially compressible pore fluid constituents are assumed as ideal gases and, therefore, form an overall gas phase, which can be considered as a mixture of ideal gases.

Therefore, it is convenient to relate their local mass dm^γ to the volume element dv^G of the overall gas phase:

$$\rho^\gamma = \frac{dm^\gamma}{dv} = \frac{dv^G}{dv} \frac{dm^\gamma}{dv^G} = n^G \rho_G^\gamma. \quad (2.9)$$

Moreover, expressing the local mass dm^γ by the molar mass M_m^γ and the local number of moles dn_m^γ , the partial density ρ_G^γ of the gas component φ^γ within the overall gas phase can be rewritten:

$$\rho_G^\gamma = \frac{dm^\gamma}{dv^G} = M_m^\gamma \frac{dn_m^\gamma}{dv^G} = M_m^\gamma c_{Gm}^\gamma, \quad \text{where} \quad c_{Gm}^\gamma = \frac{dn_m^\gamma}{dv^G} \quad (2.10)$$

is the molar concentration of the constituent φ^γ within the overall gas phase. Furthermore, taking a closer look on the partial density of the gas phase, one finds

$$\rho^G = n^G \rho^{GR} = \sum_\gamma \rho^\gamma = \sum_\gamma n^G \rho_G^\gamma = n^G \sum_\gamma \rho_G^\gamma, \quad (2.11)$$

and it follows directly that

$$\rho^{GR} = \sum_\gamma \rho_G^\gamma. \quad (2.12)$$

Relating furthermore the partial density ρ_G^γ to the material density ρ^{GR} of the overall gas phase, the mass concentration c_G^γ can be introduced via

$$c_G^\gamma = \frac{\rho_G^\gamma}{\rho^{GR}} = \frac{dm^\gamma/n^G}{dm^G/n^G} = \frac{dm^\gamma}{dm^G}. \quad (2.13)$$

Moreover, the molar fraction x_{Gm}^γ of the gas phase is defined as the ratio between the local, n_m^γ , and the total number n_m^G of moles of the gaseous constituents φ^γ :

$$x_{Gm}^\gamma = \frac{dn_m^\gamma}{dn_m^G} = \frac{c_{Gm}^\gamma}{c_{Gm}}, \quad \text{where} \quad n_m^G = \sum_\gamma n_m^\gamma, \quad c_{Gm} = \sum_\gamma c_{Gm}^\gamma. \quad (2.14)$$

Furthermore, the density of the whole porous material is given by the sum of the partial densities of all constituents:

$$\rho = \sum_\alpha \rho^\alpha. \quad (2.15)$$

2.1.2 Motion functions

In continuum mechanics of single-phasic materials, a coherent manifold of material points P defines the body \mathcal{B} and its surface $\partial\mathcal{B}$. In the frame of the Theory of Mixtures or the Theory of Porous Media, the considered body consists of material points P^α of each constituent φ^α . Proceeding from the position of the material points in the reference configuration \mathbf{X}_α , the motion function χ_α of the constituent φ^α is introduced via

$$\mathbf{x} = \chi_\alpha(\mathbf{X}_\alpha, t). \quad (2.16)$$

At this point, it is mentioned that kinematical quantities are identified via a subscript, whereas all other quantities are identified via a superscript. Following the above mentioned homogenization procedure and the basic concept of the Theory of Mixtures, where superimposed continua with internal interactions and individual motions are assumed, each spatial point \mathbf{x} is at any time t simultaneously occupied by material points P^α of all constituents φ^α , which proceed generally from different positions in the reference configuration, cf. Figure 2.2. The requirement of a unique relation between the position of the material points in the reference and the current configuration is fulfilled by the existence of unique inverse motion functions

$$\mathbf{X}_\alpha = \boldsymbol{\chi}_\alpha^{-1}(\mathbf{x}, t) \quad (2.17)$$

based on non-singular *Jacobian* determinants J_α :

$$J_\alpha = \det \frac{\partial \boldsymbol{\chi}_\alpha}{\partial \mathbf{X}_\alpha} \neq 0. \quad (2.18)$$

The assumption of individual motion functions results in different velocity and acceleration fields for every constituent, which are given in the material or *Lagrangian* description by

$$\dot{\mathbf{x}}_\alpha = \frac{d}{dt} \boldsymbol{\chi}_\alpha(\mathbf{X}_\alpha, t) \quad \text{and} \quad \ddot{\mathbf{x}}_\alpha = \frac{d^2}{dt^2} \boldsymbol{\chi}_\alpha(\mathbf{X}_\alpha, t) \quad (2.19)$$

and in the spatial or *Eulerian* description by

$$\dot{\mathbf{x}}_\alpha = \dot{\mathbf{x}}_\alpha[\boldsymbol{\chi}_\alpha^{-1}(\mathbf{x}, t), t] = \dot{\mathbf{x}}_\alpha(\mathbf{x}, t) \quad \text{and} \quad \ddot{\mathbf{x}}_\alpha = \ddot{\mathbf{x}}_\alpha(\mathbf{x}, t), \quad (2.20)$$

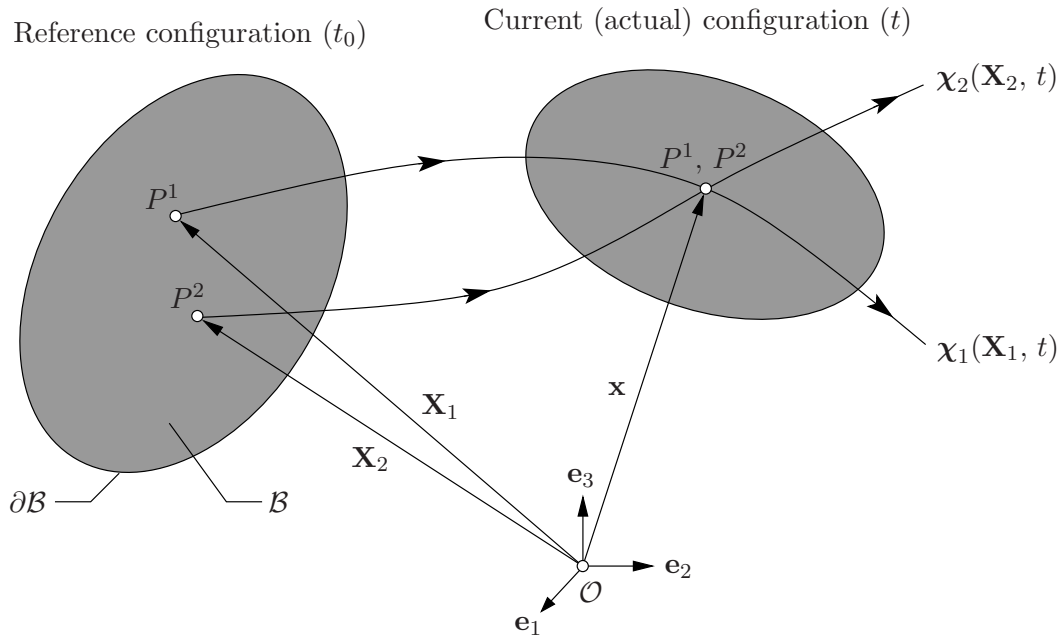


Figure 2.2: Motion of a biphasic porous material model.

where the inverse motion function (2.17) is used. It can be seen that within a *Lagrangean* representation, the constituent is described with respect to the reference, within a *Eulerian* representation with respect to the current configuration.

Proceeding from the velocity fields of the individual constituents, the velocity of the overall medium

$$\dot{\mathbf{x}} = \frac{1}{\rho} \sum_{\alpha} \rho^{\alpha} \dot{\mathbf{x}}_{\alpha} \quad (2.21)$$

can be introduced indicating the barycentric velocity of the whole aggregate. Furthermore, the mixture velocity of the gas phase is given in terms of the gas components in the following way:

$$\dot{\mathbf{x}}_G = \frac{1}{\rho^G} \sum_{\gamma} \rho^{\gamma} \dot{\mathbf{x}}_{\gamma} = \frac{1}{n^G \rho^{GR}} \sum_{\gamma} n^G \rho_G^{\gamma} \dot{\mathbf{x}}_{\gamma} = \sum_{\gamma} \frac{\rho_G^{\gamma}}{\rho^{GR}} \dot{\mathbf{x}}_{\gamma} = \sum_{\gamma} c_G^{\gamma} \dot{\mathbf{x}}_{\gamma} . \quad (2.22)$$

The relative velocity between the whole aggregate and the individual constituents is expressed via the diffusion velocity

$$\mathbf{d}_{\alpha} = \dot{\mathbf{x}}_{\alpha} - \dot{\mathbf{x}} . \quad (2.23)$$

If Γ is an arbitrary, continuous and sufficiently often continuously differentiable scalar function of (\mathbf{x}, t) , the material time derivative of Γ following the motion of φ^{α} results in

$$(\Gamma)_{\alpha}' = \frac{d_{\alpha}}{dt} \Gamma(\mathbf{x}, t) = \frac{\partial \Gamma}{\partial t} + \frac{\partial \Gamma}{\partial \mathbf{x}} \cdot \left(\frac{\partial \mathbf{x}}{\partial t} \right)_{\alpha} = \frac{\partial \Gamma}{\partial t} + \text{grad } \Gamma \cdot \dot{\mathbf{x}}_{\alpha} , \quad (2.24)$$

where the operator “grad(\cdot)” denotes the partial derivative of (\cdot) with respect to the actual position \mathbf{x} . The first term on the right-hand side of (2.24) is the so-called local part, the second term the so-called convective part, whereby a velocity field is called stationary, if the local part, i. e., the partial time derivative, is zero. If a vector-valued function $\mathbf{\Gamma}(\mathbf{x}, t)$ is considered, the material time derivative is given by

$$(\mathbf{\Gamma})_{\alpha}' = \frac{d_{\alpha}}{dt} \mathbf{\Gamma}(\mathbf{x}, t) = \frac{\partial \mathbf{\Gamma}}{\partial t} + (\text{grad } \mathbf{\Gamma}) \dot{\mathbf{x}}_{\alpha} . \quad (2.25)$$

Modeling coupled solid-fluid problems, it is convenient to describe the solid phase in a *Lagrangean* description using the displacement vector \mathbf{u}_S as primary kinematic variable, whereas the fluid phases are better described in a modified *Eulerian* representation with respect to the deformable solid skeleton.

Remark: In solid mechanics, the reference configuration and, therefore, the reference position of every material point is given at the beginning of the experiment. On the other side, in fluid mechanics only the current position of a single fluid particle within the considered control domain is known. \square

Therefore, the seepage velocity \mathbf{w}_{ζ} and the diffusion velocity $\mathbf{d}_{\gamma G}$, describing the motion of the gas components with respect to the barycentric velocity of the overall gas phase, are introduced:

$$\mathbf{u}_S = \mathbf{x} - \mathbf{X}_S , \quad \mathbf{w}_{\zeta} = \dot{\mathbf{x}}_{\zeta} - \dot{\mathbf{x}}_S , \quad \mathbf{d}_{\gamma G} = \dot{\mathbf{x}}_{\gamma} - \dot{\mathbf{x}}_G . \quad (2.26)$$

2.1.3 Deformation and strain measures

Deformation and strain measures can be introduced by comparing the square of line elements between two neighboring material points in the reference and current configuration. In general, all deformation measures are based on the material deformation gradient \mathbf{F}_α and its inverse \mathbf{F}_α^{-1} , which are obtained from (2.16) and (2.17) via

$$\mathbf{F}_\alpha = \frac{\partial \boldsymbol{\chi}_\alpha(\mathbf{X}_\alpha, t)}{\partial \mathbf{X}_\alpha} = \text{Grad}_\alpha \mathbf{x} \quad \text{and} \quad \mathbf{F}_\alpha^{-1} = \frac{\partial \boldsymbol{\chi}_\alpha^{-1}(\mathbf{x}, t)}{\partial \mathbf{x}} = \text{grad } \mathbf{X}_\alpha. \quad (2.27)$$

Therein, the operator “ $\text{Grad}_\alpha(\cdot)$ ” denotes the partial derivative of (\cdot) with respect to the reference position \mathbf{X}_α of the material point P^α . Using (2.27)₁, the *Jacobian determinant* can be also written as $J_\alpha = \det \mathbf{F}_\alpha$. Furthermore, proceeding from the initial state ($t = t_0$), where $\det \mathbf{F}_\alpha = 1$, one finds directly under consideration of the requirement for the existence of unique motion functions, cf. (2.18), that the range of the *Jacobian determinant* is limited to positive values.

Rewriting the second order tensors \mathbf{F}_α and \mathbf{F}_α^{-1} with respect to a natural basis system, one recognizes that one basis system of these tensors is located in the reference and the other one in the current configuration. Therefore, using these so-called two-field tensors, the line element $d\mathbf{X}_\alpha$ of the reference configuration can be transported to the line element $d\mathbf{x}$ of the current configuration (push-forward operation) or vice versa (pull-back operation):

$$d\mathbf{x} = \mathbf{F}_\alpha d\mathbf{X}_\alpha \quad \text{and} \quad d\mathbf{X}_\alpha = \mathbf{F}_\alpha^{-1} d\mathbf{x}. \quad (2.28)$$

Furthermore, the area element $d\mathbf{A}_\alpha$ and the volume element dV_α of the reference configuration can be mapped to their respective counterparts of the current configuration:

$$\begin{aligned} d\mathbf{a} &= (\det \mathbf{F}_\alpha) \mathbf{F}_\alpha^{T-1} d\mathbf{A}_\alpha, \\ dv &= (\det \mathbf{F}_\alpha) dV_\alpha. \end{aligned} \quad (2.29)$$

For a closer look on this topic, the interested reader is referred to the works of *de Boer* [11] or *Ehlers* [40].

With the definition of the material deformation gradient, the length of the current line element $d\mathbf{x}$ can be expressed in terms of the reference configuration:

$$\begin{aligned} \|d\mathbf{x}\|^2 &= d\mathbf{x} \cdot d\mathbf{x} = (\mathbf{F}_\alpha d\mathbf{X}_\alpha) \cdot (\mathbf{F}_\alpha d\mathbf{X}_\alpha) \\ &= d\mathbf{X}_\alpha \cdot (\mathbf{F}_\alpha^T \mathbf{F}_\alpha) d\mathbf{X}_\alpha = d\mathbf{X}_\alpha \cdot \mathbf{C}_\alpha d\mathbf{X}_\alpha. \end{aligned} \quad (2.30)$$

Therein, $\mathbf{C}_\alpha = \mathbf{F}_\alpha^T \mathbf{F}_\alpha$ is the right *Cauchy-Green* deformation tensor. Proceeding from the difference of the squares of the current and referential line elements,

$$\|d\mathbf{x}\|^2 - \|d\mathbf{X}_\alpha\|^2 = d\mathbf{X}_\alpha \cdot \mathbf{C}_\alpha d\mathbf{X}_\alpha - d\mathbf{X}_\alpha \cdot d\mathbf{X}_\alpha = d\mathbf{X}_\alpha \cdot (\mathbf{C}_\alpha - \mathbf{I}) d\mathbf{X}_\alpha, \quad (2.31)$$

the *Green-Lagrangean strain tensor*

$$\mathbf{E}_\alpha = \frac{1}{2}(\mathbf{C}_\alpha - \mathbf{I}) \quad (2.32)$$

can be introduced. Therein, \mathbf{I} denotes the second order identity and the factor $1/2$ results from the fact that the linearization of \mathbf{E}_α around the natural state ($t = t_0$) should result in the well-known 1-d *Hookean* elasticity law.

In this thesis, the occurrence of small deformations and, therefore, small strains of the solid matrix are assumed so that the finite deformation approach can be reduced to a geometrically linear one. Thus, one has to distinguish no longer between the reference and the current configuration leading to the following approximations:

$$\text{Grad}_S(\cdot) \approx \text{grad}(\cdot) \quad \text{and} \quad \text{Div}_S(\cdot) \approx \text{div}(\cdot). \quad (2.33)$$

Therein, $\text{Div}_S(\cdot)$ and $\text{div}(\cdot)$ indicate the divergence operators corresponding to $\text{Grad}_S(\cdot)$ and $\text{grad}(\cdot)$. Furthermore, the linearized form of the *Green-Lagrangean* strain tensor of the solid phase φ^S can be found via a linearization around the natural state:

$$\text{lin } \mathbf{E}_S =: \boldsymbol{\varepsilon}_S = \frac{1}{2}[\text{grad } \mathbf{u}_S + (\text{grad } \mathbf{u}_S)^T]. \quad (2.34)$$

Remark: In the same way, by expressing the length of the line element $d\mathbf{X}_\alpha$ with respect to the line element $d\mathbf{x}$ of the current configuration, the left *Cauchy-Green* deformation tensor $\mathbf{B}_\alpha = \mathbf{F}_\alpha \mathbf{F}_\alpha^T$ and, furthermore, the *Almansi* strain tensor $\mathbf{A}_\alpha = \frac{1}{2}(\mathbf{I} - \mathbf{B}_\alpha^{-1})$ can be introduced. Furthermore, a relation between the two strain tensors of the referential (\mathbf{E}_α) and current (\mathbf{A}_α) configuration is given via $\mathbf{A}_\alpha = \mathbf{F}_\alpha^T \mathbf{E}_\alpha \mathbf{F}_\alpha^{-1}$, i. e., the *Almansi* strain tensor (\mathbf{A}_α) can be computed from the *Green-Lagrangean* strain tensor (\mathbf{E}_α) via a so-called contravariant push-forward transport mechanism. In the frame of a geometrically linear theory, the linearization of both strain tensors of the solid skeleton yields the same result: $\text{lin } \mathbf{E}_S = \text{lin } \mathbf{A}_S =: \boldsymbol{\varepsilon}_S$. \square

2.1.4 Deformation and strain rates

Proceeding from a *Lagrangean* description of the constituent φ^α , the material velocity gradient is given by a total time derivative, cf. (2.25), of the material deformation gradient (2.27)₁ with respect to the constituent φ^α :

$$(\mathbf{F}_\alpha)'_\alpha = \frac{d_\alpha}{dt} \mathbf{F}_\alpha = \frac{d_\alpha}{dt} \left(\frac{\partial \mathbf{x}(\mathbf{X}_\alpha, t)}{\partial \mathbf{X}_\alpha} \right) = \frac{\partial \dot{\mathbf{x}}_\alpha(\mathbf{X}_\alpha, t)}{\partial \mathbf{X}_\alpha} = \text{Grad}_\alpha \dot{\mathbf{x}}_\alpha. \quad (2.35)$$

On the other hand, if one proceeds from an *Eulerian* description of the constituent φ^α , the total time derivative of the material deformation gradient can be computed via

$$(\mathbf{F}_\alpha)'_\alpha = \frac{\partial \dot{\mathbf{x}}_\alpha(\mathbf{x}, t)}{\partial \mathbf{x}} \frac{\partial \mathbf{x}}{\partial \mathbf{X}_\alpha} = \mathbf{L}_\alpha \mathbf{F}_\alpha, \quad (2.36)$$

where \mathbf{L}_α is the spatial velocity gradient of the constituent φ^α . After reformulating (2.36), the following relations are found directly:

$$\mathbf{L}_\alpha = (\mathbf{F}_\alpha)'_\alpha \mathbf{F}_\alpha^{-1} = \text{grad } \dot{\mathbf{x}}_\alpha \quad \text{and} \quad \mathbf{L}_\alpha \cdot \mathbf{I} = \text{div } \dot{\mathbf{x}}_\alpha. \quad (2.37)$$

As every tensor, the spatial velocity gradient can be additively split into a symmetric and a skew-symmetric part:

$$\mathbf{L}_\alpha = \mathbf{D}_\alpha + \mathbf{W}_\alpha, \quad \text{where} \quad \begin{cases} \mathbf{D}_\alpha &= \frac{1}{2}(\mathbf{L}_\alpha + \mathbf{L}_\alpha^T), \\ \mathbf{W}_\alpha &= \frac{1}{2}(\mathbf{L}_\alpha - \mathbf{L}_\alpha^T). \end{cases} \quad (2.38)$$

Therein, \mathbf{D}_α is the symmetric rate of deformation tensor, whereas \mathbf{W}_α is the skew-symmetric rate of rotation (spin or vorticity) tensor. \mathbf{D}_α is the most important tensor formulating material laws for fluids and corresponds in this frame to the linearized strain tensor $\boldsymbol{\varepsilon}_S$ in solid mechanics. In both cases, these tensors represent the symmetric part of the gradient of the respective primary kinematical variable, i. e., $\boldsymbol{\varepsilon}_S$ is a linear function of the gradient of the solid displacement vector, cf. (2.34), whereas \mathbf{D}_ζ is a linear function of the gradient of the fluid velocity.

Following the above relations, the rate of the right *Cauchy-Green* deformation tensor reads

$$\begin{aligned} (\mathbf{C}_\alpha)'_\alpha &= (\mathbf{F}_\alpha^T \mathbf{F}_\alpha)'_\alpha = (\mathbf{F}_\alpha^T)'_\alpha \mathbf{F}_\alpha + \mathbf{F}_\alpha^T (\mathbf{F}_\alpha)'_\alpha \\ &= (\mathbf{L}_\alpha \mathbf{F}_\alpha)^T \mathbf{F}_\alpha + \mathbf{F}_\alpha^T (\mathbf{L}_\alpha \mathbf{F}_\alpha) = \mathbf{F}_\alpha^T (\mathbf{L}_\alpha^T + \mathbf{L}_\alpha) \mathbf{F}_\alpha \\ &= 2 \mathbf{F}_\alpha^T \mathbf{D}_\alpha \mathbf{F}_\alpha. \end{aligned} \quad (2.39)$$

Furthermore, from the definition of the *Green-Lagrangean* strain tensor (2.32) follows directly the *Green-Lagrangean* strain rate:

$$(\mathbf{E}_\alpha)'_\alpha = \frac{1}{2}(\mathbf{C}_\alpha - \mathbf{I})'_\alpha = \frac{1}{2}(\mathbf{C}_\alpha)'_\alpha = \mathbf{F}_\alpha^T \mathbf{D}_\alpha \mathbf{F}_\alpha. \quad (2.40)$$

In the frame of a geometrically linear theory, the linearized *Green-Lagrangean* strain rate of the solid skeleton is given via

$$\text{lin } (\mathbf{E}_S)'_S = (\boldsymbol{\varepsilon}_S)'_S = \frac{1}{2} \{ \text{grad } (\mathbf{u}_S)'_S + [\text{grad } (\mathbf{u}_S)'_S]^T \}. \quad (2.41)$$

2.1.5 Stress measures

The physical quantity stress is defined as “force per unit area”. Therefore, different stress measures can be introduced due to the fact that the force can be related to area elements of both, the current or the reference configurations.

The surface traction vector $\mathbf{t}^\alpha(\mathbf{x}, t, \mathbf{n})$ describes the effects of contact forces acting on material points P^α of the surface $\partial\mathcal{B}$ characterized by the outward oriented unit surface normal \mathbf{n} of the current configuration. By *Cauchy's* theorem

$$\mathbf{t}^\alpha(\mathbf{x}, t, \mathbf{n}) = \mathbf{T}^\alpha(\mathbf{x}, t) \mathbf{n}, \quad (2.42)$$

the partial *Cauchy* stress tensor \mathbf{T}^α can be introduced. Therefore, the field function \mathbf{T}^α is only a stress measure independent of the considered surface, which is characterized by \mathbf{n} . \mathbf{T}^α relates the contact force $d\mathbf{k}^\alpha$ acting on the constituent φ^α to the oriented area element da of the current configuration,

$$d\mathbf{k}^\alpha = \mathbf{t}^\alpha da = (\mathbf{T}^\alpha \mathbf{n}) da = \mathbf{T}^\alpha (\mathbf{n} da) = \mathbf{T}^\alpha da, \quad (2.43)$$

and, thus, \mathbf{T}^α is often called true stress tensor. Transferring the area element $d\mathbf{a}$ to a weighted area element $d\bar{\mathbf{a}}_\alpha = (\det \mathbf{F}_\alpha)^{-1} d\mathbf{a}$, the partial *Kirchhoff* (or weighted *Cauchy*) stress $\boldsymbol{\tau}^\alpha$ can be introduced. Furthermore, relating the contact force to an area element $d\mathbf{A}_\alpha$ of the reference configuration using the transport theorem (2.29)₁ leads to the definition of the partial first *Piola-Kirchhoff* stress tensor \mathbf{P}^α , which is, like the material deformation gradient \mathbf{F}_α , a two-field tensor as only the second basis is pulled back to the reference configuration. Therefore, the contact force $d\mathbf{k}^\alpha$ can be expressed in the following different ways:

$$\begin{aligned} d\mathbf{k}^\alpha &= (\det \mathbf{F}_\alpha) \mathbf{T}^\alpha d\bar{\mathbf{a}}_\alpha =: \boldsymbol{\tau}^\alpha d\bar{\mathbf{a}}_\alpha \\ &= (\det \mathbf{F}_\alpha) \mathbf{T}^\alpha \mathbf{F}_\alpha^{T-1} d\mathbf{A}_\alpha =: \mathbf{P}^\alpha d\mathbf{A}_\alpha. \end{aligned} \quad (2.44)$$

Pulling back the first and the second basis of $\boldsymbol{\tau}^\alpha$ by a covariant pull-back transport mechanism, the partial second *Piola-Kirchhoff* stress tensor \mathbf{S}^α can be introduced:

$$\mathbf{S}^\alpha := \mathbf{F}_\alpha^{-1} \mathbf{P}^\alpha = \mathbf{F}_\alpha^{-1} \boldsymbol{\tau}^\alpha \mathbf{F}_\alpha^{T-1}. \quad (2.45)$$

Nevertheless, if the solid constituent is described within a geometrically linear theory, only one partial stress tensor $\boldsymbol{\sigma}^S$ is necessary due to the fact that all different stress measures are approximately the same:

$$\boldsymbol{\sigma}^S : \approx \mathbf{S}^S \approx \mathbf{P}^S \approx \boldsymbol{\tau}^S \approx \mathbf{T}^S. \quad (2.46)$$

2.2 Balance relations

The axiomatic introduction of conservation equations in continuum mechanics of single-phasic materials is based on experiences that certain physical quantities are never produced or disappear in a closed system. Furthermore, if the interaction with the environment is taken into account, balance relations can be formulated, which build the basis of a continuum mechanical model and its numerical realization. In particular, balance relations for the mechanical quantities mass, momentum and moment of momentum as well as for the first and the second fundamental law of continuum thermodynamics, i. e., the energy balance and the entropy inequality, are introduced.

The application of these fundamental relations on the modeling of multiphasic materials is based on *Truesdell's* “metaphysical principles”, cf. *Truesdell* [135]:

1. *All properties of the mixture must be mathematical consequences of properties of the constituents.*
2. *So as to describe the motion of a constituent, we may in imagination isolate it from the rest of the mixture, provided we allow properly for the actions of the other constituents upon it.*
3. *The motion of the mixture is governed by the same equations as is a single body.*

Thus, a summation of the balance equations of all constituents φ^α yields the respective balance equation of the overall porous medium φ . Furthermore, a certain constituent φ^α

can be described by the balance relations of a single-phasic material, if these balances are extended by terms describing the interactions with the other phases of the multiphasic body. Finally, the balance equations of the overall aggregate follow the structure of classical continuum mechanics.

By an examination of the individual balance relations, a general structure can be identified. Therefore, in the following this general structure is presented by means of the so-called master balance for the whole porous material and the single constituents. Afterwards, the introduced mechanical quantities are identified for the specific mechanical and thermodynamical quantities of the certain balance relations. Thereby, the presented format follows the approach given by *Ehlers* [40, 46].

2.2.1 General structure of the balance relations

The specific balance relations can be embedded into a general structure given by the master balance relation, whereas this general structure is valid for both the whole porous medium and the individual constituents. In this context, firstly, the global representation of the master balance of the mixture is introduced via

$$\boxed{\begin{aligned} \frac{d}{dt} \int_{\mathcal{B}} \Psi \, dv &= \int_{\partial \mathcal{B}} (\boldsymbol{\phi} \cdot \mathbf{n}) \, da + \int_{\mathcal{B}} \sigma \, dv + \int_{\mathcal{B}} \hat{\Psi} \, dv, \\ \frac{d}{dt} \int_{\mathcal{B}} \boldsymbol{\Psi} \, dv &= \int_{\partial \mathcal{B}} (\boldsymbol{\Phi} \mathbf{n}) \, da + \int_{\mathcal{B}} \boldsymbol{\sigma} \, dv + \int_{\mathcal{B}} \hat{\boldsymbol{\Psi}} \, dv, \end{aligned}} \quad (2.47)$$

where Ψ and $\boldsymbol{\Psi}$ are volume-specific scalar- and vector-valued mechanical quantities. It can be recognized that the temporal change of the mechanical quantity Ψ (or $\boldsymbol{\Psi}$) is balanced with the efflux $\boldsymbol{\phi}$ (or $\boldsymbol{\Phi}$) over the boundary $\partial \mathcal{B}$, the supply σ (or $\boldsymbol{\sigma}$) resulting from the external distance and the production $\hat{\Psi}$ (or $\hat{\boldsymbol{\Psi}}$) of the mechanical quantity describing possible couplings of φ with its surrounding.

In contrast to the global form of the master balance, which is valid for the overall body \mathcal{B} , the local representation of the master balance is valid for each material point P^α of \mathcal{B} . Proceeding from the global form, the local form of the master balance is given by differentiating¹ the left-hand side of (2.47), transforming the surface integrals of (2.47) into volume integrals and assuming steady and sufficiently steady differentiable integrands:

$$\boxed{\begin{aligned} \dot{\Psi} + \Psi \operatorname{div} \dot{\mathbf{x}} &= \operatorname{div} \boldsymbol{\phi} + \sigma + \hat{\Psi}, \\ \dot{\boldsymbol{\Psi}} + \boldsymbol{\Psi} \operatorname{div} \dot{\mathbf{x}} &= \operatorname{div} \boldsymbol{\Phi} + \boldsymbol{\sigma} + \hat{\boldsymbol{\Psi}}. \end{aligned}} \quad (2.48)$$

¹ $\frac{d}{dt} (\Psi \, dv) = \dot{\Psi} \, dv + \Psi (dv)^{\cdot} = \dot{\Psi} \, dv + \Psi (\det \mathbf{F} \, dV)^{\cdot} = \dot{\Psi} \, dv + \Psi [(\det \mathbf{F})^{\cdot} \, dV] =$
 $= \dot{\Psi} \, dv + \underbrace{\Psi \det \mathbf{F}}_{(\det \mathbf{F})^{\cdot}} \underbrace{\operatorname{div} \dot{\mathbf{x}} (\det \mathbf{F})^{-1} \, dv}_{dV} = (\dot{\Psi} + \Psi \operatorname{div} \dot{\mathbf{x}}) \, dv$

Proceeding from *Truesdell's* principles, the master balance for an individual constituent φ^α has the same general structure as the master balance of the overall medium. Therefore, the global master balance for a constituent is given corresponding to (2.47) via

$$\boxed{\begin{aligned} \frac{d_\alpha}{dt} \int_{\mathcal{B}} \Psi^\alpha \, dv &= \int_{\partial \mathcal{B}} (\phi^\alpha \cdot \mathbf{n}) \, da + \int_{\mathcal{B}} \sigma^\alpha \, dv + \int_{\mathcal{B}} \hat{\Psi}^\alpha \, dv, \\ \frac{d_\alpha}{dt} \int_{\mathcal{B}} \mathbf{\Psi}^\alpha \, dv &= \int_{\partial \mathcal{B}} (\mathbf{\Phi}^\alpha \mathbf{n}) \, da + \int_{\mathcal{B}} \boldsymbol{\sigma}^\alpha \, dv + \int_{\mathcal{B}} \hat{\mathbf{\Psi}}^\alpha \, dv. \end{aligned}} \quad (2.49)$$

As within the master balance of the whole mixture, the production term $\hat{\Psi}^\alpha$ (or $\hat{\mathbf{\Psi}}^\alpha$) describes the interaction with the local environment of the constituent φ^α . But, considering a porous material, this term not only describes the interaction with the environment outside, but also the interaction with the other constituents of the overall medium.

The local form of the master balance is given corresponding to (2.48) by

$$\boxed{\begin{aligned} (\Psi^\alpha)'_\alpha + \Psi^\alpha \operatorname{div} \dot{\mathbf{x}}_\alpha &= \operatorname{div} \phi^\alpha + \sigma^\alpha + \hat{\Psi}^\alpha, \\ (\mathbf{\Psi}^\alpha)'_\alpha + \mathbf{\Psi}^\alpha \operatorname{div} \dot{\mathbf{x}}_\alpha &= \operatorname{div} \mathbf{\Phi}^\alpha + \boldsymbol{\sigma}^\alpha + \hat{\mathbf{\Psi}}^\alpha. \end{aligned}} \quad (2.50)$$

As discussed in *Truesdell's* principles, the balance relations of the overall aggregate result from a summation of the balance relations of all individual constituents. Therefore, certain relations between the quantities of the single constituents and the overall porous medium can be found, which are given for a scalar-valued mechanical quantity via

$$\boxed{\begin{aligned} \text{mechanical quantity: } \Psi &= \sum_{\alpha} \Psi^\alpha, \\ \text{efflux} &: \phi \cdot \mathbf{n} = \sum_{\alpha} (\phi^\alpha - \Psi^\alpha \mathbf{d}_\alpha) \cdot \mathbf{n}, \\ \text{supply} &: \sigma = \sum_{\alpha} \sigma^\alpha, \\ \text{production} &: \hat{\Psi} = \sum_{\alpha} \hat{\Psi}^\alpha. \end{aligned}} \quad (2.51)$$

In the same way, the relations for a vector-valued mechanical quantity read

mechanical quantity :	$\Psi = \sum_{\alpha} \Psi^{\alpha},$	(2.52)
efflux :	$\Phi \mathbf{n} = \sum_{\alpha} (\Phi^{\alpha} - \Psi^{\alpha} \otimes \mathbf{d}_{\alpha}) \mathbf{n},$	
supply :	$\sigma = \sum_{\alpha} \sigma^{\alpha},$	
production :	$\hat{\Psi} = \sum_{\alpha} \hat{\Psi}^{\alpha}.$	

2.2.2 Mechanical balance laws

As mentioned above, the temporal change of the mechanical quantities mass, momentum and moment of momentum are balanced with the respective influences acting on the multiphasic body and, therefore, on the individual constituents. In this section, starting with the mass balance as the so-called lowest balance relation, the momentum balance and the balance of moment of momentum are axiomatically introduced.

Mass balances

The mass balances of the overall mixture φ and the constituent φ^{α} are axiomatically introduced via

$\frac{d}{dt} \int_{\mathcal{B}} \rho \, dv = 0, \quad \frac{d_{\alpha}}{dt} \int_{\mathcal{B}} \rho^{\alpha} \, dv = \int_{\mathcal{B}} \hat{\rho}^{\alpha} \, dv.$	(2.53)
--	--------

Therefore, the temporal change of the mass of the overall body \mathcal{B} is zero, whereas the temporal change of the mass of an individual constituent can yield a certain mass production $\hat{\rho}^{\alpha}$, if mass interactions between the constituents are taken into account, i. e., the overall mixture φ can be identified as a closed, the individual constituent φ^{α} as an open system. Comparing these relations with the master balances, the mechanical quantities can be identified by the respective densities ρ and ρ^{α} . The efflux and the supply terms as well as the production term of the overall mass balance are zero and only the production term of the constituents' mass balances can take a certain value:

overall medium φ :	$\Psi = \rho, \quad \phi = \mathbf{0}, \quad \sigma = 0, \quad \hat{\Psi} = 0,$	(2.54)
constituent φ^{α} :	$\Psi^{\alpha} = \rho^{\alpha}, \quad \phi^{\alpha} = \mathbf{0}, \quad \sigma^{\alpha} = 0, \quad \hat{\Psi}^{\alpha} = \hat{\rho}^{\alpha}.$	

With these relations, the local form of the mixture mass balance reads

$\dot{\rho} + \rho \operatorname{div} \dot{\mathbf{x}} = 0,$	(2.55)
--	--------

whereas the mass balance of an individual constituent is given via

$$\boxed{(\rho^\alpha)'_\alpha + \rho^\alpha \operatorname{div} \dot{\mathbf{x}}_\alpha = \hat{\rho}^\alpha,} \quad (2.56)$$

which can be reduced to a volume balance, if the effective density $\rho^{\alpha R}$ is constant:

$$\boxed{(n^\alpha)'_\alpha + n^\alpha \operatorname{div} \dot{\mathbf{x}}_\alpha = \hat{n}^\alpha.} \quad (2.57)$$

In this special case, the mass production $\hat{\rho}^\alpha$ can be reduced to a volume production \hat{n}^α as well. If no mass or volume productions are taken into account, i. e., $\hat{\rho}^\alpha = 0$ or $\hat{n}^\alpha = 0$, one can find directly that

$$\rho^\alpha = \rho_{0\alpha}^\alpha (\det \mathbf{F}_\alpha)^{-1} \quad \text{and} \quad n^\alpha = n_{0\alpha}^\alpha (\det \mathbf{F}_\alpha)^{-1} \quad (2.58)$$

by a comparison² of the total mass in the referential and current configuration or via a time integration of (2.56) and (2.57), respectively. If the constituent φ^α is described in an *Eulerian* description, e. g., if a fluid is considered, (2.56) and (2.57) can be reformulated:

$$\left. \begin{aligned} \frac{\partial \rho^\alpha}{\partial t} + \operatorname{grad} \rho^\alpha \dot{\mathbf{x}}_\alpha + \rho^\alpha \operatorname{div} \dot{\mathbf{x}}_\alpha &= \hat{\rho}^\alpha, \\ \frac{\partial n^\alpha}{\partial t} + \operatorname{grad} n^\alpha \dot{\mathbf{x}}_\alpha + n^\alpha \operatorname{div} \dot{\mathbf{x}}_\alpha &= \hat{n}^\alpha, \end{aligned} \right\} \longrightarrow \left\{ \begin{aligned} \frac{\partial \rho^\alpha}{\partial t} + \operatorname{div} (\rho^\alpha \dot{\mathbf{x}}_\alpha) &= \hat{\rho}^\alpha, \\ \frac{\partial n^\alpha}{\partial t} + \operatorname{div} (n^\alpha \dot{\mathbf{x}}_\alpha) &= \hat{n}^\alpha. \end{aligned} \right. \quad (2.59)$$

Proceeding furthermore from stationary conditions, i. e., $\partial \rho^\alpha / \partial t$ or $\partial n^\alpha / \partial t$ is zero, as well as zero mass or volume interactions, the mass or volume balance results in the so-called continuity equation of fluid mechanics:

$$\operatorname{div} (\rho^\alpha \dot{\mathbf{x}}_\alpha) = 0 \quad \text{or} \quad \operatorname{div} (n^\alpha \dot{\mathbf{x}}_\alpha) = 0. \quad (2.60)$$

Regarding the restrictions (2.51), one finds the following relations between the quantities of the constituents and the overall medium:

$$\rho = \sum_\alpha \rho^\alpha, \quad \mathbf{0} = \sum_\alpha \rho^\alpha \mathbf{d}_\alpha, \quad 0 = \sum_\alpha \hat{\rho}^\alpha. \quad (2.61)$$

Therefore, the density of the mixture ρ is given in analogy to (2.15) as the sum of the densities ρ^α of the constituents, whereas both the sum of the mass flows due to diffusion as well as the sum of the mass production terms must be zero.

²

$$\int_{\mathcal{B}} \rho^\alpha \, dv = \int_{\mathcal{B}} \rho_{0\alpha}^\alpha \, dV_\alpha = \int_{\mathcal{B}} \rho_{0\alpha}^\alpha (\det \mathbf{F}_\alpha)^{-1} \, dv \quad \longrightarrow \quad \rho^\alpha = \rho_{0\alpha}^\alpha (\det \mathbf{F}_\alpha)^{-1}$$

Momentum balances

The second balance equation introduced axiomatically is the momentum balance, in which the temporal change of the physical quantity momentum $\rho \dot{\mathbf{x}}$ or $\rho^\alpha \dot{\mathbf{x}}_\alpha$ is balanced with the surface and body forces acting on the body \mathcal{B} :

$$\boxed{\begin{aligned} \frac{d}{dt} \int_{\mathcal{B}} \rho \dot{\mathbf{x}} \, dv &= \int_{\partial \mathcal{B}} (\mathbf{T} \mathbf{n}) \, da + \int_{\mathcal{B}} \rho \mathbf{b} \, dv, \\ \frac{d_\alpha}{dt} \int_{\mathcal{B}} \rho^\alpha \dot{\mathbf{x}}_\alpha \, dv &= \int_{\partial \mathcal{B}} (\mathbf{T}^\alpha \mathbf{n}) \, da + \int_{\mathcal{B}} \rho^\alpha \mathbf{b}^\alpha \, dv + \int_{\mathcal{B}} \hat{\mathbf{s}}^\alpha \, dv. \end{aligned}} \quad (2.62)$$

Therein, the surface integrals on the right-hand side represent the external contact forces acting on the surface $\partial \mathcal{B}$, whereas the respective volume integrals containing the so-called supply terms $\rho \mathbf{b}$ or $\rho^\alpha \mathbf{b}^\alpha$ correspond to the external body forces acting on the body. Furthermore, $\hat{\mathbf{s}}^\alpha$ is the total momentum production. Comparing (2.62) with the master balances (2.47)₂ and (2.49)₂, the general quantities can be identified as:

$$\begin{aligned} \text{overall medium } \varphi &: \begin{cases} \Psi = \rho \dot{\mathbf{x}}, & \Phi = \mathbf{T}, \\ \sigma = \rho \mathbf{b}, & \hat{\Psi} = \mathbf{0}, \end{cases} \\ \text{constituent } \varphi^\alpha &: \begin{cases} \Psi^\alpha = \rho^\alpha \dot{\mathbf{x}}_\alpha, & \Phi^\alpha = \mathbf{T}^\alpha, \\ \sigma^\alpha = \rho^\alpha \mathbf{b}^\alpha, & \hat{\Psi}^\alpha = \hat{\mathbf{s}}^\alpha. \end{cases} \end{aligned} \quad (2.63)$$

Proceeding from the local form of the master balance (2.48)₂ of the mixture and using furthermore the mass balance (2.55), the momentum balance of the mixture is given in its local form via

$$\boxed{\rho \ddot{\mathbf{x}} = \operatorname{div} \mathbf{T} + \rho \mathbf{b}}, \quad (2.64)$$

whereas, based on (2.50)₂ and (2.56), the local form of the momentum balance of an individual constituent yields

$$\boxed{\rho^\alpha \ddot{\mathbf{x}}_\alpha = \operatorname{div} \mathbf{T}^\alpha + \rho^\alpha \mathbf{b}^\alpha + \hat{\mathbf{p}}^\alpha}. \quad (2.65)$$

Therein, the direct momentum production $\hat{\mathbf{p}}^\alpha = \hat{\mathbf{s}}^\alpha - \hat{\rho}^\alpha \dot{\mathbf{x}}_\alpha$ describes the interaction forces between φ^α and the other constituents of the overall porous material. Considering the vector-valued constraints, cf. (2.52), between the quantities of the constituents and the whole medium, the following relations have to be taken into account:

$$\rho \dot{\mathbf{x}} = \sum_{\alpha} \rho^\alpha \dot{\mathbf{x}}_\alpha, \quad \mathbf{T} = \sum_{\alpha} (\mathbf{T}^\alpha - \rho^\alpha \mathbf{d}_\alpha \otimes \mathbf{d}_\alpha), \quad \rho \mathbf{b} = \sum_{\alpha} \rho^\alpha \mathbf{b}^\alpha, \quad \mathbf{0} = \sum_{\alpha} \hat{\mathbf{s}}^\alpha. \quad (2.66)$$

Additionally, the product $\rho^G \ddot{\mathbf{x}}_G$ of the partial density and the acceleration of the overall gas phase can be computed as a function of the partial densities ρ^γ , the velocities $\dot{\mathbf{x}}_\gamma$

and accelerations $\overset{\prime\prime}{\mathbf{x}}_\gamma$, the diffusion velocities $\mathbf{d}_{\gamma G}$ and the mass production $\hat{\rho}^\gamma$ of the gas components as well as the velocity $\overset{\prime}{\mathbf{x}}_G$ and the mass production $\hat{\rho}^G$ of the overall gas phase via

$$\rho^G \overset{\prime\prime}{\mathbf{x}}_G = \sum_{\gamma} [\rho^\gamma \overset{\prime\prime}{\mathbf{x}}_\gamma - \operatorname{div}(\rho^\gamma \mathbf{d}_{\gamma G} \otimes \mathbf{d}_{\gamma G}) + \hat{\rho}^\gamma \overset{\prime}{\mathbf{x}}_\gamma] - \hat{\rho}^G \overset{\prime}{\mathbf{x}}_G . \quad (2.67)$$

Remark: Relation (2.67) can be derived based on the material time derivative of $\rho^G \overset{\prime}{\mathbf{x}}_G$ and the mass balance of the overall gas phase:

$$(\rho^G \overset{\prime}{\mathbf{x}}_G)'_G = (\rho^G)'_G \overset{\prime}{\mathbf{x}}_G + \rho^G \overset{\prime\prime}{\mathbf{x}}_G \longrightarrow \rho^G \overset{\prime\prime}{\mathbf{x}}_G = (\rho^G \overset{\prime}{\mathbf{x}}_G)'_G + \rho^G \overset{\prime}{\mathbf{x}}_G \operatorname{div} \overset{\prime}{\mathbf{x}}_G - \hat{\rho}^G \overset{\prime}{\mathbf{x}}_G .$$

Furthermore, $(\rho^G \overset{\prime}{\mathbf{x}}_G)'_G$ can be computed via

$$\begin{aligned} (\rho^G \overset{\prime}{\mathbf{x}}_G)'_G &= \sum_{\gamma} (\rho^\gamma \overset{\prime}{\mathbf{x}}_\gamma)'_G = \sum_{\gamma} [(\rho^\gamma \overset{\prime}{\mathbf{x}}_\gamma)'_\gamma - \operatorname{grad}(\rho^\gamma \overset{\prime}{\mathbf{x}}_\gamma) \mathbf{d}_{\gamma G}] \\ &= \sum_{\gamma} [(\rho^\gamma \overset{\prime}{\mathbf{x}}_\gamma)'_\gamma - \operatorname{grad}(\rho^\gamma \overset{\prime}{\mathbf{x}}_G) \mathbf{d}_{\gamma G} - \operatorname{grad}(\rho^\gamma \mathbf{d}_{\gamma G}) \mathbf{d}_{\gamma G}] , \end{aligned}$$

where relation (2.25) and the definition of the diffusion velocity $\mathbf{d}_{\gamma G} = \overset{\prime}{\mathbf{x}}_\gamma - \overset{\prime}{\mathbf{x}}_G$ is used. This relation can be reformulated building the material time derivative of $(\rho^\gamma \overset{\prime}{\mathbf{x}}_\gamma)'_\gamma$, using the mass balance of the gas components and applying the product rule to $\operatorname{grad}(\rho^\gamma \mathbf{d}_{\gamma G}) \mathbf{d}_{\gamma G}$:

$$\begin{aligned} (\rho^G \overset{\prime}{\mathbf{x}}_G)'_G &= \sum_{\gamma} [\rho^\gamma \overset{\prime\prime}{\mathbf{x}}_\gamma - \operatorname{div}(\rho^\gamma \mathbf{d}_{\gamma G} \otimes \mathbf{d}_{\gamma G}) + \hat{\rho}^\gamma \overset{\prime}{\mathbf{x}}_\gamma - \\ &\quad - \rho^\gamma \overset{\prime}{\mathbf{x}}_\gamma \operatorname{div} \overset{\prime}{\mathbf{x}}_\gamma - \operatorname{grad}(\rho^\gamma \overset{\prime}{\mathbf{x}}_G) \mathbf{d}_{\gamma G} + \rho^\gamma \mathbf{d}_{\gamma G} \operatorname{div} \mathbf{d}_{\gamma G}] . \end{aligned}$$

Reformulating the fourth term within the brackets using $\overset{\prime}{\mathbf{x}}_\gamma = \overset{\prime}{\mathbf{x}}_G + \mathbf{d}_{\gamma G}$ results in

$$\begin{aligned} (\rho^G \overset{\prime}{\mathbf{x}}_G)'_G &= \sum_{\gamma} [\rho^\gamma \overset{\prime\prime}{\mathbf{x}}_\gamma - \operatorname{div}(\rho^\gamma \mathbf{d}_{\gamma G} \otimes \mathbf{d}_{\gamma G}) + \hat{\rho}^\gamma \overset{\prime}{\mathbf{x}}_\gamma] - \rho^G \overset{\prime}{\mathbf{x}}_G \operatorname{div} \overset{\prime}{\mathbf{x}}_G - \\ &\quad - \sum_{\gamma} [\operatorname{grad}(\rho^\gamma \overset{\prime}{\mathbf{x}}_G) \mathbf{d}_{\gamma G} + \rho^\gamma \overset{\prime}{\mathbf{x}}_G \operatorname{div} \mathbf{d}_{\gamma G}] - \operatorname{div} \overset{\prime}{\mathbf{x}}_G \sum_{\gamma} \rho^\gamma \mathbf{d}_{\gamma G} . \end{aligned}$$

Incorporating this relation and taking furthermore into account that

$$\sum_{\gamma} [\operatorname{grad}(\rho^\gamma \overset{\prime}{\mathbf{x}}_G) \mathbf{d}_{\gamma G} + \rho^\gamma \overset{\prime}{\mathbf{x}}_G \operatorname{div} \mathbf{d}_{\gamma G}] = \sum_{\gamma} \operatorname{div}(\rho^\gamma \overset{\prime}{\mathbf{x}}_G \otimes \mathbf{d}_{\gamma G}) = \operatorname{div}(\overset{\prime}{\mathbf{x}}_G \otimes \sum_{\gamma} \rho^\gamma \mathbf{d}_{\gamma G}) .$$

as well as

$$\sum_{\gamma} \rho^\gamma \mathbf{d}_{\gamma G} = \mathbf{0}$$

yields

$$\rho^G \overset{\prime\prime}{\mathbf{x}}_G = \sum_{\gamma} [\rho^\gamma \overset{\prime\prime}{\mathbf{x}}_\gamma - \operatorname{div}(\rho^\gamma \mathbf{d}_{\gamma G} \otimes \mathbf{d}_{\gamma G}) + \hat{\rho}^\gamma \overset{\prime}{\mathbf{x}}_\gamma] - \hat{\rho}^G \overset{\prime}{\mathbf{x}}_G .$$

□

Moment of momentum balances

Within the axiomatically introduced balance of moment of momentum, the temporal change of the moment of momentum $\mathbf{x} \times \rho \dot{\mathbf{x}}$ or $\mathbf{x} \times \rho^\alpha \dot{\mathbf{x}}_\alpha$, is balanced with the inner and outer moments acting on the body \mathcal{B} . Therefore, this balance relation reads for the mixture and the constituents

$$\boxed{\begin{aligned} \frac{d}{dt} \int_{\mathcal{B}} (\mathbf{x} \times \rho \dot{\mathbf{x}}) dv &= \int_{\partial \mathcal{B}} [(\mathbf{x} \times \mathbf{T}) \mathbf{n}] da + \int_{\mathcal{B}} (\mathbf{x} \times \rho \mathbf{b}) dv \quad \text{and} \\ \frac{d_\alpha}{dt} \int_{\mathcal{B}} (\mathbf{x} \times \rho^\alpha \dot{\mathbf{x}}_\alpha) dv &= \int_{\partial \mathcal{B}} [(\mathbf{x} \times \mathbf{T}^\alpha) \mathbf{n}] da + \int_{\mathcal{B}} (\mathbf{x} \times \rho^\alpha \mathbf{b}^\alpha) dv + \int_{\mathcal{B}} \hat{\mathbf{h}}^\alpha dv, \end{aligned}} \quad (2.68)$$

respectively, where the outer tensor product $\mathbf{x} \times \mathbf{T}$ is introduced, cf. Appendix A.1.6. By a comparison of these equations with the master balance relations (2.47)₂ and (2.49)₂, the respective quantities can be identified:

$$\begin{aligned} \text{overall medium } \varphi &: \begin{cases} \Psi = \mathbf{x} \times \rho \dot{\mathbf{x}}, & \Phi = \mathbf{x} \times \mathbf{T}, \\ \sigma = \mathbf{x} \times \rho \mathbf{b}, & \hat{\Psi} = \mathbf{0}, \end{cases} \\ \text{constituent } \varphi^\alpha &: \begin{cases} \Psi^\alpha = \mathbf{x} \times \rho^\alpha \dot{\mathbf{x}}_\alpha, & \Phi^\alpha = \mathbf{x} \times \mathbf{T}^\alpha, \\ \sigma^\alpha = \mathbf{x} \times \rho^\alpha \mathbf{b}^\alpha, & \hat{\Psi}^\alpha = \hat{\mathbf{h}}^\alpha. \end{cases} \end{aligned} \quad (2.69)$$

Therein, $\hat{\mathbf{h}}^\alpha$ describes the total production of moment of momentum. Proceeding from (2.48)₂ and considering (2.69)₁ as well as the local form of the global mass and the momentum balance, cf. (2.55) and (2.64), the local form of the moment of momentum relation of the overall aggregate yields

$$\boxed{\mathbf{0} = \mathbf{I} \times \mathbf{T} \quad \longrightarrow \quad \mathbf{T}^T = \mathbf{T},} \quad (2.70)$$

namely, the symmetry of the *Cauchy* stress tensor. Using the local form of the mass and momentum balances, cf. (2.56) and (2.65), the local form of the moment of momentum balance for a single constituent reads

$$\boxed{\mathbf{0} = \mathbf{I} \times \mathbf{T}^\alpha + \hat{\mathbf{m}}^\alpha \quad \longrightarrow \quad (\mathbf{T}^\alpha)^T = \mathbf{T}^\alpha + \hat{\mathbf{M}}^\alpha.} \quad (2.71)$$

Therein, the direct production of moment of momentum $\hat{\mathbf{m}}^\alpha = \hat{\mathbf{h}}^\alpha - \mathbf{x} \times (\hat{\mathbf{p}}^\alpha + \hat{\rho}^\alpha \dot{\mathbf{x}}_\alpha)$ corresponds to the coupling tensor $\hat{\mathbf{M}}^\alpha$, which represents the skew-symmetric part of the stress tensor. If standard (non-polar) materials with symmetric *Cauchy* stresses on the microscale are considered, it can be shown by a homogenization procedure that the macroscopic stresses must also be symmetric, cf. [46, 85]. Thus,

$$\mathbf{T}^\alpha = (\mathbf{T}^\alpha)^T \quad \longrightarrow \quad \hat{\mathbf{m}}^\alpha \equiv \mathbf{0}. \quad (2.72)$$

Remark: In the standard (non-polar) theory, the balance of moment of momentum yields the symmetry of the overall and partial *Cauchy* stress tensors and is no longer needed as an independent equation in the frame of the closure problem of continuum mechanics. Nevertheless, describing materials within a polar (*Cosserat*) theory, the balance of moment of momentum corresponds to the rotations of the particles, which are introduced in this context as additional degrees of freedom. For a further look on this topic, the interested reader is referred to *Ammann* [2], *Ehlers* [46], *Scholz* [117] as well as to the work of the research group of Diebels [35–38]. \square

2.2.3 Thermodynamical balance laws

Considering non-isothermal conditions in the continuum mechanical modeling of materials, the energy balance, also known as first fundamental law of continuum thermodynamics, is the conditional equation for the determination of the temperature of the multiphase body in the sense of the closure problem of continuum mechanics. On the other hand, the entropy inequality, also known as second fundamental law of continuum thermodynamics, is not required as a governing equation in a numerical scheme, but provides the basis for the development of thermodynamical consistent material laws.

Energy balances

The first fundamental law of continuum thermodynamics balances the temporal change of the sum of the internal and kinetic energy with the power resulting from the surface and body forces as well as with the heat influx and the heat supply:

$$\begin{aligned}
 \frac{d}{dt} \int_{\mathcal{B}} \rho \left[\varepsilon + \frac{1}{2} (\dot{\mathbf{x}} \cdot \dot{\mathbf{x}}) \right] dv &= \int_{\partial \mathcal{B}} [(\mathbf{T}^T \dot{\mathbf{x}} - \mathbf{q}) \cdot \mathbf{n}] da + \\
 &+ \int_{\mathcal{B}} [\dot{\mathbf{x}} \cdot (\rho \mathbf{b}) + \rho r] dv, \\
 \frac{d_\alpha}{dt} \int_{\mathcal{B}} \rho^\alpha \left[\varepsilon^\alpha + \frac{1}{2} (\dot{\mathbf{x}}_\alpha \cdot \dot{\mathbf{x}}_\alpha) \right] dv &= \int_{\partial \mathcal{B}} \{ [(\mathbf{T}^\alpha)^T \dot{\mathbf{x}}_\alpha - \mathbf{q}^\alpha] \cdot \mathbf{n} \} da + \\
 &+ \int_{\mathcal{B}} [\dot{\mathbf{x}}_\alpha \cdot (\rho^\alpha \mathbf{b}^\alpha) + \rho^\alpha r^\alpha] dv + \int_{\mathcal{B}} \hat{e}^\alpha dv.
 \end{aligned} \tag{2.73}$$

Therein, the specific internal energies of the overall medium and a single constituent are given by ε and ε^α , \mathbf{q} and \mathbf{q}^α are the respective heat influx vectors, r and r^α represent the heat supplies from the external distance and \hat{e}^α indicates the total energy production of the constituent φ^α . Furthermore, the quantities of the general master balance can be

identified:

$$\begin{aligned} \text{overall medium } \varphi & : \begin{cases} \Psi = \rho \varepsilon + \frac{1}{2} \dot{\mathbf{x}} \cdot (\rho \dot{\mathbf{x}}), & \boldsymbol{\phi} = \mathbf{T}^T \dot{\mathbf{x}} - \mathbf{q}, \\ \sigma = \dot{\mathbf{x}} \cdot (\rho \mathbf{b}) + \rho r, & \hat{\Psi} = \mathbf{0}, \end{cases} \\ \text{constituent } \varphi^\alpha & : \begin{cases} \Psi^\alpha = \rho^\alpha \varepsilon^\alpha + \frac{1}{2} \dot{\mathbf{x}}_\alpha \cdot (\rho^\alpha \dot{\mathbf{x}}_\alpha), & \boldsymbol{\phi}^\alpha = (\mathbf{T}^\alpha)^T \dot{\mathbf{x}}_\alpha - \mathbf{q}^\alpha, \\ \sigma^\alpha = \dot{\mathbf{x}}_\alpha \cdot (\rho^\alpha \mathbf{b}^\alpha) + \rho^\alpha r^\alpha, & \hat{\Psi}^\alpha = \hat{\varepsilon}^\alpha. \end{cases} \end{aligned} \quad (2.74)$$

Inserting (2.74) into the local form of the scalar-valued general master balance (2.48)₁ and using furthermore the lower balance relation of mass, momentum and moment of momentum, yields the local form of the energy balance of the overall medium,

$$\boxed{\rho \dot{\varepsilon} = \mathbf{T} \cdot \mathbf{L} - \operatorname{div} \mathbf{q} + \rho r,} \quad (2.75)$$

where $\mathbf{T} \cdot \mathbf{L}$ is the stress (internal mechanical) power of the overall aggregate. Analogously, the local form of the energy balance for the constituents results in

$$\boxed{\rho^\alpha (\varepsilon^\alpha)'_\alpha = \mathbf{T}^\alpha \cdot \mathbf{L}_\alpha - \operatorname{div} \mathbf{q}^\alpha + \rho^\alpha r^\alpha + \hat{\varepsilon}^\alpha.} \quad (2.76)$$

Therein, the direct energy production $\hat{\varepsilon}^\alpha = \hat{\varepsilon}^\alpha - \hat{\mathbf{p}}^\alpha \cdot \dot{\mathbf{x}}_\alpha - \hat{\rho}^\alpha (\varepsilon^\alpha + \frac{1}{2} \dot{\mathbf{x}}_\alpha \cdot \dot{\mathbf{x}}_\alpha)$ describes the heat exchange between the individual constituents of the porous material, cf. Ghadiani [77]. Furthermore, the relations between the quantities of the constituents and the whole medium read

$$\begin{aligned} \rho \varepsilon &= \sum_\alpha \rho^\alpha (\varepsilon^\alpha + \frac{1}{2} \mathbf{d}_\alpha \cdot \mathbf{d}_\alpha), & \rho r &= \sum_\alpha \rho^\alpha (r^\alpha + \mathbf{b}^\alpha \cdot \mathbf{d}_\alpha), \\ \mathbf{q} &= \sum_\alpha [\mathbf{q}^\alpha - (\mathbf{T}^\alpha)^T \mathbf{d}_\alpha + \rho^\alpha \varepsilon^\alpha \mathbf{d}_\alpha + \frac{1}{2} \rho^\alpha (\mathbf{d}_\alpha \cdot \mathbf{d}_\alpha) \mathbf{d}_\alpha], & 0 &= \sum_\alpha \hat{\varepsilon}^\alpha. \end{aligned} \quad (2.77)$$

Entropy balances

The entropy balance takes a special place in the frame of the balance relations in continuum mechanics. As mentioned above, this relation is not needed as governing equation in the sense of the closure problem in continuum mechanics but nevertheless, it is the most important equation for the development of thermodynamically consistent constitutive relations. The basic idea is that this second law of thermodynamics has to be fulfilled for any admissible thermomechanical process. Therefore, the evaluation of the entropy inequality results in certain restrictions, which have to be taken into account, if material laws for the individual constituents are formulated.

Proceeding from the continuum mechanical description of single-phasic materials, where the restriction is made that the entropy production cannot be negative, one found out in the sixties of the last century that the postulation of this constraint for every constituent

is too restrictive. For a historical overview of this topic, the interested reader is referred to *Ehlers* [40] or *Truesdell* [133]. Thus, the restriction of a non-negative entropy production is only postulated for the overall porous medium.

Concerning the entropy balance relation, it is axiomatically introduced that the temporal change of the entropies η and η^α is balanced with the entropy effluxes, the entropy supplies and the total entropy productions $\hat{\eta}$ and $\hat{\eta}^\alpha$:

$$\boxed{\begin{aligned} \frac{d}{dt} \int_{\mathcal{B}} \rho \eta \, dv &= - \int_{\partial \mathcal{B}} (\boldsymbol{\phi}_\eta \cdot \mathbf{n}) \, da + \int_{\mathcal{B}} \sigma_\eta \, dv + \int_{\mathcal{B}} \hat{\eta} \, dv, \\ \frac{d_\alpha}{dt} \int_{\mathcal{B}} \rho^\alpha \eta^\alpha \, dv &= - \int_{\partial \mathcal{B}} \left(\frac{1}{\theta^\alpha} \mathbf{q}^\alpha \cdot \mathbf{n} \right) \, da + \int_{\mathcal{B}} \frac{1}{\theta^\alpha} \rho^\alpha r^\alpha \, dv + \int_{\mathcal{B}} \hat{\eta}^\alpha \, dv. \end{aligned}} \quad (2.78)$$

Therein, the entropy efflux $\boldsymbol{\phi}_\eta^\alpha = \mathbf{q}^\alpha / \theta^\alpha$ as well as the entropy supply $\sigma_\eta^\alpha = \rho^\alpha r^\alpha / \theta^\alpha$ of the constituent φ^α are introduced a priori, whereas the constraint has to be fulfilled that the total entropy production of the overall medium may not be negative:

$$\boxed{\int_{\mathcal{B}} \hat{\eta} \, dv \geq 0.} \quad (2.79)$$

Comparing these relations with the master balance relation (2.50)₁, the respective quantities for the constituent φ^α can be identified, while the quantities of the mixture result from a summation over all constituents of the mixture:

$$\begin{aligned} \text{overall medium } \varphi : & \begin{cases} \Psi = \rho \eta = \sum_{\alpha} \rho^\alpha \eta^\alpha, \quad \boldsymbol{\phi} = -\boldsymbol{\phi}_\eta^\alpha = -\sum_{\alpha} \left(\frac{1}{\theta} \mathbf{q}^\alpha + \rho^\alpha \eta^\alpha \mathbf{d}_\alpha \right), \\ \sigma = \sigma_\eta = \sum_{\alpha} \frac{1}{\theta} \rho^\alpha r^\alpha, \quad \hat{\Psi} = \hat{\eta} = \sum_{\alpha} \eta^\alpha \geq 0, \end{cases} \\ \text{constituent } \varphi^\alpha : & \begin{cases} \Psi^\alpha = \rho^\alpha \eta^\alpha, \quad \boldsymbol{\phi}^\alpha = -\boldsymbol{\phi}_\eta^\alpha = -\frac{1}{\theta^\alpha} \mathbf{q}^\alpha, \\ \sigma^\alpha = \frac{1}{\theta^\alpha} \rho^\alpha r^\alpha, \quad \hat{\Psi}^\alpha = \hat{\eta}^\alpha. \end{cases} \end{aligned} \quad (2.80)$$

Considering the local mass balance (2.56), the following form of the local entropy balance relation for the constituent φ^α is obtained

$$\boxed{\rho^\alpha (\eta^\alpha)'_\alpha = \operatorname{div} \left(-\frac{1}{\theta^\alpha} \mathbf{q}^\alpha \right) + \frac{1}{\theta^\alpha} \rho^\alpha r^\alpha + \hat{\zeta}^\alpha,} \quad (2.81)$$

where $\hat{\zeta}^\alpha = \hat{\eta}^\alpha - \hat{\rho}^\alpha \eta^\alpha$ is the direct entropy production. The local form of the entropy inequality of the overall medium is found by a summation over the local entropy balances

(2.81) of all constituents φ^α and by incorporating the constraint (2.79) for the total entropy production of the mixture:

$$\hat{\eta} = \sum_{\alpha} \hat{\eta}^{\alpha} = \sum_{\alpha} [\rho^{\alpha}(\eta^{\alpha})'_{\alpha} + \hat{\rho}^{\alpha}\eta^{\alpha} + \operatorname{div}(\frac{1}{\theta^{\alpha}}\mathbf{q}^{\alpha}) - \frac{1}{\theta^{\alpha}}\rho^{\alpha}r^{\alpha}] \geq 0. \quad (2.82)$$

The caloric primary variable of the internal energy ε^α is the entropy η^α . As the entropy is very difficult to measure, an additional energy, the so-called free *Helmholtz* energy ψ^α is introduced, whereas the caloric primary variable is the temperature θ^α , which is a much more observable variable as the entropy. This free *Helmholtz* energy can be introduced via a so-called *Legendre*³ transformation between the conjugated variables entropy η^α and temperature θ^α :

$$\psi^{\alpha} := \varepsilon^{\alpha} - \theta^{\alpha}\eta^{\alpha}. \quad (2.83)$$

Hence, using the definition of the free *Helmholtz* energy (2.83) and the local energy balance (2.76), the local form of the entropy inequality of the overall medium can be rewritten in the following way:

$$\sum_{\alpha} \frac{1}{\theta^{\alpha}} \{ \mathbf{T}^{\alpha} \cdot \mathbf{L}_{\alpha} - \rho^{\alpha} [(\psi^{\alpha})'_{\alpha} + (\theta^{\alpha})'_{\alpha} \eta^{\alpha}] - \hat{\mathbf{p}}^{\alpha} \cdot \dot{\mathbf{x}}_{\alpha} - \hat{\rho}^{\alpha} [\psi^{\alpha} + \frac{1}{2} \dot{\mathbf{x}}_{\alpha} \cdot \dot{\mathbf{x}}_{\alpha}] - \frac{1}{\theta^{\alpha}} \mathbf{q}^{\alpha} \cdot \operatorname{grad} \theta^{\alpha} + \hat{e}^{\alpha} \} \geq 0. \quad (2.84)$$

The evaluation of the above equation gives certain restrictions for the development of so-called constitutive relations. Based on these relations, the general closure problem of continuum mechanics can be focused to describe the respective material under study.

$$\begin{aligned} \text{}^3 \quad d\varepsilon^{\alpha} &= \frac{\partial \varepsilon^{\alpha}}{\partial(\cdot)} d(\cdot) + \underbrace{\frac{\partial \varepsilon^{\alpha}}{\partial \eta^{\alpha}}}_{\theta^{\alpha}} d\eta^{\alpha} = \frac{\partial \varepsilon^{\alpha}}{\partial(\cdot)} d(\cdot) + \underbrace{\theta^{\alpha} d\eta^{\alpha}}_{d(\theta^{\alpha}\eta^{\alpha}) - \eta^{\alpha} d\theta^{\alpha}} \\ &\longrightarrow d(\underbrace{\varepsilon^{\alpha} - \theta^{\alpha}\eta^{\alpha}}_{\psi^{\alpha}}) = \frac{\partial \varepsilon^{\alpha}}{\partial(\cdot)} d(\cdot) - \eta^{\alpha} d\theta^{\alpha} \end{aligned}$$

Chapter 3: Constitutive settings

Within a continuum mechanical modeling of porous materials, each individual constituent is governed by so-called primary variables. Particularly, as introduced in the previous chapter, the kinematical primary variable of the solid skeleton is the displacement vector, whereas the kinematical primary variable of the pore fluids is the respective seepage velocity. These primary variables are the unknowns in a system of equations composed by the respective balance relations discussed in the previous chapter. Nevertheless, there exists a certain number of unknown quantities in these governing equations, e. g., the *Cauchy* stress tensors or the momentum production terms. To close this resulting system of equations, relations between these quantities and the primary variables have to be formulated: *the so-called constitutive relations*. By means of these constitutive relations and the material parameters therein, the general balance relations can be adapted to describe the special material behavior of the considered constituents and, therefore, of the overall porous material.

In general, a porous material consists of a single solid constituent and one or more fluid constituents, whereas the solid skeleton can behave like an elastic, viscoelastic, elastoplastic or elasto-viscoplastic material and the pore fluids are governed by a viscous material behavior. Commonly, the solid skeleton and the pore liquids can be described in a mechanical sense as materially incompressible constituents, i. e., within a non-isothermal approach, their effective densities are only functions of the respective temperatures. Each of these materially incompressible constituents build a single phase with respective volume fractions. On the other hand, the materially compressible fluid constituents build together one single gas phase and are characterized, therefore, by the volume fraction of this overall gas phase. Furthermore, mass interactions between the individual constituents can appear, e. g., during fluidization, i. e., mass interactions between the solid skeleton and a pore fluid, or during evaporation or condensation, i. e., mass interactions between liquid and gaseous pore water.

Within this chapter, constitutive relations are formulated to close the system of equations resulting from a general continuum mechanical model for the description of a porous material, which consists of a solid skeleton and an arbitrary number of materially incompressible and compressible fluid constituents. Therefore, in Section 3.1, the entropy inequality is evaluated for the most general case to find restrictions for constitutive relations such that the entropy inequality is ensured for any possible thermodynamical process. Thereby, in contrast to the formulation of initial boundary-value problems, the total states of motion and temperature are given fields. In Section 3.2, constitutive relations for the fluid constituents are formulated, whereas, in Section 3.3, the solid skeleton is discussed in the frame of an elasto-viscoplastic material behavior.

3.1 Evaluation of the entropy inequality

In this section, restrictions for the development of constitutive relations are derived based on an evaluation of the entropy inequality. Therefore, in Section 3.1.1, the basic assumptions and the resulting system of equations of the underlying model are presented. In Section 3.1.2, the saturation condition (2.4) and the effective-stress principle are extended towards the description of a general porous material. The set of independent constitutive variables is presented in Section 3.1.3, whereas in Section 3.1.4 the restrictions are specified. The interested reader is referred to the works of *Coleman & Noll* [30] or *Truesdell* [134, 135] for further informations on the evaluation of the entropy inequality and the fundamentals of constitutive modeling.

3.1.1 Preliminaries

Under non-isothermal conditions, each non-polar constituent is generally governed by the balance relations of mass (2.56), momentum (2.65) and energy (2.76):

$$\begin{aligned} (\rho^\alpha)'_\alpha + \rho^\alpha \operatorname{div} \dot{\mathbf{x}}_\alpha &= \hat{\rho}^\alpha, \\ \rho^\alpha \ddot{\mathbf{x}}_\alpha &= \operatorname{div} \mathbf{T}^\alpha + \rho^\alpha \mathbf{b}^\alpha + \hat{\mathbf{p}}^\alpha, \\ \rho^\alpha (\varepsilon^\alpha)'_\alpha &= \mathbf{T}^\alpha \cdot \mathbf{L}_\alpha - \operatorname{div} \mathbf{q}^\alpha + \rho^\alpha r^\alpha + \hat{\varepsilon}^\alpha. \end{aligned} \quad (3.1)$$

Furthermore, the saturation condition (2.4) as well as the constraints for the respective production terms, i. e., (2.61)₃, (2.66)₄ and (2.77)₄, have to be fulfilled:

$$\begin{aligned} 1 &= \sum_\alpha n^\alpha, \\ 0 &= \sum_\alpha \hat{\rho}^\alpha, \\ \mathbf{0} &= \sum_\alpha \hat{\mathbf{s}}^\alpha = \sum_\alpha (\hat{\mathbf{p}}^\alpha + \hat{\rho}^\alpha \dot{\mathbf{x}}_\alpha), \\ 0 &= \sum_\alpha \hat{\varepsilon}^\alpha = \sum_\alpha [\hat{\varepsilon}^\alpha + \hat{\mathbf{p}}^\alpha \cdot \dot{\mathbf{x}}_\alpha + \hat{\rho}^\alpha (\varepsilon^\alpha + \frac{1}{2} \dot{\mathbf{x}}_\alpha \cdot \dot{\mathbf{x}}_\alpha)]. \end{aligned} \quad (3.2)$$

Additionally, the internal energy ε^α is substituted by the free *Helmholtz* energy ψ^α , cf. (2.83), introduced via

$$\psi^\alpha = \varepsilon^\alpha - \theta^\alpha \eta^\alpha. \quad (3.3)$$

In contrast to the formulation of initial boundary-value problems, the initial conditions,

$$\mathbf{x} = \boldsymbol{\chi}_\alpha(\mathcal{P}^\alpha, t_0), \quad \rho^{\alpha R}(t_0) \quad \text{and} \quad n^\alpha(t_0), \quad (3.4)$$

as well as the total state of motion and temperature,

$$\mathbf{x} = \chi_\alpha(\mathbf{X}_\alpha, t) \longrightarrow \begin{cases} \mathbf{F}_\alpha & \longrightarrow \det \mathbf{F}_\alpha, \\ \dot{\mathbf{x}}_\alpha & \longrightarrow \begin{cases} \operatorname{div} \dot{\mathbf{x}}_\alpha, \\ \mathbf{L}_\alpha, \end{cases} \\ \ddot{\mathbf{x}}_\alpha & \end{cases} \quad (3.5)$$

$$\theta^\alpha = \theta^\alpha(\mathbf{x}, t) \longrightarrow \begin{cases} \operatorname{grad} \theta^\alpha, \\ (\theta^\alpha)'_\alpha, \end{cases}$$

are assumed as given fields. Therefore, constitutive relations have to be formulated for all quantities, which cannot be computed directly from the above mentioned balance relations under consideration of the given initial conditions and the total state of motion and temperature.

In the most general case, these relations can depend on the full fundamental set of constitutive variables, which are given following *Ehlers* [40] via

$$\mathcal{V}(\mathbf{x}, t) := \{\theta^\alpha, \operatorname{grad} \theta^\alpha, n^\alpha, \operatorname{grad} n^\alpha, \rho^{\alpha R}, \operatorname{grad} \rho^{\alpha R}, \mathbf{F}_\alpha, \operatorname{Grad}_\alpha \mathbf{F}_\alpha, \dot{\mathbf{x}}_\alpha, \operatorname{Grad}_\alpha \dot{\mathbf{x}}_\alpha, \mathbf{X}_\alpha\}. \quad (3.6)$$

Therewith, the thermal state is fully described by the temperatures θ^α and the respective gradients, which govern the heat transport process. Due to the fact that in contrast to non-porous, single-phasic materials mass production can occur, the partial density $\rho^\alpha = n^\alpha \rho^{\alpha R}$ cannot be determined through an integration of the mass balance. Thus, the volume fraction n^α and the material density $\rho^{\alpha R}$ as well as their respective gradients have to be considered as independent fields to describe the deformation of an arbitrary constituent (solid or fluid). Furthermore, as porous materials have to be regarded as materials of second order, cf. [40], the first (material) deformation gradient \mathbf{F}_α as well as the second deformation gradient $\operatorname{Grad}_\alpha \mathbf{F}_\alpha$ have to be considered in (3.6) as well. Viscosity effects are described via $\dot{\mathbf{x}}_\alpha$ and $\operatorname{Grad}_\alpha \dot{\mathbf{x}}_\alpha$, whereas the position in the reference configuration \mathbf{X}_α can be used to incorporate inhomogeneities of the individual constituents. For a closer look on this topic, the interested reader is referred to *Ehlers* [40, 46].

Based on the above given fundamental set of constitutive variables, constitutive relations are required for

$$\{\psi^\alpha, \eta^\alpha, \mathbf{q}^\alpha, \hat{\varepsilon}^\alpha, \mathbf{T}^\alpha, \hat{\mathbf{p}}^\alpha, \hat{\rho}^\alpha\} = \tilde{\mathcal{R}}[\mathcal{V}(\mathbf{x}, t)], \quad (3.7)$$

whereby $\tilde{\mathcal{R}}$ indicates the set of response functions.

In the present contribution, the solid skeleton, the soil matrix, is considered as a materially incompressible constituent, whereby the physical property of material incompressibility only characterizes the mechanical behavior, i. e., the single soil grains undergo thermal expansion in dependency of the respective temperature θ^S of the solid skeleton:

$$\rho^{SR} := \rho^{SR}(\theta^S). \quad (3.8)$$

Furthermore, the solid phase is governed by an elasto-viscoplastic material behavior. No mass interactions with other constituents are assumed. The pore liquids are regarded as viscous fluids, which are, like the solid phase, materially incompressible in the sense that the material incompressibility only belongs to the mechanical behavior, whereas the material density is a function of the respective temperature θ^ξ :

$$\rho^{\xi R} := \rho^{\xi R}(\theta^\xi). \quad (3.9)$$

The pore liquids build immiscible phases and are, therefore, distinguished with individual volume fractions and different temperatures. In contrast, the viscous, materially compressible fluid constituents continuously form the overall pore gas phase, which is considered as a mixture of ideal gases. Thus, it is assumed that all compressible fluid constituents are governed by the volume fraction n^G of the overall gas phase. Furthermore, it is assumed that the compressible constituents are governed by the same temperature θ^G .

3.1.2 Saturation constraint and effective stress principle

The following evaluation of the entropy inequality is based on the formulation given via (2.84). Multiplying this equation by the temperature θ^S of the solid skeleton, including the constraints for the mass production $\hat{\rho}^\alpha$, cf. (2.61)₃, under consideration of $\hat{\rho}^S = 0$ and taking furthermore into account the total production of linear momentum $\hat{\mathbf{s}}^\alpha$ (2.66)₄ and internal energy \hat{e}^α (2.77)₄ as well as the definition of the seepage velocity \mathbf{w}_ζ , cf. (2.26)₂, yields

$$\begin{aligned} & \mathbf{T}^S \cdot \mathbf{L}_S - \rho^S [(\psi^S)'_S + (\theta^S)'_S \eta^S] + \\ & + \sum_\zeta \frac{\theta^S}{\theta^\zeta} \{ \mathbf{T}^\zeta \cdot \mathbf{L}_\zeta - \rho^\zeta [(\psi^\zeta)'_\zeta + (\theta^\zeta)'_\zeta \eta^\zeta] \} + \\ & + \sum_\zeta \hat{\rho}^\zeta [\eta^\zeta (\theta^S - \theta^\zeta) - \psi^\zeta + \dot{\mathbf{x}}_\zeta \cdot \dot{\mathbf{x}}_S - \frac{1}{2} \dot{\mathbf{x}}_\zeta \cdot \dot{\mathbf{x}}_\zeta] - \\ & - \sum_\zeta \hat{\mathbf{p}}^\zeta \cdot \mathbf{w}_\zeta + \sum_\zeta \hat{e}^\zeta \left(\frac{\theta^S}{\theta^\zeta} - 1 \right) - \\ & - \frac{1}{\theta^S} \mathbf{q}^S \cdot \text{grad } \theta^S - \sum_\zeta \frac{\theta^S}{\theta^\zeta} \frac{1}{\theta^\zeta} \mathbf{q}^\zeta \cdot \text{grad } \theta^\zeta \geq 0. \end{aligned} \quad (3.10)$$

As further constraint, the saturation condition (2.4), has to be fulfilled as well. Thus, the time derivative of the saturation constraint with respect to the solid skeleton,

$$n^S + \sum_\xi n^\xi + n^G = 1 \quad \longrightarrow \quad \boxed{(n^S)'_S + \sum_\xi (n^\xi)'_S + (n^G)'_S = 0}, \quad (3.11)$$

is added to (3.10) after a multiplication by the *Lagrangean* multiplier \mathcal{P} . Concerning the materially incompressible constituents, the mass balance (2.56) can be solved for $(n^\alpha)'_\alpha$, which results under the assumptions of $\hat{\rho}^{SR} = 0$, $\rho^{SR}(\theta^S)$ and $\rho^{\xi R}(\theta^\xi)$ as well as the definition (2.24) of the material time derivative in

$$\begin{aligned} (n^S)'_S &= -\frac{n^S}{\rho^{SR}}(\rho^{SR})'_S - n^S \operatorname{div} \dot{\mathbf{x}}_S \quad \text{and} \\ (n^\xi)'_S &= (n^\xi)'_\xi - \operatorname{grad} n^\xi \cdot \mathbf{w}_\xi \\ &= -\frac{n^\xi}{\rho^{\xi R}}(\rho^{\xi R})'_\xi - n^\xi \operatorname{div} \dot{\mathbf{x}}_\xi + \frac{\hat{\rho}^\xi}{\rho^{\xi R}} - \operatorname{grad} n^\xi \cdot \mathbf{w}_\xi. \end{aligned} \quad (3.12)$$

Within a mixture of ideal gases, the ratio between the partial pressure p_G^γ of a gaseous constituent and the overall effective gas pressure p^{GR} is governed by the molar fraction x_{Gm}^γ and not by the mass concentration c_G^γ , cf. *Baehr* [5]. Therefore, the mass balance (2.56) of the gaseous constituents is reduced at this point by taking into account that the molar mass M_m^γ is a material constant for each φ^α :

$$(n^G c_{Gm}^\gamma)'_\gamma + n^G c_{Gm}^\gamma \operatorname{div} \dot{\mathbf{x}}_\gamma = \frac{\hat{\rho}^\gamma}{M_m^\gamma}. \quad (3.13)$$

Building the sum of (3.13) over all gaseous constituents and using furthermore (2.14) and (2.24), (3.13) can be solved for $(n^G)'_S$:

$$\begin{aligned} (n^G)'_S &= -\frac{n^G}{c_{Gm}} \sum_\gamma (c_{Gm}^\gamma)'_\gamma - n^G \sum_\gamma x_{Gm}^\gamma \operatorname{div} \dot{\mathbf{x}}_\gamma + \frac{1}{c_{Gm}} \sum_\gamma \frac{\hat{\rho}^\gamma}{M_m^\gamma} - \\ &\quad - \operatorname{grad} n^G \cdot \mathbf{w}_G - \operatorname{grad} n^G \cdot \sum_\gamma x_{Gm}^\gamma \mathbf{d}_{\gamma G}. \end{aligned} \quad (3.14)$$

It is obvious that without dividing the respective mass balances by the molar masses M_m^γ , the second term on the right-hand side of (3.14) is governed by the mass concentration c_G^γ and not by the molar fraction x_{Gm}^γ . This will yield to a wrong result concerning the ratio between the partial pressure p_G^γ of a gaseous constituent and the overall effective gas pressure p^{GR} as can be seen later.

Using the relations (3.12) and (3.14) as well as the assumption that the material densities of the materially incompressible constituents are only functions of the respective temperatures, cf. (3.8) and (3.9), the saturation condition (3.11) yields

$$\begin{aligned} &n^S \mathbf{L}_S \cdot \mathbf{I} + \sum_\xi n^\xi \mathbf{L}_\xi \cdot \mathbf{I} + \sum_\gamma n^G x_{Gm}^\gamma \mathbf{L}_\gamma \cdot \mathbf{I} + \sum_\gamma \frac{n^G}{c_{Gm}} (c_{Gm}^\gamma)'_\gamma + \\ &+ \sum_\beta \operatorname{grad} n^\beta \cdot \mathbf{w}_\beta + \sum_\gamma \operatorname{grad} n^G \cdot x_{Gm}^\gamma \mathbf{d}_{\gamma G} + \\ &+ \frac{n^S}{\rho^{SR}} \frac{d\rho^{SR}}{d\theta^S} (\theta^S)'_S + \sum_\xi \frac{n^\xi}{\rho^{\xi R}} \frac{d\rho^{\xi R}}{d\theta^\xi} (\theta^\xi)'_\xi - \sum_\xi \frac{\hat{\rho}^\xi}{\rho^{\xi R}} - \sum_\gamma \frac{\hat{\rho}^\gamma}{c_{Gm} M_m^\gamma} = 0, \end{aligned} \quad (3.15)$$

where the definition of the spatial velocity gradient, cf. (2.37), is additionally used.

Furthermore, using (2.10) and (2.14), the terms, which consider the time derivative of the molar concentration c_{Gm}^γ as well as the mass production of the gaseous constituents, can be written as

$$\begin{aligned} \sum_{\gamma} \frac{n^G}{c_{Gm}} (c_{Gm}^\gamma)'_{\gamma} &= \sum_{\gamma} \frac{n^G}{c_{Gm}} (c_{Gm}^\gamma)'_{\gamma} \frac{M_m^\gamma (\rho_G^\gamma)^2}{M_m^\gamma (\rho_G^\gamma)^2} = \sum_{\gamma} \rho^\gamma \frac{x_{Gm}^\gamma}{(\rho_G^\gamma)^2} (\rho_G^\gamma)'_{\gamma}, \\ \sum_{\gamma} \frac{\hat{\rho}^\gamma}{c_{Gm} M_m^\gamma} &= \sum_{\gamma} \hat{\rho}^\gamma \frac{x_{Gm}^\gamma}{c_{Gm} M_m^\gamma} = \sum_{\gamma} x_{Gm}^\gamma \frac{\hat{\rho}^\gamma}{\rho_G^\gamma}. \end{aligned} \quad (3.16)$$

Regarding the interaction of a materially compressible gas component with the other constituents of the overall aggregate, the direct momentum production can be additively split into an external part $\hat{\mathbf{p}}_{\text{ext}}^\gamma$ describing the interaction with the other phases, i. e., the solid and the liquid phases, and an internal part $\hat{\mathbf{p}}_{\text{int}}^\gamma$, which regard the interaction with the other gas components:

$$\hat{\mathbf{p}}^\gamma = \hat{\mathbf{p}}_{\text{ext}}^\gamma + \hat{\mathbf{p}}_{\text{int}}^\gamma. \quad (3.17)$$

Furthermore, the total momentum production $\hat{\mathbf{s}}^G$ of the gas phase is given via the sum of the total momentum productions $\hat{\mathbf{s}}^\gamma$ of the gas components, cf. (2.66), where $\hat{\mathbf{s}}^\gamma$ can also be additively split into an internal and external part:

$$\begin{aligned} \hat{\mathbf{s}}^G &= \sum_{\gamma} \hat{\mathbf{s}}^\gamma = \sum_{\gamma} \hat{\mathbf{s}}_{\text{int}}^\gamma + \sum_{\gamma} \hat{\mathbf{s}}_{\text{ext}}^\gamma, \\ \hat{\mathbf{p}}^G + \hat{\rho}^G \dot{\mathbf{x}}_G &= \sum_{\gamma} (\hat{\mathbf{p}}^\gamma + \hat{\rho}^\gamma \dot{\mathbf{x}}_\gamma) = \sum_{\gamma} (\hat{\mathbf{p}}_{\text{int}}^\gamma + \hat{\rho}_{\text{int}}^\gamma \dot{\mathbf{x}}_\gamma) + \sum_{\gamma} (\hat{\mathbf{p}}_{\text{ext}}^\gamma + \hat{\rho}_{\text{ext}}^\gamma \dot{\mathbf{x}}_\gamma). \end{aligned} \quad (3.18)$$

Looking at the quantities defined above, the sum of $\hat{\mathbf{s}}_{\text{int}}^\gamma$ has to vanish, whereas the sum of $\hat{\mathbf{s}}_{\text{ext}}^\gamma$ results in the total momentum production $\hat{\mathbf{s}}^G$ of the overall gas phase:

$$\left. \begin{aligned} \sum_{\gamma} \hat{\mathbf{s}}_{\text{int}}^\gamma &= \mathbf{0}, \\ \sum_{\gamma} \hat{\mathbf{s}}_{\text{ext}}^\gamma &= \hat{\mathbf{s}}^G \end{aligned} \right\} \longrightarrow \left\{ \begin{aligned} \sum_{\gamma} \hat{\mathbf{p}}_{\text{int}}^\gamma &= - \sum_{\gamma} \hat{\rho}_{\text{int}}^\gamma \dot{\mathbf{x}}_\gamma, \\ \sum_{\gamma} \hat{\mathbf{p}}_{\text{ext}}^\gamma &= \hat{\mathbf{p}}^G + \hat{\rho}^G \dot{\mathbf{x}}_G - \sum_{\gamma} \hat{\rho}_{\text{ext}}^\gamma \dot{\mathbf{x}}_\gamma. \end{aligned} \right. \quad (3.19)$$

Within the presented continuum mechanical model, it is assumed that there are no mass interactions between the individual gas components, i. e., $\hat{\rho}_{\text{int}}^\gamma = 0$ and $\hat{\rho}^G = \sum_{\gamma} \hat{\rho}_{\text{ext}}^\gamma$. Thus,

$$\sum_{\gamma} \hat{\mathbf{p}}_{\text{int}}^\gamma = \mathbf{0} \quad \text{and} \quad \sum_{\gamma} \hat{\mathbf{p}}_{\text{ext}}^\gamma = \hat{\mathbf{p}}^G - \sum_{\gamma} \hat{\rho}_{\text{ext}}^\gamma \mathbf{d}_{\gamma G}. \quad (3.20)$$

Furthermore, the sum of the scalar products between the momentum production $\hat{\mathbf{p}}^\gamma$ and the seepage velocity \mathbf{w}_γ of the gas components can be reformulated using the definition

of the seepage velocity \mathbf{w}_G of the overall gas phase and the diffusion velocity $\mathbf{d}_{\gamma G}$ of the gas components within the overall gas phase:

$$\sum_{\gamma} \hat{\mathbf{p}}^{\gamma} \cdot \mathbf{w}_{\gamma} = \sum_{\gamma} \hat{\mathbf{p}}^{\gamma} \cdot (\mathbf{w}_G + \mathbf{d}_{\gamma G}) = (\hat{\mathbf{p}}^G - \sum_{\gamma} \hat{\rho}_{\text{ext}}^{\gamma} \mathbf{d}_{\gamma G}) \cdot \mathbf{w}_G + \sum_{\gamma} \hat{\mathbf{p}}^{\gamma} \cdot \mathbf{d}_{\gamma G}. \quad (3.21)$$

Therefore, adding the saturation constraint (3.15) after multiplication by the *Lagrangean* multiplier \mathcal{P} to relation (3.10) and taking furthermore into account the above given relations concerning the momentum production terms of the gas components, the entropy inequality yields

$$\begin{aligned} & \underbrace{(\mathbf{T}^S + \mathcal{P} n^S \mathbf{I}) \cdot \mathbf{L}_S}_{\mathbf{T}_E^S} - \rho^S (\psi^S)'_S - \underbrace{\rho^S \left(\eta^S - \mathcal{P} \frac{1}{(\rho^{SR})^2} \frac{d\rho^{SR}}{d\theta^S} \right)}_{\eta_E^S} (\theta^S)'_S + \\ & + \sum_{\xi} \underbrace{\left(\frac{\theta^S}{\theta^{\xi}} \mathbf{T}^{\xi} + \mathcal{P} n^{\xi} \mathbf{I} \right) \cdot \mathbf{L}_{\xi}}_{\mathbf{T}_E^{\xi}} + \sum_{\gamma} \underbrace{\left(\frac{\theta^S}{\theta^G} \mathbf{T}^{\gamma} + x_{Gm}^{\gamma} \mathcal{P} n^G \mathbf{I} \right) \cdot \mathbf{L}_{\gamma}}_{\mathbf{T}_E^{\gamma}} - \\ & - \sum_{\zeta} \frac{\theta^S}{\theta^{\zeta}} \rho^{\zeta} (\psi^{\zeta})'_{\zeta} - \sum_{\xi} \rho^{\xi} \underbrace{\left(\frac{\theta^S}{\theta^{\xi}} \eta^{\xi} - \mathcal{P} \frac{1}{(\rho^{\xi R})^2} \frac{d\rho^{\xi R}}{d\theta^{\xi}} \right)}_{\eta_E^{\xi}} (\theta^{\xi})'_{\xi} - \\ & - \sum_{\gamma} \frac{\theta^S}{\theta^G} \rho^{\gamma} \eta^{\gamma} (\theta^{\gamma})'_{\gamma} + \sum_{\gamma} \rho^{\gamma} \mathcal{P} \frac{x_{Gm}^{\gamma}}{(\rho_G^{\gamma})^2} (\rho_G^{\gamma})'_{\gamma} + \\ & + \sum_{\xi} \frac{\hat{\rho}^{\xi}}{\rho^{\xi R}} \underbrace{\left\{ \rho^{\xi R} [\eta^{\xi} (\theta^S - \theta^{\xi}) - \psi^{\xi} + \dot{\mathbf{x}}_{\xi} \cdot \dot{\mathbf{x}}_S - \frac{1}{2} \dot{\mathbf{x}}_{\xi} \cdot \dot{\mathbf{x}}_{\xi}] - \mathcal{P} \right\}}_{\hat{\rho}_E^{\xi}} + \quad (3.22) \\ & + \sum_{\gamma} \frac{\hat{\rho}_{\text{ext}}^{\gamma}}{\rho_G^{\gamma}} \underbrace{\left\{ \rho_G^{\gamma} [\eta^{\gamma} (\theta^S - \theta^G) - \psi^{\gamma} + \dot{\mathbf{x}}_{\gamma} \cdot \dot{\mathbf{x}}_S - \frac{1}{2} \dot{\mathbf{x}}_{\gamma} \cdot \dot{\mathbf{x}}_{\gamma}] - x_{Gm}^{\gamma} \mathcal{P} \right\}}_{\hat{\rho}_E^{\gamma}} - \\ & - \sum_{\xi} \underbrace{(\hat{\mathbf{p}}^{\xi} - \mathcal{P} \text{grad } n^{\xi}) \cdot \mathbf{w}_{\xi}}_{\hat{\mathbf{p}}_E^{\xi}} - \underbrace{(\hat{\mathbf{p}}^G - \sum_{\gamma} \hat{\rho}_{\text{ext}}^{\gamma} \mathbf{d}_{\gamma G} - \mathcal{P} \text{grad } n^G) \cdot \mathbf{w}_G}_{\hat{\mathbf{p}}_E^G} - \\ & - \sum_{\gamma} \underbrace{(\hat{\mathbf{p}}_{\text{ext}}^{\gamma} - x_{Gm}^{\gamma} \mathcal{P} \text{grad } n^G + \hat{\mathbf{p}}_{\text{int}}^{\gamma}) \cdot \mathbf{d}_{\gamma G}}_{\hat{\mathbf{p}}_{\text{ext}E}^{\gamma}} + \sum_{\zeta} \hat{\varepsilon}^{\zeta} \left(\frac{\theta^S}{\theta^{\zeta}} - 1 \right) - \\ & - \frac{1}{\theta^S} \mathbf{q}^S \cdot \text{grad } \theta^S - \sum_{\zeta} \frac{\theta^S}{\theta^{\zeta}} \frac{1}{\theta^{\zeta}} \mathbf{q}^{\zeta} \cdot \text{grad } \theta^{\zeta} \geq 0. \end{aligned}$$

Therein, so-called extra terms $(\cdot)_E$ are introduced. Using these definitions, the entropy

inequality can be written in the following way:

$$\begin{aligned}
& \mathbf{T}_E^S \cdot \mathbf{L}_S - \rho^S (\psi^S)'_S - \rho^S \eta_E^S (\theta^S)'_S + \sum_{\xi} \mathbf{T}_E^{\xi} \cdot \mathbf{L}_{\xi} + \sum_{\gamma} \mathbf{T}_E^{\gamma} \cdot \mathbf{L}_{\gamma} - \\
& - \sum_{\zeta} \frac{\theta^S}{\theta^{\zeta}} \rho^{\zeta} (\psi^{\zeta})'_{\zeta} - \sum_{\xi} \rho^{\xi} \eta_E^{\xi} (\theta^{\xi})'_{\xi} - \sum_{\gamma} \frac{\theta^S}{\theta^G} \rho^{\gamma} \eta^{\gamma} (\theta^G)'_{\gamma} + \\
& + \sum_{\gamma} \rho^{\gamma} \mathcal{P} \frac{x_{Gm}^{\gamma}}{(\rho_G^{\gamma})^2} (\rho_G^{\gamma})'_{\gamma} + \sum_{\xi} \frac{\hat{\rho}^{\xi}}{\rho^{\xi R}} \hat{\rho}_E^{\xi} + \sum_{\gamma} \frac{\hat{\rho}_{\text{ext}}^{\gamma}}{\rho_G^{\gamma}} \hat{\rho}_E^{\gamma} - \\
& - \sum_{\beta} \hat{\mathbf{p}}_E^{\beta} \cdot \mathbf{w}_{\beta} - \sum_{\gamma} (\hat{\mathbf{p}}_{\text{ext}E}^{\gamma} + \hat{\mathbf{p}}_{\text{int}}^{\gamma}) \cdot \mathbf{d}_{\gamma G} + \sum_{\zeta} \hat{\varepsilon}^{\zeta} \left(\frac{\theta^S}{\theta^{\zeta}} - 1 \right) - \\
& - \frac{1}{\theta^S} \mathbf{q}^S \cdot \text{grad } \theta^S - \sum_{\zeta} \frac{\theta^S}{\theta^{\zeta}} \frac{1}{\theta^{\zeta}} \mathbf{q}^{\zeta} \cdot \text{grad } \theta^{\zeta} \geq 0.
\end{aligned} \tag{3.23}$$

3.1.3 Constitutive variables

As was mentioned in Section 3.1.1, constitutive relations have to be formulated for the set $\tilde{\mathcal{R}}$ of response functions, cf. (3.7), whereas, in the most general case, these relation can depend on the full fundamental set of constitutive variables (3.6):

$$\begin{aligned}
\mathcal{V}(\mathbf{x}, t) := & \{ \theta^{\alpha}, \text{grad } \theta^{\alpha}, n^{\alpha}, \text{grad } n^{\alpha}, \rho^{\alpha R}, \text{grad } \rho^{\alpha R}, \\
& \mathbf{F}_{\alpha}, \text{Grad}_{\alpha} \mathbf{F}_{\alpha}, \dot{\mathbf{x}}_{\alpha}, \text{Grad}_{\alpha} \dot{\mathbf{x}}_{\alpha}, \mathbf{X}_{\alpha} \}.
\end{aligned}$$

This general set \mathcal{V} of constitutive variables can be reduced to a specific set \mathcal{S} by an incorporation of the characteristic material properties of the constituents involved.

Firstly, the constitutive variables of the solid skeleton are examined in a more detailed way, whereby the argumentation follows the work of *Ghadiani* [77]. For simplification, it is assumed in a first instance that the solid skeleton is governed by a purely elastic material behavior. As the multiphasic material is considered under non-isothermal conditions, the material deformation gradient \mathbf{F}_S of the solid matrix can be split into a purely mechanical part \mathbf{F}_{S_m} and a purely thermal part $\mathbf{F}_{S_{\theta}}$:

$$\mathbf{F}_S = \mathbf{F}_{S_m} \mathbf{F}_{S_{\theta}}. \tag{3.24}$$

Additionally, the partial density ρ_{θ}^S of the solid skeleton in the thermal intermediate configuration, where no mechanical load is included, is introduced based on (2.58)₁ via

$$\rho_{\theta}^S = \rho_{0S}^S (\det \mathbf{F}_{S_{\theta}})^{-1}. \tag{3.25}$$

Incorporating (3.24) as well as (3.25) into (2.58)₁ and taking furthermore into account that $\det(\mathbf{A}\mathbf{B}) = \det \mathbf{A} \det \mathbf{B}$, the following formulations for the partial density of the solid phase are obtained:

$$\begin{aligned}
\rho^S &= n^S \rho^{SR} = \rho_{0S}^S (\det \mathbf{F}_{S_{\theta}})^{-1} (\det \mathbf{F}_{S_m})^{-1} = n_{0S}^S \rho_{0S}^{SR} (\det \mathbf{F}_{S_{\theta}})^{-1} (\det \mathbf{F}_{S_m})^{-1} \\
&= \rho_{\theta}^S (\det \mathbf{F}_{S_m})^{-1} = n_{\theta}^S \rho_{\theta}^{SR} (\det \mathbf{F}_{S_m})^{-1}.
\end{aligned} \tag{3.26}$$

Proceeding from the assumption that the effective density ρ^{SR} is only governed by the temperature θ^S of the solid skeleton, cf. (3.8), and that a thermal loading only yields purely homogeneous expansions, which means that changes of the volume fractions only occur as a result of mechanical loading, it follows directly that

$$\rho^{SR} = \rho_{\theta}^{SR} \quad \text{and} \quad n_{\theta}^S = n_{0S}^S. \quad (3.27)$$

Inserting (3.27) into the relations (3.25) and (3.26) results in

$$\rho^{SR} = \rho_{\theta}^{SR} = \rho_{0S}^{SR} (\det \mathbf{F}_{S_{\theta}})^{-1} \quad \text{and} \quad n^S = n_{\theta}^S = n_{0S}^S (\det \mathbf{F}_{S_m})^{-1}. \quad (3.28)$$

Thus, the volume fraction n^S is directly governed by \mathbf{F}_{S_m} and can be removed from (3.6). Furthermore, at this point, an a priori constitutive relation for $\det \mathbf{F}_{S_{\theta}}$ for isotropic thermal expansion is introduced following *Ghadiani* [77]:

$$\det \mathbf{F}_{S_{\theta}} = e^{3\alpha^S(\theta^S - \theta_0^S)}. \quad (3.29)$$

Therein, α^S is the linear thermal expansion coefficient of the solid skeleton and θ_0^S indicates the initial temperature of the solid phase in the reference configuration. Following this, the material density reads

$$\rho^{SR} = \rho_{0S}^{SR} e^{-3\alpha^S(\theta^S - \theta_0^S)} \quad (3.30)$$

and is, therefore, only a function of the solid temperature θ^S so that ρ^{SR} as well as $\text{grad} \rho^{SR}$ are no longer constitutive variables.

Based on the principle of frame indifference, it can be shown that the several velocities $\dot{\mathbf{x}}_{\alpha}$ of the constituents have to be replaced by the seepage velocities $\mathbf{w}_{\beta} = \dot{\mathbf{x}}_{\beta} - \dot{\mathbf{x}}_S$ as well as the diffusion velocities $\mathbf{d}_{\gamma G} = \dot{\mathbf{x}}_{\gamma} - \dot{\mathbf{x}}_G$ of the gaseous constituents within the overall gas phase, cf. *Ehlers* [40, 46]. Furthermore, $\text{Grad}_{\alpha} \dot{\mathbf{x}}_{\alpha}$, which describes the viscous material properties, has to be replaced by \mathbf{D}_{α} , and, due to the fact that no fluid viscosity is assumed for the solid skeleton, \mathbf{D}_S is removed from \mathcal{V} as well.

As the volume fraction n^S of the solid matrix is given via (3.28), the porosity n^F of the whole porous medium can be computed using the saturation condition, cf. (2.5). Therefore, the volume fractions of the fluid phases are directly determined via their saturation s^{β} , whereas the saturation s^G of the overall gas phase can be computed using the constraint (2.6):

$$n^{\beta} = s^{\beta} n^F, \quad s^G = 1 - \sum_{\xi} s^{\xi}. \quad (3.31)$$

Concerning the special material behavior of the fluid constituents, it can be shown by use of the symmetry group of fluids that

$$\mathbf{F}_{\zeta} = (\det \mathbf{F}_{\zeta})^{1/3} \mathbf{I}, \quad (3.32)$$

cf. *Cross* [31] or *Ehlers* [40]. Additionally, *Cross* [31] showed that there is no effect on the deformation variables whether mass production is considered or not. Thus, $\det \mathbf{F}_{\zeta}$ can be substituted by $\rho^{\zeta R}$ and n^{ζ} , i. e., \mathbf{F}_{ζ} as well as $\text{Grad}_{\zeta} \mathbf{F}_{\zeta}$ can be removed from \mathcal{V} , cf. [40].

Likewise the solid phase, it is assumed that the material density $\rho^{\xi R}$ of the pore liquids depend on the respective temperature via

$$\boxed{\rho^{\xi R} = \rho_{0\xi}^{\xi R} e^{-\gamma^\xi(\theta^\xi - \theta_0^\xi)},} \quad (3.33)$$

cf. (3.9), and can be, therefore, removed together with its gradient from the set \mathcal{V} of constitutive variables. Therein, γ^ξ is the volumetric thermal expansion coefficient of the pore liquids, whereas θ_0^ξ is the liquid temperature in the reference configuration corresponding to the material density $\rho_{0\xi}^{\xi R}$. Furthermore, all constituents are assumed to be homogeneous materials and, therefore, \mathbf{X}_α can be removed from \mathcal{V} as well. Thus, the specific set \mathcal{S} of constitutive variables for the material model under study is given by

$$\mathcal{S} := \{\theta^\alpha, \text{grad } \theta^\alpha, s^\xi, \text{grad } s^\xi, \rho_G^\gamma, \text{grad } \rho_G^\gamma, \mathbf{F}_S, \text{Grad}_S \mathbf{F}_S, \mathbf{w}_\beta, \mathbf{d}_{\gamma G}, \mathbf{D}_\zeta\}. \quad (3.34)$$

Based on the principle of equipresence, the response functions collected in \mathcal{R} are assumed to be functions of the constitutive variables summarized in \mathcal{S} , cf. *Ehlers* [40, 46], i. e.,

$$\mathcal{R} := \mathcal{R}(\mathcal{S}). \quad (3.35)$$

3.1.4 Restrictions

The further evaluation of the entropy inequality is generally based on the procedure given in *Ehlers* [40, 46] and citations therein, i. e., *de Boer & Ehlers* [13], *Bowen* [15], *Coleman & Noll* [30]. Within this section, the entropy inequality is separated into two parts. One part describes the considered material in the thermodynamical equilibrium, whereas the other part, wherein the terms responsible for the dissipative effects are collected, represents the so-called dissipation inequality. This resulting inequality is evaluated around the thermodynamical equilibrium to get further restrictions for the formulation of the respective constitutive relations.

First of all, the dependency of the free *Helmholtz* energy ψ^α on the set of process variables (3.34) has to be specified. Therefore, the principle of constituent separation, cf. *Ehlers* [39], is applied meaning that ψ^α only depends on the variables of the corresponding constituent φ^α , i. e.,

$$\boxed{\begin{aligned} \psi^S &:= \psi^S(\theta^S, \mathbf{F}_S), \\ \psi^\xi &:= \psi^\xi(\theta^\xi, s^\xi), \\ \psi^\gamma &:= \psi^\gamma(\theta^G, \rho_G^\gamma). \end{aligned}} \quad (3.36)$$

Therein, the gradients of the respective variables are not considered due to a statement of *Bowen* [16, 17], after which the second-grade character of the materials only influences the interaction terms, cf. *Ehlers* [46]. Proceeding from (3.36), the material time derivative of

the free *Helmholtz* energies $(\psi^\alpha)'_\alpha$ yields

$$\begin{aligned}
(\psi^S)'_S &= \frac{\partial \psi^S}{\partial \theta^S} (\theta^S)'_S + \frac{\partial \psi^S}{\partial \mathbf{F}_S} \mathbf{F}_S^T \cdot \mathbf{L}_S, \\
(\psi^\xi)'_\xi &= \frac{\partial \psi^\xi}{\partial \theta^\xi} (\theta^\xi)'_\xi + \frac{\partial \psi^\xi}{\partial s^\xi} (s^\xi)'_\xi, \\
(\psi^\gamma)'_\gamma &= \frac{\partial \psi^\gamma}{\partial \theta^G} (\theta^G)'_\gamma + \frac{\partial \psi^\gamma}{\partial \rho_G^\gamma} (\rho_G^\gamma)'_\gamma.
\end{aligned} \tag{3.37}$$

Therein, the material time derivative $(s^\xi)'_\xi$ of the saturation functions can be computed using (2.5) as follows

$$(n^\xi)'_\xi = (s^\xi n^F)'_\xi = (s^\xi)'_\xi n^F + s^\xi (n^F)'_\xi \longrightarrow (s^\xi)'_\xi = \frac{1}{n^F} [(n^\xi)'_\xi - s^\xi (n^F)'_\xi]. \tag{3.38}$$

Incorporating furthermore the material time derivative of the saturation constraint (3.11) as well as relation (3.12), (3.38) results in

$$\begin{aligned}
(s^\xi)'_\xi &= -\frac{1}{n^F} \left[\frac{n^\xi}{\rho^{\xi R}} \frac{d\rho^{\xi R}}{d\theta^\xi} (\theta^\xi)'_\xi + n^\xi \mathbf{L}_\xi \cdot \mathbf{I} - \frac{\hat{\rho}^\xi}{\rho^{\xi R}} + \right. \\
&\quad \left. + s^\xi \frac{n^S}{\rho^{SR}} \frac{d\rho^{SR}}{d\theta^S} (\theta^S)'_S + s^\xi n^S \mathbf{L}_S \cdot \mathbf{I} + s^\xi \text{grad } n^F \cdot \mathbf{w}_\xi \right].
\end{aligned} \tag{3.39}$$

Inserting (3.37) in combination with (3.39) into (3.23), the following form of the entropy

inequality is obtained

$$\begin{aligned}
& \underbrace{\left(\mathbf{T}_E^S + \sum_{\xi} \frac{\theta^S}{\theta^{\xi}} \rho_F^{\xi} \frac{\partial \psi^{\xi}}{\partial s^{\xi}} s^{\xi} n^S \mathbf{I} - \rho^S \frac{\partial \psi^S}{\partial \mathbf{F}_S} \mathbf{F}_S^T \right)}_{\mathbf{T}_{E \text{ mech}}^S} \cdot \mathbf{L}_S - \\
& - \rho^S \underbrace{\left(\eta_E^S - \sum_{\xi} \frac{\theta^S}{\theta^{\xi}} \frac{\rho_F^{\xi}}{(\rho^{SR})^2} \frac{\partial \psi^{\xi}}{\partial s^{\xi}} s^{\xi} \frac{d\rho^{SR}}{d\theta^S} + \frac{\partial \psi^S}{\partial \theta^S} \right)}_{\eta_{E \text{ mech}}^S} (\theta^S)'_S + \\
& + \sum_{\xi} \underbrace{\left(\mathbf{T}_E^{\xi} + \frac{\theta^S}{\theta^{\xi}} \rho_F^{\xi} \frac{\partial \psi^{\xi}}{\partial s^{\xi}} n^{\xi} \mathbf{I} \right)}_{\mathbf{T}_{E \text{ mech}}^{\xi}} \cdot \mathbf{L}_{\xi} + \sum_{\gamma} \mathbf{T}_E^{\gamma} \cdot \mathbf{L}_{\gamma} - \\
& - \sum_{\xi} \rho^{\xi} \underbrace{\left(\eta_E^{\xi} - \frac{\theta^S}{\theta^{\xi}} \frac{\rho_F^{\xi}}{(\rho^{\xi R})^2} \frac{\partial \psi^{\xi}}{\partial s^{\xi}} \frac{d\rho^{\xi R}}{d\theta^{\xi}} + \frac{\theta^S}{\theta^{\xi}} \frac{\partial \psi^{\xi}}{\partial \theta^{\xi}} \right)}_{\eta_{E \text{ mech}}^{\xi}} (\theta^{\xi})'_{\xi} - \\
& - \sum_{\gamma} \rho^{\gamma} \left(\frac{\theta^S}{\theta^G} \frac{\partial \psi^{\gamma}}{\partial \theta^G} + \frac{\theta^S}{\theta^G} \eta^{\gamma} \right) (\theta^G)'_{\gamma} - \sum_{\gamma} \rho^{\gamma} \left(\frac{\theta^S}{\theta^G} \frac{\partial \psi^{\gamma}}{\partial \rho_G^{\gamma}} - \mathcal{P} \frac{x_{Gm}^{\gamma}}{(\rho_G^{\gamma})^2} \right) (\rho_G^{\gamma})'_{\gamma} + \\
& + \sum_{\xi} \frac{\hat{\rho}^{\xi}}{\rho^{\xi R}} \underbrace{\left(\hat{\rho}_E^{\xi} - \frac{\theta^S}{\theta^{\xi}} \rho_F^{\xi} \frac{\partial \psi^{\xi}}{\partial s^{\xi}} \right)}_{\hat{\rho}_{E \text{ mech}}^{\xi}} + \sum_{\gamma} \frac{\hat{\rho}_{\text{ext}}^{\gamma}}{\rho_G^{\gamma}} \hat{\rho}_E^{\gamma} - \\
& - \sum_{\xi} \underbrace{\left(\hat{\mathbf{p}}_E^{\xi} - \frac{\theta^S}{\theta^{\xi}} \rho_F^{\xi} \frac{\partial \psi^{\xi}}{\partial s^{\xi}} s^{\xi} \text{grad } n^F \right)}_{\mathbf{P}_{E \text{ mech}}^{\xi}} \cdot \mathbf{w}_{\xi} - \hat{\mathbf{p}}_E^G \cdot \mathbf{w}_G - \sum_{\gamma} (\hat{\mathbf{p}}_{\text{ext}E}^{\gamma} + \hat{\mathbf{p}}_{\text{int}}^{\gamma}) \cdot \mathbf{d}_{\gamma G} + \\
& + \sum_{\zeta} \hat{\varepsilon}^{\zeta} \left(\frac{\theta^S}{\theta^{\zeta}} - 1 \right) - \frac{1}{\theta^S} \mathbf{q}^S \cdot \text{grad } \theta^S - \sum_{\zeta} \frac{\theta^S}{\theta^{\zeta}} \frac{1}{\theta^{\zeta}} \mathbf{q}^{\zeta} \cdot \text{grad } \theta^{\zeta} \geq 0,
\end{aligned} \tag{3.40}$$

wherein $\rho_F^{\alpha} = \rho^{\alpha}/n^F$ corresponds to (2.9). In addition to the definition of the extra terms $(\cdot)_E$ coming into play as a result of the incorporation of the saturation constraint into the entropy inequality, mechanical extra terms $(\cdot)_{E \text{ mech}}$ are defined at this point.

According to the evaluation procedure of the entropy principle, cf. the argumentation in Ehlers [40], the free parameters \mathbf{L}_S , $(\theta^{\alpha})'_{\alpha}$ as well as $(\rho_G^{\gamma})'_{\gamma}$ can take arbitrary values. Therefore, to ensure the entropy inequality to be fulfilled for any case, the expressions in parentheses in front of the free parameters have to vanish. Thus, one finds the following

constraints:

$$\begin{aligned}
\mathbf{T}_{E \text{ mech}}^S &= \rho^S \frac{\partial \psi^S}{\partial \mathbf{F}_S} \mathbf{F}_S^T, \\
\eta_{E \text{ mech}}^S &= -\frac{\partial \psi^S}{\partial \theta^S}, \quad \eta_{E \text{ mech}}^\xi = -\frac{\theta^S}{\theta^\xi} \frac{\partial \psi^\xi}{\partial \theta^\xi}, \quad \eta^\gamma = -\frac{\partial \psi^\gamma}{\partial \theta^\gamma}, \\
\mathcal{P} &= \frac{\theta^S}{\theta^G} \frac{1}{x_{Gm}^\gamma} (\rho_G^\gamma)^2 \frac{\partial \psi^\gamma}{\partial \rho_G^\gamma} = \frac{\theta^S}{\theta^G} \frac{p_G^\gamma}{x_{Gm}^\gamma}.
\end{aligned} \tag{3.41}$$

Therein, the partial pressure p_G^γ of a materially compressible fluid constituent φ^γ within the overall gas phase φ^G is introduced a priori via

$$\boxed{p_G^\gamma = (\rho_G^\gamma)^2 \frac{\partial \psi^\gamma}{\partial \rho_G^\gamma}.} \tag{3.42}$$

All other terms, except of the parts describing the mass production, which will be discussed later in detail, are collected in the dissipation inequality,

$$\boxed{
\begin{aligned}
\mathcal{D} &= \sum_{\xi} \mathbf{T}_{E \text{ mech}}^\xi \cdot \mathbf{D}_\xi + \sum_{\gamma} \mathbf{T}_E^\gamma \cdot \mathbf{D}_\gamma - \\
&\quad - \sum_{\xi} \hat{\mathbf{p}}_{E \text{ mech}}^\xi \cdot \mathbf{w}_\xi - \hat{\mathbf{p}}_E^G \cdot \mathbf{w}_G - \sum_{\gamma} (\hat{\mathbf{p}}_{\text{ext}E}^\gamma + \hat{\mathbf{p}}_{\text{int}}^\gamma) \cdot \mathbf{d}_{\gamma G} - \\
&\quad - \sum_{\zeta} \hat{\varepsilon}^\zeta \left(1 - \frac{\theta^S}{\theta^\zeta}\right) - \frac{1}{\theta^S} \mathbf{q}^S \cdot \text{grad } \theta^S - \sum_{\zeta} \frac{\theta^S}{\theta^\zeta} \frac{1}{\theta^\zeta} \mathbf{q}^\zeta \cdot \text{grad } \theta^\zeta \geq 0,
\end{aligned} \tag{3.43}$$

which has to be fulfilled for any considered thermodynamical process. Therein, due to the symmetry of the *Cauchy* stress tensors, cf. (2.70), \mathbf{L}_α is replaced by its symmetric part \mathbf{D}_α .

Incorporating the definitions of the extra terms, cf. (3.22), relations for the *Cauchy* stress tensors can be found:

$$\begin{aligned}
\mathbf{T}_{E \text{ mech}}^S &= \mathbf{T}^S + \left(\mathcal{P} + \sum_{\xi} s^\xi \frac{\theta^S}{\theta^\xi} \rho_F^\xi \frac{\partial \psi^\xi}{\partial s^\xi} \right) n^S \mathbf{I} = \rho^S \frac{\partial \psi^S}{\partial \mathbf{F}_S} \mathbf{F}_S^T, \\
\mathbf{T}_{E \text{ mech}}^\xi &= \frac{\theta^S}{\theta^\xi} \mathbf{T}^\xi + \left(\mathcal{P} + \frac{\theta^S}{\theta^\xi} \rho_F^\xi \frac{\partial \psi^\xi}{\partial s^\beta} \right) n^\xi \mathbf{I}, \\
\mathbf{T}_E^\gamma &= \frac{\theta^S}{\theta^G} \mathbf{T}^\gamma + x_{Gm}^\gamma \mathcal{P} n^G \mathbf{I}.
\end{aligned} \tag{3.44}$$

Furthermore, the formulations for the entropies read

$$\begin{aligned}
\eta_{E\text{mech}}^S &= \eta^S - \left(\mathcal{P} + \sum_{\xi} s^{\xi} \frac{\theta^S}{\theta^{\xi}} \rho_F^{\xi} \frac{\partial \psi^{\xi}}{\partial s^{\xi}} \right) \frac{1}{(\rho^{SR})^2} \frac{d\rho^{SR}}{d\theta^S} = -\frac{\partial \psi^S}{\partial \theta^S}, \\
\eta_{E\text{mech}}^{\xi} &= \frac{\theta^S}{\theta^{\xi}} \eta^{\xi} - \left(\mathcal{P} + \frac{\theta^S}{\theta^{\xi}} \rho_F^{\xi} \frac{\partial \psi^{\xi}}{\partial s^{\xi}} \right) \frac{1}{(\rho^{\xi R})^2} \frac{d\rho^{\xi R}}{d\theta^{\xi}} = -\frac{\theta^S}{\theta^{\xi}} \frac{\partial \psi^{\xi}}{\partial \theta^{\xi}}, \\
\eta^{\gamma} &= -\frac{\partial \psi^{\gamma}}{\partial \theta^{\gamma}}.
\end{aligned} \tag{3.45}$$

The momentum interaction terms of the fluid constituents are given in the following way:

$$\begin{aligned}
\hat{\mathbf{p}}_{E\text{mech}}^{\xi} &= \hat{\mathbf{p}}^{\xi} - \mathcal{P} \text{grad } n^{\xi} - s^{\xi} \frac{\theta^S}{\theta^{\xi}} \rho_F^{\xi} \frac{\partial \psi^{\xi}}{\partial s^{\xi}} \text{grad } n^F, \\
\hat{\mathbf{p}}_E^G &= \hat{\mathbf{p}}^G - \mathcal{P} \text{grad } n^G - \sum_{\gamma} \hat{\rho}_{\text{ext}}^{\gamma} \mathbf{d}_{\gamma G}, \\
\hat{\mathbf{p}}_{\text{ext}E}^{\gamma} &= \hat{\mathbf{p}}_{\text{ext}}^{\gamma} - x_{Gm}^{\gamma} \mathcal{P} \text{grad } n^G.
\end{aligned} \tag{3.46}$$

Solving (3.44) for the Cauchy stress tensors yields

$$\begin{aligned}
\mathbf{T}^S &= -n^S \underbrace{\left(\mathcal{P} + \sum_{\xi} s^{\xi} \frac{\theta^S}{\theta^{\xi}} \rho_F^{\xi} \frac{\partial \psi^{\xi}}{\partial s^{\xi}} \right)}_{\bar{\mathcal{P}}} \mathbf{I} + \rho^S \underbrace{\frac{\partial \psi^S}{\partial \mathbf{F}_S}}_{\mathbf{T}_{E\text{mech}}^S} \mathbf{F}_S^T = -n^S \bar{\mathcal{P}} \mathbf{I} + \mathbf{T}_{E\text{mech}}^S, \\
\mathbf{T}^{\xi} &= -n^{\xi} \underbrace{\left(\frac{\theta^{\xi}}{\theta^S} \mathcal{P} + \rho_F^{\xi} \frac{\partial \psi^{\xi}}{\partial s^{\xi}} \right)}_{p^{\xi R}} \mathbf{I} + \frac{\theta^{\xi}}{\theta^S} \mathbf{T}_{E\text{mech}}^{\xi} = -n^{\xi} p^{\xi R} \mathbf{I} + \frac{\theta^{\xi}}{\theta^S} \mathbf{T}_{E\text{mech}}^{\xi}, \\
\mathbf{T}^{\gamma} &= -n^G \underbrace{\frac{\theta^G}{\theta^S} x_{Gm}^{\gamma} \mathcal{P}}_{p_G^{\gamma}} \mathbf{I} + \frac{\theta^G}{\theta^S} \mathbf{T}_E^{\gamma} = -n^G p_G^{\gamma} \mathbf{I} + \frac{\theta^G}{\theta^S} \mathbf{T}_E^{\gamma}.
\end{aligned} \tag{3.47}$$

Therein, the variables

$$\bar{\mathcal{P}} = \mathcal{P} + \sum_{\xi} s^{\xi} \frac{\theta^S}{\theta^{\xi}} \rho_F^{\xi} \frac{\partial \psi^{\xi}}{\partial s^{\xi}}, \quad p^{\xi R} = \frac{\theta^{\xi}}{\theta^S} \mathcal{P} + \rho_F^{\xi} \frac{\partial \psi^{\xi}}{\partial s^{\xi}} \quad \text{and} \quad p_G^{\gamma} = \frac{\theta^G}{\theta^S} x_{Gm}^{\gamma} \mathcal{P} \tag{3.48}$$

are introduced, where $p^{\xi R}$ can be identified as the effective pressure of the pore liquids and p_G^{γ} as the partial pressure of the gas components within the overall gas phase. Using (3.48)₂ and (3.48)₃, the relation for $\bar{\mathcal{P}}$ can be reformulated:

$$\begin{aligned}
\bar{\mathcal{P}} &= \mathcal{P} + \sum_{\xi} s^{\xi} \frac{\theta^S}{\theta^{\xi}} \rho_F^{\xi} \frac{\partial \psi^{\xi}}{\partial s^{\xi}} = \mathcal{P} + \sum_{\xi} s^{\xi} \frac{\theta^S}{\theta^{\xi}} (p^{\xi R} - \frac{\theta^{\xi}}{\theta^S} \mathcal{P}) = \\
&= (1 - \sum_{\xi} s^{\xi}) \mathcal{P} + \sum_{\xi} s^{\xi} \frac{\theta^S}{\theta^{\xi}} p^{\xi R} = s^G \frac{\theta^S}{\theta^G} \frac{p_G^{\gamma}}{x_{Gm}^{\gamma}} + \sum_{\xi} s^{\xi} \frac{\theta^S}{\theta^{\xi}} p^{\xi R}.
\end{aligned} \tag{3.49}$$

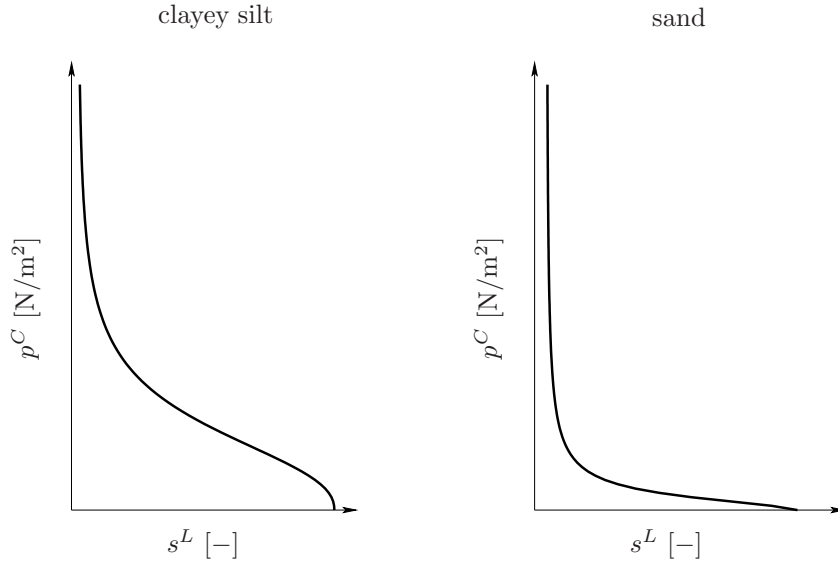


Figure 3.1: Typical capillary-pressure-saturation relations of a clayey silt and a sand.

Comparing the first and the second term of (3.49), the effective pressure p^{GR} of the overall gas phase is introduced via

$$p^{GR} := \frac{p_G^\gamma}{x_{Gm}^\gamma} \longrightarrow p_G^\gamma = x_{Gm}^\gamma p^{GR}, \quad p^{GR} = \sum_{\gamma} p_G^\gamma, \quad (3.50)$$

which means that the sum of the partial pressures p_G^γ of the individual gas components yields the effective pressure of the overall gas phase. This well-known relation was formulated by *John Dalton* in the year 1805 and is, therefore, called *Dalton's law*, cf. [32]. Using this definition, \bar{p} is given by the sum of the effective pressures $p^{\beta R}$ of the fluid phases weighted by the respective saturations s^β and the ratio between the temperature of the solid and the individual fluid phase. Therefore, \bar{p} can be identified as the effective pore pressure p^{FR} of the overall fluid constituent φ^F :

$$p^{FR} := \bar{p} = \sum_{\beta} s^{\beta} \frac{\theta^S}{\theta^{\beta}} p^{\beta R}. \quad (3.51)$$

Describing porous materials with several pore fluids, a relation between the saturation and the so-called capillary pressure p^C can be observed in suitable experiments, whereas two typical capillary-pressure-saturation relations are given exemplary in Figure 3.1 for a clayey silt and a sand. This soil capillarity and the related forces result from the interaction between the pore fluids and the soil particles and are related to the surface tension and cohesion as well as adhesion effects between the respective phases. Therefore, two pore fluids can be characterized, generally, by their wetting and non-wetting material behavior with respect to the solid skeleton. Thereby, the fluid with an acute wetting angle ω is called the wetting fluid, the other one the non-wetting fluid, cf. Figure 3.2.

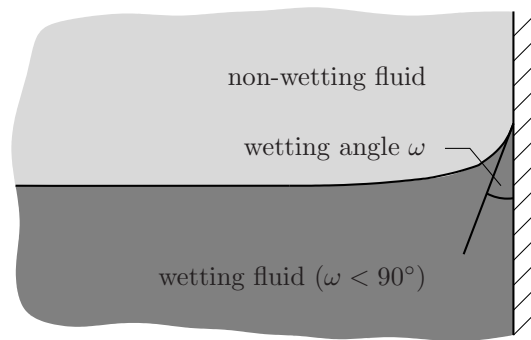


Figure 3.2: Interface of a three-phase system, i. e., solid skeleton and two fluids.

The interested reader is referred to the works of, e. g., *Bear* [7], *Cernica* [24], *Fredlund & Rahardjo* [75], *Helmig* [90] or *von Soos & Boháč* [125] and citations therein. Considering natural soils with the two pore fluids water and air, the capillary rise of pore water can be estimated by empirical relations, e. g., following *Hazen* [86]. The capillary rise of pore water within certain natural soils can be found, e. g., in *von Soos & Boháč* [125], cf. Table 3.1.

Classically, the capillary pressure is introduced as the difference between the pressure of the non-wetting and the wetting pore fluid, cf. *Brooks & Corey* [21]:

$$p^C := p^{NWR} - p^{WR}. \quad (3.52)$$

Assuming that the considered porous material includes two pore fluids, namely, pore water and the overall pore gas, the pore gas can be identified as the non-wetting, the pore water as the wetting pore fluid. In this case, the capillary pressure is given via

$$p^C := p^{GR} - p^{LR}. \quad (3.53)$$

Proceeding from this definition and using furthermore relation (3.48)₂, (3.48)₃ as well as

soil type	effective particle size [mm]	capillary rise [m]
sandy gravel	0.7	0.08
medium to coarse sand	0.35	0.2
fine to medium sand	0.1	0.5
silty sand	0.045	1.0
silt	0.01	5.0
clay	0.001	50.0

Table 3.1: Capillary rise for certain natural soils following *von Soos & Boháč* [125].

(3.50), the capillary pressure reads

$$p^C = p^{GR} - \left(\frac{\theta^L}{\theta^S} \mathcal{P} + \rho_F^L \frac{\partial \psi^L}{\partial s^L} \right) = p^{GR} \left(1 - \frac{\theta^L}{\theta^G} \right) - \rho_F^L \frac{\partial \psi^L}{\partial s^L}. \quad (3.54)$$

Finally, using $\rho_F^L = n^L \rho^{LR} / n^F = s^L \rho^{LR}$, the capillary pressure p^C is a function of the overall effective gas pressure p^{GR} , the ratio between the temperatures θ^L and θ^G of the pore liquid and the pore gas, the saturation s^L and the material density ρ^{LR} of the pore liquid as well as the derivative of the free *Helmholtz* energy ψ^L of the pore liquid with respect to its saturation s^L :

$$p^C = p^{GR} \left(1 - \frac{\theta^L}{\theta^G} \right) - s^L \rho^{LR} \frac{\partial \psi^L}{\partial s^L}. \quad (3.55)$$

Concerning the entropies η^α , one finds the following relations:

$$\begin{aligned} \eta^S &= \frac{1}{(\rho^{SR})^2} \frac{d\rho^{SR}}{d\theta^S} p^{FR} - \frac{\partial \psi^S}{\partial \theta^S}, \\ \eta^\xi &= \frac{1}{(\rho^{\xi R})^2} \frac{d\rho^{\xi R}}{d\theta^\xi} p^{\xi R} - \frac{\partial \psi^\xi}{\partial \theta^\xi}, \\ \eta^\gamma &= - \frac{\partial \psi^\gamma}{\partial \theta^G}. \end{aligned} \quad (3.56)$$

Thereby, the entropies η^α are given via the derivative of the free *Helmholtz* energies ψ^α with respect to the temperature θ^α , which corresponds directly to the introduction of ψ^α , cf. (2.83), via a *Legendre* transformation between the temperature and the entropy. In case of the materially incompressible constituents, an additional part can be recognized, which depends on the relationship between the material density and the temperature as well as on the respective effective pore pressure.

Following the argumentation of *Ehlers* [40], the dissipation inequality (3.43) is additively split into an equilibrium (\mathcal{D}_0) and a non-equilibrium (\mathcal{D}_n) part,

$$\mathcal{D}(\mathcal{S}) = \mathcal{D}_0(\mathcal{S}_0) + \mathcal{D}_n(\mathcal{S}), \quad \text{where } \mathcal{D}_0(\mathcal{S}_0) = 0 \quad \text{and} \quad \mathcal{D}_n(\mathcal{S}_0) = 0, \quad (3.57)$$

to get further restrictions for the formulation of constitutive relations for the response functions:

$$\Upsilon(\mathcal{S}) := \{ \mathbf{q}^\alpha, \mathbf{T}_{E \text{ mech}}^\xi, \mathbf{T}_E^\gamma, \hat{\varepsilon}^\zeta, \hat{\mathbf{p}}_{E \text{ mech}}^\xi, \hat{\mathbf{p}}_E^G, \hat{\mathbf{p}}_{\text{ext}E}^\gamma, \hat{\mathbf{p}}_{\text{int}}^\gamma \}. \quad (3.58)$$

The quantities summarized within the set Υ are linearized around the thermodynamic equilibrium state characterized by

$$\begin{aligned} \mathcal{S}_0 := \{ \theta^\alpha = \theta, \text{grad } \theta^\alpha = \mathbf{0}, s^\xi, \text{grad } s^\xi, \rho_G^\gamma, \text{grad } \rho_G^\gamma, \mathbf{F}_S, \text{Grad}_S \mathbf{F}_S, \\ \mathbf{w}_\beta = \mathbf{0}, \mathbf{d}_{\gamma G} = \mathbf{0}, \mathbf{D}_\zeta = \mathbf{0} \}. \end{aligned} \quad (3.59)$$

In general, all response functions can depend on the full set of constitutive variables collected in \mathcal{S} . Nevertheless, not all possibilities are meaningful and have to be considered further. Thus, one has to decide, according to the underlying material behavior, which response function depends on which constitutive variables.

Based on the principle of phase separation, it is assumed that the response functions for \mathbf{q}^α , $\mathbf{T}_{E\text{mech}}^\xi$ and \mathbf{T}_E^γ only depend on the process variables of the respective constituent φ^α . Furthermore, the interaction terms $\hat{\mathbf{p}}_{E\text{mech}}^\xi$, $\hat{\mathbf{p}}_E^G$, $\hat{\mathbf{p}}_{\text{ext}E}^\gamma$, $\hat{\mathbf{p}}_{\text{int}}^\gamma$ and $\hat{\varepsilon}^\zeta$ depend only on the interaction variables \mathbf{w}_β , $\mathbf{d}_{\gamma G}$ and the temperature differences between the individual constituents. Following the argumentation of *Ghadiani* [77], it is postulated that the mechanical response functions only depend on kinematical quantities, whereas the thermal response functions only depend on caloric process variables. More precisely, corresponding to the well-known *Fourier's* law, cf. *Grigull* [79], the heat influx vector \mathbf{q}^α is supposed to be governed by the respective temperature gradient, whereas the fluid extra terms $\mathbf{T}_{E\text{mech}}^\xi$ and \mathbf{T}_E^γ can be identified as the fluid friction stresses. Thus, these terms are assumed to be a function of the gradient of the respective primary kinematic variable, i. e., the symmetric part of the spatial velocity gradient \mathbf{D}_ζ , as it is the case in classical fluid mechanics.

The momentum production terms $\hat{\mathbf{p}}_{E\text{mech}}^\xi$, $\hat{\mathbf{p}}_E^G$ and $\hat{\mathbf{p}}_{\text{ext}E}^\gamma$ are assumed to depend on the kinematical variables \mathbf{w}_ξ and \mathbf{w}_G . As $\hat{\mathbf{p}}_{\text{int}}^\gamma$ only describes the momentum interaction with the other gas components within the overall gas phase, it is supposed that $\hat{\mathbf{p}}_{\text{int}}^\gamma$ only depends on the diffusion velocity $\mathbf{d}_{\gamma G}$. Furthermore, as the caloric interactions of two bodies are governed by the temperature difference between them, the direct energy production $\hat{\varepsilon}^\zeta$ is assumed to depend on the temperature difference $\theta^\alpha - \theta^\zeta$ between the single constituents. Therefore, it follows

$$\begin{aligned}
\mathbf{T}_{E\text{mech}}^\xi &:= \mathbf{T}_{E\text{mech}}^\xi(\mathbf{D}_\xi), & \mathbf{T}_E^\gamma &:= \mathbf{T}_E^\gamma(\mathbf{D}_\gamma), \\
\hat{\mathbf{p}}_{E\text{mech}}^\xi &:= \hat{\mathbf{p}}_{E\text{mech}}^\xi(\mathbf{w}_\xi), & \hat{\mathbf{p}}_E^G &:= \hat{\mathbf{p}}_E^G(\mathbf{w}_G), \\
\hat{\mathbf{p}}_{\text{ext}E}^\gamma &:= \hat{\mathbf{p}}_{\text{ext}E}^\gamma(\mathbf{w}_G), & \hat{\mathbf{p}}_{\text{int}}^\gamma &:= \hat{\mathbf{p}}_{\text{int}}^\gamma(\mathbf{d}_{\gamma G}), \\
\hat{\varepsilon}^\zeta &:= \hat{\varepsilon}^\zeta(\theta^\alpha), & \mathbf{q}^\alpha &:= \mathbf{q}^\alpha(\text{grad } \theta^\alpha),
\end{aligned} \tag{3.60}$$

where, in particular,

$$\begin{aligned}
\mathbf{T}_{E\text{mech}}^\xi &= \mathbf{Z}_\xi \mathbf{D}_\xi, & \mathbf{T}_E^\gamma &= \mathbf{Z}_\gamma \mathbf{D}_\gamma, \\
\hat{\mathbf{p}}_{E\text{mech}}^\xi &= -\mathbf{S}_\xi \mathbf{w}_\xi, & \hat{\mathbf{p}}_E^G &= -\mathbf{S}_G \mathbf{w}_G, \\
\hat{\mathbf{p}}_{\text{ext}E}^\gamma &= -\mathbf{S}_{\gamma\text{ext}} \mathbf{w}_G, & \hat{\mathbf{p}}_{\text{int}}^\gamma &= -\mathbf{S}_{\gamma\text{int}} \mathbf{d}_{\gamma G}, \\
\hat{\varepsilon}^\zeta &= \sum_\alpha k_{\theta^\alpha}^{\varepsilon^\zeta} (\theta^\alpha - \theta), & \mathbf{q}^\alpha &= -\mathbf{H}^\alpha \text{grad } \theta^\alpha
\end{aligned} \tag{3.61}$$

are obtained by a formal linearization of the dissipation inequality. In (3.61),

$$\begin{aligned}
\mathbf{Z}_\xi^4 &= \left. \frac{\partial \mathbf{T}_{E\text{mech}}^\xi}{\partial \mathbf{D}_\xi} \right|_{\mathcal{S}_0}, & \mathbf{Z}_\gamma^4 &= \left. \frac{\partial \mathbf{T}_E^\gamma}{\partial \mathbf{D}_\gamma} \right|_{\mathcal{S}_0}, \\
\mathbf{S}_\xi &= \left. \frac{\partial \hat{\mathbf{p}}_{E\text{mech}}^\xi}{\partial \mathbf{w}_\xi} \right|_{\mathcal{S}_0}, & \mathbf{S}_G &= \left. \frac{\partial \hat{\mathbf{p}}_E^G}{\partial \mathbf{w}_G} \right|_{\mathcal{S}_0}, \\
\mathbf{S}_{\gamma\text{ext}} &= \left. \frac{\partial \hat{\mathbf{p}}_{\text{ext}E}^\gamma}{\partial \mathbf{w}_G} \right|_{\mathcal{S}_0}, & \mathbf{S}_{\gamma\text{int}} &= \left. \frac{\partial \hat{\mathbf{p}}_{\text{int}}^\gamma}{\partial \mathbf{d}_{\gamma G}} \right|_{\mathcal{S}_0}, \\
k_{\theta^\alpha}^{\varepsilon^\zeta} &= \left. \frac{\partial \hat{\varepsilon}^\zeta}{\partial \theta^\alpha} \right|_{\mathcal{S}_0}, & \mathbf{H}^\alpha &= \left. \frac{\partial \mathbf{q}^\alpha}{\partial \text{grad } \theta^\alpha} \right|_{\mathcal{S}_0}.
\end{aligned} \tag{3.62}$$

Furthermore, it is taken into account that the response functions (3.60) have to vanish in the state of thermodynamical equilibrium, cf. *Ehlers* [40]:

$$\begin{aligned}
\mathbf{T}_{E\text{mech}}^\xi(\mathcal{S}_0) &= \mathbf{0}, & \mathbf{T}_E^\gamma(\mathcal{S}_0) &= \mathbf{0}, \\
\hat{\mathbf{p}}_{E\text{mech}}^\xi(\mathcal{S}_0) &= \mathbf{0}, & \hat{\mathbf{p}}_E^G(\mathcal{S}_0) &= \mathbf{0}, \\
\hat{\mathbf{p}}_{\text{ext}E}^\gamma(\mathcal{S}_0) &= \mathbf{0}, & \hat{\mathbf{p}}_{\text{int}}^\gamma(\mathcal{S}_0) &= \mathbf{0}, \\
\hat{\varepsilon}^\zeta(\mathcal{S}_0) &= 0, & \mathbf{q}^\alpha(\mathcal{S}_0) &= \mathbf{0}.
\end{aligned} \tag{3.63}$$

3.2 The pore fluid constituents

Concerning the fluid constituents, thermodynamical restrictions for the general structure of the response functions $\tilde{\mathcal{R}}$ could be found in the above sections. Nevertheless, the constitutive relations have to be concretized and formulated for the respective terms. Therefore, the free *Helmholtz* energies of the pore liquids are derived based on the definition of the specific heat and the capillary pressure saturation relation following *Brooks & Corey* [21], whereas the free *Helmholtz* energy of the pore gas components is furthermore based on the ideal gas law. The momentum productions of the fluid phases are governed additionally to a porous material with only one overall pore fluid by a saturation-dependent permeability tensor, whereas the internal momentum production of the gas components are governed by the gradient of the molar fraction. Furthermore, the direct energy productions are governed by the heat exchanges between the individual constituents, whereas the heat influx vectors follow the gradients of the respective temperatures and correspond, therefore, to the well-known *Fourier's* law.

3.2.1 Free *Helmholtz* energies

Following the argumentation of *Ghadiani* [77], the specific heat C_V^α is introduced via

$$C_V^\alpha = \theta^\alpha \left. \frac{\partial \eta^\alpha}{\partial \theta^\alpha} \right|_{\rho^{\alpha R} = \text{const.}} = -\theta^\alpha \left. \frac{\partial^2 \psi^\alpha}{(\partial \theta^\alpha)^2} \right|_{\rho^{\alpha R} = \text{const.}}. \tag{3.64}$$

Furthermore, the capillary pressure saturation relation following *Brooks & Corey* [21] reads

$$p^C = p^D (s^\xi)^{-1/\lambda_{bc}} \quad (3.65)$$

and was originally defined for the isothermal case ($\theta^\xi = \theta^G$). Here, it is used as constitutive relation between the capillary pressure and the saturation. Therein, p^D and λ_{bc} are two material parameters to adapt this relation to different porous mixtures. Thus, it follows with (3.55) that

$$\frac{\partial \psi^\xi}{\partial s^\xi} = -\frac{p^D}{\rho^{\xi R}} (s^\xi)^{-1/\lambda_{bc}-1}. \quad (3.66)$$

Therefore, based on (3.56)₂ as well as on (3.64) and (3.65), the entropy η^ξ can be determined:

$$\eta^\xi = C_V^\xi \ln \frac{\theta^\xi}{\theta_0^\xi} - \left\{ \frac{1}{\rho^{\xi R}} [p^{\xi R} + p^D (s^\xi)^{-1}] - \frac{1}{\rho_0^{\xi R}} [p_0^{\xi R} + p^D (s_0^\xi)^{-1}] \right\} \gamma^\xi + \eta_0^\xi, \quad (3.67)$$

wherein $\lambda_{bc} = 1$. The entropy level in the initial state defined by θ_0^ξ , $p_0^{\xi R}$, $\rho_0^{\xi R}$ and s_0^ξ is given via η_0^ξ . Furthermore, the free *Helmholtz* energy of a materially incompressible fluid yields

$$\begin{aligned} \psi^\xi = & -C_V^\xi \left[\theta^\xi \ln \frac{\theta^\xi}{\theta_0^\xi} - (\theta^\xi - \theta_0^\xi) \right] - \frac{1}{\rho_0^{\xi R}} [p_0^{\xi R} + p^D (s_0^\xi)^{-1}] \gamma^\xi (\theta^\xi - \theta_0^\xi) - \\ & - \eta_0^\xi (\theta^\xi - \theta_0^\xi) + \left[\frac{p^D}{\rho^{\xi R}} (s^\xi)^{-1} - \frac{p^D}{\rho_0^{\xi R}} (s_0^\xi)^{-1} \right] + \psi_0^\xi, \end{aligned} \quad (3.68)$$

whereas the internal energy is found based on the *Legendre* transformation between the variables θ^ξ and η^ξ , cf. (2.83),

$$\begin{aligned} \varepsilon^\xi = & C_V^\xi (\theta^\xi - \theta_0^\xi) + \left[\frac{p^D}{\rho^{\xi R}} (s^\xi)^{-1} - \frac{p^D}{\rho_0^{\xi R}} (s_0^\xi)^{-1} \right] - \\ & - \left\{ \frac{1}{\rho^{\xi R}} [p^{\xi R} + p^D (s^\xi)^{-1}] \theta^\xi - \frac{1}{\rho_0^{\xi R}} [p_0^{\xi R} + p^D (s_0^\xi)^{-1}] \theta_0^\xi \right\} \gamma + \varepsilon_0^\xi. \end{aligned} \quad (3.69)$$

Therein, ψ_0^ξ as well as ε_0^ξ denote the values of the respective energies in the initial state.

Concerning the materially compressible fluid constituents, beside the definition of the specific heat (3.64), the assumption of an ideal gas and the relation given therewith between the partial density and the partial pressure of the gas components within the overall gas phase as well as relation (3.42) serve as further constraints for the determination of the free *Helmholtz* energy of a gas component:

$$p_G^\gamma = \frac{R \rho_G^\gamma \theta^G}{M^\gamma} = (\rho_G^\gamma)^2 \frac{\partial \psi^\gamma}{\partial \rho_G^\gamma} \quad \longrightarrow \quad \frac{\partial \psi^\gamma}{\partial \rho_G^\gamma} = \frac{R \theta^G}{M^\gamma \rho_G^\gamma}. \quad (3.70)$$

Thus, the free *Helmholtz* energy of a gas component reads

$$\psi^\gamma = -C_V^\gamma \left[\theta^G \ln \frac{\theta^G}{\theta_0^G} - (\theta^G - \theta_0^G) \right] + \frac{R\theta^G}{M^\gamma} \ln \frac{\rho_G^\gamma}{\rho_{G0}^\gamma} - \eta_0^\gamma (\theta^G - \theta_0^G) + \psi_0^\gamma, \quad (3.71)$$

where ρ_{G0}^γ , θ_0^G and ψ_0^γ are the respective values in the initial state. The entropy is given therewith via

$$\eta^\gamma = C_V^\gamma \ln \frac{\theta^G}{\theta_0^G} - \frac{R}{M^\gamma} \ln \frac{\rho_G^\gamma}{\rho_{G0}^\gamma} + \eta_0^\gamma, \quad (3.72)$$

whereas the internal energy yields

$$\varepsilon^\gamma = C_V^\gamma (\theta^G - \theta_0^G) + \varepsilon_0^\gamma. \quad (3.73)$$

Thus, it can be recognized that the internal energy of an ideal gas is only governed by the temperature.

3.2.2 Mass interactions

Within this section, the mass interaction process between the pore fluids is investigated in detail. Particularly, the physical processes are exemplarily discussed examining the heating process of a pure component. Secondly, the thermomechanical description within the Theory of Porous Media is derived based on the evaluation of the entropy inequality given in the previous sections. Furthermore, it is shown, how the whole phase transition process is controlled by the coupled system of equations consisting of the mass and energy balance.

The *van der Waals* equation in the form

$$\frac{p^{\alpha R}}{p_{\text{crit}}^{\alpha R}} = \frac{8 \theta^\alpha / \theta_{\text{crit}}^\alpha}{3 \nu^{\alpha R} / \nu_{\text{crit}}^{\alpha R} - 1} - \frac{3}{(\nu^{\alpha R} / \nu_{\text{crit}}^{\alpha R})^2} \quad (3.74)$$

is given for a pure component φ^α in Figure 3.3, cf. *Abbott & van Ness* [1]. Therein, the two material parameters of the *van der Waals* equation are predetermined by the assumption that the critical isotherm has a horizontal inflection at the critical state:

$$\left(\frac{\partial p^{\alpha R}}{\partial \nu^{\alpha R}} \right)_{\theta^\alpha = \theta_{\text{crit}}^\alpha}^{\nu^{\alpha R} = \nu_{\text{crit}}^{\alpha R}} = 0 \quad \text{and} \quad \left(\frac{\partial^2 p^{\alpha R}}{\partial (\nu^{\alpha R})^2} \right)_{\theta^\alpha = \theta_{\text{crit}}^\alpha}^{\nu^{\alpha R} = \nu_{\text{crit}}^{\alpha R}} = 0. \quad (3.75)$$

Furthermore, for the identification of the liquid gas region a relation for the vaporization curve following *Antoine* [3] is used, which will be particularly discussed later in this section. All axis are normalized with respect to the values $p_{\text{crit}}^{\alpha R}$, $\nu_{\text{crit}}^{\alpha R}$ and $\theta_{\text{crit}}^\alpha$ of the critical point of the respective substance. This critical point indicates the highest pressure and highest temperature, at which liquid and gas can coexist. In case of water, the critical values

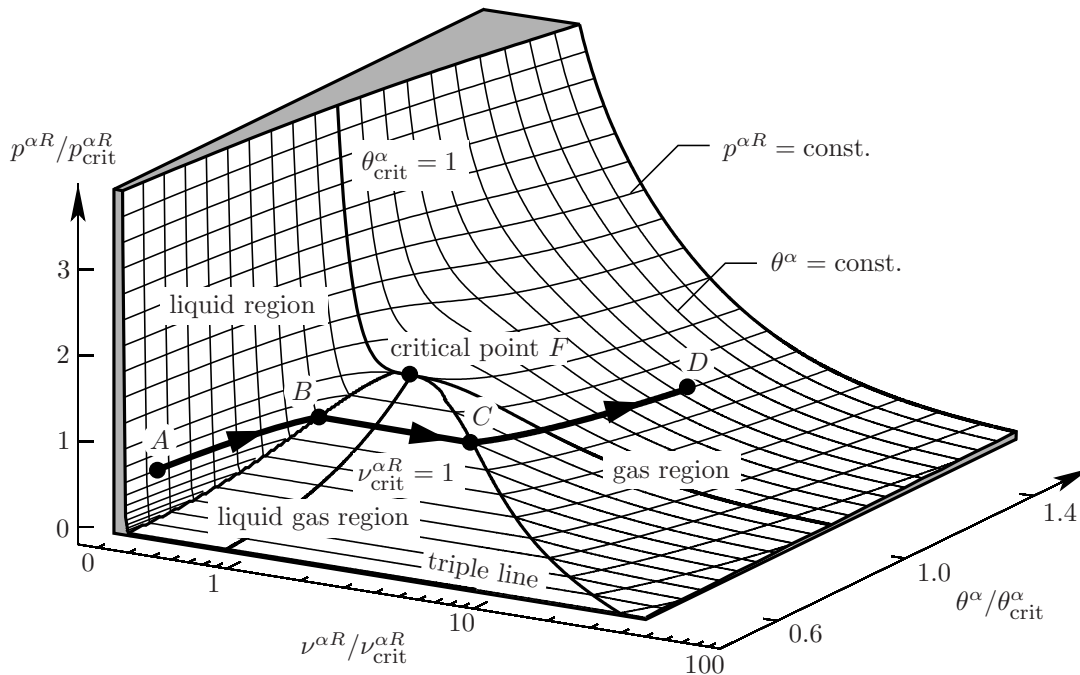


Figure 3.3: $p^{\alpha R}$ - $\nu^{\alpha R}$ - θ^{α} surface of a pure component, cf. Abbott & van Ness [1].

are $p_{crit}^{WR} = 22.064$ MPa, $\nu_{crit}^{WR} = 3.106$ dm³/kg and $\theta_{crit}^W = 647.1$ K. At higher pressures or temperatures, no clear distinction between the liquid and the gas phases can be made (overcritical state). Due to the fact that only mass interactions between the fluid phases are taken into account within this contribution, the regions concerning the solid phase are omitted in Figure 3.3. Nevertheless, the triple line represents the states, where all three phases of the component can coexist. This triple line is characterized in case of water via $p_{trip}^{WR} = 611.66$ Pa and $\theta_{trip}^W = 273.16$ K.

The heating process of a pure component under constant pressure conditions:

Three different regions can be separated in Figure 3.3: The liquid region, the gas region and a region, where both, the liquid and the gaseous phase can coexist. If, exemplary, the liquid component is heated up starting from point A, the specific volume as well as the temperature increases until the liquid gas region is reached in point B (line A – B). At this point, the liquid begins to vaporize. During further heating, the temperature remains constant and more and more vapor is produced, whereby a strong increase of the overall specific volume can be observed (line B – C). Leaving the liquid gas region in point C, all of the liquid is vaporized and point D in the gas region is reached, where the heating process is stopped (line C – D).

The pressure-temperature projection of the $p^{\alpha R}$ - $\nu^{\alpha R}$ - θ^{α} surface is given in Figure 3.4. Therein, the liquid and gas region of the component can be furthermore identified. Due to the fact that within the liquid gas region at constant pressure the temperature is constant as well, the left and right boundary of the liquid gas region, seen with respect to the critical specific volume $\nu_{crit}^{\alpha R}$, coincide in one curve, the so-called vaporization curve. This curve starts at the triple point E and ends at the critical point F.

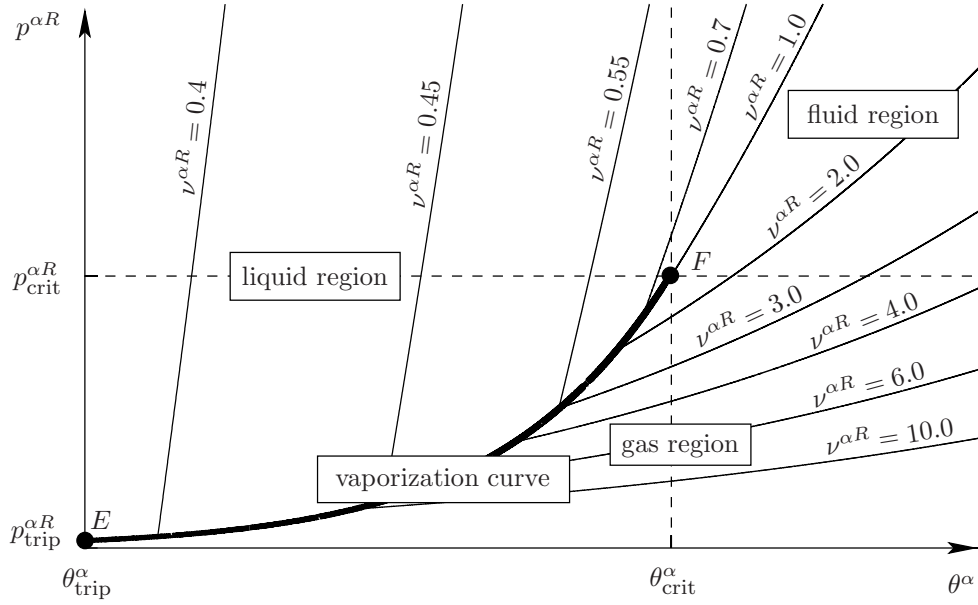


Figure 3.4: $p^{\alpha R}$ - θ^{α} projection of the $p^{\alpha R}$ - $\nu^{\alpha R}$ - θ^{α} surface of a pure component approximated via the vaporization curve following Antoine [3].

Restrictions from the entropy inequality: Taking a closer look at the mass interaction terms of the fluid constituents within the entropy inequality results in

$$\begin{aligned} \hat{\rho}_{E\text{mech}}^{\xi} &= \rho^{\xi R} [\eta^{\xi}(\theta^S - \theta^{\xi}) - \psi^{\xi} + \dot{\mathbf{x}}_{\xi} \cdot \dot{\mathbf{x}}_S - \frac{1}{2} \dot{\mathbf{x}}_{\xi} \cdot \dot{\mathbf{x}}_{\xi}] - \\ &\quad - \left(\mathcal{P} + \frac{\theta^S}{\theta^{\xi}} \rho_F^{\xi} \frac{\partial \psi^{\xi}}{\partial s^{\xi}} \right), \end{aligned} \quad (3.76)$$

$$\hat{\rho}_E^{\gamma} = \rho_G^{\gamma} [\eta^{\gamma}(\theta^S - \theta^G) - \psi^{\gamma} + \dot{\mathbf{x}}_{\gamma} \cdot \dot{\mathbf{x}}_S - \frac{1}{2} \dot{\mathbf{x}}_{\gamma} \cdot \dot{\mathbf{x}}_{\gamma}] - x_{Gm}^{\gamma} \mathcal{P}.$$

As only mass exchanges between liquid and gaseous pore water are considered, pore water exists within the porous material as materially incompressible pore liquid φ^L and materially compressible water vapor φ^V . Due to the constraint that the sum of the mass interactions has to vanish, (2.61)₃, it follows:

$$\hat{\rho}^L + \hat{\rho}_{\text{ext}}^V = 0 \quad \longrightarrow \quad \hat{\rho}^L = -\hat{\rho}_{\text{ext}}^V. \quad (3.77)$$

Thus, the corresponding parts in the dissipation inequality depending on the mass interaction, cf. (3.76), can be reorganized using (3.48)_{2,3}:

$$\begin{aligned} (\dots) - \hat{\rho}^L \left(\frac{\hat{\rho}_{E\text{mech}}^V}{\rho_G^V} - \frac{\hat{\rho}_{E\text{mech}}^L}{\rho^{LR}} \right) - (\dots) &\geq 0 \\ (\dots) - \hat{\rho}^L \left\{ \psi^L + \frac{p^{LR}}{\rho^{LR}} - \eta^L(\theta^S - \theta^L) + \frac{1}{2} \mathbf{w}_L \cdot \mathbf{w}_L - \right. & \\ \left. - \left[\psi^V + \frac{p^V}{\rho_G^V} - \eta^V(\theta^S - \theta^G) + \frac{1}{2} \mathbf{w}_V \cdot \mathbf{w}_V \right] \right\} - (\dots) &\geq 0. \end{aligned} \quad (3.78)$$

Within this contribution, the mass interaction describes a phase transition of one component, i. e., between liquid water and water vapor. This mass interaction is a fully reversible process, and, therefore, the mass interaction terms have to be considered within the equilibrium part of the entropy inequality.

Remark: Describing purely dissipative mass interaction processes, e. g., erosion processes, the mass interaction terms have to be examined within the evaluation of the dissipation inequality:

$$\begin{aligned} \mathcal{D} = (\dots) - \hat{\rho}^L \{ \psi^L + \eta^L(\theta^L - \theta^S) + \frac{\theta^S p^{LR}}{\theta^L \rho^{LR}} + \frac{1}{2} \mathbf{w}_L \cdot \mathbf{w}_L - \\ - [\psi^V + \eta^V(\theta^G - \theta^S) + \frac{\theta^S p_G^V}{\theta^G \rho_G^V} + \frac{1}{2} \mathbf{w}_V \cdot \mathbf{w}_V] \} - (\dots) \geq 0. \end{aligned}$$

This relation has to be fulfilled for any thermomechanical process. Therefore, the mass interaction $\hat{\rho}^L$ has to be formulated within a thermodynamically consistent approach in the following way:

$$\begin{aligned} \hat{\rho}^L = -\alpha \{ \psi^L + \eta^L(\theta^L - \theta^S) + \frac{\theta^S p^{LR}}{\theta^L \rho^{LR}} + \frac{1}{2} \mathbf{w}_L \cdot \mathbf{w}_L - \\ - [\psi^V + \eta^V(\theta^G - \theta^S) + \frac{\theta^S p_G^V}{\theta^G \rho_G^V} + \frac{1}{2} \mathbf{w}_V \cdot \mathbf{w}_V] \}, \end{aligned}$$

wherein α is a positive scalar function. For a closer look at this topic, the interested reader is referred to *Steeb & Diebels* [127] and *Steeb et al.* [128], where erosion processes are examined under isothermal conditions. \square

As the mass production $\hat{\rho}^L$ can take arbitrary values, the terms in parenthesis of relation (3.78) have to vanish to ensure the entropy inequality to be fulfilled for any case, i. e.,

$$\boxed{\xi^L - \eta^L(\theta^S - \theta^L) + \frac{1}{2} \mathbf{w}_L \cdot \mathbf{w}_L = \xi^V - \eta^V(\theta^S - \theta^G) + \frac{1}{2} \mathbf{w}_V \cdot \mathbf{w}_V,} \quad (3.79)$$

where the *Gibbs* free enthalpies are introduced via

$$\xi^L(\theta, p^{LR}) := \psi^L + \frac{p^{LR}}{\rho^{LR}} \quad \text{and} \quad \xi^V(\theta, p_G^V) := \psi^V + \frac{p_G^V}{\rho_G^V}. \quad (3.80)$$

This means, mass interactions between the liquid and gaseous pore water can only occur, if relation (3.79) is fulfilled. Furthermore, in the thermomechanical equilibrium ($\theta^\alpha = \theta$ and $\mathbf{w}_L = \mathbf{w}_V = \mathbf{0}$), liquid and gaseous water have the same *Gibbs* free enthalpies, $\xi^L = \xi^V$. This condition can be found in the literature of technical thermodynamics as well, cf. *Baehr* [5]. Thus, liquid and gaseous pore water can only coexist, if condition (3.79) is fulfilled

Relation (3.79) has to hold as well, if no capillary effects are considered ($s^L = 0$), the overall pore gas consists only of water vapor ($\rho_G^A = 0$) and under the assumption of a rigid solid skeleton ($n^F = \text{const.}$). Therefore, relation (3.79) could be reduced to a further

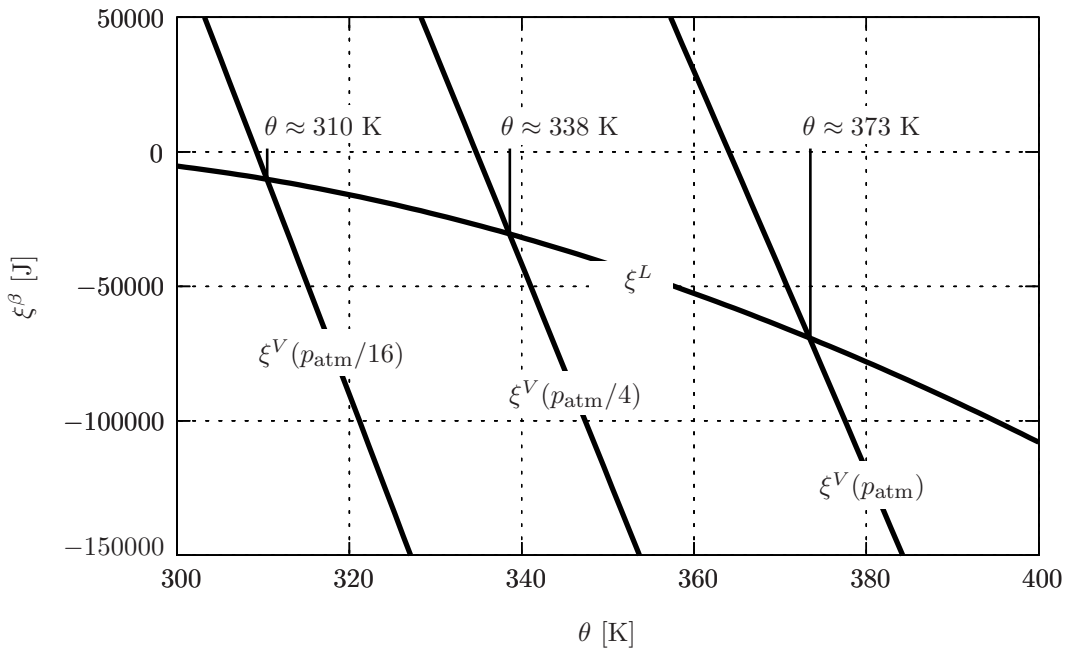


Figure 3.5: The *Gibbs* free enthalpies of liquid and gaseous water for three different existing pressures.

condition between the process variables ρ_G^V (or the pressure p_G^V) and the temperatures θ^α . Thus, if both liquid and gaseous pore water coexist, the partial density ρ_G^V (or the partial pressure p_G^V) loses the character of a process variable.

If no air component and no capillary effects are taken into account, the whole system is governed by one overall effective pressure p^{WR} . In Figure 3.5, the *Gibbs* free enthalpies of liquid and gaseous water, which are based on the definitions of the free *Helmholtz* energies (3.68) and (3.71) as well as relation (3.80), are given as a function of the temperature for different effective pressures, i. e., $p^{WR} = p_{atm}$, $p^{WR} = p_{atm}/4$ and $p^{WR} = p_{atm}/16$. Whereas the existing effective pressure has a strong influence on the water vapor's *Gibbs* free enthalpy, the influence of the effective pressure on the *Gibbs* free enthalpy of the liquid water is obviously negligible. Therefore, the three different *Gibbs* free enthalpies of the liquid pore water coincide in one curve. If the whole system is governed by atmospheric pressure, the *Gibbs* free enthalpies take the same value for $\theta \approx 373$ K, which represents the vaporization temperature of water at atmospheric pressure. The other temperature values, which were found for the pressures $p^{WR} = p_{atm}/4$ and $p^{WR} = p_{atm}/16$ agree very well with values found in the literature, cf. *Abbott & van Ness* [1], as well. Furthermore, it is obvious that the difference $\xi^V - \xi^L$ of the *Gibbs* free enthalpies is greater zero, if the temperature is lower than the vaporization temperature, i. e., only liquid water is present. If the difference $\xi^V - \xi^L$ of the *Gibbs* free enthalpies is lower than zero, the temperature is higher than the vaporization temperature and only water vapor exists.

The situation is a little bit different, if the overall gas phase consists of more than one component, e. g., water vapor and air. If both the liquid and the gas phase coexists, i. e., $0 < s^L < 1$, water vapor can exist within the overall gas phase, if the temperature is lower than the vaporization temperature corresponding to the dominating overall effective

pressure as well, because the pressure difference between the overall effective gas pressure and the partial pressure of the water vapor within the overall gas phase is balanced by the partial pressure of the air component within the overall gas phase. In this case, the partial pressure of the water vapor within the overall gas phase has to be determined in such a way that the *Gibbs* free enthalpies of the liquid and gaseous water are equal depending on the predominating temperature.

Thus, the whole process can be generalized and summarized in the following way:

$$\left. \begin{array}{l} s^L = 1 \quad \text{and} \\ \xi^L - \eta^L(\theta^S - \theta^L) + \frac{1}{2} \mathbf{w}_L \cdot \mathbf{w}_L - \\ \quad - [\xi^V - \eta^V(\theta^S - \theta^G) + \frac{1}{2} \mathbf{w}_V \cdot \mathbf{w}_V] > 0 \end{array} \right\} \hat{\rho}^L = 0 \\
 \left. \begin{array}{l} 0 \leq s^L \leq 1 \quad \text{and} \\ \xi^L - \eta^L(\theta^S - \theta^L) + \frac{1}{2} \mathbf{w}_L \cdot \mathbf{w}_L - \\ \quad - [\xi^V - \eta^V(\theta^S - \theta^G) + \frac{1}{2} \mathbf{w}_V \cdot \mathbf{w}_V] = 0 \end{array} \right\} \hat{\rho}^L \neq 0 \quad (3.81) \\
 \left. \begin{array}{l} s^L = 0 \quad \text{and} \\ \xi^L - \eta^L(\theta^S - \theta^L) + \frac{1}{2} \mathbf{w}_L \cdot \mathbf{w}_L - \\ \quad - [\xi^V - \eta^V(\theta^S - \theta^G) + \frac{1}{2} \mathbf{w}_V \cdot \mathbf{w}_V] < 0 \end{array} \right\} \hat{\rho}^L = 0$$

The vaporization curve: Based on (3.79), a relation for the vaporization curve, cf. Figure 3.4, can be derived. Building the differential of (3.79), assuming thermomechanical equilibrium and taking into account the definition (3.53) of the capillary pressure, relation (3.50) for the overall gas pressure as well as the definitions of the free *Helmholtz* energies and the entropies of a materially incompressible and a materially compressible fluid constituent yields

$$(\eta^V - \eta^L) d\theta = \left(\frac{1}{\rho_G^V} - \frac{1}{\rho^{LR}} \right) dp_{G\text{sat}}^V - \frac{1}{\rho^{LR}} dp_G^A, \quad (3.82)$$

where $p_{G\text{sat}}^V$ indicates the saturated partial water vapor pressure within the overall gas phase. If the overall pore gas is only governed by water vapor, i. e., $p_G^A = 0$, (3.82) can be solved for the slope of the vaporization curve:

$$\frac{dp_{G\text{sat}}^V}{d\theta} = \frac{\eta^V - \eta^L}{1/\rho_G^V - 1/\rho^{LR}}. \quad (3.83)$$

This equation is well-known as *Clausius-Clapeyron* equation. Furthermore, by an introduction of the enthalpy $\zeta(\eta, p)$ as a further energy measure formulated in the process variables entropy and pressure,

$$\zeta^L(\eta^L, p^{LR}) = \psi^L + \theta\eta^L + \frac{p^{LR}}{\rho^{LR}} \quad \text{and} \quad \zeta^V(\eta^V, p_G^V) = \psi^V + \theta\eta^V + \frac{p_G^V}{\rho_G^V}, \quad (3.84)$$

the entropy difference $\Delta\eta^{VL} = \eta^V - \eta^L$ between the two phases, also known as the standard entropy change of vaporization, can be reformulated using (3.79):

$$\Delta\eta^{VL} = \frac{1}{\theta}(\zeta^V - \zeta^L) = \frac{\Delta\zeta^{VL}}{\theta}. \quad (3.85)$$

Therein, $\Delta\zeta^{VL} = \zeta^G - \zeta^L$ is introduced as the standard enthalpy change of vaporization. The combination of (3.83) and (3.85) as well as the introduction of the specific volume difference $\Delta\nu^{VL} = 1/\rho_G^V - 1/\rho^{LR}$ yields

$$\frac{dp_{Gsat}^V}{d\theta} = \frac{\Delta\zeta^{VL}}{\theta\Delta\nu^{VL}}, \quad (3.86)$$

which is the most used form of the *Clausius-Clapeyron* equation [25, 29].

Taking into account that the specific volume ν^{LR} of the liquid is negligible in comparison to the specific volume ν_G^V of the water vapor ($\rho^{LR} \approx 1000.0 \rho_G^V$), that the standard enthalpy change of vaporization $\Delta\zeta^{VL}$ is constant and that the vapor can be described as an ideal gas, relation (3.82) in combination with (3.85) can be integrated and reformulated yielding

$$\ln\left(\frac{p_{Gsat}^V}{p_0}\right) = C_1 - \frac{C_2}{\theta}, \quad (3.87)$$

where C_1 and C_2 are two material parameters. Note that this relation is only valid within a small region of the vaporization curve at low pressures. A more accurate approximation of the vaporization curve is given via a formulation following *Antoine* [3]:

$$\ln\left(\frac{p_{Gsat}^V}{p_0}\right) = C_1 - \frac{C_2}{\theta - C_3}. \quad (3.88)$$

Therein, the three constants C_1 , C_2 and C_3 can be used to describe the respective component, whereas $p_0 = 1 \text{ mmHg} = 133.322 \text{ Pa}$, i. e., p_0 corresponds to the pressure of a mercury column of one millimeter height. In the literature, the *Antoine* equation is generally given based on the common logarithm. Thus, the saturation pressure can be computed via

$$p_{Gsat}^V(\theta) = p_0 \cdot 10^{(C_1 - \frac{C_2}{\theta - C_3})}, \quad (3.89)$$

whereas, e. g., for the water component the constants take the values $C_1 = 8.07131$, $C_2 = 1730.63 \text{ K}$, $C_3 = -39.574 \text{ K}$, cf. *Class* [26].

In this case, the partial pressure of the water vapor depends not on the whole set of process variables but only on the predominating temperature. Thus, (3.81) can be simplified:

$$\begin{array}{lll} s^L = 1 & \text{and } p^{LR} > p_{Gsat}^V(\theta) & \longrightarrow \hat{\rho}^L = 0, \\ 0 \leq s^L \leq 1 & \text{and } p_G^V = p_{Gsat}^V(\theta) & \longrightarrow \hat{\rho}^L \neq 0, \\ s^L = 0 & \text{and } p_G^V < p_{Gsat}^V(\theta) & \longrightarrow \hat{\rho}^L = 0. \end{array} \quad (3.90)$$

As the partial density ρ_G^V of the water vapor has to be determined in such a way that the *Gibbs* free enthalpies of the liquid and gaseous water are equal, the partial density loses the character of a process variable, if mass interactions occur. This means, the mass balance of the water vapor cannot be used to determine the time derivative of the partial density of the water vapor but to compute the mass interaction:

$$\begin{aligned} \hat{\rho}^L &= -\hat{\rho}_{\text{ext}}^V = -[(\rho^V)'_V + \rho^V \text{div } \dot{\mathbf{x}}_V] \\ &= -\{ [s^G n^F \rho_G^V(\theta)]'_S + s^G n^F \rho_G^V(\theta) \text{div } \dot{\mathbf{x}}_S + \\ &\quad + \text{div} [s^G n^F \rho_G^V(\theta) \mathbf{w}_V] \}. \end{aligned} \quad (3.91)$$

The heating process of a porous material at constant pressure: In the following, the heating process of a porous material at a constant overall effective gas pressure $p^{GR} = p_0$ is discussed, where the pore space is filled with pore water, water vapor and air building together the overall gas phase. The initial temperature is assumed to be θ_1 . The partial pressure p_G^V of the water vapor within the overall gas phase equals the saturated partial water vapor pressure $p_{G\text{sat}}^V$, which has to be computed in such a way that condition (3.79) is fulfilled. Furthermore, the sum of the partial pressures of the gas components yields the overall effective gas pressure:

$$p^{GR} = p_G^V + p_G^A = p_0, \quad \text{where } p_G^V = p_{G\text{sat}}^V(\theta), \quad (3.92)$$

cf. Figure 3.6. The partial pressure p_G^A decreases in the same way as the partial pressure p_G^V increases, if the temperature is increased ($\theta = \theta_2$), because the overall effective gas pressure p^{GR} is fixed via boundary conditions.

If the saturated partial water vapor pressure equals the boundary condition during further heating ($\theta = \theta_3$), the overall gas phase is only governed via the water vapor, because the partial pressure of the air within the overall gas phase is zero. Therefore, the overall

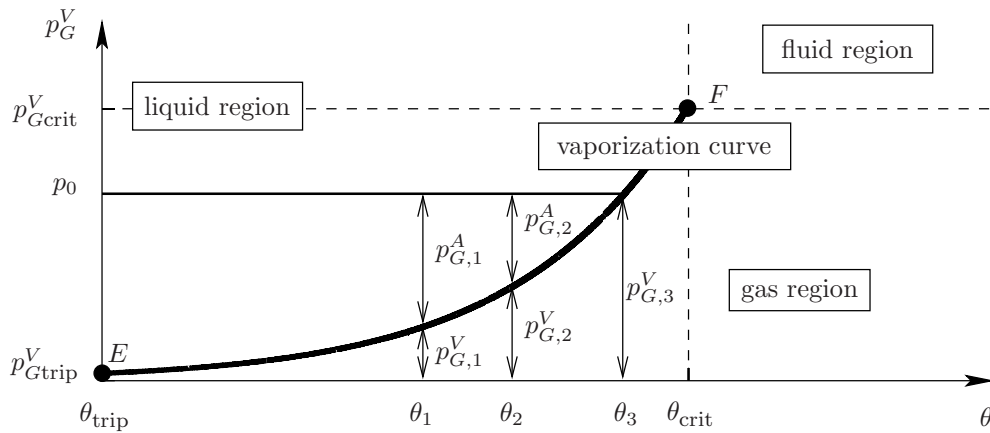


Figure 3.6: Development of the partial vapor pressure during a heating process.

effective gas pressure p^{GR} equals the saturated partial water vapor pressure and is, consequently, directly coupled with the dominating temperature. This means, the temperature is fixed at a certain value as long as the partial water vapor pressure is a function of the temperature. This is the case as long as mass interactions occur, i. e., as long as liquid water exists in the pore space:

$$s^L > 0 : \quad p^{GR} = p_G^V(\theta) = p_{G\text{sat}}^V(\theta) = p_0 = \text{const.} \quad \longrightarrow \quad \theta = \text{const.} \quad (3.93)$$

In a next step, a closer look is taken on the energy balance of the overall porous material, which loses the character of a governing equation for the temperature as long as the temperature of the porous material is constant. Assuming a rigid solid skeleton, a homogeneous temperature distribution ($\text{grad } \theta^\alpha = \mathbf{0}$) as well as a negligible stress power of the pore fluids and a negligible dependency of the internal energy of the liquid pore water on the saturation, the energy balance of the overall porous material yields for constant temperature

$$\left\{ \hat{\rho}^L \left[(\varepsilon^L + \frac{1}{2} \mathbf{w}_L \cdot \mathbf{w}_L) - (\varepsilon^V + \frac{1}{2} \mathbf{w}_V \cdot \mathbf{w}_V) \right] - \rho r \right\} \Big|_{\theta=\text{const.}} = 0, \quad (3.94)$$

where

$$\varepsilon^L(\theta = \text{const.}) = \text{const.} \quad \text{and} \quad \varepsilon^V(\theta = \text{const.}) = \text{const.} \quad (3.95)$$

Furthermore, in porous materials the kinetic energy of the pore fluids is negligible in comparison with the internal energy so that (3.94) can be reduced to

$$\left\{ \hat{\rho}^L (\varepsilon^L - \varepsilon^V) - \rho r \right\} \Big|_{\theta=\text{const.}} = 0, \quad \text{where} \quad \varepsilon^L - \varepsilon^V = \text{const.} \quad (3.96)$$

Assuming that the heat load is applied via the radiation r and taking into account that the internal energy of the water vapor is greater than of liquid water,

$$\Delta\varepsilon^{VL} = \varepsilon^V - \varepsilon^L = \text{const.} > 0, \quad (3.97)$$

it is obvious that the energy balance drives the mass production ($\theta = \text{const.}$):

$$\hat{\rho}^L = -\frac{\rho r}{\Delta\varepsilon^{VL}} \quad \longrightarrow \quad \begin{cases} r > 0 \text{ (heating)} : & \hat{\rho}^L < 0 \text{ (vaporization)}, \\ r < 0 \text{ (cooling)} : & \hat{\rho}^L > 0 \text{ (condensation)}. \end{cases} \quad (3.98)$$

Thus, it could be shown by the above given argumentation that the whole phase transition process of a pure component, like, e. g., water, is driven by the coupled system of equations consisting of the respective mass and energy balances extended by condition (3.79), which ensures the equality of their respective *Gibbs* free enthalpies, if mass interactions occur. In particular, the mass balances are responsible, besides the conservation of mass, for fixing the temperature to the vaporization temperature in dependency of the dominating effective pressure. If the temperature is, therefore, fixed to a constant value, the only free variable within the energy balances is the mass production term $\hat{\rho}^L$. Therefore, applying a further heat load, the energy balances can only be fulfilled, if the mass production term takes a certain value.

Furthermore, as the temperature is constant, the partial density of the water vapor is constant as well. Thus, relation (3.91) yields

$$\hat{\rho}^L = \frac{\partial s^L}{\partial t} n^F \rho_G^V - \operatorname{div}(s^G n^F \rho_G^V \mathbf{w}_V). \quad (3.99)$$

Inserting (3.99) into (3.98), the local time derivative of the saturation yields

$$\frac{\partial s^L}{\partial t} = \frac{1}{n^F \rho_G^V} \left[-\frac{\rho r}{\Delta \varepsilon^{VL}} + \operatorname{div}(s^G n^F \rho_G^V \mathbf{w}_V) \right]. \quad (3.100)$$

Therefore, it is obvious that under constant temperature conditions the mass production results directly in a volume production governed by a change of the saturation.

3.2.3 Momentum productions

In a next step, constitutive relations for the momentum production terms of the pore fluids are derived. Therefore, firstly, a relation for the seepage velocity of a materially incompressible fluid constituent is discussed. In a second step, it is shown that a summation over the momentum balances of the materially compressible gas components yields the momentum balance of the overall pore gas, which results in the same relation for the seepage velocity as in case of a materially incompressible pore fluid. Furthermore, as the terms, which vanish during this summation are responsible for the momentum interaction within the overall gas phase, a relation for the diffusion velocity $\mathbf{d}_{\gamma G}$ can be derived by taking a closer look at these terms.

The materially incompressible pore fluid constituent: The momentum balance of a materially incompressible pore fluid φ^ξ is given by (3.1)₂:

$$\rho^\xi \mathbf{x}_\xi'' = \operatorname{div} \mathbf{T}^\xi + \rho^\xi \mathbf{b} + \hat{\mathbf{p}}^\xi. \quad (3.101)$$

Therein, the momentum production $\hat{\mathbf{p}}^\xi$ is given following (3.46)₁, which can be reformulated using (3.48)

$$\begin{aligned} \hat{\mathbf{p}}^\xi &= \mathcal{P} \operatorname{grad} n^\xi + s^\xi \frac{\theta^S}{\theta^\xi} \rho_F^\xi \frac{\partial \psi^\xi}{\partial s^\xi} \operatorname{grad} n^F + \mathbf{p}_{E \text{ mech}}^\xi \\ &= \mathcal{P} (n^F \operatorname{grad} s^\xi + s^\xi \operatorname{grad} n^F) + s^\xi \frac{\theta^S}{\theta^\xi} \rho_F^\xi \frac{\partial \psi^\xi}{\partial s^\xi} \operatorname{grad} n^F + \mathbf{p}_{E \text{ mech}}^\xi \\ &= \mathcal{P} n^F \operatorname{grad} s^\xi + \underbrace{\operatorname{grad} n^F s^\xi \left(\mathcal{P} + \frac{\theta^S}{\theta^\xi} \rho_F^\xi \frac{\partial \psi^\xi}{\partial s^\xi} \right)}_{= \theta^S / \theta^\xi p^{\xi R}} + \mathbf{p}_{E \text{ mech}}^\xi \\ \hat{\mathbf{p}}^\xi &= \mathcal{P} n^F \operatorname{grad} s^\xi + \operatorname{grad} n^F \frac{\theta^S}{\theta^\xi} s^\xi p^{\xi R} + \mathbf{p}_{E \text{ mech}}^\xi. \end{aligned} \quad (3.102)$$

According to the argumentation of *Ehlers et al.* [55], the mechanical extra stress $\mathbf{T}_{E \text{ mech}}^\xi$ of the pore fluids is negligible in comparison with the mechanical extra momentum production $\mathbf{p}_{E \text{ mech}}^\xi$. Therefore, incorporating (3.102) into (3.101) and using furthermore relation

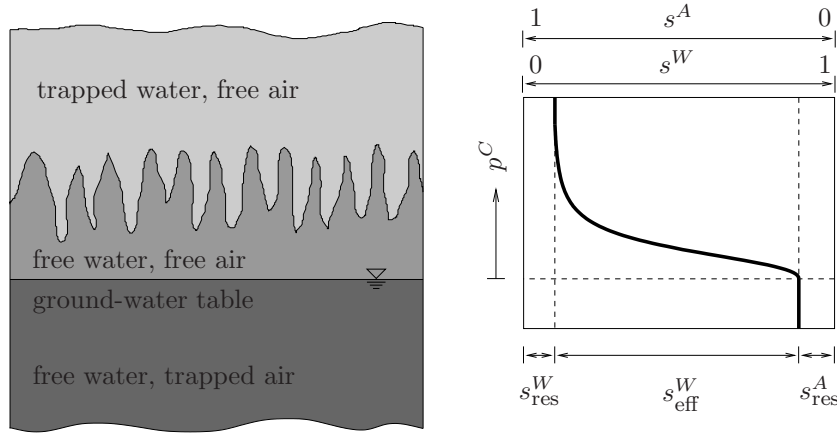


Figure 3.7: Vertical cut through a partially saturated natural soil.

(3.47)₂ for the *Cauchy* stress tensor of the pore liquids yields under consideration of quasi-static conditions ($\mathbf{x}_\xi = \mathbf{0}$)

$$\begin{aligned}
 -\hat{\mathbf{p}}_{E\text{mech}}^\xi &= \text{div}(-n^\xi p^{\xi R} \mathbf{I}) + \rho^\xi \mathbf{b} + \text{grad} n^F \frac{\theta^S}{\theta^\xi} s^\xi p^{\xi R} + \mathcal{P} n^F \text{grad} s^\xi \\
 &= -n^\xi \text{grad} p^{\xi R} + n^\xi \rho^{\xi R} \mathbf{b} - p^{\xi R} \text{grad} n^\xi + \\
 &\quad + \text{grad} n^\xi \frac{\theta^S}{\theta^\xi} p^{\xi R} + n^F \left(\mathcal{P} - \frac{\theta^S}{\theta^\xi} p^{\xi R} \right) \text{grad} s^\xi \tag{3.103} \\
 -\hat{\mathbf{p}}_{E\text{mech}}^\xi &= -n^\xi \left\{ \text{grad} p^{\xi R} - \rho^{\xi R} \mathbf{b} - p^{\xi R} \left[\frac{1}{n^\xi} \text{grad} n^\xi \left(\frac{\theta^S}{\theta^\xi} - 1 \right) \right] - \right. \\
 &\quad \left. - \frac{1}{s^\xi} \left(\mathcal{P} - \frac{\theta^S}{\theta^\xi} p^{\xi R} \right) \text{grad} s^\xi \right\}.
 \end{aligned}$$

At this point, a constitutive relation for the mechanical extra momentum production is introduced following *Ehlers* [46] via

$$\boxed{\hat{\mathbf{p}}_{E\text{mech}}^\xi = -\mathbf{S}_\xi \mathbf{w}_\xi = - (n^\xi)^2 \gamma^{\xi R} (\kappa_r^\xi \mathbf{K}^\xi)^{-1} \mathbf{w}_\xi.} \tag{3.104}$$

Therein, $\gamma^{FR} = \rho^{FR} |\mathbf{b}|$ is the specific weight, \mathbf{K}^ξ is the *Darcy* permeability tensor measured under fully-saturated conditions and κ_r^ξ is introduced as a so-called relative permeability factor, cf. *Brooks & Corey* [21] or *van Genuchten* [76] as well as *Burdine* [23] and *Mualem* [109].

Using this relative permeability factor, a special behavior of a multiphasic flow process can be described. Taking a closer look at a porous material with two pore fluids, generally, three different domains can be distinguished, whereby the borders are runny. In one domain, one fluid can stream freely, whereas the other is trapped with a residual saturation s_{res}^β . In a second domain, the situation is vice versa. Between these two areas, both fluids can stream, but, due to a strong interaction, the velocity is lower than under fully saturated conditions. This fact is exemplary shown in Figure 3.7 for a partially

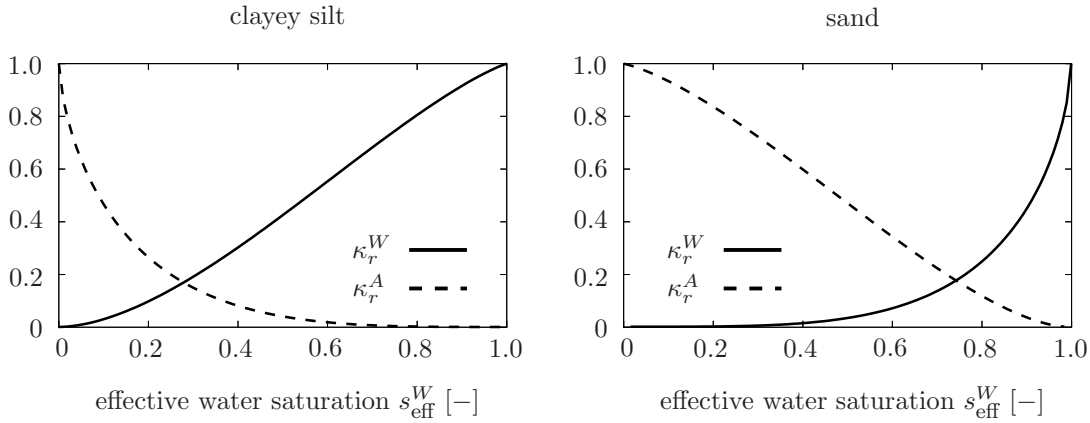


Figure 3.8: Typical relations for the relative permeability factors of a clayey silt and a sand.

saturated soil with the pore fluids water and air. With the relative permeability factor, the permeability, measured under fully saturated conditions, is weighted as far as the permeability is zero for the respective residual saturation. It is obvious that the effective saturation describing the saturation between the two residual saturations of the pore fluids is the suitable variable, in which the relative permeability factor has to be formulated.

In Figure 3.8, typical relations for the relative permeability factors of the pore fluids water and air in a clayey silt and in a sand are given following the formulation by *van Genuchten* [76] and corresponding to the capillary pressure saturation relations given in Figure 3.1. Considering, e. g., the pore water, it is obvious that if the effective water saturation

$$s_{\text{eff}}^W = \frac{s^W - s_{\text{res}}^W}{1 - s_{\text{res}}^W - s_{\text{res}}^A} \quad (3.105)$$

tends to one, the relative permeability factor of the pore water tends towards one as well, and, thus, the overall permeability of the pore water tends to the permeability measured under fully saturated conditions. On the other hand, if the effective water saturation tends to zero, the relative permeability factor tends to zero, and thus, the overall permeability as well as the seepage velocity of the pore water tends to zero, i. e., the pore water is trapped within the porous material. The situation is just vice versa for the pore air.

Following *Ehlers* [46], a relation between the *Darcy* permeability and the so-called intrinsic permeability \mathbf{K}^S , which is a pure permeability measure of the solid skeleton, is in general given via

$$\mathbf{K}^\xi = \frac{\gamma^{\xi R}}{\mu^{\xi R}} \mathbf{K}^S, \quad (3.106)$$

where $\mu^{\xi R}$ is the shear viscosity of the considered pore liquid.

Considering furthermore a deformable solid skeleton, it is obvious that the intrinsic permeability depends on the deformation of the solid phase. Therefore, proceeding from a fully isotropic material behavior, a relation following *Eipper* [67],

$$\mathbf{K}^S = \left(\frac{1 - n^S}{1 - n_{0S}^S} \right)^\pi K_{0S}^S \mathbf{I} = \left(\frac{n^F}{n_{0S}^F} \right)^\pi K_{0S}^S \mathbf{I}, \quad (3.107)$$

particle size		coefficient of Darcy permeability	
		k^F [10^{-4} cm/s]	k^F [m/s]
sand	coarse	3000 – 5000	$3 - 5 \cdot 10^{-3}$
	medium	1000	$1 \cdot 10^{-3}$
	fine	50 – 150	$5 \cdot 10^{-5} - 1.5 \cdot 10^{-4}$
silt	coarse, sandy	1 – 20	$1 \cdot 10^{-6} - 2 \cdot 10^{-5}$
	medium	0.1 – 1	$1 \cdot 10^{-7} - 1 \cdot 10^{-6}$
	fine, clayey	0.01 – 0.1	$1 \cdot 10^{-8} - 1 \cdot 10^{-7}$
clay	coarse, silty	0.001 – 0.01	$1 \cdot 10^{-9} - 1 \cdot 10^{-8}$
	medium	0.0001 – 0.001	$1 \cdot 10^{-10} - 1 \cdot 10^{-9}$
	fine, colloidal	0.00001 – 0.0001	$1 \cdot 10^{-11} - 1 \cdot 10^{-10}$

Table 3.2: Darcy permeability for different natural soils following *Cernica* [24].

can be introduced, wherein the referential and the current intrinsic permeability are related to each other via the ratio of the referential, n_{0S}^F , and current, n^F , porosity. Therein, K_{0S}^S is the intrinsic permeability in the reference configuration and π is an additional material parameter. The intrinsic permeability K_{0S}^S of natural soils can be estimated by several relations, cf. *Bear* [7], which are based, e. g., on the effective grain diameter d_{10} . Estimations for the Darcy permeability factor of soils can be obtained, e. g., from *Cernica* [24], cf. Table 3.2. The reader, who is interested in the description of anisotropic permeability behavior of porous materials is referred to *Markert* [108].

Using relation (3.104), it is obvious that if the permeability tensor \mathbf{K}^ξ is positive definite, \mathbf{S}_ξ is positive definite as well and the entropy inequality (3.43) is fulfilled. Inserting (3.104) into (3.103) results in a relation for the filter velocity $n^\xi \mathbf{w}_\xi$ of an individual materially incompressible pore fluid:

$$\begin{aligned}
 n^\xi \mathbf{w}_\xi = & -\frac{\kappa_r^\xi \mathbf{K}^\xi}{\gamma^{\xi R}} \left\{ \text{grad } p^{\xi R} - \rho^{\xi R} \mathbf{b} - p^{\xi R} \left[\frac{1}{n^\xi} \text{grad } n^\xi \left(\frac{\theta^S}{\theta^\xi} - 1 \right) \right] - \right. \\
 & \left. - \frac{1}{s^\xi} \left(\mathcal{P} - \frac{\theta^S}{\theta^\xi} p^{\xi R} \right) \text{grad } s^\xi \right\}.
 \end{aligned} \tag{3.108}$$

Note that for isothermal ($\theta^\alpha = \theta$) and fully saturated ($s^\xi = 1$) conditions, (3.108) reduces to the well-known relation for the seepage velocity of biphasic materials, cf. *Ehlers* [46], which conforms to the Darcy law derived from experimental tests, cf. *Darcy* [33].

Regarding the realization of experimental tests for the determination of the relative permeability factor for a certain fluid in a porous material, one has to consider that the seepage velocity is measured for a defined, homogeneous saturation distribution of the test specimen and a certain pressure gradient. Therefore, the relative permeability factor

belonging to a specific saturation is computed via the one-dimensional relation

$$\kappa_r^\xi = -\frac{n^\xi w_\xi \gamma^{\xi R}}{K^\xi} \frac{\Delta x}{\Delta p^{\xi R}}. \quad (3.109)$$

Thus, it is obvious that the effects resulting from a saturation gradient are not included within the measured relation for κ_r^ξ . Therefore, the last term in (3.108) is neglected in the following, and one finds finally

$$\boxed{n^\xi \mathbf{w}_\xi = -\frac{\kappa_r^\xi \mathbf{K}^\xi}{\gamma^{\xi R}} \left\{ \text{grad } p^{\xi R} - \rho^{\xi R} \mathbf{b} - p^{\xi R} \left[\frac{1}{n^\xi} \text{grad } n^\xi \left(\frac{\theta^S}{\theta^\xi} - 1 \right) \right] \right\}. \quad (3.110)}$$

The materially compressible pore gas components: Taking a closer look on the materially compressible fluid constituents, the momentum balance (3.1)₂ yields in combination with (3.46)₃, (3.47)₃ as well as (3.50)

$$\begin{aligned} \rho^\gamma \ddot{\mathbf{x}}_\gamma &= -x_{Gm}^\gamma p^{GR} \text{grad } n^G - n^G p^{GR} \text{grad } x_{Gm}^\gamma - n^G x_{Gm}^\gamma \text{grad } p^{GR} + \\ &+ \rho^\gamma \mathbf{b} + \hat{\mathbf{p}}_{\text{ext}}^\gamma + \hat{\mathbf{p}}_{\text{int}}^\gamma, \end{aligned} \quad (3.111)$$

where it is taken into account that the mechanical extra stress $\mathbf{T}_{E\text{mech}}^\gamma$ of the gas components is negligible in comparison with the mechanical extra momentum production $\mathbf{p}_{E\text{mech}}^\gamma$, cf. [55]. Furthermore, the momentum balance of the overall gas phase can be computed via a summation over the momentum balances of all gas components:

$$\begin{aligned} \sum_\gamma \rho^\gamma \ddot{\mathbf{x}}_\gamma &= -p^{GR} \text{grad } n^G \sum_\gamma x_{Gm}^\gamma - n^G p^{GR} \sum_\gamma \text{grad } x_{Gm}^\gamma - \\ &- n^G \text{grad } p^{GR} \sum_\gamma x_{Gm}^\gamma + \mathbf{b} \sum_\gamma \rho^\gamma + \sum_\gamma \hat{\mathbf{p}}_{\text{ext}}^\gamma + \sum_\gamma \hat{\mathbf{p}}_{\text{int}}^\gamma \\ \sum_\gamma \rho^\gamma \ddot{\mathbf{x}}_\gamma &= \text{div}(-n^G p^{GR} \mathbf{I}) + \rho^G \mathbf{b} + \hat{\mathbf{p}}^G + \hat{\rho}^G \dot{\mathbf{x}}_G - \sum_\gamma \hat{\rho}_{\text{ext}}^\gamma \dot{\mathbf{x}}_\gamma \\ \rho^G \ddot{\mathbf{x}}_G &= \text{div} \sum_\gamma (\mathbf{T}^\gamma - \rho^\gamma \mathbf{d}_{\gamma G} \otimes \mathbf{d}_{\gamma G}) + \rho^G \mathbf{b} + \hat{\mathbf{p}}^G \\ \rho^G \ddot{\mathbf{x}}_G &= \text{div } \mathbf{T}^G + \rho^G \mathbf{b} + \hat{\mathbf{p}}^G. \end{aligned} \quad (3.112)$$

Thereby, use is made of the relations (2.66)₂, (2.67) and (3.20). Incorporating (3.46)₂ into (3.112)₃ results under the assumption of quasi-static conditions ($\ddot{\mathbf{x}}_\alpha = \mathbf{0}$) in

$$\mathbf{0} = \text{div}(-n^G p^{GR} \mathbf{I}) + \rho^G \mathbf{b} + \mathcal{P} \text{grad } n^G + \hat{\mathbf{p}}_E^G. \quad (3.113)$$

This relation is equal to the momentum balance of a materially incompressible fluid constituent, cf. (3.101) and (3.102), under consideration that the free *Helmholtz* energy

of the gaseous constituents is independent of the saturation. Therefore, the relation for the filter velocity $n^G \mathbf{w}_G$ yields finally

$$\boxed{n^G \mathbf{w}_G = -\frac{\kappa_r^G \mathbf{K}^G}{\gamma^{GR}} \left\{ \text{grad } p^{GR} - \rho^{GR} \mathbf{b} - p^{GR} \left[\frac{1}{n^G} \text{grad } n^G \left(\frac{\theta^S}{\theta^G} - 1 \right) \right] \right\}}, \quad (3.114)$$

which corresponds to relation (3.110). To ensure the entropy inequality (3.43), the relation

$$-\sum_{\gamma} (\hat{\mathbf{p}}_{\text{ext}E}^{\gamma} \cdot \mathbf{d}_{\gamma G}) \geq 0 \quad (3.115)$$

must hold. Proceeding from (3.46)₃ and incorporating (3.20)₂ as well as (3.46)₂ yields

$$\sum_{\gamma} \hat{\mathbf{p}}_{\text{ext}E}^{\gamma} = \hat{\mathbf{p}}_E^G. \quad (3.116)$$

Due to the fact that the linear momentum is governed by the density, it is assumed that the external momentum production $\hat{\mathbf{p}}_{\text{ext}E}^{\gamma}$ of the individual gas components is given by the momentum production $\hat{\mathbf{p}}_E^G$ of the overall gas phase weighted by the mass concentration c_G^{γ} :

$$\hat{\mathbf{p}}_{\text{ext}E}^{\gamma} = \hat{\mathbf{p}}_E^G c_G^{\gamma} \quad \longrightarrow \quad -\hat{\mathbf{p}}_E^G \cdot \sum_{\gamma} c_G^{\gamma} \mathbf{d}_{\gamma G} \geq 0. \quad (3.117)$$

Generally, the velocity of the overall porous material is given by the sum of the velocities of its constituents weighted by the partial densities, cf. (2.21). Thus, a relation between the seepage velocity \mathbf{w}_G of the gas phase and the seepage velocities \mathbf{w}_{γ} of the gas components can be found:

$$n^G \rho^{GR} \mathbf{w}_G = \sum_{\gamma} n^G \rho_G^{\gamma} \mathbf{w}_{\gamma} \quad \longrightarrow \quad \rho^{GR} \mathbf{w}_G = \sum_{\gamma} \rho_G^{\gamma} \mathbf{w}_{\gamma}. \quad (3.118)$$

Furthermore, this relation can be reformulated using the definition of the diffusion velocity (2.26)₃,

$$\rho^{GR} \mathbf{w}_G = \sum_{\gamma} \rho_G^{\gamma} \mathbf{w}_{\gamma} = \sum_{\gamma} \rho_G^{\gamma} (\mathbf{w}_G + \mathbf{d}_{\gamma G}) = \rho^{GR} \mathbf{w}_G + \sum_{\gamma} \rho_G^{\gamma} \mathbf{d}_{\gamma G}, \quad (3.119)$$

and, therefore, one finds finally:

$$\sum_{\gamma} \rho_G^{\gamma} \mathbf{d}_{\gamma G} = \sum_{\gamma} c_G^{\gamma} \mathbf{d}_{\gamma G} = \mathbf{0}. \quad (3.120)$$

Thus, it follows that

$$-\hat{\mathbf{p}}_E^G \cdot \sum_{\gamma} c_G^{\gamma} \mathbf{d}_{\gamma G} = 0. \quad (3.121)$$

The diffusion velocity of the gas components within the overall gas phase: At this point, the assumption is made that the terms describing the momentum interaction

between the individual gas components within the overall gas phase have to vanish during a summation over all gas components. Taking this into account, one finds proceeding from (3.112) that

$$\boxed{-\hat{\mathbf{p}}_{\text{int}}^{\gamma} = -n^G p^{GR} \text{grad } x_{Gm}^{\gamma}} \quad (3.122)$$

Therefore, it is obvious that the driving force for the momentum interaction between the individual gas components is given by the gradient of the molar fraction x_{Gm}^{γ} .

Remark: If no mass interactions between the fluid phases are taken into account, i. e., the total number of moles n_m^G is constant, relation (3.122) can be rewritten using (2.14):

$$-\hat{\mathbf{p}}_{\text{int}}^{\gamma} = -n^G \frac{p^{GR}}{c_{Gm}^{\gamma}} \text{grad } c_{Gm}^{\gamma}.$$

In this case, the driving force for the momentum interaction between the gas components is given by the gradient of the molar concentration c_{Gm}^{γ} , which agrees with *Fick's* first law, cf. *Fick* [70]. \square

Based on a formulation for the diffusion coefficient given in *Class* [26] and citations therein, a constitutive relation for $\hat{\mathbf{p}}_{\text{int}}^{\gamma}$ is introduced via

$$-\hat{\mathbf{p}}_{\text{int}}^{\gamma} = \mathbf{S}_{\gamma \text{int}} \mathbf{d}_{\gamma G} = (n^G)^2 (p^{GR})^2 (\rho_G^{\gamma} / \rho^{GR}) (p_0^{GR} d \mathbf{I})^{-1} \left(\frac{\theta^G}{\theta_0^G}\right)^{-z} \mathbf{d}_{\gamma G}, \quad (3.123)$$

where z is an additional material parameter and d is the binary diffusion coefficient measured under consideration of an overall gas phase with two components at the temperature θ_0^G and the pressure p_0^{GR} . Furthermore, it is ensured that $\mathbf{S}_{\gamma \text{int}}$ is a positive definite tensor, if d and p_0^{GR} take positive values. Therefore, with this constitutive relation the entropy inequality (3.43) is fulfilled. Finally, solving (3.122) for the diffusion velocity yields

$$\boxed{n^G \mathbf{d}_{\gamma G} = -\frac{\rho^{GR} p_0^{GR}}{\rho_G^{\gamma} p^{GR}} d \left(\frac{\theta^G}{\theta_0^G}\right)^z \text{grad } x_{Gm}^{\gamma}} \quad (3.124)$$

3.2.4 Direct energy productions

The total energy production $\hat{\varepsilon}^{\alpha}$ of a single constituent consists in general of three different parts, cf. Section 2.2.3. One part is governed by the product of the momentum production and the velocity and can therefore be interpreted as heat exchange due to frictional effects, a second part results from a possible mass in- or decrease, whereas the third part, the direct energy production $\hat{\varepsilon}^{\alpha}$, can be understood as the caloric interaction between the individual constituents, cf. *Ghadiani* [77].

Proceeding from the dissipation inequality (3.43), the constraint concerning the direct energy production terms is given via

$$-\sum_{\zeta} \hat{\varepsilon}^{\zeta} \left(1 - \frac{\theta^S}{\theta^{\zeta}}\right) = \sum_{\zeta} \frac{\hat{\varepsilon}^{\zeta}}{\theta^{\zeta}} (\theta^S - \theta^{\zeta}) \stackrel{!}{\geq} 0, \quad (3.125)$$

where

$$\hat{\varepsilon}^\zeta = \sum_{\alpha} k_{\theta^\alpha}^{\varepsilon\zeta} (\theta^\alpha - \theta) \quad (3.126)$$

results from Equation (3.61)₇. Thereby, the change of $\hat{\varepsilon}^\zeta$ with respect to θ^ζ , given by $k_{\theta^\zeta}^{\varepsilon\zeta}$, can be additively split into terms describing the change of $\hat{\varepsilon}^\zeta$ with respect to the temperatures of the other constituents:

$$\boxed{k_{\theta^\zeta}^{\varepsilon\zeta} = \sum_{\alpha \neq \zeta} k_{\theta^\alpha}^{\varepsilon\alpha\zeta}.} \quad (3.127)$$

Furthermore, the caloric interaction is driven by the temperature difference between two bodies, cf. *Grigull* [79]. Therefore, the negative change of $\hat{\varepsilon}^\zeta$ with respect to the temperature θ^α has to be equal to that part of the change of $\hat{\varepsilon}^\zeta$ with respect to the temperature θ^ζ describing the caloric interaction with the constituent φ^α :

$$\boxed{k_{\theta^\alpha}^{\varepsilon\zeta} = -k_{\theta^\zeta}^{\varepsilon\alpha\zeta}.} \quad (3.128)$$

Incorporating (3.127) and (3.128) into relation (3.126) yields

$$\begin{aligned} \hat{\varepsilon}^\zeta &= \sum_{\alpha} k_{\theta^\alpha}^{\varepsilon\zeta} (\theta^\alpha - \theta) = \sum_{\alpha \neq \zeta} k_{\theta^\alpha}^{\varepsilon\zeta} (\theta^\alpha - \theta) + \sum_{\alpha \neq \zeta} k_{\theta^\zeta}^{\varepsilon\alpha\zeta} (\theta^\zeta - \theta) \\ &= \sum_{\alpha \neq \zeta} (k_{\theta^\alpha}^{\varepsilon\zeta} \theta^\alpha - k_{\theta^\alpha}^{\varepsilon\zeta} \theta + k_{\theta^\zeta}^{\varepsilon\alpha\zeta} \theta^\zeta - k_{\theta^\zeta}^{\varepsilon\alpha\zeta} \theta) = \sum_{\alpha \neq \zeta} k_{\theta^\alpha}^{\varepsilon\zeta} (\theta^\alpha - \theta^\zeta). \end{aligned} \quad (3.129)$$

Considering exemplary a caloric interaction between the constituents φ^1 and φ^2 , it is obvious that the change of $\hat{\varepsilon}^1$ with respect to θ^2 has to be equal to the change of $\hat{\varepsilon}^2$ with respect to θ^1 . Thus, one can introduce the following variables

$$k_{S_n}^\varepsilon := k_{\theta^S}^{\varepsilon n}, \quad k_{mn}^\varepsilon := k_{\theta^m}^{\varepsilon n} = k_{\theta^n}^{\varepsilon m} = k_{nm}^\varepsilon, \quad (3.130)$$

where $m, n \in \zeta$ and $m \neq n$. Therefore, the direct energy production of the fluid constituent φ^n reads finally

$$\boxed{\hat{\varepsilon}^n = k_{S_n}^\varepsilon (\theta^S - \theta^n) + \sum_{m \neq n} k_{mn}^\varepsilon (\theta^m - \theta^n).} \quad (3.131)$$

Relation (3.125) results under the usage of (3.131) in

$$\sum_n \frac{\hat{\varepsilon}^n}{\theta^n} (\theta^S - \theta^n) = \sum_n \frac{k_{S_n}^\varepsilon}{\theta^n} (\theta^S - \theta^n)^2 + \sum_n \sum_{m \neq n} \frac{k_{mn}^\varepsilon}{\theta^n} (\theta^m - \theta^n) (\theta^S - \theta^n) \stackrel{!}{\geq} 0. \quad (3.132)$$

To check, if the second part of this relation is always greater than zero, it is assumed that the porous material φ consists of n constituents φ^n , where the solid skeleton is identified

via φ^1 . Therefore, (3.132) can be reformulated under consideration of (3.130) in the following way:

$$\begin{aligned} \sum_{i=2}^n \sum_{j \neq i}^n \frac{k_{ji}^\varepsilon}{\theta^i} (\theta^j - \theta^i) (\theta^S - \theta^i) &= \sum_{i=2}^n \sum_{j>i}^n k_{ji}^\varepsilon (\theta^j - \theta^i) \left(\frac{\theta^S - \theta^i}{\theta^i} - \frac{\theta^S - \theta^j}{\theta^j} \right) \\ &= \sum_{i=2}^n \sum_{j>i}^n k_{ji}^\varepsilon (\theta^j - \theta^i)^2 \frac{\theta^S}{\theta^j \theta^i} \geq 0. \end{aligned} \quad (3.133)$$

Therefore, it is obvious that the entropy inequality is fulfilled if the heat exchange coefficients

$$k_{S\zeta}^\varepsilon, k_{\pi\zeta}^\varepsilon \geq 0. \quad (3.134)$$

The heat exchange coefficients are given in the literature as surface-specific material parameters, but within the TPM, volume-specific quantities are required. Therefore, the surface-specific heat exchange coefficients, introduced at this point via $k_{S\zeta}^{\varepsilon S}$ and $k_{\pi\zeta}^{\varepsilon S}$, have to be transformed by certain relations to the volume-specific material parameters $k_{S\zeta}^{\varepsilon V}$ and $k_{\pi\zeta}^{\varepsilon V}$. Within this contribution, it is assumed that the contact area between the overall pore fluid phase and the solid skeleton can be described by the surface of a sphere, whereby the volume of the sphere is characterized by the radius r^F . The following discussion is exemplary given under consideration of two pore fluids, namely, pore water and an overall pore gas phase. The contact area between the pore gas and the solid phase is given via A^{SG} , the contact area between the pore water and the solid phase via A^{SL} and the contact area between the two pore fluid phases via A^{GL} , cf. Figure 3.9. These areas, the volume V^F of the whole sphere and the partial volumes V^β of the individual fluids can be computed based on the radius r^F as well as the fill height h^β via

$$V^F = \frac{4}{3}\pi(r^F)^3, \quad V^\beta = \frac{1}{3}\pi(h^\beta)^2(3r^F - h^\beta) \quad (3.135)$$

and

$$A^{S\beta} = 2\pi r^F h^\beta, \quad A^{GL} = \pi h^\beta(2r^F - h^\beta). \quad (3.136)$$

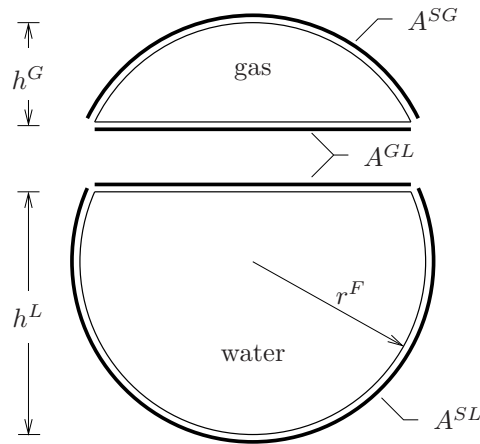


Figure 3.9: Surface equivalent sphere of the pore space.

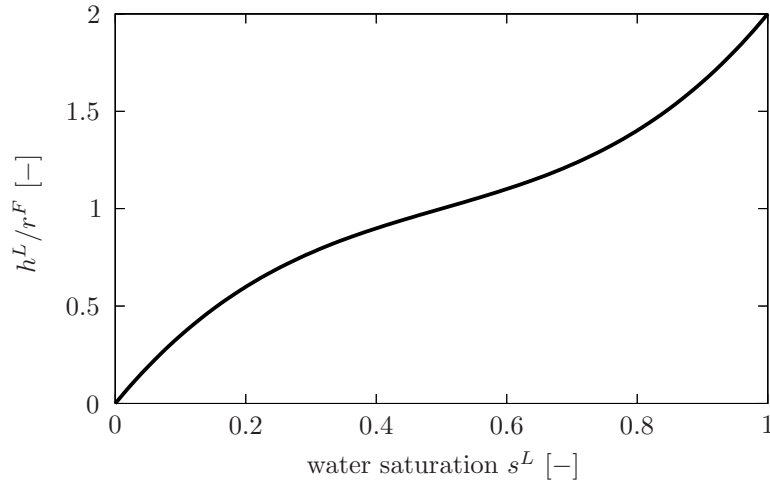


Figure 3.10: Ratio between the fill height h^L and the equivalent pore fluid radius r^F as function of the saturation s^L .

Based on the above introduced quantities and assumptions, the saturation s^β can be given as follows:

$$s^\beta = \frac{V^\beta}{V^F} = \frac{(h^\beta)^2(3r^F - h^\beta)}{4(r^F)^3}. \quad (3.137)$$

On the other hand, the fill height h^β of the pore fluids in the sphere can be formulated as a function of the saturation s^β and the equivalent pore fluid radius r^F , cf. Figure 3.10:

$$h^\beta = \left[\frac{36864}{8910} (s^\beta)^3 - \frac{18432}{2970} (s^\beta)^2 + \frac{12084}{2970} s^\beta \right] r^F. \quad (3.138)$$

Therefore, the conversion factor to transform the surface-specific heat exchange coefficients into volume-specific material parameters can be derived by relating the above introduced contact surfaces to the overall volume V of the whole porous material, where the volume fraction of the pore fluid is assumed to be $n^F = V^F/V$:

$$\frac{A^{S\beta}}{V} = \frac{A^{S\beta} V^F}{V^F V} = n^F \frac{A^{S\beta}}{V^F} \quad \text{and} \quad \frac{A^{GL}}{V} = \frac{A^{GL} V^F}{V^F V} = n^F \frac{A^{GL}}{V^F}. \quad (3.139)$$

Finally, this results in, cf. Figure 3.11,

$$\begin{aligned} k_{S\beta}^{\varepsilon V} \left[\frac{\text{W}}{\text{m}^3 \text{K}} \right] &= \frac{3 n^F h^\beta}{2 (r^F)^2} k_{S\beta}^{\varepsilon S} \left[\frac{\text{W}}{\text{m}^2 \text{K}} \right], \\ k_{GL}^{\varepsilon V} \left[\frac{\text{W}}{\text{m}^3 \text{K}} \right] &= \frac{3 n^F h^\beta (2 r^F - h^\beta)}{4 (r^F)^3} k_{GL}^{\varepsilon S} \left[\frac{\text{W}}{\text{m}^2 \text{K}} \right]. \end{aligned} \quad (3.140)$$

Furthermore, based on (2.4), the following relation between the volume elements and the volume fractions of the solid and the overall fluid phase holds:

$$dv = \frac{dv^S}{n^S} = \frac{dv^F}{n^F}. \quad (3.141)$$

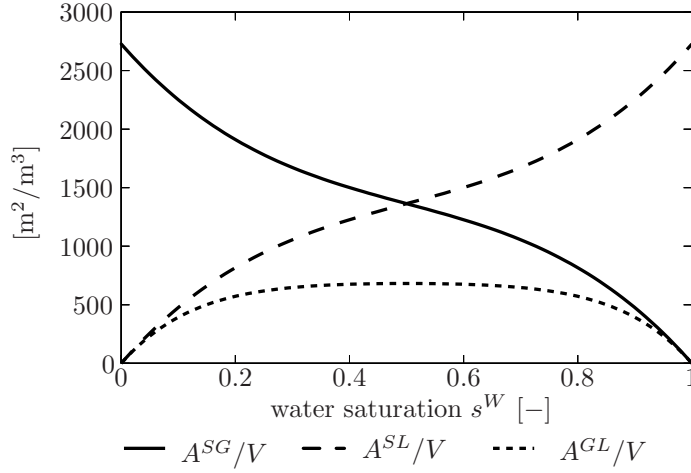


Figure 3.11: Conversion factors to transform surface-specific heat exchange coefficients into volume-specific material parameters.

Therefore, under the assumption that the volume elements are related to the volume of a sphere, the radius r^F can be computed based on a characteristic solid radius r^S via

$$r^F = \left(\frac{n^F}{n^S} \right)^{1/3} r^S \quad \text{and} \quad r^S = \frac{1}{2} d_{50}. \quad (3.142)$$

Therein, d_{50} is the medial grain diameter of the considered natural soil.

For simplicity, it is assumed within this thesis that the volume-specific heat exchange coefficients can be computed in this way from the surface-specific heat exchange coefficients, i. e., the conversion factors depend only on the volume fractions and a characteristic soil radius. Nevertheless, it can be expected that these coefficients depend on the heat conduction of the pore fluids as well as on the internal geometric parameters of the porous material, cf. *Ghadiani* [77]. Therefore, the correct volume-specific heat exchange coefficients can be determined only by performing an adequate experiment.

3.2.5 Heat influx vectors and mechanical fluid extra stresses

Heat influx vectors: Proceeding from the entropy inequality (3.43), the constraint

$$-\frac{1}{\theta^S} \mathbf{q}^S \cdot \text{grad } \theta^S - \sum_{\zeta} \frac{\theta^S}{\theta^{\zeta}} \frac{1}{\theta^{\zeta}} \mathbf{q}^{\zeta} \cdot \text{grad } \theta^{\zeta} \geq 0 \quad (3.143)$$

for the heat influx vectors \mathbf{q}^{α} has to hold. Furthermore, constitutive relations for \mathbf{q}^{α} can be introduced, based on (3.61)₈, via

$$\mathbf{q}^S = -n^S \mathbf{H}_r^S \text{grad } \theta^S, \quad \mathbf{q}^{\xi} = -n^{\xi} \mathbf{H}_r^{\xi} \text{grad } \theta^{\xi}, \quad \mathbf{q}^{\gamma} = -n^G x_{Gm}^{\gamma} \mathbf{H}_r^{\gamma} \text{grad } \theta^G, \quad (3.144)$$

where \mathbf{H}_r^{α} is the heat conduction tensor of the constituent φ^{α} . Relation (3.144) corresponds to the well-known *Fourier's law*, cf. *Fourier* [72], wherein the heat influx is governed

by the respective temperature gradient. Nevertheless, modeling porous materials with different constituents, the composition of the overall medium has to be taken into account. This is done in relation (3.144) via the consideration of the respective volume fraction n^α , whereas the heat influx vector of the gaseous constituents additionally depends on the molar fraction x_{Gm}^γ .

Incorporating this relation into (3.143) yields

$$\frac{n^S \mathbf{H}_r^S}{\theta^S} (\text{grad } \theta^S)^2 + \sum_{\xi} \frac{\theta^S}{\theta^\xi} \frac{n^\xi \mathbf{H}_r^\xi}{\theta^\xi} (\text{grad } \theta^\xi)^2 + \sum_{\gamma} \frac{\theta^S}{\theta^G} \frac{n^G x_{Gm}^\gamma \mathbf{H}_r^\gamma}{\theta^G} (\text{grad } \theta^G)^2 \geq 0. \quad (3.145)$$

Therefore, it is obvious that the entropy inequality is fulfilled, if each heat conduction tensor \mathbf{H}_r^α is positive definite.

Mechanical fluid extra stresses: Due to the fact that the mechanical fluid friction stress is negligible in comparison with the momentum productions, i. e., $\mathbf{T}_{E\text{mech}}^\zeta \approx \mathbf{0}$, cf. *Ehlers et al.* [55], a constitutive relation for the mechanical extra stress of the pore fluids is not necessary in the modeling of porous materials, but for completeness, this topic is still considered here.

The entropy inequality (3.43) is fulfilled, if \mathbf{Z}_ζ , cf. (3.61)₁ is a positive definite fourth order tensor. Therefore, a constitutive approach is, generally, given via

$$\mathbf{Z}_\zeta = 2\mu^\zeta (\mathbf{I} \otimes \mathbf{I})^{23} + \lambda^\zeta (\mathbf{I} \otimes \mathbf{I}), \quad (3.146)$$

where μ^ζ and λ^ζ are the shear and the volumetric viscosities of the pore fluid. Therein, the transposition $(\cdot)^{23}$ indicates an exchange of the 2nd and 3rd basis systems included into the tensor basis of higher order tensors, cf. Appendix A.1.3. Thus, the mechanical extra stress of the pore fluid yields

$$\mathbf{T}_{E\text{mech}}^\zeta = 2\mu^\zeta \mathbf{D}_\zeta + \lambda^\zeta (\mathbf{D}_\zeta \cdot \mathbf{I}) \mathbf{I}, \quad (3.147)$$

which can be reformulated using the deviator \mathbf{D}_ζ^D , cf. Appendix A.1.4, of the symmetric rate of deformation tensor \mathbf{D}_ζ :

$$\mathbf{T}_{E\text{mech}}^\zeta = 2\mu^\zeta \mathbf{D}_\zeta^D + (\lambda^\zeta + \frac{2}{3}\mu^\zeta) (\mathbf{D}_\zeta \cdot \mathbf{I}) \mathbf{I}. \quad (3.148)$$

To ensure the entropy inequality, the material parameters have to fulfill the following constraints:

$$\mu^\zeta \geq 0 \quad \text{and} \quad \lambda^\zeta + \frac{2}{3}\mu^\zeta \geq 0. \quad (3.149)$$

Remark: It can be realized that the friction stress is governed by the gradient of the primary kinematical variable $\dot{\mathbf{x}}_\zeta$ of the pore fluid ($\mathbf{D}_\zeta = \frac{1}{2}[\text{grad } \dot{\mathbf{x}}_\zeta + (\text{grad } \dot{\mathbf{x}}_\zeta)^T]$). A fluid, which can be described by such a linear constitutive approach is called *Newtonian fluid*. The special importance of this approach is due to the fact that most of the technically relevant fluids can be described by this relation. Furthermore, use can be made of *Stokes'*

assumption, i. e., $\lambda^\zeta + \frac{2}{3}\mu^\zeta = 0$. Therefore, the mechanical extra stress is only governed by the shear viscosity. Finally, relation (3.146) is comparable to the elastic tangent of the *Hookean* elasticity law, where the governing variable is also the gradient of the primary kinematic variable, i. e., the displacement vector \mathbf{u}_S , of the solid skeleton ($\boldsymbol{\varepsilon}_S = \frac{1}{2}[\text{grad } \mathbf{u}_S + (\text{grad } \mathbf{u}_S)^T]$). \square

3.3 The solid constituent

Considering geotechnical problems of practical relevance, e. g., consolidation, slope failure or base failure problems, one is, first of all, interested in the initiation of the respective failure mechanism. This is due to the fact that the usability of natural soils as subsoil is not guaranteed even if only small deformations occur. Therefore, it is assumed in the presented continuum mechanical model that the solid skeleton only undergoes small deformations and, thus, can be described within a geometrically linear theory. For a closer look on the continuum mechanical modeling of porous materials considering large (finite) deformations, the interested reader is referred to the works of, e. g., *Ehlers* [41], *Eipper* [67] or *Markert* [108]. Furthermore, it is maintainable to proceed from a thermal linear theory as well, due to fact that, within the considered temperature spectrum, the physical properties of the solid skeleton do not change significantly.

Assuming small deformations of the solid skeleton ($\alpha^S \approx 1.0^{-6} \text{ 1/K}$), the material density ρ^{SR} , cf. (3.30), as well as the volume fraction n^S , cf. (3.28)₁, of the solid skeleton can be linearized around the natural state indicated by $\mathbf{F}_S = \mathbf{I}$ and $\theta^S = \theta_0^S$. Therefore, a *Taylor* series is carried out around this initial state, in which higher order terms are neglected. As the material density of the solid skeleton only depends on the temperature, one finds

$$\rho_{\text{lin}}^{SR} = \rho^{SR} \Big|_{\theta^S = \theta_0^S} + \frac{d\rho^{SR}}{d\theta^S} \Big|_{\theta^S = \theta_0^S} (\theta^S - \theta_0^S), \quad (3.150)$$

which results under consideration of (3.30) in

$$\rho_{\text{lin}}^{SR} = \rho_{0S}^{SR} [1 - 3\alpha^S(\theta^S - \theta_0^S)]. \quad (3.151)$$

Furthermore, proceeding from (3.24), the relation between the determinants of the overall material deformation gradient \mathbf{F}_S and its mechanical, \mathbf{F}_{S_m} , and thermal, \mathbf{F}_{S_θ} , parts is given via

$$\det \mathbf{F}_S = \det \mathbf{F}_{S_m} \det \mathbf{F}_{S_\theta} \quad (3.152)$$

and can be reformulated as follows:

$$(\det \mathbf{F}_{S_m})^{-1} = (\det \mathbf{F}_S)^{-1} \det \mathbf{F}_{S_\theta}. \quad (3.153)$$

Thus, the linearized volume fraction depends on the overall material deformation gradient and the respective temperature of the solid skeleton and can be computed via

$$n_{\text{lin}}^S = n^S \Big|_{\theta^S = \theta_0^S}^{\mathbf{F}_S = \mathbf{I}} + \frac{\partial n^S}{\partial \mathbf{F}_S} \Big|_{\theta^S = \theta_0^S}^{\mathbf{F}_S = \mathbf{I}} (\mathbf{F}_S - \mathbf{I}) + \frac{\partial n^S}{\partial \theta^S} \Big|_{\theta^S = \theta_0^S}^{\mathbf{F}_S = \mathbf{I}} (\theta^S - \theta_0^S), \quad (3.154)$$

which yields

$$\boxed{n_{\text{lin}}^S = n_{0S}^S [1 - \text{div } \mathbf{u}_S + 3\alpha^S(\theta^S - \theta_0^S)]}. \quad (3.155)$$

3.3.1 Free *Helmholtz* energy, entropy and effective stress

Within this contribution, it is assumed, cf. (3.36), that the free *Helmholtz* energy of the solid skeleton depends on the temperature θ^S and the material deformation gradient \mathbf{F}_S . As a result of the principle of frame indifference, cf. [46], the free *Helmholtz* energy of the solid skeleton has to depend on the material deformation gradient in such a way that this dependency can also be described by the right *Cauchy-Green* deformation tensor \mathbf{C}_S and the *Green-Lagrangean* strain tensor \mathbf{E}_S ,

$$\psi^S(\theta^S, \mathbf{F}_S) = \psi^S(\theta^S, \mathbf{C}_S) = \psi^S(\theta^S, \mathbf{E}_S), \quad (3.156)$$

whereas in the frame of a geometrically linear theory, the *Green-Lagrangean* strain tensor \mathbf{E}_S can be replaced by its linearized form $\boldsymbol{\varepsilon}_S$, cf. (2.34),

$$\psi_{\text{lin}}^S(\theta^S, \boldsymbol{\varepsilon}_S). \quad (3.157)$$

Therefore, assuming small deformations, the free *Helmholtz* energy of the solid skeleton is introduced as follows via

$$\boxed{\begin{aligned} \rho_{0S}^S \psi_{\text{lin}}^S &= \mu^S \boldsymbol{\varepsilon}_S \cdot \boldsymbol{\varepsilon}_S + \frac{1}{2} \lambda^S (\boldsymbol{\varepsilon}_S \cdot \mathbf{I})^2 + m^S (\theta^S - \theta_0^S) \boldsymbol{\varepsilon}_S \cdot \mathbf{I} - \\ &\quad - \rho_{0S}^S C_V^S \left[\theta^S \ln \frac{\theta^S}{\theta_0^S} - (\theta^S - \theta_0^S) \right] - \rho_{0S}^S \eta_0^S (\theta^S - \theta_0^S) - \\ &\quad - \rho_{0S}^S \frac{p_0^{FR}}{\rho_{0S}^{SR}} 3\alpha^S (\theta^S - \theta_0^S) + \rho_{0S}^S \psi_0^S, \end{aligned}} \quad (3.158)$$

where ψ_0^S specifies a certain energy and η_0^S a certain entropy level in the initial state. Therein, μ^S and λ^S are the *Lamé* constants, whereas $m^S = -(2\mu^S + 3\lambda^S)\alpha^S$ is the stress-temperature modulus of the solid skeleton. As a consequence, the linearized entropy η_{lin}^S of the solid skeleton can be computed via (3.56)₁ and (3.151), which yields

$$\boxed{\eta_{\text{lin}}^S = C_V^S \ln \frac{\theta^S}{\theta_0^S} - (p^{FR} - p_0^{FR}) \frac{3\alpha^S}{\rho_{0S}^{SR}} - \frac{1}{\rho_{0S}^S} m^S \boldsymbol{\varepsilon}_S \cdot \mathbf{I} + \eta_0^S}. \quad (3.159)$$

Furthermore, the linearized internal energy $\varepsilon_{\text{lin}}^S$ can be computed based on (2.83), i. e.,

$$\boxed{\begin{aligned} \varepsilon_{\text{lin}}^S &= \frac{1}{\rho_{0S}^S} [\mu^S \boldsymbol{\varepsilon}_S \cdot \boldsymbol{\varepsilon}_S + \frac{1}{2} \lambda^S (\boldsymbol{\varepsilon}_S \cdot \mathbf{I})^2 - m^S \theta_0^S \boldsymbol{\varepsilon}_S \cdot \mathbf{I}] + \\ &\quad + C_V^S (\theta^S - \theta_0^S) - \left(\frac{p^{FR}}{(\rho_{0S}^{SR})^2} \theta^S - \frac{p_0^{FR}}{(\rho_{0S}^{SR})^2} \theta_0^S \right) 3\alpha^S \rho_{0S}^{SR} + \varepsilon_0^S, \end{aligned}} \quad (3.160)$$

wherein ε_0^S indicates the internal energy in the referential state. As a consequence of (3.47)₁, the linearized mechanical solid extra stress $\boldsymbol{\sigma}_{E\text{mech}}^S$ is given by the derivative of the linearized free *Helmholtz* energy with respect to the linearized strain tensor $\boldsymbol{\varepsilon}_S$. Therefore, based on (3.158), one finds the *Hookean* elasticity law extended towards thermal conditions:

$$\boxed{\boldsymbol{\sigma}_{E\text{mech}}^S = \rho_{0S}^S \frac{\partial \psi_{\text{lin}}^S}{\partial \boldsymbol{\varepsilon}_S} = 2\mu^S \boldsymbol{\varepsilon}_S + \lambda^S (\boldsymbol{\varepsilon}_S \cdot \mathbf{I}) \mathbf{I} + m^S (\theta^S - \theta_0^S) \mathbf{I}.} \quad (3.161)$$

Concerning the purely thermal part of (3.158), one obtains, by building the second derivative with respect to the temperature, the specific heat of the solid skeleton as it is postulated:

$$C_V^S = \theta^S \left. \frac{\partial \eta^S}{\partial \theta^S} \right|_{\rho^{SR} = \text{const.}} = -\theta^S \left. \frac{\partial^2 \psi^S}{(\partial \theta^S)^2} \right|_{\rho^{SR} = \text{const.}}. \quad (3.162)$$

Remark: Assuming large (finite) deformations, a relation for the free *Helmholtz* energy can be introduced following *Ehlers* [44], wherein an extension of the *Simo-Pister* law is given via

$$\begin{aligned} \rho_{0S}^S \psi^S &= \frac{1}{2} \mu^S (\text{I}_{C_S} - 3) + [m^S (\theta^S - \theta_0^S) - \mu^S] \ln (\text{III}_{C_S})^{1/2} + \\ &+ \frac{1}{2} \lambda^S [\ln (\text{III}_{C_S})^{1/2}]^2 - \rho_{0S}^S C_V^S [\theta^S \ln \frac{\theta^S}{\theta_0^S} - (\theta^S - \theta_0^S)] - \\ &- \rho_{0S}^S \eta_0^S (\theta^S - \theta_0^S) - \rho_{0S}^S \frac{p_0^{FR}}{\rho_{0S}^{SR}} 3\alpha^S (\theta^S - \theta_0^S) + \rho_{0S}^S \psi_0^S. \end{aligned}$$

This relation is based on the *Simo-Pister* law, where the deformation state of the solid skeleton is described by the first I_{C_S} and third III_{C_S} invariant of the right *Cauchy-Green* deformation tensor \mathbf{C}_S . This is done to fulfill the restrictions resulting from the principle of frame indifference (3.156), cf. *Ehlers* [46]. The entropy η^S of the solid skeleton yields as a consequence

$$\eta^S = C_V^S \ln \frac{\theta^S}{\theta_0^S} - \left(\frac{p^{FR}}{\rho^{SR}} - \frac{p_0^{FR}}{\rho_{0S}^{SR}} \right) 3\alpha^S - \frac{1}{\rho_{0S}^S} m^S \ln (\text{III}_{C_S})^{1/2} + \eta_0^S,$$

whereas the internal energy is given via

$$\begin{aligned} \varepsilon^S &= \frac{1}{\rho_{0S}^S} \left\{ \frac{1}{2} \mu^S (\text{I}_{C_S} - 3) - (m^S \theta_0^S + \mu^S) \ln (\text{III}_{C_S})^{1/2} + \frac{1}{2} \lambda^S [\ln (\text{III}_{C_S})^{1/2}]^2 \right\} + \\ &+ C_V^S (\theta^S - \theta_0^S) - \left(\frac{p^{FR}}{\rho^{SR}} \theta^S - \frac{p_0^{FR}}{\rho_{0S}^{SR}} \theta_0^S \right) 3\alpha^S + \varepsilon_0^S. \end{aligned}$$

The mechanical extra term of the *Cauchy* stress tensor can be directly computed based on (3.47)₁:

$$\mathbf{T}_{E\text{mech}}^S = \rho^S \frac{\partial \psi^S}{\partial \mathbf{F}_S} \mathbf{F}_S^T = (\det \mathbf{F}_S)^{-1} [2\mu^S \mathbf{K}_S + \lambda^S \ln (\det \mathbf{F}_S) \mathbf{I} + m^S (\theta^S - \theta_0^S) \mathbf{I}],$$

where $\mathbf{K}_S = \frac{1}{2}(\mathbf{B}_S - \mathbf{I})$ is the so-called *Karni-Reiner* strain tensor. Considering the definition of the *Kirchhoff* stress $\boldsymbol{\tau}^S$, the mechanical extra term of this stress tensor of the current configuration reads

$$\boldsymbol{\tau}_{E \text{ mech}}^S = \det \mathbf{F}_S \mathbf{T}_{E \text{ mech}}^S = 2\mu^S \mathbf{K}_S + \lambda^S \ln(\det \mathbf{F}_S) \mathbf{I} + m^S(\theta^S - \theta_0^S) \mathbf{I}.$$

Furthermore, performing a covariant pull-back transport mechanism of the first and second basis yields the mechanical extra term of the second *Piola-Kirchhoff* stress tensor:

$$\mathbf{S}_{E \text{ mech}}^S = \mathbf{F}_S^{-1} \boldsymbol{\tau}_E^S \mathbf{F}_S^{T-1} = 2\mu^S \mathbf{K}_S^R + \lambda^S \ln(\det \mathbf{F}_S) \mathbf{C}_S^{-1} + m^S(\theta^S - \theta_0^S) \mathbf{C}_S^{-1}.$$

As constraint for every finite elasticity law, its linearization around the initial state must result in the well-known *Hookean* elasticity law. Generally, this linearization can be carried out via

$$\mathbf{S}_{E \text{ mech lin}}^S = \mathbf{S}_E^S \Big|_{\theta^S = \theta_0^S}^{\mathbf{E}_S = \mathbf{I}} + \frac{\partial \mathbf{S}_E^S}{\partial \mathbf{E}_S} \Big|_{\theta^S = \theta_0^S}^{\mathbf{E}_S = \mathbf{I}} (\mathbf{E}_S - \mathbf{I}) + \frac{\partial \mathbf{S}_E^S}{\partial \theta^S} \Big|_{\theta^S = \theta_0^S}^{\mathbf{E}_S = \mathbf{I}} (\theta^S - \theta_0^S),$$

which yields for the given ansatz

$$\boldsymbol{\sigma}_{E \text{ mech}}^S = 2\mu^S \boldsymbol{\varepsilon}_S + \lambda^S (\boldsymbol{\varepsilon}_S \cdot \mathbf{I}) \mathbf{I} + m^S(\theta^S - \theta_0^S) \mathbf{I},$$

and, therefore, the underlying restriction is fulfilled. \square

3.3.2 Plastic material behavior

Modeling natural soils, one can proceed from the assumption that the solid skeleton is governed by an elastoplastic material behavior. In this case, it can be shown that the total strains can be split additively into an elastic and a plastic part, cf. *Ehlers* [46]:

$$\boldsymbol{\varepsilon}_S = \boldsymbol{\varepsilon}_{Se} + \boldsymbol{\varepsilon}_{Sp}. \quad (3.163)$$

As a consequence, based on (3.157), the free *Helmholtz* energy depends in general on both, the elastic and plastic parts of the strain tensor. Thereby, the dependency on the plastic part of the strain tensor can be interpreted as a dependency of the material parameters of the solid skeleton on different plastic intermediate configurations. Within this thesis, such a behavior of the material parameters as well as hardening and softening effects of the solid skeleton are neglected. Thus, one can postulate that the free *Helmholtz* energy is only a function of the temperature θ^S and the elastic part of the strain tensor $\boldsymbol{\varepsilon}_{Se}$:

$$\psi^S(\theta^S, \boldsymbol{\varepsilon}_{Se}). \quad (3.164)$$

Therefore, the entropy inequality (3.23) has to be reformulated. Proceeding from

$$\mathbf{T}_E^S \cdot \mathbf{L}_S - \rho^S (\psi^S)'_S + (\dots) \geq 0, \quad (3.165)$$

the spatial velocity gradient \mathbf{L}_S can be replaced by its symmetric part \mathbf{D}_S due to the symmetry of the *Cauchy* stress tensor. Furthermore, the mechanical part of the stress power of the solid skeleton can be reformulated using (2.26)₁ and (2.38)₁:

$$\begin{aligned} \mathbf{T}_{E\text{mech}}^S \cdot \mathbf{L}_S &= \mathbf{T}_{E\text{mech}}^S \cdot \mathbf{D}_S = \mathbf{T}_{E\text{mech}}^S \cdot \frac{1}{2} [\text{grad } \dot{\mathbf{x}}_S + (\text{grad } \dot{\mathbf{x}}_S)^T] \\ &= \mathbf{T}_{E\text{mech}}^S \cdot \frac{1}{2} \{ \text{grad } (\mathbf{u}_S)'_S + [\text{grad } (\mathbf{u}_S)'_S]^T \}. \end{aligned} \quad (3.166)$$

Therefore, the mechanical stress power yields under the assumption of a geometrically linear theory

$$\mathbf{T}_{E\text{mech}}^S \cdot \mathbf{L}_S \approx \boldsymbol{\sigma}_{E\text{mech}}^S \cdot (\boldsymbol{\varepsilon}_S)'_S = \boldsymbol{\sigma}_{E\text{mech}}^S \cdot [(\boldsymbol{\varepsilon}_{Se})'_S + (\boldsymbol{\varepsilon}_{Sp})'_S]. \quad (3.167)$$

Thus, the entropy inequality reads

$$\left(\boldsymbol{\sigma}_{E\text{mech}}^S - \rho_{0S}^S \frac{\partial \psi_{\text{lin}}^S}{\boldsymbol{\varepsilon}_{Se}} \right) \cdot (\boldsymbol{\varepsilon}_{Se})'_S + \boldsymbol{\sigma}_{E\text{mech}}^S \cdot (\boldsymbol{\varepsilon}_{Sp})'_S + (\dots) \geq 0. \quad (3.168)$$

Thus, it is obvious that the dissipative material behavior of the solid skeleton is described by the plastic part of the strain rate. Furthermore, to fulfill relation (3.168), one has to ensure that

$$\boldsymbol{\sigma}_{E\text{mech}}^S \cdot (\boldsymbol{\varepsilon}_{Sp})'_S \geq 0. \quad (3.169)$$

Remark: Relation (3.163) is based on a constitutive split of the material deformation gradient \mathbf{F}_S in an elastic and an inelastic (plastic) part, $\mathbf{F}_S = \mathbf{F}_{Se} \mathbf{F}_{Sp}$. Taking into account that in the non-isothermal case \mathbf{F}_S is split in a thermal and mechanical part, it follows:

$$\mathbf{F}_S = \mathbf{F}_{Se} \mathbf{F}_{S_\theta} \mathbf{F}_{Sp}.$$

Therefore, the line element $d\mathbf{X}_S$ is firstly transported via \mathbf{F}_{Sp} from the reference to the stress free intermediate configuration. Furthermore, $d\mathbf{X}_S$ is transported via \mathbf{F}_{S_θ} from the stress free intermediate configuration to a configuration, where only a purely thermal load is applied, and, finally, $d\mathbf{X}_S$ is transported via \mathbf{F}_{Se} to the current configuration, cf. *Ghadiani* [77].

Furthermore, proceeding from finite deformations of the solid phase, the elastic part of the *Green-Lagrangean* strain tensor depends on the elastic part $\hat{\mathbf{C}}_{Se}$ of the right *Cauchy-Green* deformation tensor, which has to be transported back from the intermediate to the reference configuration by a contravariant transport mechanism with the plastic part \mathbf{F}_{Sp} of the material deformation gradient:

$$\mathbf{E}_{Se} = \mathbf{E}_{Se}(\hat{\mathbf{C}}_{Se}, \mathbf{F}_{Sp}) = \frac{1}{2} \mathbf{F}_{Sp}^T (\hat{\mathbf{C}}_{Se} - \mathbf{I}) \mathbf{F}_{Sp}.$$

Thus, the free *Helmholtz* energy of the solid skeleton depends, within a geometrically non-linear theory, similarly on both, the elastic and the plastic part of the deformation:

$$\psi^S(\theta^S, \hat{\mathbf{C}}_{Se}, \mathbf{F}_{Sp}).$$

Furthermore, considering hardening and softening effects of the solid skeleton, the set of variables of the free *Helmholtz* energy has to be extended by the set $\boldsymbol{\alpha}$ of internal variables:

$$\psi^S(\theta^S, \boldsymbol{\varepsilon}_{Se}, \boldsymbol{\alpha}).$$

For a closer look on this topic, the interested reader is referred to the works of *Ehlers & Müllerschön* [65], *Müllerschön* [110] and *Scholz* [117]. \square

Concerning the basic ideas of an elastoplastic concept, one has to define, on the one hand, an adequate yield surface confining the elastic domain and, on the other hand, an evolution equation for the plastic strains, the so-called flow rule.

Furthermore, regarding the elastoplastic material behavior of natural soils, one observes that, in contrast to metallic, non-porous materials, these materials undergo plastic deformations during a purely hydrostatic loading and that they show a contractant or dilatant plastic material behavior depending on the stress state, cf. *Lade & Duncan* [100].

Therefore, to consider all of these effects, the single-surface yield criterion F following *Ehlers* [41, 42] for granular materials is used to bound the elastic domain, cf. Figure 3.12:

$$\begin{aligned} F &= \Phi^{1/2} + \beta I + \epsilon I^2 - \kappa = 0, \\ \Phi &= \mathbb{I}^D (1 + \gamma \vartheta)^m + \frac{1}{2} \alpha I^2 + \delta^2 I^4, \\ \vartheta &= \mathbb{III}^D / (\mathbb{II}^D)^{3/2}. \end{aligned} \tag{3.170}$$

Therein, I is the first principle invariant of the mechanical effective stress tensor $\boldsymbol{\sigma}_{E\text{mech}}^S$, whereas \mathbb{II}^D and \mathbb{III}^D are the (negative) second and third principle invariants of the deviator of the mechanical effective stress tensor, cf. Appendix A.2.

This yield criterion is governed all together by seven material parameters,

$$\mathcal{S}_h = \{\alpha, \beta, \delta, \epsilon, \kappa\}, \quad \mathcal{S}_d = \{\gamma, m\}, \tag{3.171}$$

which are responsible for the shape of the yield surface in the hydrostatic (\mathcal{S}_h) and deviatoric (\mathcal{S}_d) plane. Generally, an evolution equation for the plastic strains can be formulated following *Hill* [92] and citations therein via

$$\left(\boldsymbol{\varepsilon}_{Sp} \right)'_S = \Lambda \frac{\partial G}{\partial \boldsymbol{\sigma}_{E\text{mech}}^S}, \tag{3.172}$$

where G is an additional potential, the so-called plastic potential, and Λ is the plastic multiplier or consistency parameter. For the completion of the governing equations of plasticity theory, the *Kuhn-Tucker* (loading/unloading) conditions,

$$F \leq 0, \quad \Lambda \geq 0, \quad \Lambda F = 0, \tag{3.173}$$

and the consistency condition,

$$\dot{F} = 0, \tag{3.174}$$

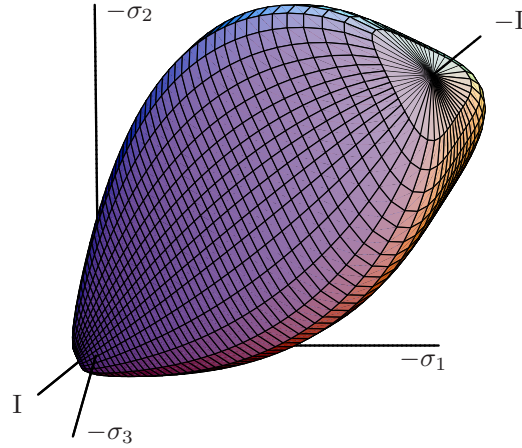


Figure 3.12: Single-surface yield criterion F for cohesive-frictional materials in the principal stress space (tension positive).

are required. The yield surface is introduced based on the definition that for $F < 0$ the material behaves elastically, whereas $F = 0$ indicates the elastic limit. Stress points outside the elastic domain are not allowed, and, therefore, the function F has always to be lower or equal zero. On the other hand, the direction of the plastic strains are determined via the derivative of the plastic potential with respect to the stress point. Thus, the plastic multiplier has always to be greater or equal zero. Furthermore, in the elastic domain ($F < 0$) no change of the plastic strains take place ($(\boldsymbol{\varepsilon}_{Sp})'_S = \mathbf{0}$) and so the plastic multiplier has to be zero. The plastic strains $(\boldsymbol{\varepsilon}_{Sp})'_S$ can only be unequal to zero, i. e., $\Lambda > 0$, if the stress point is on the yield surface ($F = 0$). These two constraints can be ensured via $\Lambda F = 0$. The consistency condition corresponds to the physical requirement that for $(\boldsymbol{\varepsilon}_{Sp})'_S > \mathbf{0}$, the stress point has to stay on the yield surface and is used to determine the plastic multiplier Λ . For a more detailed view on this topic, the interested reader is referred to *Lemaitre & Chaboche* [104] or *Simo & Hughes* [122].

Remark: The general frame, where $G \neq F$ is called non-associated plasticity. In the special case, where the plastic potential is chosen equal to the yield surface ($G = F$), one talks about associated plasticity. In this case, the direction of plastic flow is given via the normal on the yield surface. For a closer look on the associated plasticity concept, the interested reader is referred to the works of *Hill* [92], *Lemaitre & Chaboche* [104], *Simo & Hughes* [122]. \square

The yield surface F is given for a natural soil with low cohesion ($\kappa \approx 0$) in a hydrostatic plane of the principle stress space in Figure 3.13, wherein the stress and strain tensors can be geometrically interpreted as vectors. Taking a closer look on the scalar product $\partial F / \partial \boldsymbol{\sigma}_{E\text{mech}}^S \cdot (\boldsymbol{\sigma}_{E\text{mech}}^S)'_S$ one finds

$$\partial F / \partial \boldsymbol{\sigma}_{E\text{mech}}^S \cdot (\boldsymbol{\sigma}_{E\text{mech}}^S)'_S \begin{cases} > 0 & : \text{ plastic loading,} \\ = 0 & : \text{ neutral loading,} \\ < 0 & : \text{ unloading.} \end{cases} \quad (3.175)$$

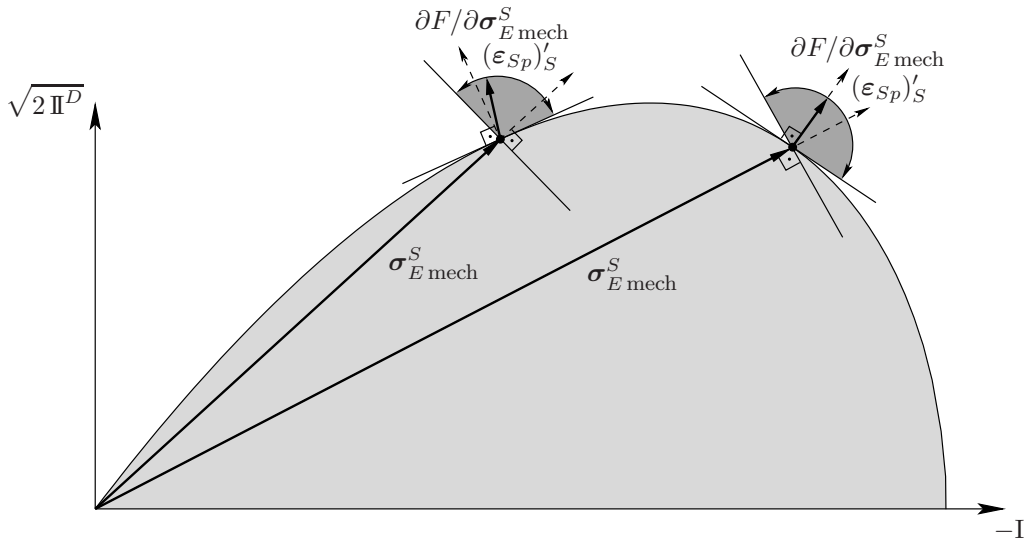


Figure 3.13: Single-surface yield criterion F following *Ehlers* [41, 42] for cohesive-frictional materials given in the hydrostatic plane ($\kappa \approx 0$).

To ensure the dissipation inequality (3.169), the scalar product $\boldsymbol{\sigma}_{E \text{ mech}}^S \cdot (\boldsymbol{\epsilon}_{Sp})'_S$ has to be greater than or equal to zero. On the other hand, the scalar product between the normal $\partial F / \partial \boldsymbol{\sigma}_{E \text{ mech}}^S$ on the yield surface and $(\boldsymbol{\epsilon}_{Sp})'_S$ has to be greater than or equal to zero as well. Thus, as a result $(\boldsymbol{\epsilon}_{Sp})'_S$ must lie within the gray domains. Furthermore, the demand of convexity of the plastic potential can be motivated from a numerical point of view, where the unique assignment of stress points has to be ensured during a back projection of a trial stress outside the elastic domain, cf. *Müllerschön* [110].

Due to the fact that the associated plasticity concept is not suitable for the description of frictional materials, cf., e. g., *Ehlers & Volk* [66], *Lade & Duncan* [100] or *Davis & Selvadurai* [34], the plastic potential G is introduced similar to the yield surface F , cf. *Mahnkopf* [107],

$$\begin{aligned} G &= \Gamma^{1/2} + \psi_2 I + \epsilon I^2, \\ \Gamma &= \psi_1 \mathbb{I}^D + \frac{1}{2} \alpha I^2 + \delta^2 I^4, \end{aligned} \quad (3.176)$$

where ψ_1 and ψ_2 are two material parameters to relate the dilatation angle to experimental data. In comparison with (3.170), one can observe that the plastic potential is independent of \mathbb{I}^D and describes, therefore, a circle in the deviatoric plane. This is based on the results of experiments on frictional materials published by *Kim & Lade* [95], wherein the direction of the plastic flow in the deviatoric plane was found to be near to the coaxial direction. The capability of the above presented formulation to describe contractant and dilatant plastic material behavior depending on the hydrostatic pressure state is shown in *Ehlers et al.* [54].

Concerning the numerical treatment of the presented plasticity model within the FEM, a strong dependency of simulation results on the chosen spatial discretization can be observed. Such an unphysical, mesh-dependent behavior can be prevented by the usage of suitable regularization techniques as, e. g., the viscoplasticity concept or the *Cosserat* theory. For a closer look on this topic, the interested reader is referred to the work of

Ammann [2] and citations therein.

Within this work, the viscoplasticity concept is applied to regularize the occurring numerical problems within the elastoplastic theory. Therefore, the plastic multiplier is given following an overstress approach of Perzyna type [114]:

$$\Lambda = \frac{1}{\eta} \left\langle \frac{F(\boldsymbol{\sigma}_{E\text{mech}}^S)}{\sigma_0} \right\rangle^r \quad \text{or} \quad \Lambda \eta \langle \sigma_0 \rangle^r - \langle F(\boldsymbol{\sigma}_{E\text{mech}}^S) \rangle^r = 0. \quad (3.177)$$

Therein, η is the relaxation time (viscosity), σ_0 is the reference stress usually chosen equal to κ , r is the viscoplastic exponent and $\langle \cdot \rangle$ are the Macauley brackets defined by $\langle x \rangle = \max\{0, x\}$, cf. Hartmann *et al.* [84].

The governing equations of elasto-viscoplasticity are given by (3.172) and (3.177)₂, where the primary variables are the plastic strains $\boldsymbol{\varepsilon}_{Sp}$ and the plastic multiplier Λ . For $\eta > 0$ and $r = 1$, one can observe from Equation (3.177)₂ that positive values for the yield criterion are possible, and, therefore, stresses outside the elastic domain, so-called overstresses, are allowed. Nevertheless, for $\eta = 0$, Equation (3.177)₂ results in the constraint $F = 0$ for the determination of Λ and, thus, an elastoplastic material behavior is modeled. Thereby, both, an elastoplastic ($\eta = 0$, $r = 1$) as well as an elasto-viscoplastic ($\eta > 0$) material behavior can be described using the same formulation only by changing the material parameters, cf. Ehlers & Ellsiepen [53], Ellsiepen [68] or Wiens *et al.* [140].

Taking into account the special material behavior of partially saturated soils, Bolzano *et al.* [14] or Laloui & Nuth [102] postulated that the yield surface is a function of the stress state as well as of the saturation of the pore water. Additionally, Laloui *et al.* [101] have enhanced this set of variables by the temperature to include the non-isothermal material behavior.

Remark: Concerning the modeling of the hardening or softening material behavior of the solid skeleton, where an evolution equation for a certain set of material parameters of the yield surface is introduced, the interested reader is referred to Müllerschön [110] or Scholz [117]. Furthermore, in these publications, the material parameters of the solid skeleton are identified for Berliner Sand [65, 110] and Hostun Sand [117] using results of biaxial and triaxial experiments. \square

3.4 A triphasic porous material model

Within this section, the constitutive relations derived in the previous sections of this chapter are applied to the description of natural, partially saturated soils under non-isothermal conditions. The three different components are the solid skeleton φ^S , pore water φ^W and pore air φ^A , whereas the pore water can appear in both, a liquid and a gaseous state. Therefore, the considered porous material consists of three phases: a solid phase φ^S , a liquid phase φ^L and an overall gas phase φ^G . The overall gas phase is assumed as an ideal mixture of two gaseous components, i. e., pore air and the gaseous pore water (pore vapor φ^V). Nevertheless, the presented model can be adapted to describe any other porous material with two different pore fluids.

The primary variables for the mechanical description of initial boundary-value problems are chosen in the quasi-static case as follows:

$$\theta^S, \theta^L, \theta^G, \mathbf{u}_S, p^{LR}, p_G^V \text{ and } p_G^A. \quad (3.178)$$

Recall that the gaseous constituents are governed by the same temperature θ^G . Due to the fact that for practical reasons the chosen primary variables have to be observable variables, the densities are replaced by the corresponding partial pressures. Thereby, one have to keep in mind that the effective pressure p^{LR} of the materially incompressible pore liquid cannot be determined based on the free *Helmholtz* energy but results from the boundary conditions of the problem under study. Furthermore, if both the liquid and the gas phase coexists, the partial pressure p_G^V of the water vapor within the overall gas phase is no longer a primary variable.

The governing equations for the individual temperatures θ^S , θ^L and θ^G are the energy balances of the respective phases. Furthermore, due to practical reasons regarding the handling of boundary conditions within a numerical scheme, the momentum balance of the overall porous material is used as governing equation for the displacement vector \mathbf{u}_S of the solid skeleton. More precisely, using the momentum balance of the overall material, the resulting *Neumann* boundary conditions correspond to the overall stress vector. If only the momentum balance of the solid skeleton is used as governing equation, one have to manually split the stress acting on the overall porous material in the stress acting only on the solid phase, because the *Neumann* boundary conditions correspond to the stress vector of the solid skeleton. Considering the pore fluids, constitutive relations between the primary kinematical variables \mathbf{w}_L , \mathbf{w}_G , \mathbf{d}_{VG} and \mathbf{d}_{AG} and the corresponding effective (p^{LR}) and partial (p_G^V , p_G^A) pressures are given via (3.110) and (3.124), and, therefore, the primary kinematical variables of the pore fluids lose their character of primary variables of the global continuum mechanical model. As the partial pressure p_G^V of the water vapor within the overall gas phase is no longer a primary variable, if phase transitions between the liquid and gaseous water are taken into account and both, the liquid and the gas phase coexists, the mass balance of the water vapor is no longer a governing equation in that case. Instead, condition (3.79) must hold and the mass production $\hat{\rho}^L$ is given via relation (3.91).

Thus, the system of governing equations for the triphasic porous material model under

study reads

solid skeleton:

$$\operatorname{div}(\boldsymbol{\sigma}^S + \mathbf{T}^L + \mathbf{T}^V + \mathbf{T}^A) + [n^S \rho^{SR} + n^L \rho^{LR} + n^G(\rho_G^V + \rho_G^A)] \mathbf{b} = \mathbf{0},$$

if $\hat{\rho}^L \neq 0$:

$$\operatorname{div}(\boldsymbol{\sigma}^S + \mathbf{T}^L + \mathbf{T}^V + \mathbf{T}^A - \rho^L \mathbf{d}_L \otimes \mathbf{d}_L - \rho^V \mathbf{d}_V \otimes \mathbf{d}_V) + [n^S \rho^{SR} + n^L \rho^{LR} + n^G(\rho_G^V + \rho_G^A)] \mathbf{b} = \mathbf{0},$$

$$n^S \rho^{SR} (\boldsymbol{\varepsilon}^S)'_S - \boldsymbol{\sigma}^S \cdot (\boldsymbol{\varepsilon}_S)'_S + \operatorname{div} \mathbf{q}^S - n^S \rho^{SR} r^S - \hat{\varepsilon}^S = 0,$$

liquid pore water:

$$(n^L \rho^{LR})'_S + n^L \rho^{LR} \operatorname{div}(\mathbf{u}_S)'_S + \operatorname{div}(n^L \rho^{LR} \mathbf{w}_L) - \hat{\rho}^L = 0, \quad (3.179)$$

$$n^L \rho^{LR} [(\boldsymbol{\varepsilon}^L)'_S + \operatorname{grad} \boldsymbol{\varepsilon}^L \cdot \mathbf{w}_L] - \mathbf{T}^L \cdot \mathbf{L}_L + \operatorname{div} \mathbf{q}^L - n^L \rho^{LR} r^L - \hat{\varepsilon}^L = 0,$$

gaseous pore vapor and pore air:

if $\hat{\rho}^V = 0$:

$$(n^G \rho_G^V)'_S + n^G \rho_G^V \operatorname{div}(\mathbf{u}_S)'_S + \operatorname{div}[n^G \rho_G^V (\mathbf{w}_G + \mathbf{d}_{VG})] = 0,$$

$$(n^G \rho_G^A)'_S + n^G \rho_G^A \operatorname{div}(\mathbf{u}_S)'_S + \operatorname{div}[n^G \rho_G^A (\mathbf{w}_G + \mathbf{d}_{AG})] = 0,$$

$$n^G \rho_G^V [(\boldsymbol{\varepsilon}^V)'_S + \operatorname{grad} \boldsymbol{\varepsilon}^V \cdot (\mathbf{w}_G + \mathbf{d}_{VG})] + n^G \rho_G^A [(\boldsymbol{\varepsilon}^A)'_S + \operatorname{grad} \boldsymbol{\varepsilon}^A \cdot (\mathbf{w}_G + \mathbf{d}_{AG})] - \mathbf{T}^V \cdot \mathbf{L}_V - \mathbf{T}^A \cdot \mathbf{L}_A + \operatorname{div} \mathbf{q}^V + \operatorname{div} \mathbf{q}^A - n^G(\rho_G^V + \rho_G^A) r^G - \hat{\varepsilon}^V - \hat{\varepsilon}^A = 0.$$

Therein, the momentum balance of the overall porous material is given by the sum of the momentum balances of the individual constituents under quasi-static conditions, whereas the term considering mass interaction processes is reformulated using relation (2.67), which is applied to the overall mixture. Furthermore, the energy balance of the gas phase results from a summation over the energy balances of the single gaseous constituents. All time derivatives in (3.179) are given with respect to the deformable solid skeleton, which is described within a geometrically linear theory using the linearized stress tensor $\boldsymbol{\sigma}^S$ and the linearized strain tensor $\boldsymbol{\varepsilon}_S$.

The volume fractions and densities included in (3.179) are related to the primary variables as discussed in the sections before. Therefore, the volume fractions read

$$\begin{aligned} n^S &= n_{0S}^S [1 - \operatorname{div} \mathbf{u}_S + 3 \alpha^S (\theta^S - \theta_0^S)], \\ n^F &= 1 - n^S, \\ s^L &= s^L(p^C) = s^L(p^{LR}, p_G^V, p_G^A), \text{ depends on the problem,} \\ n^L &= s^L n^F, \\ n^G &= (1 - s^L) n^F. \end{aligned} \quad (3.180)$$

The relation between the capillary pressure p^C and the saturation of the pore liquid s^L depends in the following on the particular problem under study and is specified in the respective sections.

The material densities of the solid skeleton and the liquid pore water as well as the partial densities of the gas components within the overall gas phase are given via

$$\begin{aligned}
 \rho^{SR} &= \rho_{0S}^{SR} [1 - 3\alpha^S(\theta^S - \theta_0^S)], \\
 \rho^{LR} &= \rho_{0L}^{LR} e^{-\gamma^L(\theta^L - \theta_0^L)}, \\
 \rho_G^V &= p_G^V M^V / (R\theta^G), \quad \rho_G^A = p_G^A M^A / (R\theta^G), \\
 c_G^V &= \rho_G^V / (\rho_G^V + \rho_G^A), \quad c_G^A = \rho_G^A / (\rho_G^V + \rho_G^A), \\
 x_{Gm}^V &= p_G^V / (p_G^V + p_G^A), \quad x_{Gm}^A = p_G^A / (p_G^V + p_G^A).
 \end{aligned} \tag{3.181}$$

The mass production between the liquid and gaseous pore water is governed, generally, by the following relations:

$$\begin{aligned}
 \hat{\rho}^L &= - \{ [(n^G \rho_G^V)'_S + n^G \rho_G^V \operatorname{div}(\mathbf{u}_S)'_S + \operatorname{div}[n^G \rho_G^V (\mathbf{w}_G + \mathbf{d}_{VG})]] \}, \\
 \left. \begin{aligned}
 s^L &= 1 \quad \text{and} \\
 \xi^L - \eta^L(\theta^S - \theta^L) + \frac{1}{2} \mathbf{w}_L \cdot \mathbf{w}_L \\
 &\quad - [\xi^V - \eta^V(\theta^S - \theta^G) + \frac{1}{2} \mathbf{w}_V \cdot \mathbf{w}_V] > 0
 \end{aligned} \right\} \hat{\rho}^L = 0, \\
 \left. \begin{aligned}
 0 \leq s^L \leq 1 \quad \text{and} \\
 \xi^L - \eta^L(\theta^S - \theta^L) + \frac{1}{2} \mathbf{w}_L \cdot \mathbf{w}_L \\
 &\quad - [\xi^V - \eta^V(\theta^S - \theta^G) + \frac{1}{2} \mathbf{w}_V \cdot \mathbf{w}_V] = 0
 \end{aligned} \right\} \hat{\rho}^L \neq 0, \\
 \left. \begin{aligned}
 s^L &= 0 \quad \text{and} \\
 \xi^L - \eta^L(\theta^S - \theta^L) + \frac{1}{2} \mathbf{w}_L \cdot \mathbf{w}_L \\
 &\quad - [\xi^V - \eta^V(\theta^S - \theta^G) + \frac{1}{2} \mathbf{w}_V \cdot \mathbf{w}_V] < 0
 \end{aligned} \right\} \hat{\rho}^L = 0.
 \end{aligned} \tag{3.182}$$

As in this contribution, mass interactions are only considered in the thermal equilibrium, (3.182) can be simplified, if furthermore the kinetic energies of the pore fluids are

neglected:

$$\begin{aligned}
& \text{assuming: } \theta^\alpha = \theta, \quad p_G^V = p_{G\text{sat}}^V(\theta), \quad \frac{1}{2} \mathbf{w}_L \cdot \mathbf{w}_L \approx \frac{1}{2} \mathbf{w}_V \cdot \mathbf{w}_V \approx 0 \\
& \hat{\rho}^L = - \{ [(n^G \rho_G^V)'_S + n^G \rho_G^V \operatorname{div}(\mathbf{u}_S)'_S + \operatorname{div}[n^G \rho_G^V (\mathbf{w}_G + \mathbf{d}_{VG})]] \}, \\
& p_{G\text{sat}}^V(\theta) = p_0 \cdot 10^{(C_1 - \frac{C_2}{\theta + C_3})} \quad \text{following Antoine, cf. (3.89)}, \\
& s^L = 1 \quad \text{and} \quad p^{LR} > p_{G\text{sat}}^V(\theta) \quad \longrightarrow \quad \hat{\rho}^L = 0, \\
& 0 \leq s^L \leq 1 \quad \text{and} \quad p_G^V = p_{G\text{sat}}^V(\theta) \quad \longrightarrow \quad \hat{\rho}^L \neq 0, \\
& s^L = 0 \quad \text{and} \quad p_G^V < p_{G\text{sat}}^V(\theta) \quad \longrightarrow \quad \hat{\rho}^L = 0.
\end{aligned} \tag{3.183}$$

The solid skeleton is governed within an elasto-viscoplastic scheme by the yield criterion F , the plastic potential G , the flow rule and a relation for the plastic multiplier:

$$\begin{aligned}
& \text{yield criterion:} \\
& \quad F = \Phi^{1/2} + \beta \mathbf{I} + \epsilon \mathbf{I}^2 - \kappa = 0, \\
& \quad \Phi = \mathbb{I}^D (1 + \gamma \vartheta)^m + \frac{1}{2} \alpha \mathbf{I}^2 + \delta^2 \mathbf{I}^4, \\
& \quad \vartheta = \mathbb{III}^D / (\mathbb{II}^D)^{3/2}, \\
& \text{plastic potential:} \\
& \quad G = \Gamma^{1/2} + \psi_2 \mathbf{I} + \epsilon \mathbf{I}^2, \\
& \quad \Gamma = \psi_1 \mathbb{I}^D + \frac{1}{2} \alpha \mathbf{I}^2 + \delta^2 \mathbf{I}^4, \\
& \text{flow rule and plastic multiplier:} \\
& \quad (\boldsymbol{\varepsilon}_{Sp})'_S = \Lambda \frac{\partial G}{\partial \boldsymbol{\sigma}_{E\text{mech}}^S}, \quad \Lambda = \frac{1}{\eta} \left\langle \frac{F(\boldsymbol{\sigma}_{E\text{mech}}^S)}{\sigma_0} \right\rangle_r.
\end{aligned} \tag{3.184}$$

The stress tensors of the pore fluids are only governed by the respective pressures, while the frictional stresses are neglected. The linearized stress tensor of the solid skeleton consists of both, one part governed by the overall effective pore fluid pressure and a second part, where the extra stress is related to the linearized strain and the temperature of the solid phase via the well-known *Hookean* elasticity law extended for the description of thermal effects:

$$\begin{aligned}
\mathbf{T}^L &= -n^L p^{LR} \mathbf{I}, \quad \mathbf{T}^V = -n^G p_G^V \mathbf{I}, \quad \mathbf{T}^A = -n^G p_G^A \mathbf{I}, \\
\boldsymbol{\sigma}^S &= -n^S p^{FR} \mathbf{I} + 2\mu^S \boldsymbol{\varepsilon}_{Se} + \lambda^S (\boldsymbol{\varepsilon}_{Se} \cdot \mathbf{I}) \mathbf{I} + m^S (\theta^S - \theta_0^S) \mathbf{I}, \\
p^{FR} &= s^L \frac{\theta^S}{\theta^L} p^{LR} + (1 - s^L) \frac{\theta^S}{\theta^G} (p_G^V + p_G^A), \\
\boldsymbol{\varepsilon}_S &= \boldsymbol{\varepsilon}_{Se} + \boldsymbol{\varepsilon}_{Sp}, \quad \boldsymbol{\varepsilon}_S = \frac{1}{2} [\operatorname{grad} \mathbf{u}_S + (\operatorname{grad} \mathbf{u}_S)^T].
\end{aligned} \tag{3.185}$$

The velocities of the pore fluids are described with respect to the deformable solid skeleton. Therefore, the so-called filter as well as diffusion velocities are introduced. The constitutive relations, which were found in the last sections, relate these velocities to the respective gradients of the pressures, whereas, in the non-isothermal case, the filter velocities are additionally related to the gradient of the porosity:

$$\begin{aligned}
n^L \mathbf{w}_L &= -\frac{\kappa_r^L \mathbf{K}^S}{\mu^{LR}} \left\{ \text{grad } p^{LR} - \rho^{LR} \mathbf{b} - p^{LR} \left[\frac{1}{n^F} \text{grad } n^F \left(\frac{\theta^S}{\theta^L} - 1 \right) \right] \right\}, \\
n^G \mathbf{w}_G &= -\frac{\kappa_r^G \mathbf{K}^S}{\mu^{GR}} \left\{ \text{grad } (p_G^V + p_G^A) - (\rho_G^V + \rho_G^A) \mathbf{b} - \right. \\
&\quad \left. - (p_G^V + p_G^A) \left[\frac{1}{n^F} \text{grad } n^F \left(\frac{\theta^S}{\theta^G} - 1 \right) \right] \right\}, \\
\kappa_r^L &= \kappa_r^L(s^L), \quad \kappa_r^G = \kappa_r^G(s^L), \quad \text{depends on the problem,} \\
\mathbf{K}^S &= \left(\frac{1 - n^S}{1 - n_{0S}^S} \right)^\pi K_{0S}^S \mathbf{I}, \\
n^G \mathbf{d}_{VG} &= -\frac{\rho_G^V + \rho_G^A}{\rho_G^V} \frac{p_0^{GR}}{p_G^V + p_G^A} d \left(\frac{\theta^G}{\theta_0^G} \right)^z \text{grad } x_{Gm}^V, \\
n^G \mathbf{d}_{AG} &= -\frac{\rho_G^V + \rho_G^A}{\rho_G^A} \frac{p_0^{GR}}{p_G^V + p_G^A} d \left(\frac{\theta^G}{\theta_0^G} \right)^z \text{grad } x_{Gm}^A.
\end{aligned} \tag{3.186}$$

At this point, the relative permeability factors κ_r^L and κ_r^G are not specified, because these relations correspond to the capillary pressure saturation relation, which depends on the considered initial boundary-value problem.

Concerning the free *Helmholtz* energies ψ^α of the constituents, these terms are based on the respective specific heats C_V^α , whereas the free *Helmholtz* energies of the solid skeleton and the pore liquid are governed, furthermore, by the linearized strain tensor $\boldsymbol{\varepsilon}_S$ and the temperature dependency of the material densities ρ^{SR} and ρ^{LR} . The free *Helmholtz*

energy ψ^L of the pore liquid is additionally a function of the saturation s^L :

$$\begin{aligned}
\rho_{0S}^S \psi^S &= \mu^S \boldsymbol{\varepsilon}_S \cdot \boldsymbol{\varepsilon}_S + \frac{1}{2} \lambda^S (\boldsymbol{\varepsilon}_S \cdot \mathbf{I})^2 + m^S (\theta^S - \theta_0^S) \boldsymbol{\varepsilon}_S \cdot \mathbf{I} - \\
&\quad - \rho_{0S}^S C_V^S \left[\theta^S \ln \frac{\theta^S}{\theta_0^S} - (\theta^S - \theta_0^S) \right] - \rho_{0S}^S \eta_0^S (\theta^S - \theta_0^S) - \\
&\quad - \rho_{0S}^S \frac{p_0^{FR}}{\rho_{0S}^S} 3\alpha^S (\theta^S - \theta_0^S) + \rho_{0S}^S \psi_0^S, \\
\psi^L &= -C_V^L \left[\theta^L \ln \frac{\theta^L}{\theta_0^L} - (\theta^L - \theta_0^L) \right] - \eta_0^L (\theta^L - \theta_0^L) - \\
&\quad - \frac{1}{\rho_0^{LR}} [p_0^{LR} + p^D (s^L)^{-1}] \gamma^L (\theta^L - \theta_0^L) + \\
&\quad + \left[\frac{p^D}{\rho_0^{LR}} (s^L)^{-1} - \frac{p^D}{\rho_0^{LR}} (s_0^L)^{-1} \right] + \psi_0^L, \\
\psi^V &= -C_V^V \left[\theta^G \ln \frac{\theta^G}{\theta_0^G} - (\theta^G - \theta_0^G) \right] + \frac{R\theta^G}{M^V} \ln \frac{\rho_G^V}{\rho_{G0}^V} - \\
&\quad - \eta_0^V (\theta^G - \theta_0^G) + \psi_0^V, \\
\psi^A &= -C_V^A \left[\theta^G \ln \frac{\theta^G}{\theta_0^G} - (\theta^G - \theta_0^G) \right] + \frac{R\theta^G}{M^A} \ln \frac{\rho_G^A}{\rho_{G0}^A} - \\
&\quad - \eta_0^A (\theta^G - \theta_0^G) + \psi_0^A.
\end{aligned} \tag{3.187}$$

The entropy η^α of a single constituent is given by the derivative of the free *Helmholtz* energy ψ^α with respect to the corresponding temperature θ^α . Concerning the materially incompressible constituents, i. e., the solid and pore liquid phase, an additional part results from the assumption that the effective densities ρ^{SR} and ρ^{LR} depend on the temperature:

$$\begin{aligned}
\eta^S &= C_V^S \ln \frac{\theta^S}{\theta_0^S} - (p^{FR} - p_0^{FR}) \frac{3\alpha^S}{\rho_{0S}^S} - \frac{1}{\rho_{0S}^S} m^S \boldsymbol{\varepsilon}_S \cdot \mathbf{I} + \eta_0^S, \\
\eta^L &= C_V^L \ln \frac{\theta^L}{\theta_0^L} - \left\{ \frac{1}{\rho_0^{LR}} [p^{LR} + p^D (s^L)^{-1}] - \right. \\
&\quad \left. - \frac{1}{\rho_0^{LR}} [p_0^{LR} + p^D (s_0^L)^{-1}] \right\} \gamma^L + \eta_0^L, \\
\eta^V &= C_V^V \ln \frac{\theta^G}{\theta_0^G} - \frac{R}{M^V} \ln \frac{\rho_G^V}{\rho_{G0}^V} + \eta_0^V, \\
\eta^A &= C_V^A \ln \frac{\theta^G}{\theta_0^G} - \frac{R}{M^A} \ln \frac{\rho_G^A}{\rho_{G0}^A} + \eta_0^A.
\end{aligned} \tag{3.188}$$

Based on the above presented free *Helmholtz* energies and entropies, the internal energy can be computed via (2.83).

The stress powers of the pore fluids, e. g., $\mathbf{T}^L \cdot \mathbf{L}_L = -n^L p^{LR} \mathbf{I} \cdot \mathbf{L}_L = -n^L p^{LR} \operatorname{div} \dot{\mathbf{x}}_L$, can be computed using the respective mass balances, which are solved for $\operatorname{div} \dot{\mathbf{x}}_\xi$. Furthermore, the heat influx vectors \mathbf{q}^α depend on the temperature gradients, whereas the heat conduction tensor is reduced to the isotropic case, $\mathbf{H}_r^\alpha = h_r^\alpha \mathbf{I}$:

stress powers:

$$\begin{aligned} \mathbf{T}^L \cdot \mathbf{L}_L &= -\frac{p^{LR}}{\rho^{LR}} [\hat{\rho}^L - (n^L \rho^{LR})'_S - \operatorname{grad} (n^L \rho^{LR}) \cdot \mathbf{w}_L], \\ \mathbf{T}^V \cdot \mathbf{L}_V &= -\frac{p_G^V}{\rho_G^V} [-\hat{\rho}^L - (n^G \rho_G^V)'_S - \operatorname{grad} (n^G \rho_G^V) \cdot (\mathbf{w}_G + \mathbf{d}_{VG})], \\ \mathbf{T}^A \cdot \mathbf{L}_A &= -\frac{p_G^A}{\rho_G^A} [-(n^G \rho_G^A)'_S - \operatorname{grad} (n^G \rho_G^A) \cdot (\mathbf{w}_G + \mathbf{d}_{AG})], \end{aligned} \quad (3.189)$$

heat influx vectors:

$$\begin{aligned} \mathbf{q}^S &= -n^S h_r^S \operatorname{grad} \theta^S, & \mathbf{q}^L &= -n^L h_r^L \operatorname{grad} \theta^L, \\ \mathbf{q}^V &= -n^G x_{Gm}^V h_r^V \operatorname{grad} \theta^G, & \mathbf{q}^A &= -n^G x_{Gm}^A h_r^A \operatorname{grad} \theta^G. \end{aligned}$$

The constitutive relation for the direct energy production of the pore fluids is governed by the temperature difference between the single phases, whereas the direct energy production $\hat{\varepsilon}^S$ of the solid skeleton can be computed using the constraints (3.2)₂₋₄:

$$\begin{aligned} \hat{\varepsilon}^L &= k_{SL}^{\varepsilon V} (\theta^S - \theta^L) + (k_{VL}^{\varepsilon V} + k_{AL}^{\varepsilon V}) (\theta^G - \theta^L), \\ \hat{\varepsilon}^V &= k_{SV}^{\varepsilon V} (\theta^S - \theta^G) + k_{LV}^{\varepsilon V} (\theta^L - \theta^G), \\ \hat{\varepsilon}^A &= k_{SA}^{\varepsilon V} (\theta^S - \theta^G) + k_{LA}^{\varepsilon V} (\theta^L - \theta^G), \\ \hat{\varepsilon}^S &= -\hat{\varepsilon}^L - \hat{\varepsilon}^V - \hat{\varepsilon}^A - \\ &\quad - \hat{\mathbf{p}}^L \cdot \mathbf{w}_L - \hat{\mathbf{p}}^V \cdot (\mathbf{w}_G + \mathbf{d}_{VG}) - \hat{\mathbf{p}}^A \cdot (\mathbf{w}_G + \mathbf{d}_{AG}) - \\ &\quad - \hat{\rho}^L [\varepsilon^L - \varepsilon^V + \frac{1}{2} \mathbf{w}_L \cdot \mathbf{w}_L - \frac{1}{2} (\mathbf{w}_G + \mathbf{d}_{VG}) \cdot (\mathbf{w}_G + \mathbf{d}_{VG})], \\ \hat{\mathbf{p}}^L &= (\theta^S / \theta^L) p^{LR} \operatorname{grad} n^L - (n^L)^2 \mu^{LR} (\kappa_r^L \mathbf{K}^S)^{-1} \mathbf{w}_L + \\ &\quad + [(\theta^S / \theta^G) p^{GR} - (\theta^S / \theta^L) p^{LR}] n^F \operatorname{grad} s^L, \\ \hat{\mathbf{p}}^V &= (\theta^S / \theta^G) p_G^V \operatorname{grad} n^G - c_G^V (n^G)^2 \mu^{GR} (\kappa_r^G \mathbf{K}^S)^{-1} \mathbf{w}_G - \\ &\quad - (n^G)^2 (p^{GR})^2 c_G^V (p_0^{GR} d\mathbf{I})^{-1} (\theta^G / \theta_0^G)^{-z} \mathbf{d}_{VG}, \\ \hat{\mathbf{p}}^A &= (\theta^S / \theta^G) p_G^A \operatorname{grad} n^G - c_G^A (n^G)^2 \mu^{GR} (\kappa_r^G \mathbf{K}^S)^{-1} \mathbf{w}_G - \\ &\quad - (n^G)^2 (p^{GR})^2 c_G^A (p_0^{GR} d\mathbf{I})^{-1} (\theta^G / \theta_0^G)^{-z} \mathbf{d}_{AG}. \end{aligned} \quad (3.190)$$

Within this work, phase transitions between liquid and gaseous pore water are only considered assuming thermal equilibrium, cf. $\theta^\alpha = \theta$. In this case, only one energy balance is

required and, therefore, the energy balance of the overall mixture is chosen as governing equation for the temperature θ of the overall medium. This balance relation is given via the sum of the energy balances of the individual constituents:

$$\begin{aligned}
& n^S \rho^{SR} (\varepsilon^S)'_S - \boldsymbol{\sigma}^S \cdot (\boldsymbol{\varepsilon}_S)'_S + \\
& + (n^L \rho^{LR} \varepsilon^L)'_S + n^L \rho^{LR} \zeta^L \operatorname{div}(\mathbf{u}_S)'_S + \\
& + \operatorname{div}(n^L \rho^{LR} \zeta^L \mathbf{w}_L) - \mathbf{w}_L \cdot \operatorname{grad}(n^L p^{LR}) + \\
& + (n^G \rho_G^V \varepsilon^V)'_S + n^G \rho_G^V \zeta^V \operatorname{div}(\mathbf{u}_S)'_S + \\
& + \operatorname{div}[n^G \rho_G^V \zeta^V (\mathbf{w}_G + \mathbf{d}_{VG})] - (\mathbf{w}_G + \mathbf{d}_{VG}) \cdot \operatorname{grad}(n^G p_G^V) + \\
& + (n^G \rho_G^A \varepsilon^A)'_S + n^G \rho_G^A \zeta^A \operatorname{div}(\mathbf{u}_S)'_S + \\
& + \operatorname{div}[n^G \rho_G^A \zeta^A (\mathbf{w}_G + \mathbf{d}_{AG})] - (\mathbf{w}_G + \mathbf{d}_{AG}) \cdot \operatorname{grad}(n^G p_G^A) + \\
& + \operatorname{div} \mathbf{q}^S + \operatorname{div} \mathbf{q}^L + \operatorname{div} \mathbf{q}^V + \operatorname{div} \mathbf{q}^A - \\
& - [n^S \rho^{SR} + n^L \rho^{LR} + n^G (\rho_G^V + \rho_G^A)] r^G = 0.
\end{aligned} \tag{3.191}$$

Therein, the mass balances of the pore fluids, cf. (2.56), are used to eliminate the mass production terms and are furthermore added to the energy balances multiplied by the internal energies. The resulting terms are then reorganized using the definition of the enthalpy $\zeta^\zeta = \varepsilon^\zeta + p^{\zeta R} / \rho^{\zeta R}$. Furthermore, it is assumed that the kinetic energies of the pore fluids can be neglected describing multiphasic flow processes in porous materials.

Chapter 4: Numerical Treatment

After the introduction of the governing balance equations as well as the constitutive relations of the continuum mechanical model under study in the previous chapters, its numerical realization is presented now. Thereby, after the derivation of the required weak formulations of the governing equations, the spatial and temporal discretization as well as the solution of the resulting nonlinear system of equations are discussed. Finally, a special regard is taken on the numerical treatment of multiphasic flow processes in porous materials.

In particular, the weak formulations of the governing equations, which are required for the numerical treatment, are derived in Section 4.1. Furthermore, in Section 4.2 the spatial discretization of the considered domain is carried out using the finite element method (FEM), whereas the temporal domain is discretized based on a finite difference scheme. Additionally, the solution of the resulting nonlinear system of equations is discussed, whereby a special focus is taken on the difficulties resulting from the elastoplastic material behavior of the solid skeleton. The argumentation and notations within these sections follow the works of *Ammann* [2], *Ellsiepen* [68] and *Wieners et al.* [140]. For a more fundamental view on the FEM, the reader is referred to *Bathe* [6], *Braess* [18], *Eriksson et al.* [69], *Hughes* [93], *Oden & Reddy* [112], *Schwarz* [121], *Strang & Fix* [129] or *Zienkiewicz & Taylor* [146,147], whereas a detailed discussion of different time integration schemes can be found in *Hairer et al.* [80,81], *Strehmel & Weiner* [130], *Törnig & Spellucci* [132] or *Wood* [143]. Finally, the special numerical treatment of multiphasic flow processes in porous materials are discussed in Section 4.3, which leads to the application of a certain stabilization technique to overcome the occurring numerical problems. A detailed discussion of this topic under the assumption of a rigid solid skeleton is given in *Class et al.* [28], *Forsyth* [71], *Knabner & Angermann* [98], *Helmig* [90], *Helmig & Huber* [91], *Niessner et al.* [111] and *Paul* [113]. The reader, who is generally interested in the numerical treatment of porous media models, where a deformable solid behavior is taken into account is referred to the works of the research group of Ehlers [46, 48, 49, 53, 54, 56, 108] as well as Schrefler and coworkers, e. g., [105, 118–120].

4.1 Weak formulations of the governing equations

The numerical treatment of the continuum mechanical model is based on the governing equations derived in Section 3.4. Therewith, together with the respective initial and boundary conditions, the strong formulation of the initial boundary-value problem of continuum mechanics is given. The resulting system of equations has to be fulfilled at each material point \mathbf{x} of the considered domain Ω . Due to the fact that only for some special initial boundary-value problems an exact solution can be found, this restriction is generally too strict. Therefore, it is required that the balance equations have only to be fulfilled in an integral manner, i. e., in a weak sense, and no longer point-wise at each

material point. To obtain such a weak formulation, the governing equations of the model under study are scalarly multiplied with a test function and integrated over the domain Ω .

First of all, the trial (ansatz) spaces, i. e.,

$$\begin{aligned}
\mathcal{S}_u(t) &= \{ \mathbf{u}_S \in H^1(\Omega)^D : \mathbf{u}_S(\mathbf{x}) = \bar{\mathbf{u}}_S(\mathbf{x}, t) \text{ on } \Gamma_u \}, \\
\mathcal{S}_{pl}(t) &= \{ p^{LR} \in H^1(\Omega) : p^{LR}(\mathbf{x}) = \bar{p}^{LR}(\mathbf{x}, t) \text{ on } \Gamma_{pl} \}, \\
\mathcal{S}_{pvg}(t) &= \{ p_G^V \in H^1(\Omega) : p_G^V(\mathbf{x}) = \bar{p}_G^V(\mathbf{x}, t) \text{ on } \Gamma_{pvg} \}, \\
\mathcal{S}_{pag}(t) &= \{ p_G^A \in H^1(\Omega) : p_G^A(\mathbf{x}) = \bar{p}_G^A(\mathbf{x}, t) \text{ on } \Gamma_{pag} \}, \\
\mathcal{S}_{ts}(t) &= \{ \theta^S \in H^1(\Omega) : \theta^S(\mathbf{x}) = \bar{\theta}^S(\mathbf{x}, t) \text{ on } \Gamma_{ts} \}, \\
\mathcal{S}_{tl}(t) &= \{ \theta^L \in H^1(\Omega) : \theta^L(\mathbf{x}) = \bar{\theta}^L(\mathbf{x}, t) \text{ on } \Gamma_{tl} \}, \\
\mathcal{S}_{tg}(t) &= \{ \theta^G \in H^1(\Omega) : \theta^G(\mathbf{x}) = \bar{\theta}^G(\mathbf{x}, t) \text{ on } \Gamma_{tg} \},
\end{aligned} \tag{4.1}$$

and test spaces, i. e.,

$$\begin{aligned}
\mathcal{T}_u &= \{ \delta \mathbf{u}_S \in H^1(\Omega)^D : \delta \mathbf{u}_S(\mathbf{x}) = \mathbf{0} \text{ on } \Gamma_u \}, \\
\mathcal{T}_{pl} &= \{ \delta p^{LR} \in H^1(\Omega) : \delta p^{LR}(\mathbf{x}) = 0 \text{ on } \Gamma_{pl} \}, \\
\mathcal{T}_{pvg} &= \{ \delta p_G^V \in H^1(\Omega) : \delta p_G^V(\mathbf{x}) = 0 \text{ on } \Gamma_{pvg} \}, \\
\mathcal{T}_{pag} &= \{ \delta p_G^A \in H^1(\Omega) : \delta p_G^A(\mathbf{x}) = 0 \text{ on } \Gamma_{pag} \}, \\
\mathcal{T}_{ts} &= \{ \delta \theta^S \in H^1(\Omega) : \delta \theta^S(\mathbf{x}) = 0 \text{ on } \Gamma_{ts} \}, \\
\mathcal{T}_{tl} &= \{ \delta \theta^L \in H^1(\Omega) : \delta \theta^L(\mathbf{x}) = 0 \text{ on } \Gamma_{tl} \}, \\
\mathcal{T}_{tg} &= \{ \delta \theta^G \in H^1(\Omega) : \delta \theta^G(\mathbf{x}) = 0 \text{ on } \Gamma_{tg} \},
\end{aligned} \tag{4.2}$$

are defined, where $D \in \{1, 2, 3\}$ indicates the dimension of the considered problem and $H^1(\Omega)$ indicates the standard *Sobolev* space. $\bar{\mathbf{u}}_S$, \bar{p}^{LR} , \bar{p}_G^V , \bar{p}_G^A , $\bar{\theta}^S$, $\bar{\theta}^L$ and $\bar{\theta}^G$ are the *Dirichlet* (or essential) boundary conditions of the underlying model, which give the value of the respective primary variables on the *Dirichlet* boundaries Γ_u , Γ_{pl} , Γ_{pvg} , Γ_{pag} , Γ_{ts} , Γ_{tl} and Γ_{tg} . One can recognize that the trial functions are exactly equal to the *Dirichlet* boundary conditions, whereas the test functions $\delta \mathbf{u}_S$, δp^{LR} , δp_G^V , δp_G^A , $\delta \theta^S$, $\delta \theta^L$ and $\delta \theta^G$ vanish at the *Dirichlet* boundaries.

The derivation of the weak formulations is now presented exemplary for the momentum balance of the overall mixture, cf. (3.179)_{1,2}. Firstly, this equation is multiplied scalarly by the respective test function $\delta \mathbf{u}_S$ and integrated over the domain Ω . In a second step, the term governed by the divergence operator is reformulated using the product rule and the *Gaußian* integral theorem. Thus, the weak formulation of the momentum balance of

the overall mixture reads for $\hat{\rho}^L = 0$

$$\begin{aligned} \mathcal{G}_{\text{MM}} \equiv & \int_{\Omega} (\boldsymbol{\sigma}^S + \mathbf{T}^L + \mathbf{T}^V + \mathbf{T}^A) \cdot \text{grad } \delta \mathbf{u}_S \, dv - \int_{\Omega} \rho \mathbf{b} \cdot \delta \mathbf{u}_S \, dv - \\ & - \int_{\Gamma_t} \bar{\mathbf{t}} \cdot \delta \mathbf{u}_S \, da = 0 \quad \forall \delta \mathbf{u}_S \in \mathcal{T}_u. \end{aligned} \quad (4.3)$$

Taking mass interactions into account, i. e., $\hat{\rho}^L \neq 0$, one finds:

$$\begin{aligned} \mathcal{G}_{\text{MM}} \equiv & \int_{\Omega} (\boldsymbol{\sigma}^S + \mathbf{T}^L + \mathbf{T}^V + \mathbf{T}^A - \rho^L \mathbf{d}_L \otimes \mathbf{d}_L - \rho^V \mathbf{d}_V \otimes \mathbf{d}_V) \cdot \text{grad } \delta \mathbf{u}_S \, dv - \\ & - \int_{\Omega} \rho \mathbf{b} \cdot \delta \mathbf{u}_S \, dv - \int_{\Gamma_t} \bar{\mathbf{t}} \cdot \delta \mathbf{u}_S \, da = 0 \quad \forall \delta \mathbf{u}_S \in \mathcal{T}_u. \end{aligned} \quad (4.4)$$

Therein, a surface integral appears, which is governed by the overall surface traction $\bar{\mathbf{t}} = (\boldsymbol{\sigma}^S + \mathbf{T}^L + \mathbf{T}^V + \mathbf{T}^A) \mathbf{n}$ or $\bar{\mathbf{t}} = (\boldsymbol{\sigma}^S + \mathbf{T}^L + \mathbf{T}^V + \mathbf{T}^A - \rho^L \mathbf{d}_L \otimes \mathbf{d}_L - \rho^V \mathbf{d}_V \otimes \mathbf{d}_V) \mathbf{n}$ acting on the so-called *Neumann* boundary Γ_t of the overall mixture. Therefore, two different boundary conditions can be identified generally: the *Dirichlet* and the *Neumann* boundary conditions. Thus, the boundary $\Gamma = \partial\Omega$ of the domain Ω is split for each primary variable \mathbf{u}_S , p^{LR} , p_G^V , p_G^A , θ^S , θ^L and θ^G into a *Dirichlet* and a *Neumann* boundary Γ_t , Γ_{ml} , Γ_{mv} , Γ_{ma} , Γ_{qs} , Γ_{ql} and Γ_{qg} in the following way:

$$\begin{aligned} \Gamma &= \Gamma_u \cup \Gamma_t, & \emptyset &= \Gamma_u \cap \Gamma_t, \\ \Gamma &= \Gamma_{pl} \cup \Gamma_{ml}, & \emptyset &= \Gamma_{pl} \cap \Gamma_{ml}, \\ \Gamma &= \Gamma_{pvg} \cup \Gamma_{mv}, & \emptyset &= \Gamma_{pvg} \cap \Gamma_{mv}, \\ \Gamma &= \Gamma_{pag} \cup \Gamma_{ma}, & \emptyset &= \Gamma_{pag} \cap \Gamma_{ma}, \\ \Gamma &= \Gamma_{ts} \cup \Gamma_{qs}, & \emptyset &= \Gamma_{ts} \cap \Gamma_{qs}, \\ \Gamma &= \Gamma_{tl} \cup \Gamma_{ql}, & \emptyset &= \Gamma_{tl} \cap \Gamma_{ql}, \\ \Gamma &= \Gamma_{tg} \cup \Gamma_{qg}, & \emptyset &= \Gamma_{tg} \cap \Gamma_{qg}. \end{aligned} \quad (4.5)$$

Thereby, it is assumed that on a certain boundary point only one, a *Dirichlet* or a *Neumann* boundary condition, can be specified. Furthermore, using the momentum balance of the mixture as governing equation for the displacement vector \mathbf{u}_S of the solid skeleton, the *Neumann* boundary condition acts on the overall mixture. Therefore, the applied surface traction has not to be separated into certain parts acting on the several constituents, which is very convenient for the numerical modeling of porous materials, because the volume fractions can change during the computation.

By the same procedure, the weak formulations of the pore liquids mass balance,

$$\begin{aligned} \mathcal{G}_{ML} \equiv & \int_{\Omega} [(\rho^L)'_S + \rho^L \operatorname{div}(\mathbf{u}_S)'_S] \delta p^{LR} dv - \int_{\Omega} \rho^{LR} n^L \mathbf{w}_L \cdot \operatorname{grad} \delta p^{LR} dv - \\ & - \int_{\Omega} \hat{\rho}^L \delta p^{LR} dv + \int_{\Gamma_{mt}} \bar{m}^L \delta p^{LR} da = 0 \quad \forall \quad \delta p^{LR} \in \mathcal{T}_{pl}, \end{aligned} \quad (4.6)$$

the water vapors mass balance,

$$\begin{aligned} \mathcal{G}_{MV} \equiv & \int_{\Omega} [(\rho^V)'_S + \rho^V \operatorname{div}(\mathbf{u}_S)'_S] \delta p_G^V dv - \int_{\Omega} \rho_G^V n^G \mathbf{w}_V \cdot \operatorname{grad} \delta p_G^V dv + \\ & + \int_{\Gamma_{mv}} \bar{m}^V \delta p_G^V da = 0 \quad \forall \quad \delta p_G^V \in \mathcal{T}_{pvG}, \end{aligned} \quad (4.7)$$

and the pore airs mass balance,

$$\begin{aligned} \mathcal{G}_{MA} \equiv & \int_{\Omega} [(\rho^A)'_S + \rho^A \operatorname{div}(\mathbf{u}_S)'_S] \delta p_G^A dv - \int_{\Omega} \rho_G^A n^G \mathbf{w}_A \cdot \operatorname{grad} \delta p_G^A dv + \\ & + \int_{\Gamma_{ma}} \bar{m}^A \delta p_G^A da = 0 \quad \forall \quad \delta p_G^A \in \mathcal{T}_{pag}, \end{aligned} \quad (4.8)$$

result from a formal scalar multiplication of the mass balances of the fluid constituents by the test functions δp^{LR} , δp_G^V as well as δp_G^A and a further integration over the considered domain Ω . Therein, the resulting surface integrals, i. e., the *Neumann* boundaries, are governed by the respective mass effluxes $\bar{m}^L = \rho^{LR} n^L \mathbf{w}_L \cdot \mathbf{n}$, $\bar{m}^V = \rho_G^V n^G \mathbf{w}_V \cdot \mathbf{n}$ and $\bar{m}^A = \rho_G^A n^G \mathbf{w}_A \cdot \mathbf{n}$ over the boundary of the considered domain Ω . Remember that the water vapors mass balance is only a governing equation, if no liquid pore water exists. Therefore, $\hat{\rho}^L$ does not appear in equation (4.7).

After the scalar multiplication with the test function $\delta \theta^S$, a further integration over the domain Ω and the reformulation of the part governed by the heat influx vector, the weak formulation of the energy balance of the solid phase reads

$$\begin{aligned} \mathcal{G}_{ES} \equiv & \int_{\Omega} [\rho^S (\varepsilon^S)'_S - \boldsymbol{\sigma}^S \cdot (\boldsymbol{\varepsilon}_S)'_S] \delta \theta^S dv - \int_{\Omega} (\rho^S r^S + \hat{\varepsilon}^S) \delta \theta^S dv - \\ & - \int_{\Omega} \mathbf{q}^S \cdot \operatorname{grad} \delta \theta^S dv + \int_{\Gamma_{qs}} \bar{q}^S \delta \theta^S da = 0 \quad \forall \quad \delta \theta^S \in \mathcal{T}_{ts}, \end{aligned} \quad (4.9)$$

where $\bar{q}^S = \mathbf{q}^S \cdot \mathbf{n}$ is the heat influx of the solid skeleton through the *Neumann* boundary Γ_{qs} . The same procedure yields the weak formulation of the energy balance of the pore

liquid,

$$\begin{aligned}
\mathcal{G}_{\text{EL}} \equiv & \int_{\Omega} [(\rho^L \varepsilon^L)'_S + \rho^L \zeta^L \text{div}(\mathbf{u}_S)'_S] \delta\theta^L \, dv + \\
& + \int_{\Omega} (\mathbf{w}_L \cdot \text{div} \mathbf{T}^L - \hat{\varepsilon}^L - \varepsilon^L \hat{\rho}^L - \rho^L r) \delta\theta^L \, dv - \\
& - \int_{\Omega} (\rho^L \zeta^L \mathbf{w}_L + \mathbf{q}^L) \cdot \text{grad} \delta\theta^L \, dv + \int_{\Gamma_{qt}} \bar{q}^L \delta\theta^L \, da = 0 \quad \forall \delta\theta^L \in \mathcal{T}_{tl},
\end{aligned} \tag{4.10}$$

and the weak formulation of the energy balance of the overall gas phase,

$$\begin{aligned}
\mathcal{G}_{\text{EG}} \equiv & \int_{\Omega} [(\rho^V \varepsilon^V)'_S + (\rho^A \varepsilon^A)'_S + (\rho^V \zeta^V + \rho^A \zeta^A) \text{div}(\mathbf{u}_S)'_S] \delta\theta^G \, dv + \\
& + \int_{\Omega} (\mathbf{w}_V \cdot \text{div} \mathbf{T}^V + \mathbf{w}_A \cdot \text{div} \mathbf{T}^A) \delta\theta^G \, dv + \\
& + \int_{\Omega} [\varepsilon^V \hat{\rho}^L - \hat{\varepsilon}^V - \hat{\varepsilon}^A - (\rho^A + \rho^V) r] \delta\theta^G \, dv - \\
& - \int_{\Omega} (\rho^V \zeta^V \mathbf{w}_V + \rho^A \zeta^A \mathbf{w}_A + \mathbf{q}^V + \mathbf{q}^A) \cdot \text{grad} \delta\theta^G \, dv + \\
& + \int_{\Gamma_{gg}} \bar{q}^G \delta\theta^G \, da = 0 \quad \forall \delta\theta^G \in \mathcal{T}_{tg}.
\end{aligned} \tag{4.11}$$

Therein, the mass balances of the pore fluids, cf. (2.56), are used to eliminate the mass production terms and are added furthermore to the energy balances multiplied by the internal energies. The resulting terms are then reorganized using the definition of the enthalpy $\zeta^\zeta = \varepsilon^\zeta + p^{\zeta R}/\rho^{\zeta R}$. Thus, the *Neumann* boundary conditions are governed by $\bar{q}^L = (\rho^L \zeta^L \mathbf{w}_L + \mathbf{q}^L) \cdot \mathbf{n}$ and $\bar{q}^G = (\rho^V \zeta^V \mathbf{w}_V + \rho^A \zeta^A \mathbf{w}_A + \mathbf{q}^V + \mathbf{q}^A) \cdot \mathbf{n}$ and, therefore, not only by the respective heat influx vectors \mathbf{q}^ζ , but also by the enthalpy flux $\rho^\zeta \zeta^\zeta \mathbf{w}_\zeta$ through the boundary.

Within this contribution, mass interactions are only considered under thermal equilibrium ($\theta^\alpha = \theta$). Thus, the governing equation for the overall temperature is given by the energy balance of the overall mixture. The respective weak formulation is not explicitly given here, but can be easily computed by summing up the weak formulations of the single energy balances. In this case, the mass production only appears in a product with the kinetic energy $\frac{1}{2} \mathbf{w}_\zeta \cdot \mathbf{w}_\zeta$. Due to the fact that the seepage velocity \mathbf{w}_ζ in porous materials is very low, this product is neglected. Furthermore, the pressures can be approximated by linear ansatz functions, because all volume integrals governed by the divergence of the seepage velocity $\text{div}([\dots] \mathbf{w}_\zeta)$, i. e., governed by $\text{div}([\dots] \text{grad} p^{\zeta R})$, can be reformulated using the product rule and the *Gaussian* integral theorem. Therefore, only first derivatives in space are required.

4.2 Spatial and temporal discretization

For a numerical treatment of the governing equations, the above presented continuous formulation has to be discretized in the spatial as well as in the temporal domain. Within this contribution, the spatial discretization is carried out using the finite element method (FEM), whereas the implicit (backward) *Euler* method is used for the time integration.

4.2.1 Finite element method

The considered domain Ω is approximated by a spatially discretized domain Ω^h , which consists of a finite number of non-overlapping subdomains, the finite elements, or, more general, the cells C :

$$\Omega \approx \Omega^h = \bigcup_{C \in \mathcal{C}} C, \quad (4.12)$$

where \mathcal{C} is the set of all cells in the finite element mesh. In a further step, the continuously defined trial spaces $\mathcal{S}(t)$ and test spaces \mathcal{T} have to be approximated by finite-dimensional (N -dimensional) subspaces $\mathcal{S}^h(t)$ and \mathcal{T}^h , respectively, cf. *Ehlers & Ellsiepen* [53] and *Ellsiepen* [68]. Thus, the space discrete ansatz functions

$$\begin{aligned} \mathbf{u}_S(\mathbf{x}, t) &\approx \mathbf{u}_S^h(\mathbf{x}, t) = \bar{\mathbf{u}}_S^h(\mathbf{x}, t) + \sum_{j=1}^N \phi_u^j(\mathbf{x}) \mathbf{u}_S^j(t) \in \mathcal{S}_u^h(t), \\ p^{LR}(\mathbf{x}, t) &\approx p^{LRh}(\mathbf{x}, t) = \bar{p}^{LRh}(\mathbf{x}, t) + \sum_{j=1}^N \phi_{pl}^j(\mathbf{x}) p^{LRj}(t) \in \mathcal{S}_{pl}^h(t), \\ p_G^V(\mathbf{x}, t) &\approx p_G^{Vh}(\mathbf{x}, t) = \bar{p}_G^{Vh}(\mathbf{x}, t) + \sum_{j=1}^N \phi_{pvg}^j(\mathbf{x}) p_G^{Vj}(t) \in \mathcal{S}_{pvg}^h(t), \\ p_G^A(\mathbf{x}, t) &\approx p_G^{Ah}(\mathbf{x}, t) = \bar{p}_G^{Ah}(\mathbf{x}, t) + \sum_{j=1}^N \phi_{pag}^j(\mathbf{x}) p_G^{Aj}(t) \in \mathcal{S}_{pag}^h(t), \\ \theta^S(\mathbf{x}, t) &\approx \theta^{Sh}(\mathbf{x}, t) = \bar{\theta}^{Sh}(\mathbf{x}, t) + \sum_{j=1}^N \phi_{ts}^j(\mathbf{x}) \theta^{Sj}(t) \in \mathcal{S}_{ts}^h(t), \\ \theta^L(\mathbf{x}, t) &\approx \theta^{Lh}(\mathbf{x}, t) = \bar{\theta}^{Lh}(\mathbf{x}, t) + \sum_{j=1}^N \phi_{tl}^j(\mathbf{x}) \theta^{Lj}(t) \in \mathcal{S}_{tl}^h(t), \\ \theta^G(\mathbf{x}, t) &\approx \theta^{Gh}(\mathbf{x}, t) = \bar{\theta}^{Gh}(\mathbf{x}, t) + \sum_{j=1}^N \phi_{tg}^j(\mathbf{x}) \theta^{Gj}(t) \in \mathcal{S}_{tg}^h(t) \end{aligned} \quad (4.13)$$

and test functions

$$\begin{aligned}
\delta \mathbf{u}_S(\mathbf{x}) &\approx \delta \mathbf{u}_S^h(\mathbf{x}) = \sum_{j=1}^N \phi_u^j(\mathbf{x}) \delta \mathbf{u}_S^j \in \mathcal{T}_u^h, \\
\delta p^{LR}(\mathbf{x}) &\approx \delta p^{LRh}(\mathbf{x}) = \sum_{j=1}^N \phi_{pl}^j(\mathbf{x}) \delta p^{LRj} \in \mathcal{T}_{pl}^h, \\
\delta p_G^V(\mathbf{x}) &\approx \delta p_G^{Vh}(\mathbf{x}) = \sum_{j=1}^N \phi_{pvg}^j(\mathbf{x}) \delta p_G^{Vj} \in \mathcal{T}_{pvg}^h, \\
\delta p_G^A(\mathbf{x}) &\approx \delta p_G^{Ah}(\mathbf{x}) = \sum_{j=1}^N \phi_{pag}^j(\mathbf{x}) \delta p_G^{Aj} \in \mathcal{T}_{pag}^h, \\
\delta \theta^S(\mathbf{x}) &\approx \delta \theta^{Sh}(\mathbf{x}) = \sum_{j=1}^N \phi_{ts}^j(\mathbf{x}) \delta \theta^{Sj} \in \mathcal{T}_{ts}^h, \\
\delta \theta^L(\mathbf{x}) &\approx \delta \theta^{Lh}(\mathbf{x}) = \sum_{j=1}^N \phi_{tl}^j(\mathbf{x}) \delta \theta^{Lj} \in \mathcal{T}_{tl}^h, \\
\delta \theta^G(\mathbf{x}) &\approx \delta \theta^{Gh}(\mathbf{x}) = \sum_{j=1}^N \phi_{tg}^j(\mathbf{x}) \delta \theta^{Gj} \in \mathcal{T}_{tg}^h
\end{aligned} \tag{4.14}$$

are introduced, wherein N indicates the total number of nodal points in the mesh and the set $\{\bar{\mathbf{u}}_S^h, \bar{p}^{LRh}, \bar{p}_G^{Vh}, \bar{p}_G^{Ah}, \bar{\theta}^{Sh}, \bar{\theta}^{Lh}, \bar{\theta}^{Gh}\}$ defines the *Dirichlet* boundary conditions. Furthermore, $\{\phi_u^j, \phi_{pl}^j, \phi_{pvg}^j, \phi_{pag}^j, \phi_{ts}^j, \phi_{tl}^j, \phi_{tg}^j\}$ are the global basis functions of the respective ansatz and test functions, wherein $\phi_u^j = [\phi_{u_1}^j, \dots, \phi_{u_D}^j]$. They are linearly independent, fulfill homogeneous *Dirichlet* boundary conditions, i. e.,

$$\begin{aligned}
\phi_{u_d}^j &= 0 \quad \text{on } \Gamma_{u_d}^h, \quad j = 1, \dots, N, \quad d = 1, \dots, D, \\
\phi_{pl}^j &= 0 \quad \text{on } \Gamma_{pl}^h, \quad j = 1, \dots, N, \\
\phi_{pvg}^j &= 0 \quad \text{on } \Gamma_{pvg}^h, \quad j = 1, \dots, N, \\
\phi_{pag}^j &= 0 \quad \text{on } \Gamma_{pag}^h, \quad j = 1, \dots, N, \\
\phi_{ts}^j &= 0 \quad \text{on } \Gamma_{ts}^h, \quad j = 1, \dots, N, \\
\phi_{tl}^j &= 0 \quad \text{on } \Gamma_{tl}^h, \quad j = 1, \dots, N, \\
\phi_{tg}^j &= 0 \quad \text{on } \Gamma_{tg}^h, \quad j = 1, \dots, N,
\end{aligned} \tag{4.15}$$

and depend only on the spatial position \mathbf{x} , whereas the unknown nodal quantities are only time-dependent.

Remark: By the above given definitions, the same basis functions for the ansatz and test functions are used. This assumption is well-known as *Bubnov-Galerkin* method. In

general, different basis functions can be chosen for the ansatz and test functions (*Petrov-Galerkin* method), which is done, e. g., in the frame of certain numerical stabilization techniques, cf. [20, 51, 90]. \square

Furthermore, each nodal point $\bar{P} \in \mathcal{N}$, where \mathcal{N} is the set of all nodal points of the finite element mesh, corresponds to a basis function ϕ_{dof}^j , which yields non-zero values only in the cells $C \in \mathcal{C}_{\bar{P}}$, where the set $\mathcal{C}_{\bar{P}}$ collects all finite elements including the nodal point \bar{P} . To ensure furthermore that the nodal quantities correspond exactly to the approximated solution, the basis functions are normalized:

$$\begin{aligned} \phi_{dof}^j(\mathbf{x}) &= 0, & \text{if } \mathbf{x} \notin \bigcup_{C \in \mathcal{C}_{\bar{P}}} C, & \quad dof \in \{u_d, pl, pvg, pag, ts, tl, tg\}, \\ \phi_{dof}^j(\mathbf{x}_i) &= \delta_i^j, & i, j &= 1, \dots, N. \end{aligned} \quad (4.16)$$

Therein, the *Kronecker* symbol δ_i^j gives non-zero values only if $i = j$.

Using the above introduced relations, the whole procedure of spatial discretization yields finally a system of linearly independent equations for the determination of the unknown nodal quantities (degrees of freedom), where each degree of freedom corresponds to one linearly independent equation.

Considering multiphase problems, the spatial discretized model under study is governed by several primary variables, which results within the FEM in a so-called mixed finite element formulation. Thereby, the ansatz functions for the individual primary variables can be chosen differently. Nevertheless, one has to be careful in the choice of the ansatz functions to prevent oscillations in the numerical solutions. Mathematically, the chosen ansatz functions have to fulfill the *Ladyzhenskaya-Babuška-Brezzi* (or inf-sub) condition specifying the spaces of the ansatz functions to each other. For a closer look on this topic, the interested reader is referred to *Braess* [18], *Brezzi & Fortin* [19], *Langtangen & Tveito* [103] and *Wieners* [138].

Regarding the *Stokes* equation in fluid mechanics, where the primary variables are the velocity and the pressure of the respective fluid, often so-called *Taylor-Hood* elements, which are based on quadratic ansatz functions for the velocity field and linear ansatz functions for the pressure field are used, cf. [18, 103]. *Brezzi & Fortin* [19] show that such a combination of ansatz functions fulfills the above mentioned inf-sub condition. The inf-sub condition is not fulfilled, if linear ansatz functions for both unknowns are used, cf. [18, 94, 145]. From an engineering point of view, one can find the same result by taking a closer look on the stress tensor, which consists of two parts. One part is governed by the pressure, whereas the second part is governed by the gradient of the kinematical primary variable. Choosing the ansatz functions of the kinematical primary variable by one order higher, both stress parts are approximated by the same polynomial order. Furthermore, assuming a materially incompressible fluid, the volume balance as the governing equation for the pressure is independent of its respective primary variable. This results in zero values on the main diagonal of the overall stiffness matrix concerning the primary variable pressure, which can yield to a singular and, therefore, a none invertible stiffness matrix in case that the pressure unknowns are dominating. Based on these findings, extended *Taylor-Hood* elements are used for the spatial discretization of the model under study. This means,

the solid displacement is approximated by quadratic ansatz functions, whereas the pore fluid pressures as well as the temperatures are approximated by linear ansatz functions.

Remark: In fluid mechanics, unstable solutions are avoided by applying certain numerical stabilization techniques, while the same ansatz functions for the velocity and the pressure are used. Thereby, the test functions are modified in such a way that no zero values on the main diagonal of the stiffness matrix appear, cf. [20, 73, 74, 145]. *Ehlers et al.* [55] used such a technique for the numerical treatment of a biphasic porous media model, where both the solid displacement as well as the pore fluid pressure are approximated by linear ansatz functions. \square

Concerning the numerical implementation within a finite element program, all necessary quantities like the residual or the tangent are firstly computed on the element level before they are assembled to the respective global quantities. Thereby, the certain ansatz and test functions are given with respect to a reference element C_r , i. e., they are given with respect to some local coordinates $\boldsymbol{\xi}$. Thus, a geometry transformation has to be carried out to relate the physical coordinate system \mathbf{x} to the local coordinates $\boldsymbol{\xi}$:

$$\mathbf{x}(\boldsymbol{\xi}) = \sum_{j=1}^{N_g} \phi_{geo}^j(\boldsymbol{\xi}) \mathbf{x}_j. \quad (4.17)$$

Therein, N_g indicates the number of nodes in the element and $\phi_{geo}^j(\boldsymbol{\xi})$ are the basis functions of the geometry transformation, which are formulated with respect to the local coordinates and fulfill condition (4.16).

Remark: Within this contribution, quadratic ansatz functions for the geometry transformation are chosen. This means that, using extended *Taylor-Hood* elements, an isoparametric mapping for the solid displacement and a superparametric mapping for the pressures and the temperatures are used [2]. \square

As the weak formulations are evaluated on the element level as well, the appearing integrals have to be reformulated with respect to the above introduced local coordinates:

$$\int_C f(\mathbf{x}) dv = \int_{C_r} f(\mathbf{x}(\boldsymbol{\xi})) J_C(\boldsymbol{\xi}) dv_r, \quad \text{where} \quad J_C(\boldsymbol{\xi}) = \det \left(\frac{d\mathbf{x}(\boldsymbol{\xi})}{d\boldsymbol{\xi}} \right) \quad (4.18)$$

is the *Jacobian determinant* and dv_r is the incremental volume element of C_r . Furthermore, the integration is carried out numerically using the *Gauß* quadrature:

$$\int_C f(\mathbf{x}) dv \approx \sum_{k=1}^{\tilde{K}} f(\mathbf{x}(\boldsymbol{\xi}_k)) J_C(\boldsymbol{\xi}_k) w_k. \quad (4.19)$$

Thereby, the integrals are approximated via an evaluation of the weak formulations on \tilde{K} integration points $\boldsymbol{\xi}_k$ multiplied by certain weight factors w_k . Due to the fact that this integration is carried out on the element level with respect to a special reference element, the integration points as well as the weight factors are fixed quantities for every reference element.

As the problem has to be discretized in the spatial as well as in the temporal domain, a so-called semi-discrete initial-value problem can be formulated after the spatial discretization:

$$\mathbf{F}(t, \mathbf{y}, \mathbf{y}') = \begin{bmatrix} \mathbf{F}_1(t, \mathbf{u}, \mathbf{u}', \mathbf{q}) \\ \mathbf{F}_2(t, \mathbf{q}, \mathbf{q}', \mathbf{u}) \end{bmatrix} = \begin{bmatrix} \mathbf{M}\mathbf{u}' + \mathbf{k}(\mathbf{u}, \mathbf{q}) - \mathbf{f} \\ \mathbf{A}\mathbf{q}' - \mathbf{g}(\mathbf{q}, \mathbf{u}) \end{bmatrix} \stackrel{!}{=} \mathbf{0}. \quad (4.20)$$

Thereby, the governing equations ($\mathbf{F}_1 = \mathbf{0}$) as well as the plastic evolution equations ($\mathbf{F}_2 = \mathbf{0}$) are combined to one overall system of equations. Furthermore, the space-discrete variables are collected within the vectors

$$\begin{aligned} \mathbf{u} &= [(\mathbf{u}_S^1, p^{LR1}, p_G^{V1}, p_G^{A1}, \theta^{S1}, \theta^{L1}, \theta^{G1}), \dots, \\ &\quad \dots, (\mathbf{u}_S^N, p^{LRN}, p_G^{VN}, p_G^{AN}, \theta^{SN}, \theta^{LN}, \theta^{GN})]^T \quad \text{and} \\ \mathbf{q} &= [(\boldsymbol{\varepsilon}_{Sp}^1, \Lambda^1), \dots, (\boldsymbol{\varepsilon}_{Sp}^K, \Lambda^K)]^T, \end{aligned} \quad (4.21)$$

where N is the number of nodal points and K the number of integration points of the FE mesh. Furthermore, in the vector $\mathbf{y} = (\mathbf{u}^T, \mathbf{q}^T)^T$ all unknown quantities of the problem are summarized. The vector \mathbf{u} contains all degrees of freedom, whereby it is assumed for simplicity that at each nodal point all primary variables are present, which is not the case, if extended *Taylor-Hood* elements are used, because different ansatz functions are chosen for the different primary variables. All internal (history) variables, i. e., the plastic strain $\boldsymbol{\varepsilon}_{Sp}$ and the plastic multiplier Λ , are summarized in the vector \mathbf{q} . These internal variables are evaluated element-wise at the integration points by solving the plastic evolution equations:

$$\mathbf{A}\mathbf{q}' - \mathbf{g}(\mathbf{q}, \mathbf{u}) = \begin{bmatrix} (\boldsymbol{\varepsilon}_{Sp})' \\ 0 \end{bmatrix} - \begin{bmatrix} \Lambda \frac{\partial G}{\partial \boldsymbol{\sigma}_{E \text{ mech}}^S} \\ \frac{1}{\eta} \left\langle \frac{F(\boldsymbol{\sigma}_{E \text{ mech}}^S)}{\sigma_0} \right\rangle^r - \Lambda \end{bmatrix} = \mathbf{0}. \quad (4.22)$$

Furthermore, \mathbf{M} is the generalized mass matrix, \mathbf{k} the generalized stiffness vector and \mathbf{f} the vector of external forces. The time derivative $(\cdot)'_S$ with respect to the solid skeleton is expressed via $(\cdot)'$. For completeness, initial conditions $\mathbf{y}(t_0) = \mathbf{y}_0$ are necessary, which give the values of the unknowns at the initial time t_0

4.2.2 Time integration

After the spatial discretization, the occurring time dependent quantities within the governing equations have to be discretized as well. Generally, one can choose between explicit or implicit time integration methods, but only the application of an implicit time integration scheme leads to unconditionally stable solutions of the problem under study, cf. [68, 82]. Therefore, the implicit (or backward) *Euler* scheme, which belongs to the wide range of *Runge-Kutta* methods, is used for the time discretization within this contribution, because of its low numerical effort.

Regarding the general, nonlinear problem

$$\mathbf{u}'(t_n) = \mathbf{h}(\mathbf{u}_n, t_n) \quad (4.23)$$

formulated at the actual time t_n , where $\mathbf{u}' = d\mathbf{u}/dt$ represents the first order time derivative of the vector \mathbf{u} , in which the unknown quantities are collected. Furthermore, \mathbf{h} is an arbitrary, nonlinear function of the unknown quantities and the time t . The time derivative $\mathbf{u}'(t_n)$ is discretized by

$$\mathbf{u}'(t_n) = \frac{\mathbf{u}_n - \mathbf{u}_{n-1}}{\Delta t_n} \quad \longrightarrow \quad \mathbf{u}_n = \mathbf{u}_{n-1} + \mathbf{u}'(t_n)\Delta t_n, \quad (4.24)$$

where the time increment $\Delta t_n = t_n - t_{n-1}$ is introduced. Note that within an explicit time integration scheme, the nonlinear problem (4.23) is formulated at the last time step t_{n-1} . Inserting (4.24) into (4.23), one finds finally

$$\mathbf{u}_n - \mathbf{u}_{n-1} - \mathbf{h}(\mathbf{u}_n, t_n)\Delta t_n = 0. \quad (4.25)$$

Obviously, in contrast to an explicit time integration scheme, relation (4.25) cannot be solved directly for the actual unknown quantities \mathbf{u} , but has to be evaluated during an iterative procedure like, e. g., the *Newton-Raphson* method. For a more detailed view on the topic of time integration schemes, the interested reader is referred to the work of *Ellsiepen* [68].

4.2.3 Solution of the nonlinear system of equations

After the weak formulations have been discretized in the spatial as well as in the temporal domain, the resulting nonlinear system of equations has to be solved for a certain initial boundary-value problem. Therefore, one has to determine the new values of the vectors \mathbf{u}_n and \mathbf{q}_n such that

$$\mathcal{R}^{h,n}(t_n, \mathbf{u}_n, \mathbf{q}_n) = \begin{bmatrix} \mathcal{R}_{MM}^{h,n}(t_n, \mathbf{u}_n, \mathbf{q}_n) \\ \mathcal{R}_{ML}^{h,n}(t_n, \mathbf{u}_n) \\ \mathcal{R}_{MV}^{h,n}(t_n, \mathbf{u}_n) \\ \mathcal{R}_{MA}^{h,n}(t_n, \mathbf{u}_n) \\ \mathcal{R}_{ES}^{h,n}(t_n, \mathbf{u}_n, \mathbf{q}_n) \\ \mathcal{R}_{EL}^{h,n}(t_n, \mathbf{u}_n) \\ \mathcal{R}_{EG}^{h,n}(t_n, \mathbf{u}_n) \end{bmatrix} \stackrel{!}{=} \mathbf{0}, \quad (4.26)$$

where

$$\begin{aligned}
\mathcal{R}_{MM}^{h,n}(t_n, \mathbf{u}_n, \mathbf{q}_n) &= \left[\mathcal{R}_{MM}^{h,n}(t_n, \mathbf{u}_n, \mathbf{q}_n; \phi_{u_1}^1), \dots, \mathcal{R}_{MM}^{h,n}(t_n, \mathbf{u}_n, \mathbf{q}_n; \phi_{u_D}^N) \right]^T, \\
\mathcal{R}_{ML}^{h,n}(t_n, \mathbf{u}_n) &= \left[\mathcal{R}_{ML}^{h,n}(t_n, \mathbf{u}_n; \phi_{pl}^1), \dots, \mathcal{R}_{ML}^{h,n}(t_n, \mathbf{u}_n; \phi_{pl}^N) \right]^T, \\
\mathcal{R}_{MV}^{h,n}(t_n, \mathbf{u}_n) &= \left[\mathcal{R}_{MV}^{h,n}(t_n, \mathbf{u}_n; \phi_{pvg}^1), \dots, \mathcal{R}_{MV}^{h,n}(t_n, \mathbf{u}_n; \phi_{pvg}^N) \right]^T, \\
\mathcal{R}_{MA}^{h,n}(t_n, \mathbf{u}_n) &= \left[\mathcal{R}_{MA}^{h,n}(t_n, \mathbf{u}_n; \phi_{pag}^1), \dots, \mathcal{R}_{MA}^{h,n}(t_n, \mathbf{u}_n; \phi_{pag}^N) \right]^T, \\
\mathcal{R}_{ES}^{h,n}(t_n, \mathbf{u}_n, \mathbf{q}_n) &= \left[\mathcal{R}_{ES}^{h,n}(t_n, \mathbf{u}_n, \mathbf{q}_n; \phi_{ts}^1), \dots, \mathcal{R}_{ES}^{h,n}(t_n, \mathbf{u}_n, \mathbf{q}_n; \phi_{ts}^N) \right]^T, \\
\mathcal{R}_{EL}^{h,n}(t_n, \mathbf{u}_n) &= \left[\mathcal{R}_{EL}^{h,n}(t_n, \mathbf{u}_n; \phi_{il}^1), \dots, \mathcal{R}_{EL}^{h,n}(t_n, \mathbf{u}_n; \phi_{il}^N) \right]^T, \\
\mathcal{R}_{EG}^{h,n}(t_n, \mathbf{u}_n) &= \left[\mathcal{R}_{EG}^{h,n}(t_n, \mathbf{u}_n; \phi_{tg}^1), \dots, \mathcal{R}_{EG}^{h,n}(t_n, \mathbf{u}_n; \phi_{tg}^N) \right]^T
\end{aligned} \tag{4.27}$$

is the residual formulation of the discretized weak formulations (4.3) or (4.4) and (4.6)-(4.11). The procedure for the solution of the nonlinear system (4.26) reads:

- Start the *Newton-Raphson* method:
 - ▷ Compute the element-wise residual $(\mathcal{R}^{h,n,j})_C$ based on the element solution vector $(\mathbf{u}_n^j)_C$, the old element solution vector $(\mathbf{u}_{n-1})_C$ and the old element vector of the internal variables $(\mathbf{q}_{n-1})_C$ and assemble the global residual $\mathcal{R}^{h,n,j}$. The index j indicates the current *Newton* step.
 - ▷ Incorporate the *Neumann* and the *Dirichlet* boundary conditions by subtracting the respective values of the surface integrals and the difference between the old nodal and the new *Dirichlet* value, respectively, on the corresponding positions in the global residual $\mathcal{R}^{h,n,j}$.
 - ▷ Compute the element-wise consistent tangent $(D\mathcal{R}^{h,n,j})_C$ based on the element solution vector $(\mathbf{u}_n^j)_C$, the old element solution vector $(\mathbf{u}_{n-1})_C$ and the old element vector of the internal variables $(\mathbf{q}_{n-1})_C$ and assemble the global consistent tangent $D\mathcal{R}^{h,n,j}$.
 - ▷ Set those rows of the global consistent tangent $D\mathcal{R}^{h,n,j}$ to zero, which correspond to the unknowns determined via a *Dirichlet* boundary condition, and, additionally, set a “1” on the main diagonal entries of those rows.
 - ▷ Solve the global linear system $D\mathcal{R}^{h,n,j} \Delta \mathbf{u}_n^j = \mathcal{R}^{h,n,j}$ for the *Newton* increment $\Delta \mathbf{u}_n^j$ and update the solution vector: $\mathbf{u}_n^{j+1} = \mathbf{u}_n^j - \Delta \mathbf{u}_n^j$.
- If the residual norm fulfills the user-defined tolerance,

$$\|\mathcal{R}^{h,n,j+1}\| < tol,$$

update the vector of the internal variables and accept the last solution vector. If no convergence within the *Newton-Raphson* method is obtained after $j = j_{max}$ *Newton* steps, bisect the time step size and start the *Newton* iteration again.

Although this is a standard procedure within the finite element method, a closer look should be done on the discretized formulation of the plastic evolution equations and the consistent tangent, which is necessary for the *Newton-Raphson* procedure.

Concerning the numerical treatment of the elastoplastic material behavior of the solid skeleton, a so-called trial stress $\boldsymbol{\sigma}_{E\text{trial}}^{Sn} = \mathbf{C}[\boldsymbol{\varepsilon}(\mathbf{u}_S^{h,n}) - \boldsymbol{\varepsilon}_{Sp}^{h,n-1}]$ is determined at every integration point. Therein, $\mathbf{C} := \overset{4}{\mathbf{C}} = 2\mu^S(\mathbf{I} \otimes \mathbf{I})^{\overset{23}{T}} + \lambda^S(\mathbf{I} \otimes \mathbf{I})$ denotes the fourth order elasticity tensor, where the transposition $(\cdot)^{\overset{ik}{T}}$ indicates an exchange of the i -th and k -th basis systems included into the tensor basis of higher order tensors, cf. Appendix A.1.3. Note that this trial stress is computed based on the current solid displacement $\mathbf{u}_S^{h,n}$ and the old plastic strains $\boldsymbol{\varepsilon}_{Sp}^{h,n-1}$. If the trial stress violates the yield criterion, the plastic evolution equations (4.22) are entered, which read after the spatial and temporal discretization

$$\begin{aligned}\boldsymbol{\varepsilon}_{Sp}^{h,n} &= \boldsymbol{\varepsilon}_{Sp}^{h,n-1} + \Delta t_n \Lambda^{h,n} \frac{\partial G(\boldsymbol{\sigma}_{E\text{mech}}^S(\mathbf{u}_S^{h,n}, \boldsymbol{\varepsilon}_{Sp}^{h,n}))}{\partial \boldsymbol{\sigma}_{E\text{mech}}^S}, \\ \Lambda^{h,n} &= \frac{1}{\eta} \left\langle \frac{F(\boldsymbol{\sigma}_{E\text{mech}}^S(\mathbf{u}_S^{h,n}, \boldsymbol{\varepsilon}_{Sp}^{h,n}))}{\sigma_0} \right\rangle_r.\end{aligned}\quad (4.28)$$

By solving (4.28), a compatible strain increment $\Delta \boldsymbol{\varepsilon}_{Sp}^{h,n} = \boldsymbol{\varepsilon}_{Sp}^{h,n} - \boldsymbol{\varepsilon}_{Sp}^{h,n-1}$ is determined. Thus, one can require alternatively: Find $\Delta \boldsymbol{\varepsilon}_{Sp}^{h,n}$ and the plastic multiplier $\Lambda^{h,n}$ such that

$$\begin{aligned}\Delta \boldsymbol{\varepsilon}_{Sp}^{h,n} &= \Delta t_n \Lambda^{h,n} \frac{\partial G(\boldsymbol{\sigma}_{E\text{trial}}^{Sn} - \mathbf{C}\Delta \boldsymbol{\varepsilon}_{Sp}^{h,n})}{\partial \boldsymbol{\sigma}_{E\text{mech}}^S}, \\ \eta \Lambda^{h,n} &= \left\langle \frac{F(\boldsymbol{\sigma}_{E\text{trial}}^{Sn} - \mathbf{C}\Delta \boldsymbol{\varepsilon}_{Sp}^{h,n})}{\sigma_0} \right\rangle_r\end{aligned}\quad (4.29)$$

or by using the new stress state $\boldsymbol{\sigma}_{E\text{mech}}^{Sn} = \boldsymbol{\sigma}_{E\text{trial}}^{Sn} - \mathbf{C}\Delta \boldsymbol{\varepsilon}_{Sp}^{h,n}$: For a given trial stress $\boldsymbol{\sigma}_{E\text{trial}}^{Sn}$, find the stress response $\boldsymbol{\sigma}_{E\text{mech}}^{Sn}$ and the plastic multiplier $\Lambda^{h,n}$ such that

$$\begin{aligned}\boldsymbol{\sigma}_{E\text{mech}}^{Sn} &= \boldsymbol{\sigma}_{E\text{trial}}^{Sn} - \Delta t_n \Lambda^{h,n} \mathbf{C} \frac{\partial G(\boldsymbol{\sigma}_{E\text{mech}}^{Sn})}{\partial \boldsymbol{\sigma}_{E\text{mech}}^S}, \\ \eta \Lambda^{h,n} &= \left\langle \frac{F(\boldsymbol{\sigma}_{E\text{mech}}^{Sn})}{\sigma_0} \right\rangle_r.\end{aligned}\quad (4.30)$$

Thus, the resulting stress response

$$\boldsymbol{\sigma}_{E\text{mech}}^{Sn} = \bar{\mathbf{P}}^n(\boldsymbol{\sigma}_{E\text{trial}}^{Sn}) = \bar{\mathbf{P}}^n(\mathbf{u}_S^{h,n}, \boldsymbol{\varepsilon}_{Sp}^{h,n-1}) \quad (4.31)$$

has to be inserted into the weak formulation of the momentum balance to get the final formulation of $\mathcal{R}_{MM}^{h,n}$. Finally, if the norm of the global residual fulfills the user-defined tolerance, the plastic strains are updated:

$$\boldsymbol{\varepsilon}_{Sp}^{h,n} = \boldsymbol{\varepsilon}(\mathbf{u}_S^{h,n}) - \mathbf{C}^{-1} \bar{\mathbf{P}}^n(\mathbf{C}[\boldsymbol{\varepsilon}(\mathbf{u}_S^{h,n}) - \boldsymbol{\varepsilon}_{Sp}^{h,n-1}]). \quad (4.32)$$

It is obvious following the above given argumentation that the new internal variables \mathbf{q}_n^j depend on the solid displacement $\mathbf{u}_S^{h,n}$. This fact has to be taken into account, while the global tangent is computed,

$$D\mathcal{R}^{h,n,j} = \frac{d\mathcal{R}^{h,n,j}}{d\mathbf{u}_n^j} = \frac{\partial\mathcal{R}^{h,n,j}}{\partial\mathbf{u}_n^j} + \frac{\partial\mathcal{R}^{h,n,j}}{\partial\mathbf{q}_n^j} \frac{d\mathbf{q}_n^j}{d\mathbf{u}_n^j}, \quad (4.33)$$

leading directly to the introduction of the term “algorithmically consistent linearization”, cf. [67, 123, 144]. The derivation of the internal variables \mathbf{q}_n^j with respect to the primary variables \mathbf{u}_n^j can be computed in the following way

$$\begin{aligned} \mathcal{R}_{\text{local}}^{h,n,j} &\stackrel{!}{=} \mathbf{0}, \quad \frac{d\mathcal{R}_{\text{local}}^{h,n,j}}{d\mathbf{u}_n^j} = \frac{\partial\mathcal{R}_{\text{local}}^{h,n,j}}{\partial\mathbf{u}_n^j} + \frac{\partial\mathcal{R}_{\text{local}}^{h,n,j}}{\partial\mathbf{q}_n^j} \frac{d\mathbf{q}_n^j}{d\mathbf{u}_n^j} = \mathbf{0} \\ \longrightarrow \quad \frac{d\mathbf{q}_n^j}{d\mathbf{u}_n^j} &= - \left[\frac{\partial\mathcal{R}_{\text{local}}^{h,n,j}}{\partial\mathbf{q}_n^j} \right]^{-1} \frac{\partial\mathcal{R}_{\text{local}}^{h,n,j}}{\partial\mathbf{u}_n^j}. \end{aligned} \quad (4.34)$$

Therein,

$$\mathcal{R}_{\text{local}}^{h,n}(t_n, \mathbf{u}_n, \mathbf{q}_n) = \begin{bmatrix} \mathcal{R}_{\text{local } 1}^{h,n}(t_n, \mathbf{u}_n, \mathbf{q}_n) \\ \vdots \\ \mathcal{R}_{\text{local } K}^{h,n}(t_n, \mathbf{u}_n, \mathbf{q}_n) \end{bmatrix} \stackrel{!}{=} \mathbf{0} \quad (4.35)$$

is the residual formulation of (4.28), K indicates the number of integration points and

$$\mathcal{R}_{\text{local } k}^{h,n}(t_n, \mathbf{u}_n, \mathbf{q}_n) = \begin{bmatrix} \boldsymbol{\varepsilon}_{Sp}^{h,n} - \boldsymbol{\varepsilon}_{Sp}^{h,n-1} - \Delta t_n \Lambda^{h,n} \frac{\partial G(\boldsymbol{\sigma}_{E \text{ mech}}^S(\mathbf{u}_S^{h,n}, \boldsymbol{\varepsilon}_{Sp}^{h,n}))}{\partial \boldsymbol{\sigma}_{E \text{ mech}}^S} \\ \Lambda^{h,n} - \frac{1}{\eta} \left\langle \frac{F(\boldsymbol{\sigma}_{E \text{ mech}}^S(\mathbf{u}_S^{h,n}, \boldsymbol{\varepsilon}_{Sp}^{h,n}))}{\sigma_0} \right\rangle_r \end{bmatrix}_{\mathbf{x}=\mathbf{x}_k} \quad (4.36)$$

is obtained at each integration point $k = 1, \dots, K$ with the global position \mathbf{x}_k . The indicator j of the current *Newton* iteration is thereby omitted. Thus, using (4.34) the consistent global tangent reads finally

$$D\mathcal{R}^{h,n,j} = \frac{\partial\mathcal{R}^{h,n,j}}{\partial\mathbf{u}_n^j} - \frac{\partial\mathcal{R}^{h,n,j}}{\partial\mathbf{q}_n^j} \left[\frac{\partial\mathcal{R}_{\text{local}}^{h,n,j}}{\partial\mathbf{q}_n^j} \right]^{-1} \frac{\partial\mathcal{R}_{\text{local}}^{h,n,j}}{\partial\mathbf{u}_n^j}. \quad (4.37)$$

4.3 Multiphasic flow processes

Within the numerical treatment of porous materials, special attention has to be taken on the correct modeling of the multiphasic flow process. Assuming a porous material with two pore fluids, the primary variables are generally the displacement of the solid skeleton and the pressures of the two pore fluids. Furthermore, the saturation is a function of

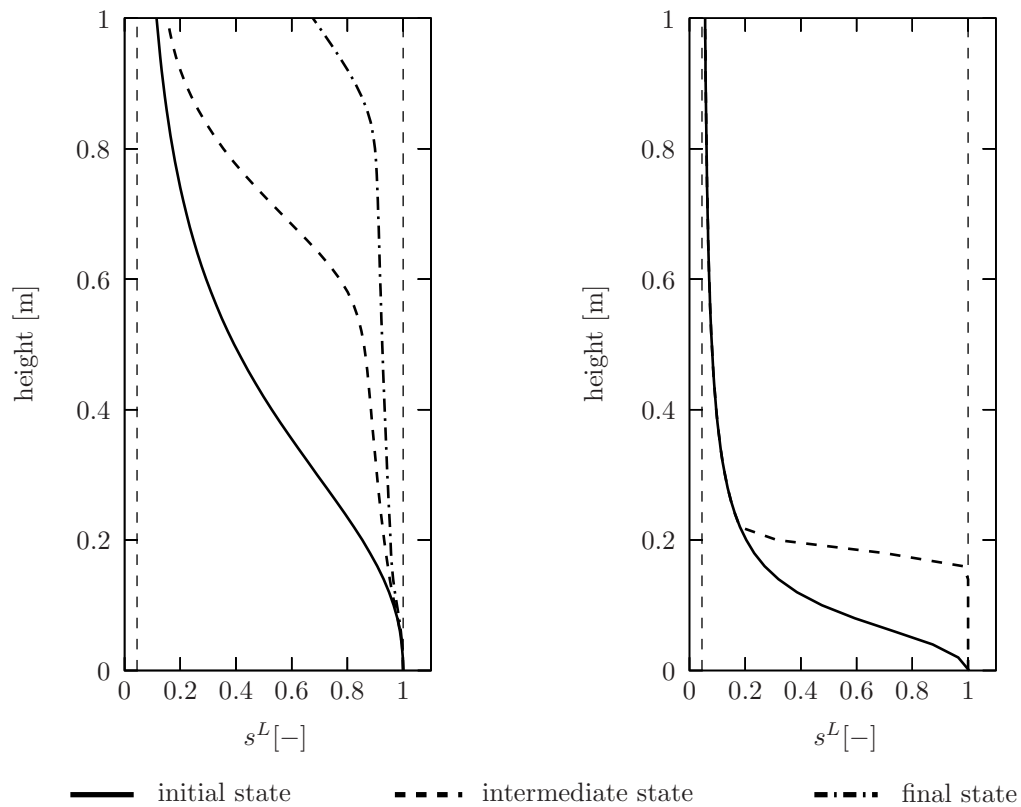


Figure 4.1: Saturation s^L of the pore water over the height of a clayey silt (left) and a sand (right) column computed using a *Bubnov-Galerkin* procedure.

the capillary pressure and can be computed via the capillary pressure saturation relation. Problems occur, if porous materials with low capillary effects, e. g., granular materials like sand, are considered, because the derivative of the capillary pressure saturation relation tends to minus infinity for such materials, cf. [90]. To overcome this problem, the inverse formulation of the capillary pressure saturation relation has to be used, which means that the saturation has to be chosen as primary variable. Due to the fact that high gradients can occur in the saturation distribution, numerical stabilization techniques have to be applied to the numerical procedure to prevent oscillations and unphysical values of the saturation, cf. [71, 90, 91, 113].

This fact is now pointed out by a simple numerical example, where the wetting process of a natural soil column is investigated. The simulations were carried out using a fixed number of finite elements and constant time-steps. In Figure 4.1, the saturation distributions of a clayey silt (left) and a sand (right) soil column are given. In both cases, the solid lines represent the saturation distribution in the initial states, the dashed lines represents the saturation distribution during the wetting process, whereas the dashed-dotted line represent the saturation distribution at the end of the simulation. This final state is only reached, if the clayey silt column is considered. The computation of the wetting process of the sand column failed due to a non converging numerical procedure.

In the worst case, the derivative of the capillary pressure saturation relation with respect to the capillary pressure tends to minus infinity, if no capillary effect is considered and

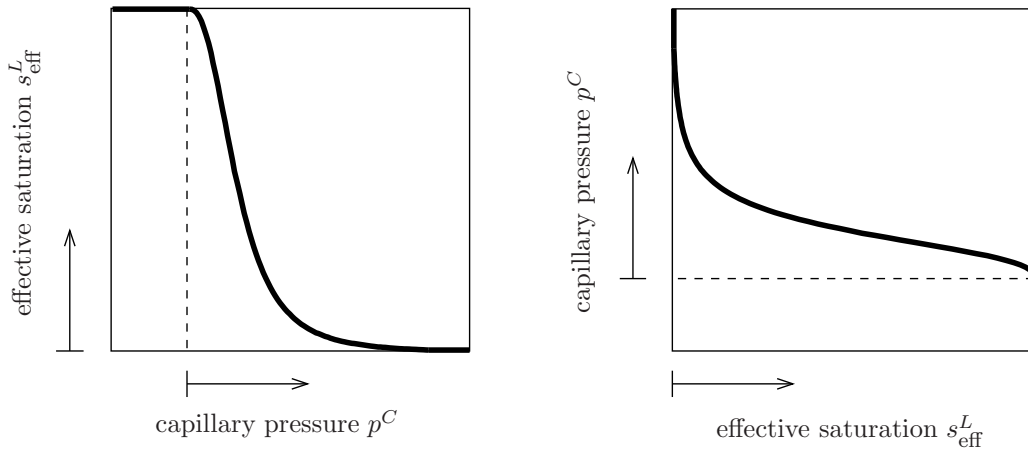


Figure 4.2: Capillary pressure saturation relation: $s_{\text{eff}}^L = s_{\text{eff}}^L(p^C)$ (left), $p^C = p^C(s_{\text{eff}}^L)$ (right).

consequently, a computation is impossible, cf. Figure 4.2 (left). To overcome this problem, the inverse formulation of the capillary pressure saturation relation, cf. Figure 4.2 (right), is used. Following this, the primary variables of the pore fluids have to be switched from the two pressures to one pressure and one saturation. For a more detailed discussion of this topic, the interested reader is referred to the work of *Helmig* [90] and citations therein. On the other hand, high gradients in the solution of the saturation can appear, e. g., if the capillary influence is very low. From numerical examinations of general transport equations, e. g., the heat transport equation or the *Navier-Stokes* equation, it is well-known that oscillations of the primary variables occur, if the spatial discretization is too coarse at boundary layers, i. e., in zones with high gradients of the primary variables.

For a better understanding, this topic will be discussed now taking a closer look at the 1-d convection diffusion equation

$$v \frac{d\phi}{dx} - \kappa \frac{d^2\phi}{dx^2} = 0. \quad (4.38)$$

This equation describes the transport of the scalar-valued variable ϕ , e. g., the temperature, by the velocity v and a simultaneous diffusion characterized by the diffusion coefficient κ . The solution of (4.38) within a region $\Omega = [0, L]$ is given for a constant velocity v and a constant diffusion coefficient κ via

$$\frac{\phi(x) - \phi(x=0)}{\phi(x=L) - \phi(x=0)} = \frac{1 - e^{Pe(x/L)}}{1 - e^{Pe}}, \quad (4.39)$$

where $Pe = vL/\kappa$ is the so-called *Péclet* number, cf. [78]. The *Péclet* number relates the convective transport properties represented by vL to the diffusive transport properties represented by κ . For $Pe > 1$, the convection part, and for $Pe < 1$, the diffusion part dominates the overall transport behavior. In the region $0 \text{ m} \leq x \leq 1 \text{ m}$, (4.39) results considering the *Dirichlet* boundary condition $\phi(x = 0 \text{ m}) = 1$ and $\phi(x = 1 \text{ m}) = 0$ in

$$\phi(x) = 1 - \frac{1 - e^{Pe(x/L)}}{1 - e^{Pe}}, \quad \text{where } L = 1 \text{ m}. \quad (4.40)$$

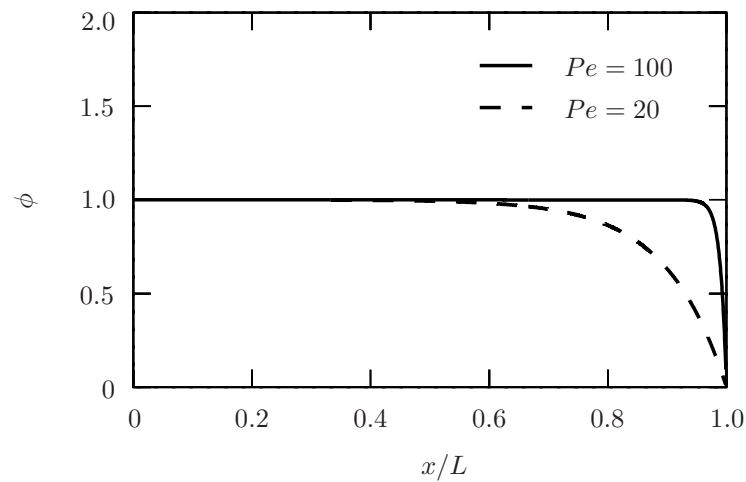


Figure 4.3: Exact solution of the 1-d convection diffusion equation for two different *Péclet* numbers.

Exemplary, $\phi(x)$ is given in Figure 4.3 for two different *Péclet* numbers, i. e., $Pe = 20$ and $Pe = 100$. It can be recognized that increasing *Péclet* numbers, which means a domination of the convective transport properties, yield high gradients in the solution near $x = 1$ m, cf. [78, 126].

An approximation of the considered transport equation (4.38) by a centered finite difference method (FDM) or the *Bubnov-Galerkin* finite element method yields with linear shape functions for the primary variable ϕ

$$v \frac{\phi_{i+1} - \phi_{i-1}}{2h_e} - \kappa \frac{\phi_{i+1} - 2\phi_i + \phi_{i-1}}{h_e^2} = 0, \quad (4.41)$$

where h_e is the element size and i the index of the respective node. This relation can be reformulated:

$$(\phi_{i+1} - \phi_{i-1}) - \frac{1}{Pe_e}(\phi_{i+1} - 2\phi_i + \phi_{i-1}) = 0. \quad (4.42)$$

Therein, the element *Péclet* number

$$Pe_e = \frac{v h_e}{2\kappa} = \frac{h_e Pe}{2L} = \frac{Pe}{2N} \quad (4.43)$$

is introduced, where $N = L/h_e$ is the total number of elements. The discrete solution for this equation is given by

$$\phi(i) = 1 - \frac{1 - r^i}{1 - r^N}, \quad \text{where } r = \frac{1 + Pe_e}{1 - Pe_e}, \quad (4.44)$$

cf. [78, 126]. It is obvious that for $r < 0$ the value of $\phi(i)$ oscillates from node to node. Thus, $Pe_e < 1$ should be required to prevent oscillations in the numerical solution. A graphical interpretation of this behavior is given in Figure 4.4, where a discretization with $N = 12$ elements is used. The dashed lines indicate two solutions, where no oscillations occur due to the fact that the highest gradient, which appears at $x/L = 1$, can be

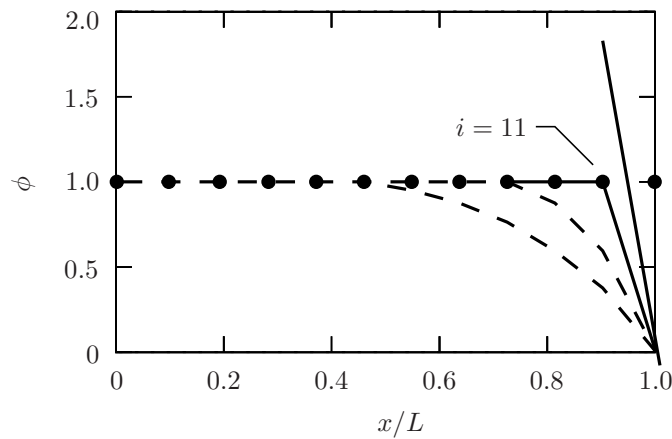


Figure 4.4: Schematic diagram for the occurring of oscillations depending on the element size.

approximated by nodal values lying in the physically correct range. Therefore, the highest possible gradient, which yields no oscillations in the numerical solution is predetermined through the condition that $\phi(11) = 1$. In this case, Equation (4.42) yields

$$(0 - 1) - \frac{1}{Pe_e}(0 - 2 \cdot 1 + 1) = 0, \quad (4.45)$$

which results the following constraint for the prevention of oscillations

$$Pe_e = \frac{v h_e}{2 \kappa} < 1 \quad \longrightarrow \quad h_e < \frac{2 \kappa}{v}. \quad (4.46)$$

It seems that oscillations can be prohibited by using an adequate spatial discretization, which is able to approximate the respective gradient of the primary variable in a physical correct way.

As example for the above presented argumentation, the discrete solution for $Pe = 100$ using a spatial discretization with $N = 10$ and $N = 51$ elements is given in Figure 4.5.

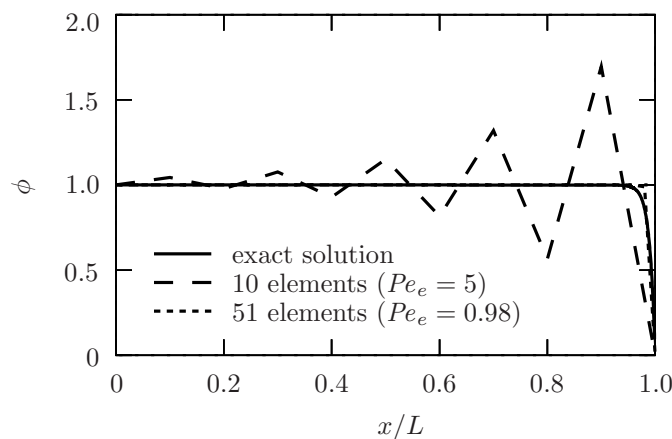


Figure 4.5: 1-d convection diffusion equation for $Pe = 100$.

The coarse spatial discretization results in an element *Péclet* number of $Pe_e = 5$ and high oscillations in the solution, whereas the fine spatial discretization results in an element *Péclet* number of $Pe_e = 0.98$ and, as result, no oscillations occur. This means, the element size should be reduced with increasing element velocity or the diffusivity should be increased in order to keep the element *Péclet* number lower than one in order to prohibit oscillations in the solution. Due to the fact that it is very ineffective and numerically expensive to refine the element size in areas, where oscillations occur and not in areas, where a better solution is desired, the only way to prevent oscillations is to increase the diffusivity in the respective areas. Therefore, an additional (or artificial) diffusivity has to be added to the numerical procedure. This can be realized, e. g., by a modification of the test functions. Generally, this method can be interpreted as a higher weighting of the upstream information with respect to the respective element velocity. Therefore, this method is called an upwinding procedure, cf. [20].

This knowledge can be transferred to the description of multiphasic flow processes within porous materials. In general, two pore fluids can be distinguished by their wetting behavior with respect to the solid skeleton. Therefore, assuming that the effective pressure p^{NWR} of the non-wetting fluid φ^{NW} and the saturation s^W of the wetting fluid φ^W are the respective primary variables of the pore fluids, the strong formulation of the volume balance of the materially incompressible wetting fluid yields, where, for the sake of simplicity, a rigid solid skeleton, isothermal conditions and no mass interactions are considered:

$$(n^W)'_S - \operatorname{div}(n^W \mathbf{w}_W) = 0. \quad (4.47)$$

Proceeding from (3.53), (3.106), (3.107) and (3.110), this equation reads

$$n^F(s^W)'_S + \operatorname{div}\left[\frac{\kappa_r^W(s^W)K_{0S}^S}{\mu^{WR}}(\operatorname{grad} p^{NWR} + \operatorname{grad} p^C(s^W) - \rho^{WR} \mathbf{g})\right] = 0 \quad (4.48)$$

or

$$\begin{aligned} & \overbrace{\frac{\partial \kappa_r^W}{\partial s^W} \frac{K_{0S}^S}{\mu^{WR}} (\operatorname{grad} p^{NWR} + \frac{\partial p^C}{\partial s^W} \operatorname{grad} s^W - \rho^{WR} \mathbf{g}) \cdot \operatorname{grad} s^W}^{\text{convective transport}} + \\ & + n^F(s^W)'_S + \frac{\kappa_r^W K_{0S}^S}{\mu^{WR}} \Delta p^{NWR} + \underbrace{\frac{\partial p^C}{\partial s^W} \frac{\kappa_r^W K_{0S}^S}{\mu^{WR}} \Delta s^W}_{\text{diffusive transport}} = 0. \end{aligned} \quad (4.49)$$

Therein, both, the convective and the diffusive transport properties depend on the capillary behavior of the porous material, i. e., on the derivative of the relative permeability factor and the capillary pressure saturation relation with respect to the saturation. Oscillations in the saturation occur, if the finite element mesh is not suitable for the computation of the saturation distribution for a given capillary pressure saturation relation and relative permeability factors. A stabilization method like the *Streamline-upwind/Petrov-Galerkin* or *Galerkin-least-squares* method cannot be applied to this kind of stabilization problem as it is done, e. g., discretizing the *Navier-Stokes* equation, cf. [73, 83, 106]. The reason therefore is that the factors responsible for the transport properties are not constant material parameters; instead, they depend on nonlinear constitutive relations. Thus,

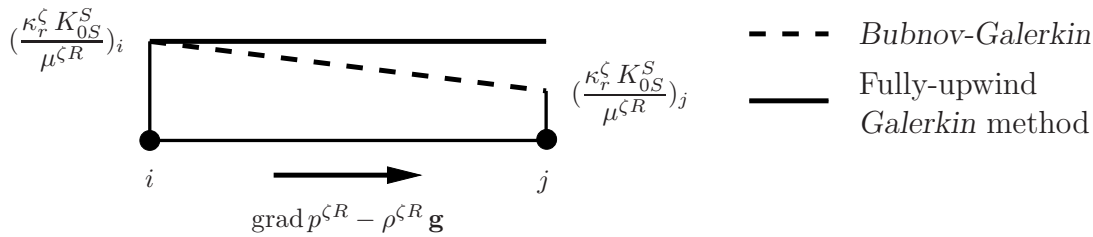


Figure 4.6: Fully-upwind *Galerkin* method.

an upwinding procedure called the fully-upwind *Galerkin* method (FUG), cf. [90], is chosen as stabilization technique, where $\kappa_r^\zeta K_{0S}^S / \mu^{\zeta R}$ is considered constant within an element and holds the value of the upstream node, whereas no modification of the test functions is required, cf. Figure 4.6. For a detailed discussion of this method, the interested reader is referred to *Forsyth* [71], *Helmig* [90] or *Helmig & Huber* [91].

A standard benchmark for the verification of a multiphasic flow model is the *Buckley-Leverett* problem [22], where the instationary replacement of a materially incompressible pore fluid by another one in a horizontal soil column is simulated. Thereby, no capillary and gravitational effects are considered and linear relations for the relative permeability factors are assumed. Due to the fact that no capillarity is considered, it is impossible to compute this problem by using the two pore fluid pressures as primary variables. Furthermore, as capillarity can be interpreted as a diffusivity, cf. [90], the *Buckley-Leverett* problem describes the worst case for the occurring of oscillations within a numerical computation of multiphasic flow problems. Therefore, this problem is a good test for the considered stabilization technique. The sketch of the problem is given in Figure 4.7 according to [113], where the length of the soil column is $L = 300$ m and the height is $H = 75$ m. The governing material parameters are given in Table 4.1, whereas the solid skeleton is assumed to behave like a rigid body. The results of several computations are given in Figure 4.8. Therein, the solid line represents the analytical solution after 500 days. The computations were carried out on two different meshes, a coarse one with 32 and a fine one with 512 quadratic finite elements in horizontal direction. One can recognize that the solutions converge to the analytical solution, if the chosen stabilization technique is applied, whereas unphysical solutions and wrong approximations of the front between the two pore fluids occur, if a *Bubnov-Galerkin* procedure is used. By adding an artificial

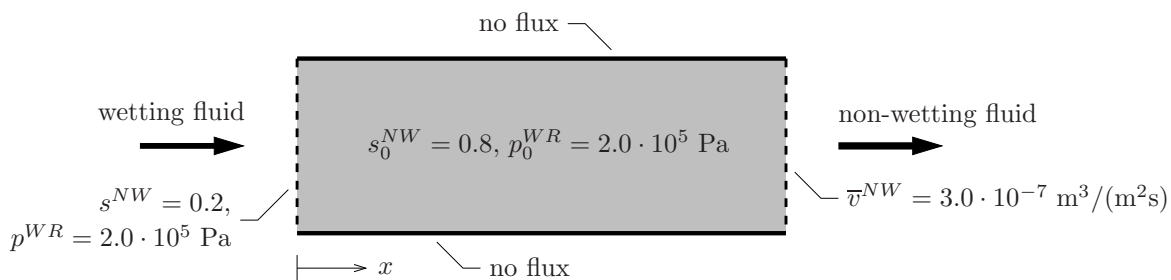


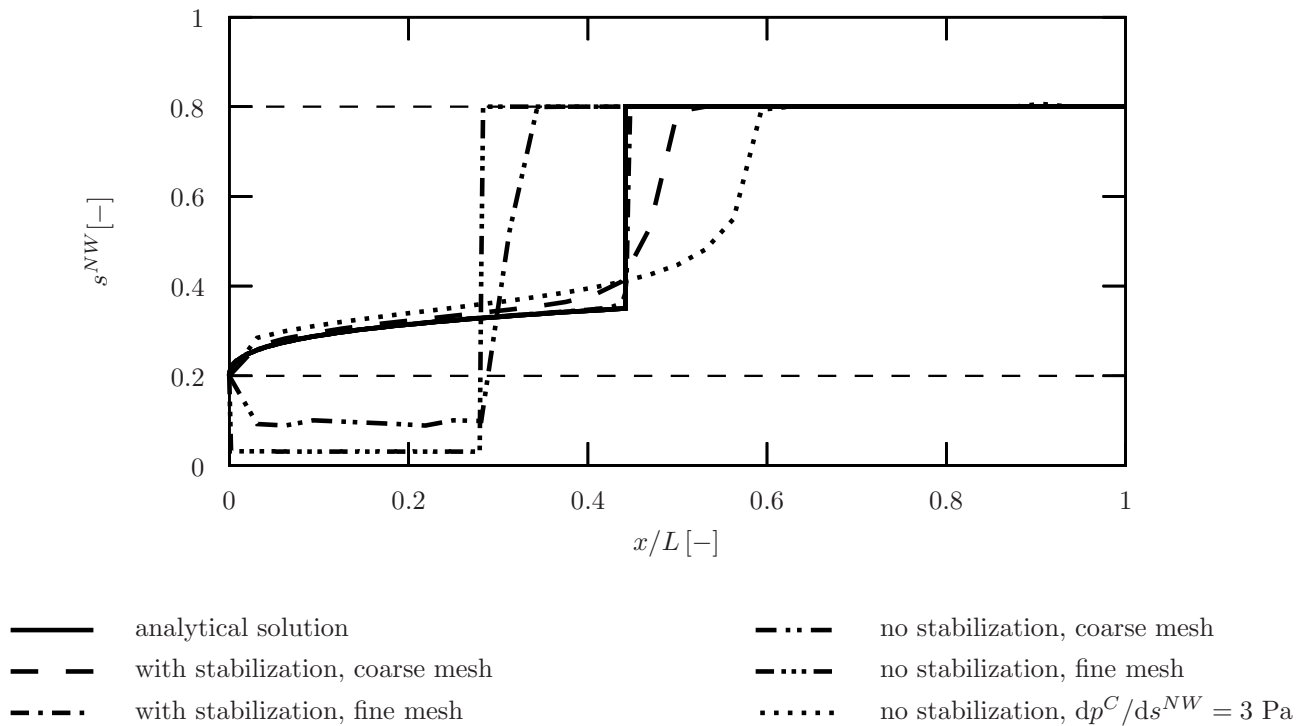
Figure 4.7: Sketch of the *Buckley-Leverett* problem [113].

volume fractions	$n_{0S}^S = 0.8, n_{0S}^F = 0.2$
intrinsic permeability	$K_{0S}^S = 1.0 \cdot 10^{-7} \text{ m}^2$
effective densities	$\rho^{WR} = 1000 \text{ kg/m}^3, \rho^{NWR} = 1000 \text{ kg/m}^3$
fluid viscosities	$\mu^{WR} = 10^{-3} \text{ Ns/m}^2, \mu^{NWR} = 10^{-3} \text{ Ns/m}^2$
residual saturations	$s_{\text{res}}^W = 0.2, s_{\text{res}}^{NW} = 0.2$

Table 4.1: Material parameters of the *Buckley-Leverett* problem [113].

diffusion, e. g., considering a linear capillary pressure saturation relation ($dp^C/ds^{NW} = 3 \text{ Pa}$), no oscillations occur even though no stabilization technique is used, but the front is not approximated in a correct way. Consequently, the fully-upwind *Galerkin* method seems to be a suitable numerical technique to stabilize the convection-dominated problem.

Using this stabilization technique, no problems occur computing the soil column example even for a sandy soil material, cf. Figure 4.9. Hence, considering the presented stabilization technique in the numerical scheme, the presented triphasic model is able to simulate typical initial boundary-value problems independent of the chosen soil material represented through the corresponding capillary pressure saturation relation.

Figure 4.8: Solutions of the *Buckley-Leverett* problem after the time $t = 500 \text{ d}$.

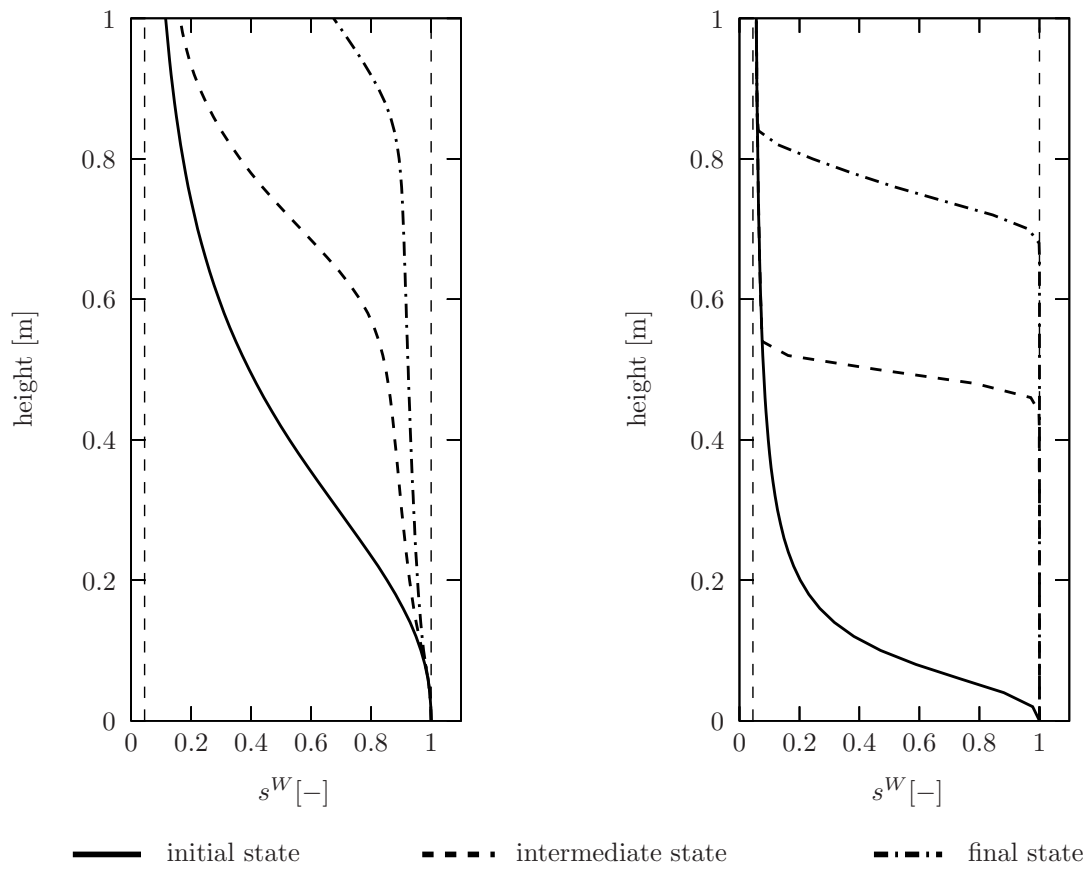


Figure 4.9: Saturation distribution over the height of a clayey silt (left) and a sand (right) column computed using the fully-upwind *Galerkin* method.

Chapter 5: Numerical Examples

In this chapter, the presented porous media model is applied to several two- and three-dimensional initial boundary-value problems, thus, demonstrating the efficiency of the overall formulation. In particular, the triphasic model is used for the simulation of typical pollutant infiltration problems, which show the capability of the model and the applied stabilization method to describe the correct physical behavior of multiphasic flow processes in inhomogeneous materials. Furthermore, the coupled failure mechanism of natural slopes is investigated, whereby the strong interaction between the pore fluids flow and the solid skeleton has to be described in a proper way. Finally, two numerical examples are presented, where the triphasic model under non-isothermal conditions is discussed and mass interactions between liquid and gaseous pore water are taken into account.

All computations presented in this chapter were carried out using the FE package PANDAS [52], which provides certain time- and space adaptive methods. Several numerical examples, where the FE tool PANDAS is applied to geotechnical problems, gas saturated polyurethane foams, biological soft tissues and rocket thrust chambers under isothermal as well as non-isothermal conditions can be found in the works of *Blome* [10], *Ellsiepen* [68], *Ghadiani* [77], *Markert* [108] and *Ehlers* and coworkers [4, 45, 48–50, 53, 54, 56–64].

Further numerical examples concerning partially saturated soils, where a deformable solid skeleton is assumed as well, can be found in the works of *Klubertanz* [96] and *Klubertanz et al.* [97] or *Schrefler* and coworkers, e. g., [105, 115, 118–120]. For a closer look on numerical simulations concerning multiphasic flow processes in rigid porous materials, the interested reader is referred to the works of *Helmig* [90], *Helmig & Huber* [91], *Class & Helmig* [27] or *Bielinski* [8] and citations therein.

In the following, the deformable solid skeleton is assumed to behave like a clayey silt, whereby the elasto-viscoplastic material parameters, which are constant within the following numerical examples are collected in Table 5.1, cf. [46, 131]. All other material parameters will be given within the individual numerical examples. Furthermore, extended *Taylor-Hood* elements are used, where the displacement vector of the solid skeleton is approximated by quadratic ansatz functions, whereas the pore fluid pressures as well as the saturation are approximated by linear ansatz functions.

<i>Lamé</i> constants	$\mu^S = 5\,583 \text{ kN/m}^2, \lambda^S = 8\,375 \text{ kN/m}^2$
yield criterion	$\alpha = 1.074 \cdot 10^{-2}, \beta = 0.1195, \gamma = 1.555,$ $\delta = 1.377 \cdot 10^{-4} \text{ m}^2/\text{kN}, \epsilon = 4.33 \cdot 10^{-6} \text{ m}^2/\text{kN},$ $\kappa = 10.27 \text{ kN/m}^2, m = 0.5935$
viscoplasticity	$\sigma_0 = 10.27 \text{ kN/m}^2, r = 1$
plastic potential	$\psi_1 = 1.33, \psi_2 = 0.107$

Table 5.1: Material parameters of the elasto-viscoplastic solid skeleton [46].

5.1 Pollutant infiltration problems in inhomogeneous porous materials

In this section, the presented model is applied to simulate pollutant infiltration processes in an inhomogeneous water saturated porous material in the 2-d as well as the 3-d case. As the pollutant has a comparable density as the pore water, the interaction between the pore fluids and the solid skeleton is approximately constant during the infiltration process. Thus, considering the numerical examples within this section, the deformation of the solid phase can be neglected and, therefore, the solid skeleton is supposed to be rigid. Furthermore, isothermal conditions and materially incompressible pore fluids are assumed. Due to the fact that a natural sand is used as solid material, the numerical problems discussed in the previous chapter occur. Therefore, the saturation of the pollutant and the effective pressure of the pore water are the primary variables of the presented initial boundary-value problems.

The main focus in the modeling of multiphasic flow processes in heterogeneous materials lies on the correct description of the fluid behavior at the interfaces between the different soil materials corresponding directly to their so-called entry pressure p^D . Therefore, the capillary pressure saturation relation,

$$s_{\text{eff}}^W = (p^D/p^C)^{\lambda_{bc}}, \quad (5.1)$$

as well as the ansatz for the relative permeability factors,

$$\kappa_r^W = (s_{\text{eff}}^W)^{\frac{2+3\lambda_{bc}}{\lambda_{bc}}} \quad \text{and} \quad \kappa_r^P = (1 - s_{\text{eff}}^W)^2 [1 - (s_{\text{eff}}^W)^{\frac{2+\lambda_{bc}}{\lambda_{bc}}}], \quad (5.2)$$

following *Brooks & Corey* [21] and *Burdine* [23] are used for the numerical examples within this section. This is done, because the entry pressure p^D is explicitly included in this constitutive relation, whereby λ_{bc} is an additional material parameter.

2-d example: Kueper et al. [99] carried out a laboratory experiment of tetrachlorethylene (TCE) infiltration in a water-filled sand box with four different soil materials. Therewith, one of the first experimental data sets for the verification of multiphasic flow models describing infiltration problems in heterogeneous porous materials was given. In this example, the pore water (φ^W) is identified as the wetting, the TCE (pollutant φ^P) as the non-wetting fluid. The four different homogeneous quartz sands were filled in a acrylic glass box with the dimensions $70 \times 50 \times 0.6 \text{ cm}^3$ as shown in Figure 5.1. The material parameters, cf. Table 5.2, as well as the initial boundary-value problem itself have been taken from [90, 99]. The four different soils are arranged by their permeabilities, where material I is the sand with the highest permeability and the lowest entry pressure, whereas material IV has the lowest permeability and the highest entry pressure.

The domain is discretized by quadratic finite elements with an element size of $h_e = 1.25 \text{ cm}$, whereas the time steps are chosen constant to $\Delta t = 1 \text{ s}$. In the initial state, the saturation of the pollutant is $s_0^P = 0$ and a hydrostatic pressure distribution is assumed for the effective pressure of the pore water in the whole domain, with the water table at the top of the sand box, cf. Figure 5.1. The edges at the top and the bottom of

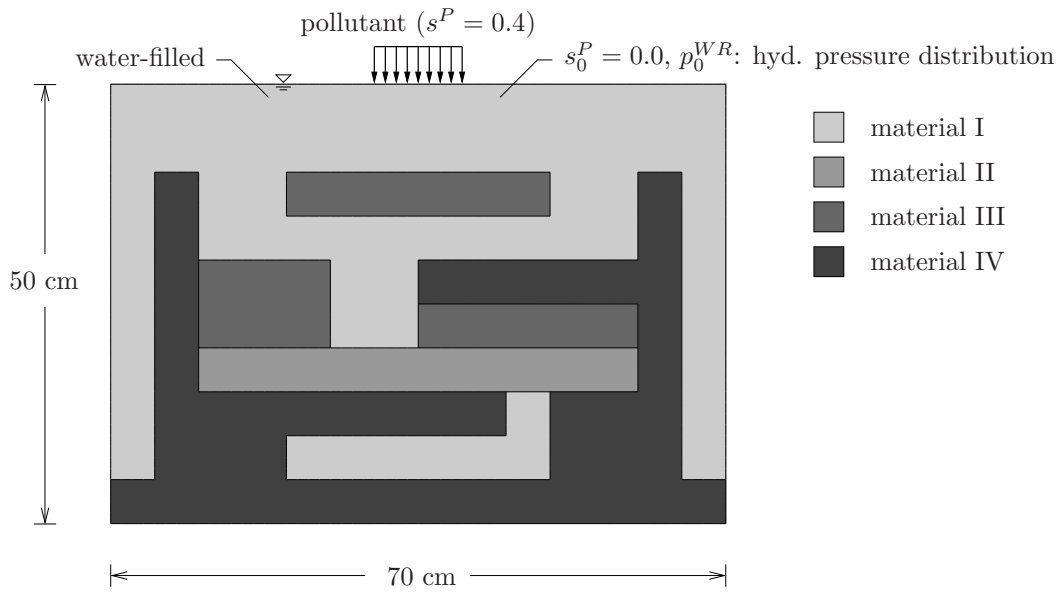


Figure 5.1: Sketch of the 2-d infiltration problem.

the sand box are modeled as no flux boundaries except of the infiltration zone, where the saturation of the pollutant is set to $s^P = 0.4$ corresponding to the 4 cm TCE-column boundary condition in the laboratory experiment. On the left and right edges the effective pressure of the pore water corresponds to a hydrostatic pressure distribution, whereas the saturation of the pollutant is fixed to $s^P = 0$.

In Figure 5.2, the distribution of the pollutant saturation is given at several times during the infiltration process. By a comparison with the experimental data set [99] as well

volume fractions	material I: $n_{0S}^S = 0.6$, material II: $n_{0S}^S = 0.61$, material III: $n_{0S}^S = 0.61$, material IV: $n_{0S}^S = 0.59$
intrinsic permeabilities	mat. I: $K_{0S}^S = 5.04 \cdot 10^{-10} \text{ m}^2$, mat. II: $K_{0S}^S = 2.05 \cdot 10^{-10} \text{ m}^2$, mat. III: $K_{0S}^S = 5.26 \cdot 10^{-11} \text{ m}^2$, mat. IV: $K_{0S}^S = 8.19 \cdot 10^{-12} \text{ m}^2$
effective densities	$\rho^{WR} = 1000 \text{ kg/m}^3$, $\rho^{PR} = 1621 \text{ kg/m}^3$
fluid viscosities	$\mu^{WR} = 10^{-3} \text{ Ns/m}^2$, $\mu^{PR} = 9 \cdot 10^{-4} \text{ Ns/m}^2$
Brooks & Corey model	mat. I: $p^D = 369.837 \text{ N/m}^2$, $\lambda_{bc} = 3.86$, mat. II: $p^D = 434.58 \text{ N/m}^2$, $\lambda_{bc} = 3.51$, mat. III: $p^D = 1324.35 \text{ N/m}^2$, $\lambda_{bc} = 2.49$, mat. IV: $p^D = 3247.11 \text{ N/m}^2$, $\lambda_{bc} = 3.3$
residual saturations	mat. I: $s_{\text{res}}^W = 0.078$, $s_{\text{res}}^P = 0.0$, mat. II: $s_{\text{res}}^W = 0.069$, $s_{\text{res}}^P = 0.0$, mat. III: $s_{\text{res}}^W = 0.098$, $s_{\text{res}}^P = 0.0$, mat. IV: $s_{\text{res}}^W = 0.189$, $s_{\text{res}}^P = 0.0$
gravitation	$g = 9.81 \text{ m/s}^2$

Table 5.2: Material parameters of the 2-d infiltration experiment [90, 99].

as with the numerical results given in *Helmig* [90], it can be realized that the model is able to simulate such a kind of infiltration processes very well. The flow behavior of the pore fluids at the interfaces is computed in a correct way. In particular, an infiltration of the pollutant can only take place over the interfaces between the materials I and II, cf. Figure 5.2 (middle right), or II and III, cf. Figure 5.2 (bottom). At the other interfaces, the pollutant saturation is not high enough to reach the entry-pressure and, therefore, the TCE cannot infiltrates over these interfaces.

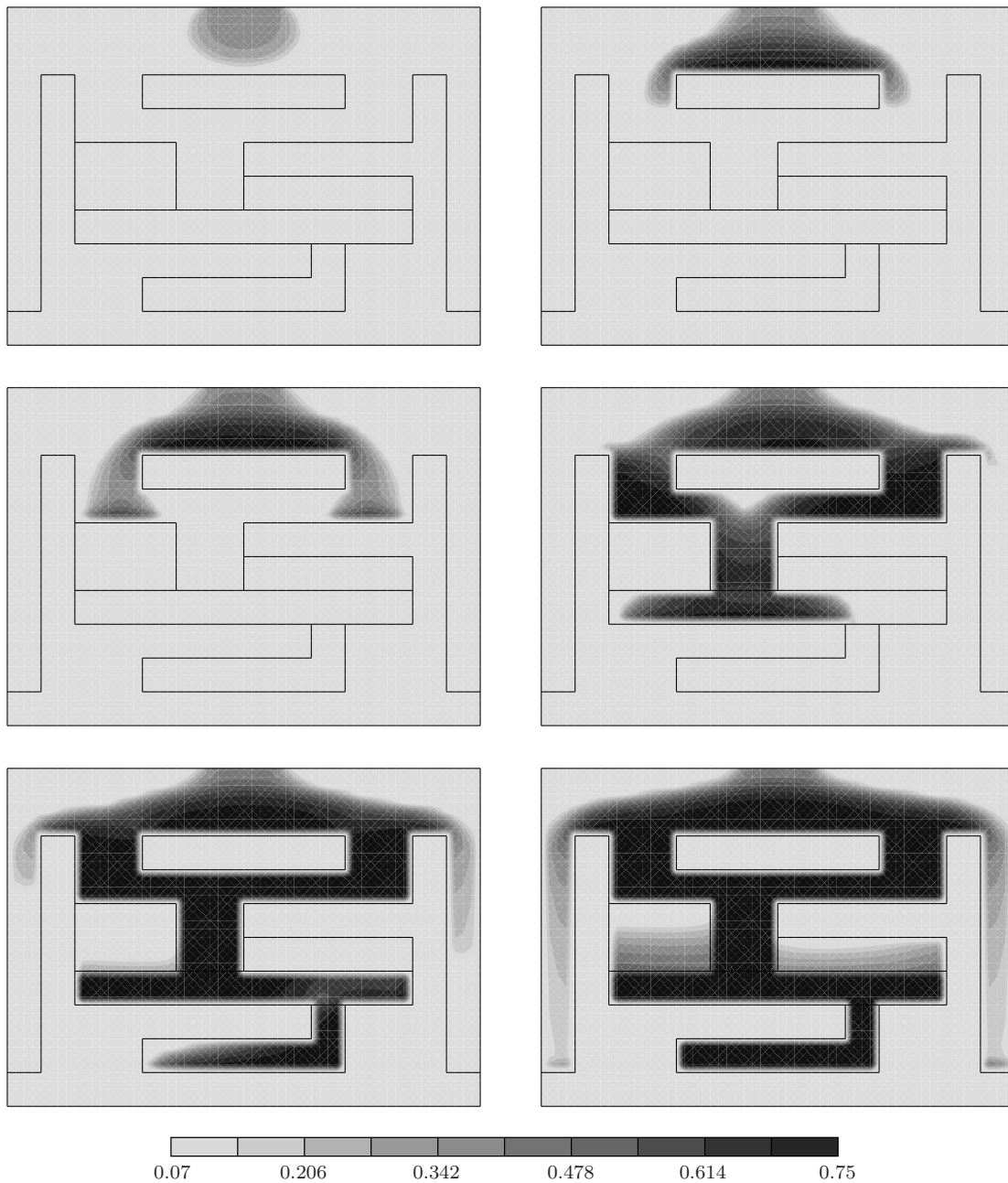


Figure 5.2: Pollutant saturation s^P at $t = 34$ s (top left), $t = 126$ s (top right), $t = 184$ s (middle left), $t = 500$ s (middle right), $t = 800$ s (bottom left) and $t = 1500$ s (bottom right).

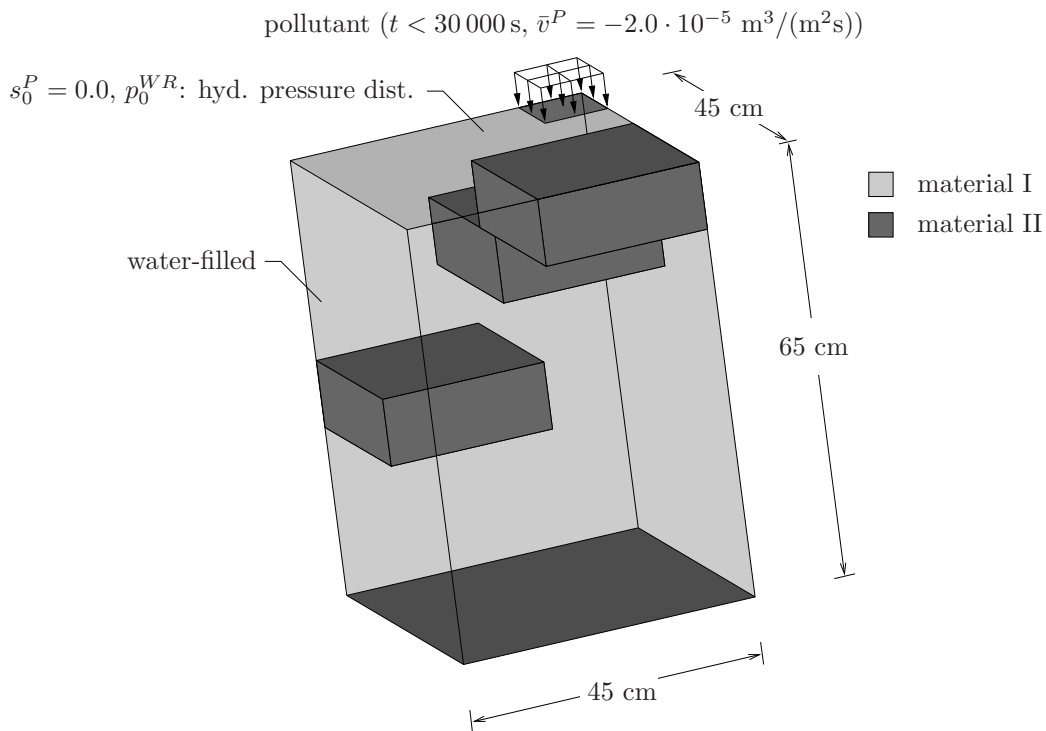


Figure 5.3: Sketch of the 3-d infiltration problem.

3-d example: As example for a 3-d initial boundary-value problem, the infiltration of TCE into a water-filled sand box (material I) with three fine sand lenses (material II) is considered. The sketch of the problem is given in Figure 5.3, where the water table is assumed to be at the top of the box. The infiltration of the pollutant during the first 30 000 s is modeled by an influx of $\bar{v}^P = -2.0 \cdot 10^{-5}\text{ m}^3/(\text{m}^2\text{s})$. The material parameters are given in Table 5.3 according to a 2-d infiltration problem presented in [91], where material II is a soil with a lower permeability and a higher entry pressure than material I.

volume fractions	material I: $n_{0S}^S = 0.6$, material II: $n_{0S}^S = 0.61$,
intrinsic permeabilities	mat. I: $K_{0S}^S = 6.64 \cdot 10^{-11}\text{ m}^2$, mat. II: $K_{0S}^S = 7.15 \cdot 10^{-12}\text{ m}^2$
effective densities	$\rho^{WR} = 1\,000\text{ kg/m}^3$, $\rho^{PR} = 1\,460\text{ kg/m}^3$
fluid viscosities	$\mu^{WR} = 10^{-3}\text{ Ns/m}^2$, $\mu^{PR} = 9 \cdot 10^{-4}\text{ Ns/m}^2$
Brooks & Corey model	mat. I: $p^D = 755\text{ N/m}^2$, $\lambda_{bc} = 2.7$, mat. II: $p^D = 2060\text{ N/m}^2$, $\lambda_{bc} = 2.0$
residual saturations	mat. I: $s_{\text{res}}^W = 0.09$, $s_{\text{res}}^P = 0.0$, mat. II: $s_{\text{res}}^W = 0.12$, $s_{\text{res}}^P = 0.0$
gravitation	$g = 9.81\text{ m/s}^2$

Table 5.3: Material parameters of the 3-d infiltration problem [91].

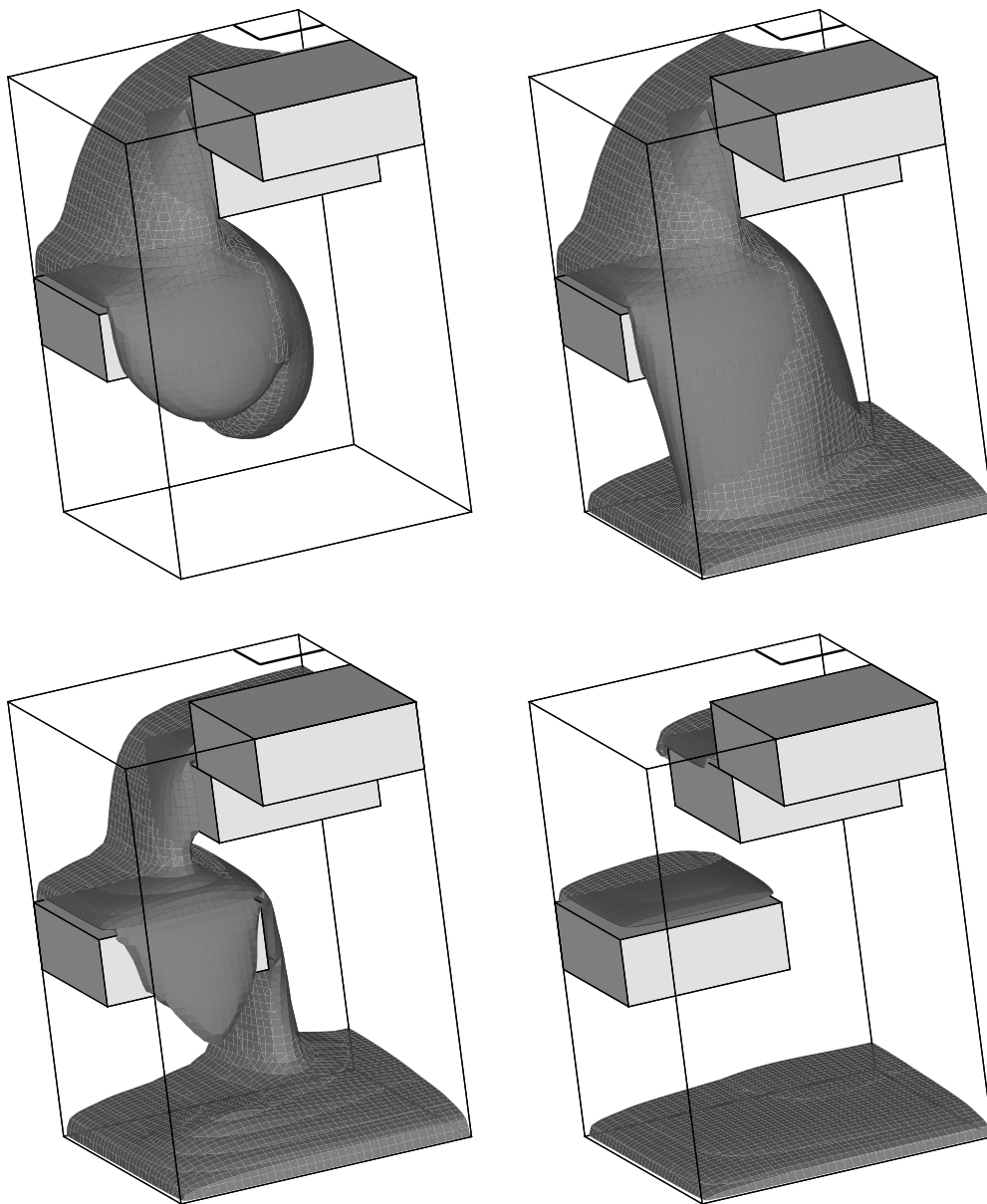


Figure 5.4: Isosurface of the pollutant saturation $s^P = 0.1$ at $t = 13000$ s (top left), $t = 30000$ s (top right), $t = 40000$ s (bottom left) and $t = 120000$ s (bottom right).

The isosurface of the pollutant saturation $s^P = 0.1$ is given at certain times in Figure 5.4. The TCE follows the path predetermined by the different sand materials. During the whole simulation, no infiltration into the fine sand (material II) takes place due to the fact that the capillary pressure in the coarse sand (material I) is lower than the entry pressure of the fine sand material.

Recapitulating, the numerical examples presented in this section show that the continuum mechanical model in combination with the applied stabilization method is capable to simulate the physically correct behavior of multiphasic flow processes in inhomogeneous porous materials in the 2-d as well as in the 3-d case.

5.2 Slope failure problems

In this section, numerical simulations of natural slope failure problems are discussed, where a strong interaction between the fluid and the solid phases destabilizes the solid material. Particularly, the overall pore fluid pressure acts like an “inner” load on the solid skeleton. Due to the fact that the density of water is by the factor 1000 higher than the density of air, the overall pore fluid pressure increases in the same magnitude, if the saturation of the pore water increases. The resulting overall pore fluid pressure acting on the solid skeleton is not negligible anymore. Thus, the displacement process of pore air by pore water has a strong influence on the deformation behavior of the solid skeleton and is therefore a convenient test to prove the capability of the model to describe the interaction between the fluid phases and the solid material. As temperature effects have no significant influence on this phenomenon, isothermal conditions are assumed. The additional, common material parameters of both initial boundary-value problems presented within this section are collected in Table 5.4.

permeabilities	$\pi = 1.0$
effective densities	$\rho^{SR} = 2720 \text{ kg/m}^3, \rho^{WR} = 1000 \text{ kg/m}^3$
gas phase	$\bar{R}^G = 287.17 \text{ J/(kg K)}, \theta = 283 \text{ K}, p_0 = 10^5 \text{ N/m}^2$
fluid viscosities	$\mu^{WR} = 10^{-3} \text{ Ns/m}^2, \mu^{GR} = 1.8 \cdot 10^{-5} \text{ Ns/m}^2$
gravitation	$g = 9.81 \text{ m/s}^2$

Table 5.4: Common material parameters of the slope failure problems.

2-d example: In this numerical example, the failure problem of a natural slope with a gradient of $s = 6/5$ is discussed, where the solid skeleton is assumed to behave like a clayey silt and the two pore fluids are identified by a materially incompressible pore liquid (pore water φ^W) and a materially compressible pore gas (φ^G). A comparable example was presented in [56], where it was shown that the failure process is initialized, if the pore water seeps out of the slope. Within the numerical example presented here, the capillary pressure saturation relation follows a sandy soil material so that, due to the occurring numerical difficulties, the saturation s^W of the pore water and the effective pressure p^{GR} of the pore gas (pore air) are chosen as primary variables of the pore fluids. The capillary pressure saturation relation as well as the relative permeability factors follows the formulation given by *Brooks & Corey* and *Burdine*, cf. relation (5.1) and (5.2). The set of material parameters is completed by the parameters collected in Table 5.5, which correspond to the material parameters of the sand material II collected in Table 5.3 except of the intrinsic permeability, which is chosen by the factor 10 higher to save computing time. Furthermore, this computation was carried out using a space adaptive method, whereby the error indicator was governed by both, the saturation s^W and the plastic part of the strain tensor represented by the accumulated plasticity.

As it was shown in [56], the natural slope under study results in a stable situation under gravitational load as long as the pore liquid does not seep out of the slope, cf. Figure 5.5

volume fractions	$n_{0S}^S = 0.61$
intrinsic permeabilities	$K_{0S}^S = 7.15 \cdot 10^{-11} \text{ m}^2$
<i>Brooks & Corey</i> model	$p^D = 2060 \text{ N/m}^2, \lambda_{bc} = 2.0$
residual saturations	$s_{\text{res}}^W = 0.12, s_{\text{res}}^G = 0.0$
viscoplasticity	$\eta = 400 \text{ s}$

Table 5.5: Remaining material parameters of the 2-d slope-failure problem.

(top). Within this example, this stable configuration is changed due to an increase of the ground-water table from 3 m to 10 m on the left boundary. If the pore water seeps out of the slope, the solid material in this part gets under buoyancy. The resulting destabilization of this part of the slope leads to a development of a shearing domain with a certain thickness, cf. Figure 5.5 (bottom), which indicates the failure of the considered natural slope.

In contrast to [56], where a clayey silt with a smooth capillary pressure saturation relation is assumed as solid material, this numerical example is pointing out that the presented triphasic model in combination with the applied stabilization method is capable to simulate the strong interaction between the streaming pore fluids and the deformable solid skeleton for a natural soil governed by a much more steep capillary pressure saturation relation as well.

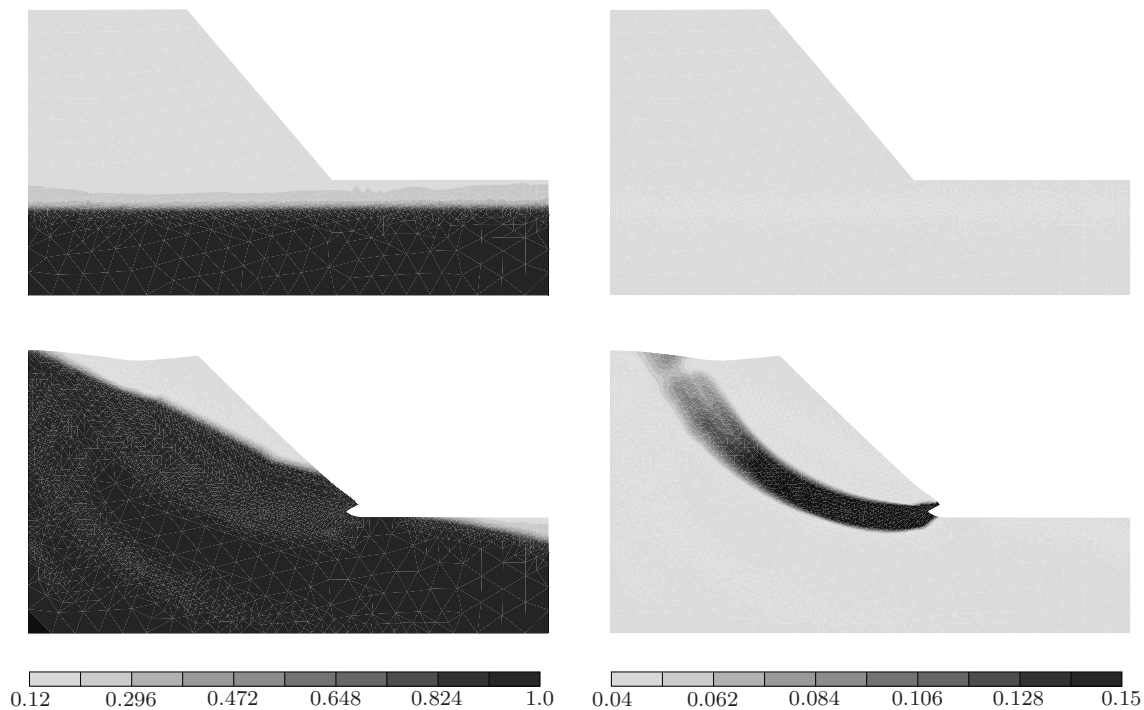


Figure 5.5: Saturation of the pore water s^W (left) and accumulated plastic strains (right) of the 2-d slope-failure problem (scaled 3 times).

Remark: Concerning the boundary conditions of the pore water at the slope, one has to realize that s^W cannot be predetermined via a *Dirichlet* boundary condition, because for a realistic description of the material behavior, the saturation of the pore water has to be allowed to take arbitrary values at the slope. Therefore, as only a *Dirichlet* or a *Neumann* boundary condition can be applied, the boundary condition of the pore water at the slope has to be governed by a *Neumann* (no flux) boundary condition at the beginning. This means that in this case the slope is impermeable for pore water. As long as pore water does not reach the slope, this no flux boundary condition is tenable. But, if the pore water reaches the slope, this boundary condition results in an unrealistic flow behavior, i. e., unrealistic high pressures of the pore water occur, which act on the solid skeleton. To avoid this unrealistic behavior, the *Neumann* (no flux) boundary condition of the pore water is changed into a *Dirichlet* ($s^W = 1.0$) boundary condition, if a critical saturation is exceeded below the slope. This means, pore water can leak over this part of the boundary, unrealistic high pore water pressures are prevented and the whole mechanical process is described in a correct manner. \square

3-d example: The reason for an increasing water saturation and therewith an increasing failure risk of natural slopes is directly coherent to occurring rainfall events. Therefore, the 3-d failure situation of a railroad embankment after a heavy rainfall event is discussed now, whereby the heavy rainfall event is simulated via an infiltration rate (negative efflux of pore water) of $\bar{v}^W = -10^{-5} \text{ m}^3/(\text{m}^2\text{s})$ corresponding to $\bar{v}^W = -36 \text{ l}/(\text{m}^2\text{h})$ at the top of the railroad embankment. Because of the high number of unknowns, this example was solved using parallel solution strategies, where the sequential FE code PANDAS was coupled with the solver M++ (Meshes, Multigrid and more). For a closer look on this topic, the interested reader is referred to the works of Ammann [2], Wieners [139] and Wieners et al. [140–142].

The railroad embankment is considered as an inhomogeneous natural soil material consisting of three different soil strata, cf. Figure 5.6. In particular, both, soil strata 1 and 2 are assumed to behave like a clayey silt, cf. Table 5.1, whereas soil stratum 3 is regarded as a rock material, i. e., this soil stratum is governed by a purely elastic material behavior. Furthermore, soil stratum 2 is modeled as a less permeable soil material and, therefore, the belonging intrinsic permeability is by the factor 100 lower than the intrinsic permeability coefficient of the other two soil strata, cf. Table 5.6. Due to the fact that

volume fractions	$n_{0S}^S = 0.54$
intrinsic permeabilities	soil strata 1 and 3: $K_{0S}^S = 10^{-10} \text{ m}^2$, soil stratum 2: $K_{0S}^S = 10^{-12} \text{ m}^2$
<i>van Genuchten</i> model	$\alpha_{\text{gen}} = 2 \cdot 10^{-4}$, $j_{\text{gen}} = 2.3$, $h_{\text{gen}} = 1.5$, $\epsilon_{\text{gen}} = 0.5$, $\gamma_{\text{gen}} = 0.333$
residual saturations	$s_{\text{res}}^W = 0.1$, $s_{\text{res}}^G = 0.1$
viscoplasticity	$\eta = 100 \text{ s}$

Table 5.6: Remaining material parameters of the 3-d slope-failure problem.

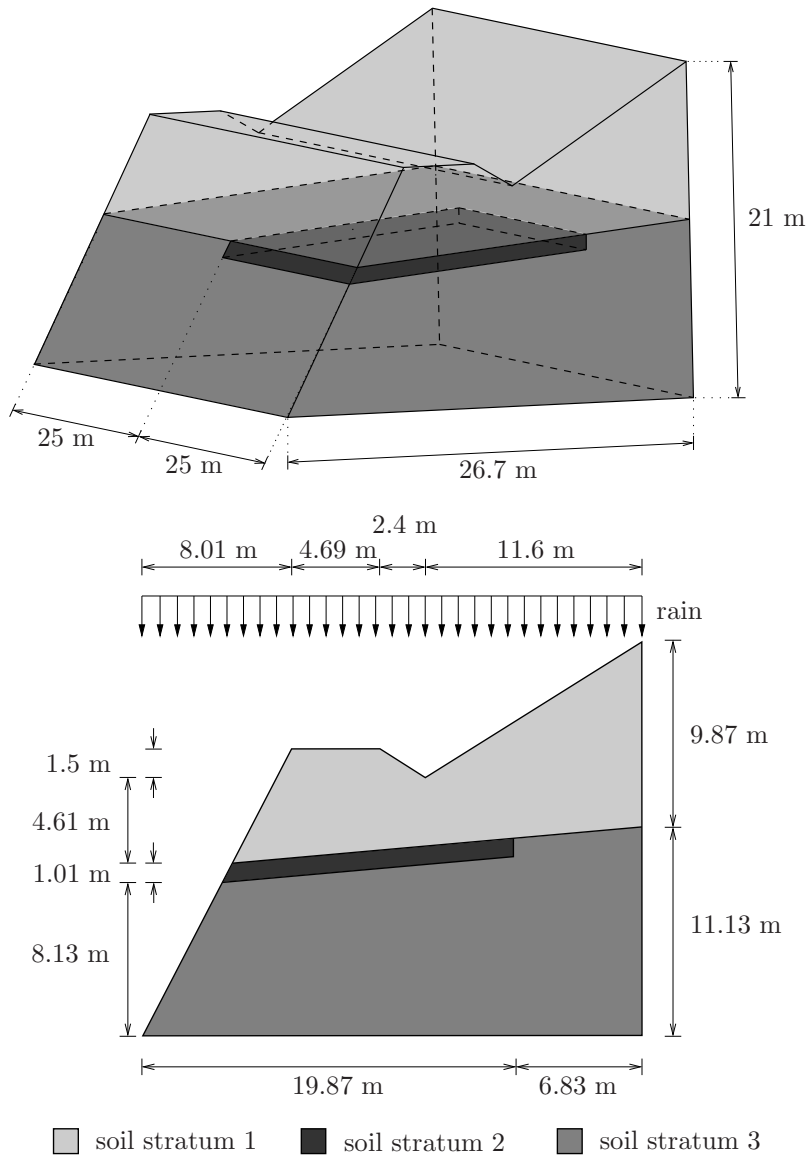


Figure 5.6: Sketch of the 3-d slope failure problem.

the current version of the iterative solver is very sensible with respect to small values of the intrinsic permeability, the values of the intrinsic permeability coefficients are chosen much more larger than it is the case for a realistic clayey silt material. Nevertheless, this assumption has no influence on the qualitative interpretation of the numerical results.

Within this example, the capillary pressure saturation relation as well as the constitutive relation for the relative permeability factors following *van Genuchten* [76] and *Mualem* [109] are used:

$$s_{\text{eff}}^W = [1 + (\alpha_{\text{gen}} p^C)^{j_{\text{gen}}}]^{-h_{\text{gen}}} \quad (5.3)$$

and

$$\begin{aligned} \kappa_r^W &= (s_{\text{eff}}^W)^{c_{\text{gen}}} \{1 - [1 - (s_{\text{eff}}^W)^{1/h_{\text{gen}}}]^{h_{\text{gen}}}\}^2, \\ \kappa_r^G &= (1 - s_{\text{eff}}^W)^{\gamma_{\text{gen}}} [1 - (s_{\text{eff}}^W)^{1/h_{\text{gen}}}]^{2h_{\text{gen}}}. \end{aligned} \quad (5.4)$$

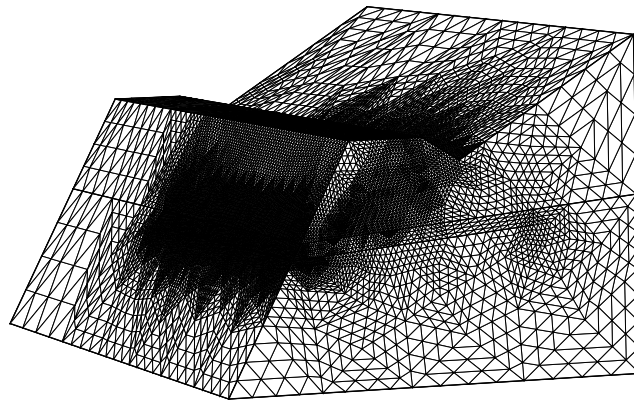


Figure 5.7: Finite element mesh of the 3-d slope failure problem.

The finite element mesh was generated with the mesh generator NETGEN [116] and consists of 2 562 048 tetrahedral cells, cf. Figure 5.7. This results in 11 208 869 degrees of freedom and 968 454 144 internal variables. The numerical simulation was carried out using 88 processors on the Linux cluster *Leonardo da Vinci* of the Institute of Applied

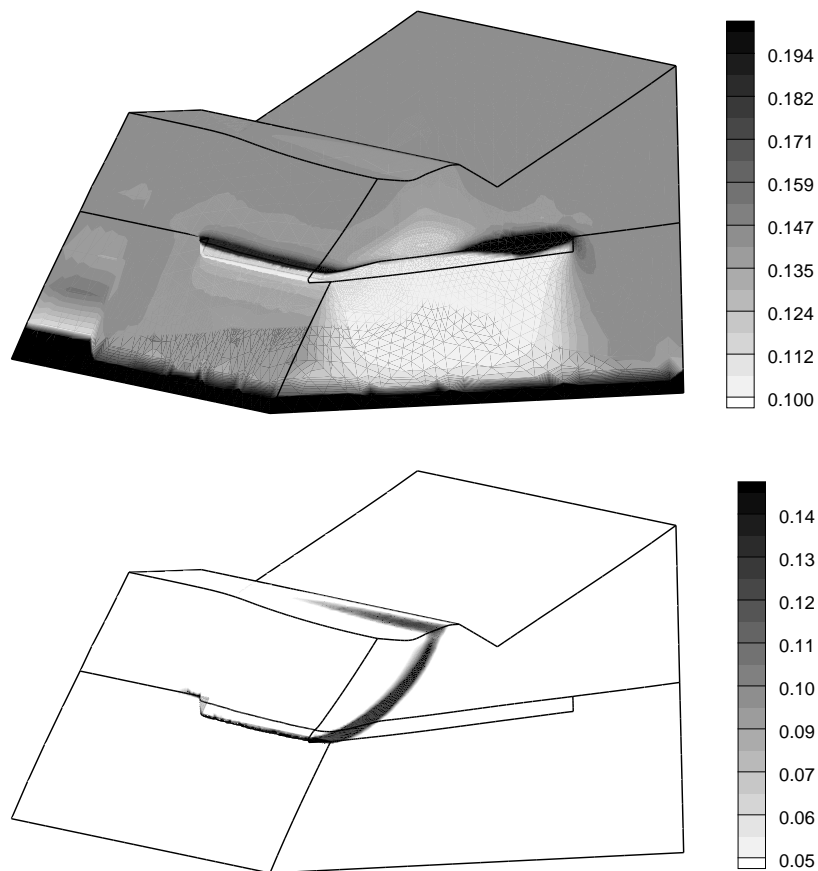


Figure 5.8: Saturation s^W of the pore water (top) and accumulated plastic strains $[10^{-1}]$ (bottom) of a railroad embankment after a heavy rainfall event (scaled 6 times).

Mechanics (Chair 2) at the University of Stuttgart, whereas the computing time was 1070:22 [h:m].

The railroad embankment is in a stable situation before the heavy rainfall event starts. It can be realized from the distribution of the water saturation, cf. Figure 5.8 (top), that the infiltrating pore water is retained by the less permeable soil stratum. Therefore, the pore water is leaking from the slope at the top of this stratum. Thus, as a result of buoyancy, failure of this part of the slope is initiated, which can be identified by a 3-d localization zone of the plastic strains, cf. Figure 5.8 (bottom). The other part of the railroad embankment remains stable.

This numerical example shows the capability of the presented model as well as the combined FE tool PANDAS/M++ to simulate realistic 3-d slope failure problems in a proper way.

5.3 Heat transport problems

Within this section, the presented triphasic porous media model is applied to non-isothermal initial boundary-value problems. Particularly, the injection process of heated pore gas into a water-saturated natural soil is presented, where the different phases are governed by individual temperatures. In a further example, the so-called heatpipe problem is simulated. Thereby, the different phases are governed by one temperature and mass interaction (phase transition) between the liquid and gaseous (vapor) water are taken into account.

Injection of heated pore gas into a water-saturated porous material: Heated pore gas is injected into a water-saturated porous material, whereby a soil stratum with a lower permeability inhibits the pore gas to volatilize to the atmosphere. The primary variables of the problem under study are the three different temperatures of the solid, the pore liquid (water) and the pore gas (air) phase, the displacement of the solid skeleton as well as the effective pressures of the pore liquid and the pore air.

As the main focus of this numerical example lies on the correct description of the injection behavior and the heat transfer phenomena, the solid skeleton is assumed to behave purely elastic, whereby the *Lamé* constants are given in Table 5.1. Furthermore, no mass interactions are taken into account within this numerical example and, for simplicity, the dependency of the pore liquids inner energy on the saturation is neglected.

The additional material parameters are collected in Table 5.7. Therein, the values of the pore waters and the pore airs inner energies at the initial temperature θ_0 are given following *Abbott & van Ness* [1] and *Class* [26]. Furthermore, for the determination of the thermal expansion coefficient α^S as well as the thermal conductivity h_r^S of the solid skeleton, the solid phase is assumed to behave like a sand stone. The thermal expansion coefficient γ^W of the pore water is assumed to be independent of the temperature and is determined according to the considered temperature range of the numerical example at $\theta \approx 315$ K. The specific heats C_V^S and C_V^G of the solid skeleton and the pore gas as well as the thermal conductivities h_r^W and h_r^G of the liquid pore water and pore gas follow

volume fractions and characteristic grain diameter	$n_{0S}^S = 0.54, d_{50} = 0.001$ m
intrinsic permeabilities	soil stratum 1: $K_{0S}^S = 10^{-12}$ m ² , soil stratum 2: $K_{0S}^S = 10^{-15}$ m ²
effective densities	$\rho_0^{SR} = 2720$ kg/m ³ , $\rho_0^{WR} = 999.7$ kg/m ³
gas phase	$\bar{R}^G = 287.17$ J/(kg K), $p_0 = 101325$ N/m ²
fluid viscosities	$\mu^{WR} = 10^{-3}$ Ns/m ² , $\mu^{GR} = 1.8 \cdot 10^{-5}$ Ns/m ²
<i>van Genuchten</i> model	$\alpha_{\text{gen}} = 2 \cdot 10^{-4}$, $j_{\text{gen}} = 2.3$, $h_{\text{gen}} = 1.5$, $\epsilon_{\text{gen}} = 0.5$, $\gamma_{\text{gen}} = 0.333$
residual saturations	$s_{\text{res}}^W = 0.1$, $s_{\text{res}}^G = 0.1$
thermal conductivity	$h_r^S = 2.0$ W/(m K), $h_r^W = 0.62$ W/(m K), $h_r^G = 0.026$ W/(m K)
thermal expansion coefficients	$\alpha^S = 1.2 \cdot 10^{-5}$ 1/K, $\gamma^W = 0.4 \cdot 10^{-3}$ 1/K
specific heats	$C_V^S = 700.0$ J/(kg K), $C_V^W = 4187.0$ J/(kg K), $C_V^G = 733.0$ J/(kg K)
heat exchange coefficients	$k_{SW}^{\epsilon S} = 1.0 \cdot 10^3$ W/(m ² K), $k_{SG}^{\epsilon S} = 10.0$ W/(m ² K), $k_{GW}^{\epsilon S} = 11.7$ W/(m ² K)
initial inner energies	$\epsilon_0^S = 0$, $\epsilon_0^W = 4.199 \cdot 10^4$ J/kg, $\epsilon_0^G = 7.33 \cdot 10^3$ J/kg
initial temperature and initial water pressure	$\theta_0 = 283$ K, $p_0^{WR} = 101325$ N/m ²
gravitation and radiation	$g = 9.81$ m/s ² , $r = 0$

Table 5.7: Additional material parameters of the heated pore gas injection problem.

the material parameters given in *Class* [26]. Taking a closer look on the heat exchange coefficients between the individual phases, the heat exchange coefficients between various shapes and air lies in the range between 2-23 W/(m² K), the heat exchange coefficients between various shapes and water in the range between 300-1700 W/(m² K), whereas the heat exchange coefficients between water and air is given by 11.7 W/(m² K). Finally, the capillary pressure saturation relation as well as the constitutive relation for the relative permeability factors following *van Genuchten* [76] and *Mualem* [109] are used, cf. (5.3) and (5.4).

The sketch of the problem is given in Figure 5.9. The whole domain is discretized by quadratic finite elements with an element size of $h_e = 0.25$ m. The water table is assumed to be 3 m below the top, whereas the soil stratum with the lower permeability has a thickness of 3 m. At the top and the left boundary, the individual temperatures are set to $\theta^\alpha = 283$ K. Furthermore, on the left boundary the effective pressure of the pore liquid corresponds to a hydrostatic pressure distribution determined by the given water table, whereas at the top boundary, the effective pressure of the pore gas is given by $p^{GR} = 0$. The injection of the heated pore gas is simulated via a mass influx of $\bar{m}^G = -1.0 \cdot 10^{-5}$ kg/(m²s) with a pore gas temperature of 363 K over a time period of 22 h.

The distribution of the water saturation s^W as well as the pore gas temperature θ^G is given in Figure 5.10 at four different time steps. The injected pore gas displaces the pore water around the injection zone. Due to the density difference between the pore gas and

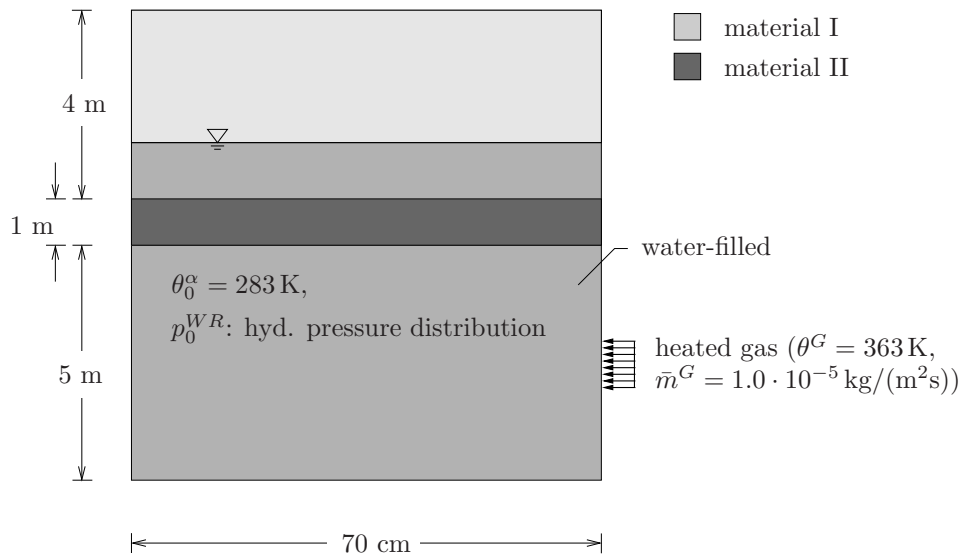


Figure 5.9: Sketch of the infiltration problem.

the pore water, the pore gas raises up until this motion is limited via the soil stratum with the lower permeability. Furthermore, one can realize that the temperature influence is concentrated in a small domain around the injection zone. To analyze this effect, the

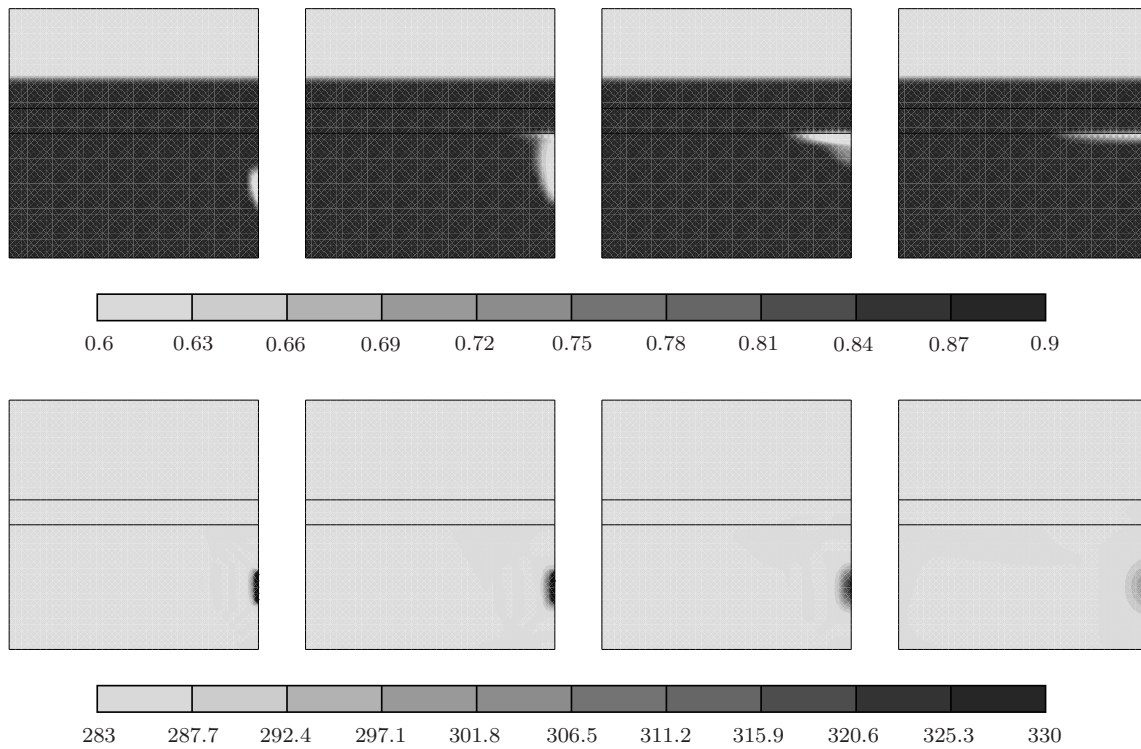


Figure 5.10: Water saturation s^W (upper row) and pore gas temperature θ^G (lower row) at certain time steps: $t \approx 9 \text{ h}$, $t \approx 23 \text{ h}$, $t \approx 36 \text{ h}$ and $t \approx 90 \text{ h}$ (from left to right).

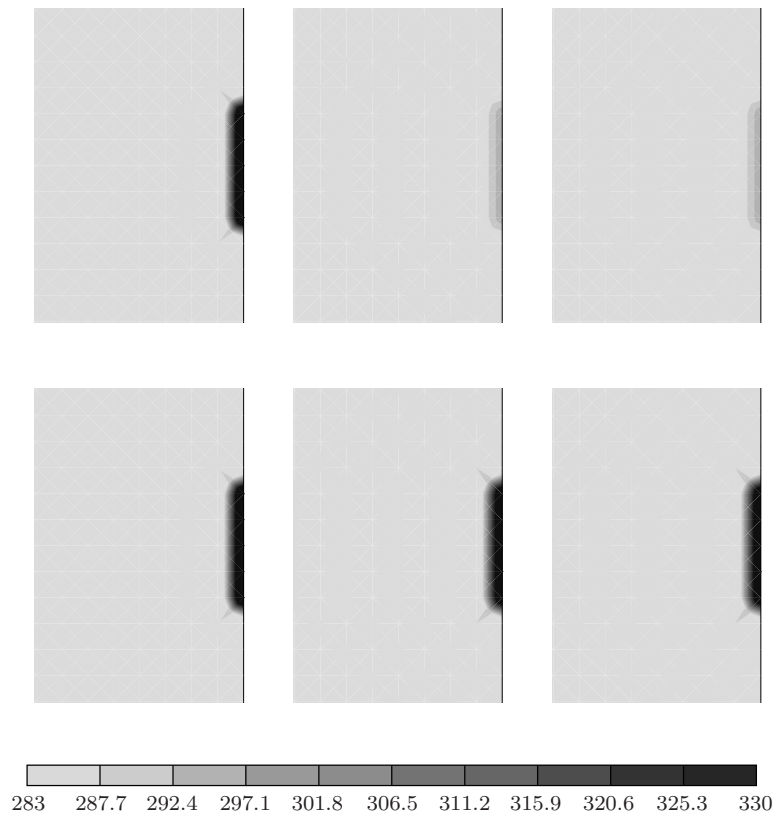


Figure 5.11: Distribution of the pore gas temperature θ^G (left), the solid temperature θ^S (middle) and the pore liquid temperature θ^W (right) immediately (upper row) and 15 minutes (lower row) after the injection process was started.

distribution of the individual phase temperatures are investigated. In Figure 5.11, the distribution of the pore gas temperature θ^G (left), the solid temperature θ^S (middle) and the pore liquid temperature θ^W (right) are given immediately (upper row) and 15 minutes (lower row) after the injection process was started. It can be observed that the temperatures of the different phases are equalized after this small time period, which is governed by the given heat exchange coefficients between the individual phases. Therefore, applying the presented non-isothermal model to unsaturated natural soil problems and taking into account the long time periods, which are considered thereby, it is not necessary to introduce the three different phase temperatures as primary variables. It is sufficient to introduce the temperature of the mixture as primary variable governing the thermal effects. Nevertheless, if other porous materials are investigated, where the interesting period of time is much shorter and the respective material parameters take other values, the introduction of three different phase temperatures could be necessary.

For a further verification of the presented triphasic model, the whole simulation was computed once again, while the heat exchange coefficients between the pore gas and the other phases are assumed to be zero. The distribution of the water saturation s^W as well as the pore gas temperature θ^G is given in Figure 5.12, whereby the time steps correspond to the time steps given in Figure 5.10. In contrast to the simulation results given in

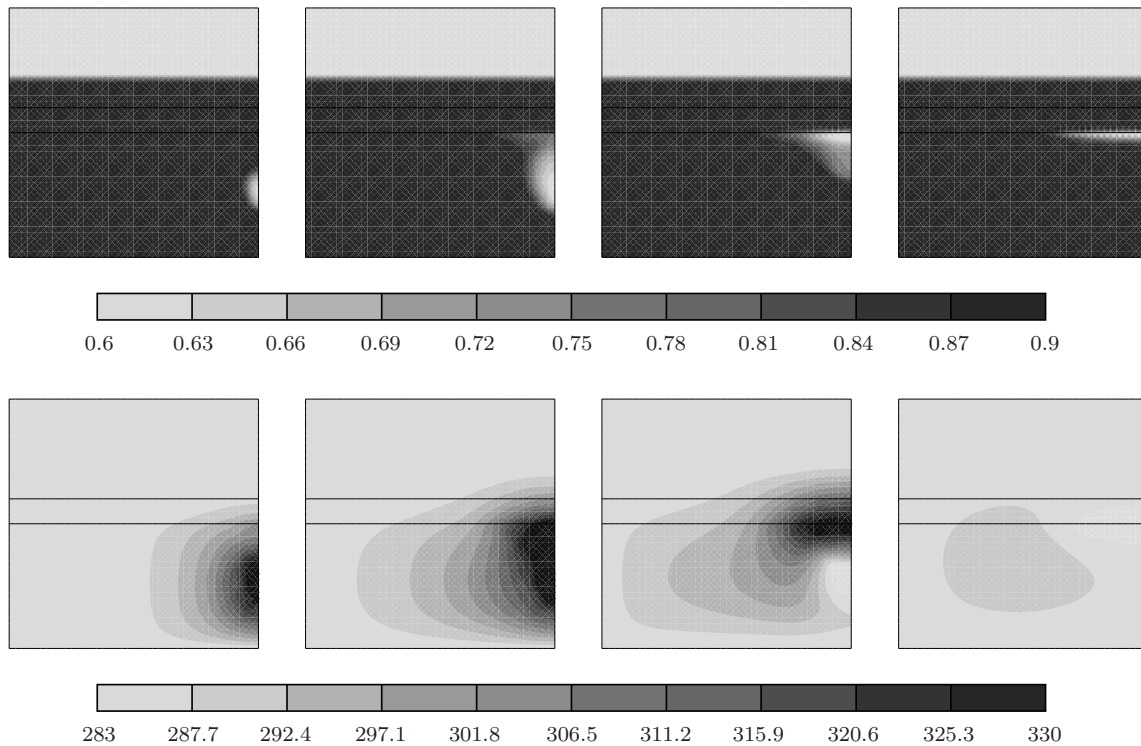


Figure 5.12: Water saturation s^W (upper row) and pore gas temperature θ^G (lower row) at certain time steps: $t \approx 9$ h, $t \approx 23$ h, $t \approx 36$ h and $t \approx 90$ h (from left to right), if no heat transfer between the phases is taken into account.

Figure 5.10, the heat transport phenomena is concentrated within this example to the pore gas phase, whereby the overall transport process of the temperature is governed by a combination of pure thermal conductivity and a transport via the motion of the pore gas.

The heatpipe problem: Within this initial boundary-value problem, a partially saturated, horizontal soil column is heated up at one boundary via a constant heat flux, which is chosen high enough to reach the vaporization temperature of water. Thus, due to the arising water vapor, the effective pressure of the overall gas phase increases and the resulting gradient of the overall effective gas pressure yields a pore gas flow from the hotter to the colder boundary. Furthermore, the occurring capillary effects yield a liquid water flow in the opposite direction in fact of a decreasing liquid saturation. Finally, three regions can be differentiated in the stationary state. On the one hand, there are two regions, where only liquid or gaseous water exist and, on the other hand, one region between them, where both liquid and gaseous water coexists, cf. Figure 5.13.

The material parameters are taken from *Udell & Fitch* [137] and *Class* [26] and are summarized in Table 5.8. Therein, the material densities of the solid skeleton φ^S as well as the liquid pore water φ^L are assumed to be constant. Thus, the dependency of both material densities on the temperature are not taken into account within this numerical example as well ($\alpha^S = 0$, $\gamma^W = 0$). Furthermore, the overall porous medium is governed by one overall temperature ($\theta^\alpha = \theta$), where the governing balance relation is the overall

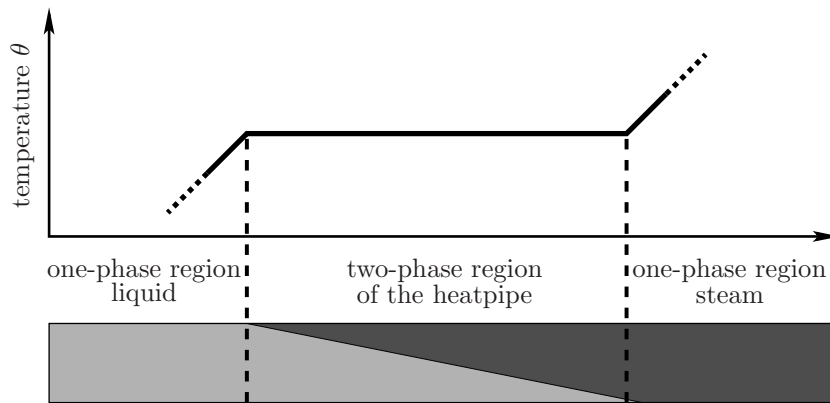


Figure 5.13: Schematic description of the heatpipe problem.

energy balance of the porous medium. This is a tenable assumption for a natural soil with the pore fluids water and air as was shown in the last example. The shear viscosity μ^{GR} of the overall gas phase is a function of the shear viscosities μ^{VR} and μ^{AR} of the gas components water vapor and air as well as the composition of the overall gas phase given by the molar fractions x_m^A and x_m^A , cf. [26]:

$$\mu^{GR} = \mu^{VR} x_m^A + \mu^{AR} x_m^A. \quad (5.5)$$

The heat conduction of the overall medium is given following a formulation of *Somerton et al.* [124],

$$h_r = h_0 + (s^L)^{1/2}(h_1 - h_0), \quad (5.6)$$

volume fractions	$n_{0S}^S = 0.6$
intrinsic permeability	$K_{0S}^S = 10^{-12} \text{ m}^2$
effective densities	$\rho^{SR} = 2600 \text{ kg/m}^3, \rho^{LR} = 958.4 \text{ kg/m}^3$
gas phase	$R^G = 8.31441 \text{ J/(mol K)}, M^V = 0.018 \text{ kg/mol}, M^A = 0.028953 \text{ kg/mol}$
fluid viscosities	$\mu^{LR} = 2.938 \cdot 10^{-4} \text{ Ns/m}^2, \mu^{VR} = 1.2 \cdot 10^{-5} \text{ Ns/m}^2,$ $\mu^{AR} = 2.08 \cdot 10^{-5} \text{ Ns/m}^2$
linear capillary pressure saturation relation	$p_{\max}^C = 15000 \text{ N/m}^2$
residual saturations	$s_{\text{res}}^L = 0.15, s_{\text{res}}^G = 0.0$
thermal conductivity	$h_0 = 0.582 \text{ W/(m K)}, h_1 = 1.13 \text{ W/(m K)}$
diffusivity	$\tau = 0.5, d_G^{AV} = 2.6 \cdot 10^{-5} \text{ m}^2/\text{s}$
specific heats	$C_V^S = 700.0 \text{ J/(kg K)}, C_V^L = 4187.0 \text{ J/(kg K)},$ $C_V^V = 1618.0 \text{ J/(kg K)}, C_V^A = 733.0 \text{ J/(kg K)}$
initial inner energies	$\varepsilon_0^S = 0, \varepsilon_0^W = 4.199 \cdot 10^4 \text{ J/kg}, \varepsilon_0^V = 2.389 \cdot 10^6 \text{ J/kg}, \varepsilon_0^A = 7.33 \cdot 10^3 \text{ J/kg}$
initial temperature and atmospheric pressure	$\theta_0 = 283 \text{ K}, p_{\text{atm}} = 101330.0 \text{ Pa}$

Table 5.8: Material parameters of the heatpipe problem.

where h_0 and h_1 are the heat conduction coefficient for the fully dry and fully wet soil. The diffusion velocity is computed via

$$n^G \mathbf{d}_{\gamma G} = -\frac{1}{\rho_G^\gamma} \rho^G \tau d_G^{AV} \text{grad } x_{Gm}^\gamma, \quad (5.7)$$

where τ is a tortuosity parameter and d_G^{AV} is the binary diffusion coefficient. Furthermore, no gravitation and radiation load is taken into account.

Udell & Fitch as well as *Class* used the effective pressure p^{GR} of the overall gas phase as well as the liquid pore water saturation s^L as primary variables in their numerical examples. Here, both effective pressures of the fluid phases are chosen as primary variables. Therefore, the capillary pressure saturation relation given in *Udell & Fitch* [137] and *Class* [26] cannot be used. Thus, it is assumed that the capillary pressure is related to the liquid water saturation via a linear function:

$$s_{\text{eff}}^L = -\frac{p^C - p_{\text{max}}^C}{p_{\text{max}}^C}. \quad (5.8)$$

Therefore, as the *Helmholtz* free energy of a materially incompressible pore fluid is only derived based on a capillary pressure saturation relation following *Brooks & Corey*, this dependency is neglected within this example. Furthermore, the relative permeability factors are given via a cubic function of the effective saturation of the liquid pore water:

$$\kappa_r^L = (1 - s_{\text{eff}}^L)^3, \quad \kappa_r^G = (s_{\text{eff}}^L)^3. \quad (5.9)$$

The sketch of the initial boundary-value problem is given in Figure 5.14. The length of the horizontal column is chosen to $L = 2.4$ m, which corresponds to the value given in *Class* [26]. The whole column is discretized by quadratic finite elements with an element size of $h_e = 0.04$ m. In the initial state, the overall effective gas pressure p^{GR} corresponds to the atmospheric pressure $p_{\text{atm}} = 101\,330.0$ Pa, whereas the effective liquid water pressure p^{LR} is chosen in such a way that a liquid saturation distribution of $s^L = 0.5$ is initiated. The initial temperature is chosen to $\theta_0 = 341.6$ K. On the left boundary, the initial values of the overall effective gas pressure as well as the temperature are fixed, whereas the effective liquid water pressure is chosen in such a way that a liquid saturation of $s^L = 1$ is prescribed. The heat load is applied on the left boundary via a heat influx of $\bar{\mathbf{q}} = 130$ J/(m²s). Furthermore, the edges at the top and the bottom of the sand box are modeled as no flux boundaries.

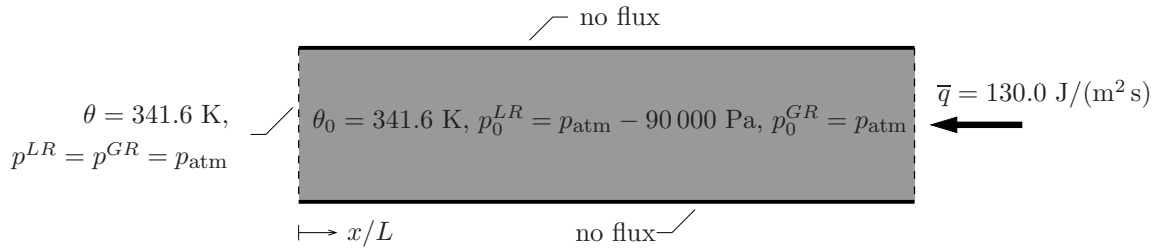


Figure 5.14: Sketch of the heatpipe problem.

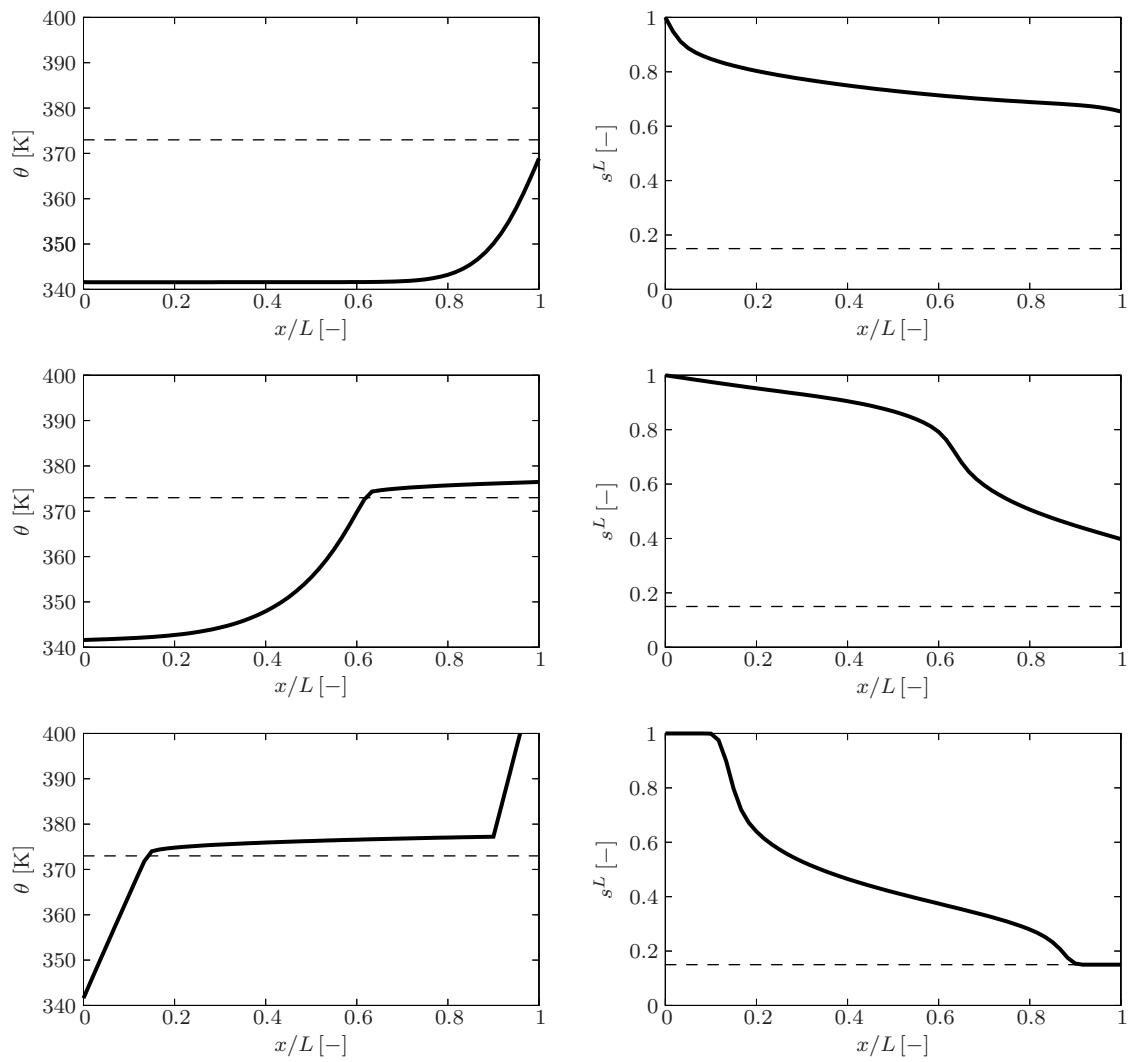


Figure 5.15: Distribution of the temperature and the liquid water saturation at certain times.

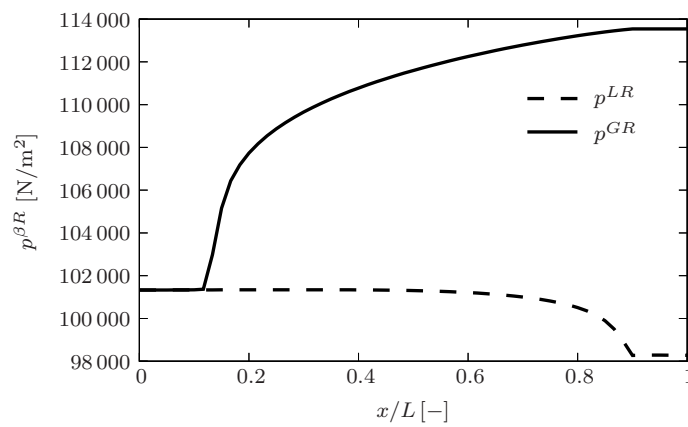


Figure 5.16: Pressure distribution of the two pore fluids in the stationary state.

The temperature and the corresponding liquid saturation distribution within the horizontal heatpipe are given for certain times in Figure 5.15. It can be recognized that the presented model is capable to describe the heating process of water, which was discussed in detail in Section 3.2.2. The overall temperature increases until a critical temperature is reached, which dependence directly on the existing pressure. This dependency is maintained as long as the liquid water saturation is greater than the residual water saturation. If the residual liquid water saturation is reached, the dependency between the temperature and the pressure is solved and the temperature can increase. In Figure 5.16, the pressure distribution of the overall gas phase and the liquid pore water are given in the stationary state. Thereby, the resulting pressure gradients yield the predicted liquid water flow from the left to the right boundary and an overall pore gas flow in the opposite direction.

As discussed in Section 3.2.2, the temperature is fixed during a vaporization process as soon as the overall gas pressure is only governed by the water vapor. This can be recognized from Figure 5.17, where certain molar fractions x_{Gm}^V and corresponding temperature distributions are given. If $x_{Gm}^V = 1$, one can see directly that the gradient of the temperature at the right boundary decreases and tends to zero.

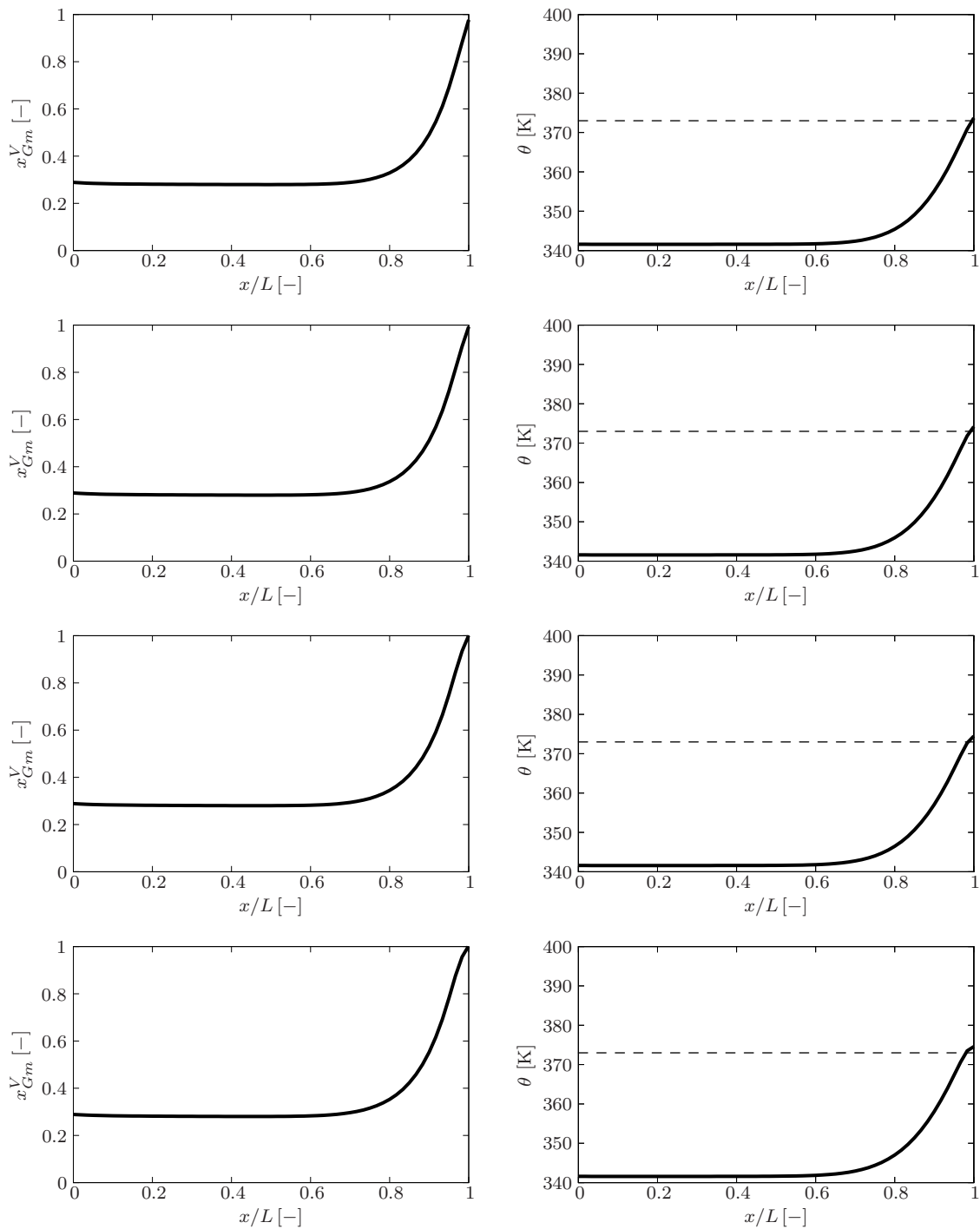


Figure 5.17: Distribution of the molar fraction x_{Gm}^V of the water vapor within the overall gas phase and the temperature θ , if x_{Gm}^V tends towards one at the right boundary.

Chapter 6: Summary and outlook

6.1 Summary

Within this contribution, a multiphasic, continuum mechanical model for the description of porous materials with several fluid constituents under consideration of non-isothermal conditions and phase transition processes between liquid and gaseous pore water was presented based on the well-founded framework of the Theory of Porous Media (TPM). The required thermodynamically consistent constitutive relations were derived via an evaluation of the entropy inequality. In the following, this general model was reduced to a triphasic one consisting of a solid, a liquid water and an overall gas phase, which was built by water vapor and air. Furthermore, a special attention was taken on the numerical treatment of multiphasic flow processes. Finally, the presented initial-boundary value problems showed the capability of the discussed model to simulate engineering problems of practical relevance.

In particular, concerning the derived continuum mechanical model, each phase of the porous material is governed by its individual temperature. The solid skeleton is assumed to behave like an elasto-viscoplastic, the pore fluids like viscous materials. Furthermore, the solid skeleton as well as the pore liquids are described in a mechanical sense as materially incompressible constituents, whereby their effective densities are only a function of the respective temperatures. The gaseous pore fluid constituents are assumed to behave like ideal gases building together one overall pore gas phase. It could be shown that the ratio between the partial pressure of a gaseous component within the overall gas phase and the overall effective gas pressure is given by the respective molar fraction, whereas the overall effective gas pressure is given by the sum of the partial pressures of the gaseous constituents, which corresponds directly to *Dalton's law*.

As each phase is governed by its individual temperature and, furthermore, phase transition between liquid and gaseous pore water is taken into account, constitutive relations are not only required for the free *Helmholtz* energies of each individual constituent and the direct momentum productions of the pore fluids, but also for the mass production of the liquid pore water and the direct energy productions of the pore fluids. Appropriate constitutive relations could be formulated for the direct momentum as well as for the direct energy productions. The results are *Darcy*-type equations for the seepage velocities of the pore fluid phases and relations for the diffusion velocities of the gaseous components within the overall gas phase. As the phase transition between liquid and gaseous water is a reversible process, the evaluation of the entropy inequality gives no restriction for a special constitutive relation, but a further condition for the process variables, which has to be ensured as long as mass interactions take place. This condition serves as constraint for the determination of the partial pressure of water vapor within the overall gas phase. Furthermore, if the overall porous material is only governed by one temperature and the kinetic energies of the water component are neglected, this condition results in the fact

that during phase transition processes the *Gibbs* free enthalpies of the liquid and gaseous pore water have to be equal. Based on this fact, a relation between the partial pressure of the water vapor within the overall gas phase and the temperature of the overall porous material, i. e., the so-called vaporization curve, can be derived. Therefore, the mass balance of water vapor loses the character of a governing equation and can be used for the determination of the mass interaction. Consequently, the whole phase transition process of liquid and gaseous pore water is described by a coupled system of equations consisting of the mass balance of the overall water component, the mass balance of the air component and the overall energy balance.

The numerical treatment of the presented triphasic model is based on the finite element method (FEM), whereas extended *Taylor-Hood* elements with quadratic ansatz functions for the solid displacement vector and linear ansatz functions for the pore fluid pressures and saturations as well as the temperatures are used. Furthermore, the special numerical treatment of multiphasic flow processes in porous materials was discussed, which led to the application of a certain stabilization technique to overcome the occurring numerical problems.

Finally, the presented multiphasic porous media model was applied to several two- and three-dimensional initial boundary-value problems, where the FE tool PANDAS/M++ was used. Particularly, typical pollutant infiltration and slope failure problems, injection processes of heated pore gas into a water saturated porous material and the so-called heatpipe problem were discussed. It could be shown that the model is capable to describe the strong interaction between the pore fluids flow and the deformable soil matrix as well as the occurring thermal effects and phase transitions processes between liquid and gaseous pore water.

6.2 Outlook

With the multiphasic, non-isothermal porous media model presented in this thesis, the basis for the simulation of initial boundary-value problems is given, where a deformable solid skeleton and two pore fluid phases are taken into account. Nevertheless, this model can be extended in different directions depending on the considered mechanical problems.

Additionally to the description of reversible phase transition processes, dissipative mass interaction processes, e. g., erosion processes driven by interaction forces between the pore fluids and the solid skeleton, can be included. Thereby, a constitutive relation for the mass production term can be formulated based on the evaluation of the entropy inequality. Furthermore, applying the presented model to problems, where the assumption of small deformations cannot be hold, the whole model has to be described within a geometrically non-linear theory.

Furthermore, the triphasic model can be extended towards the most general case, where the pore space can be filled only by liquid water, only gaseous water or by both types of water phase states. Thereby, a special attention has to be taken on the changes between these different phase states. The constraint, which has to be ensured during phase transition processes take place, should then be considered directly within the numerical scheme

instead of using this condition as basis for the derivation of the vaporization curve. Additionally, for a more efficient numerical treatment of complex, realistic 3-d slope failure problems, space and time adaptive strategies should be taken into account within the FE tool PANDAS/M++.

Appendix A: Tensor calculus

In this chapter, the definitions of the main tensorial expressions used within this theses are summarized, whereby the notations follow the rules and definitions given in the work by *de Boer* [11] and in the lecture notes on vector and tensor calculus by *Ehlers* [47]. These relations are valid for an arbitrary basis system. Nevertheless, a normalized *Cartesian* basis system is assumed, if the expressions are given in basis notation. Furthermore, the well-known summation convention of *Einstein* holds.

A.1 Tensor algebra

A.1.1 Basic tensor products

Dyadic product

The dyadic product is defined in the following way:

$$\begin{aligned}\mathbf{C} &= \mathbf{a} \otimes \mathbf{b} = a_i b_j \mathbf{e}_i \otimes \mathbf{e}_j, \\ \overset{4}{\mathbf{C}} &= \mathbf{A} \otimes \mathbf{B} = A_{ij} B_{kl} \mathbf{e}_i \otimes \mathbf{e}_j \otimes \mathbf{e}_k \otimes \mathbf{e}_l.\end{aligned}\tag{A.1}$$

Thereby, the basis vectors \mathbf{e}_i of the involved tensors are combined in a dyadic sense, i. e., the order (or rank) of the resulting tensor equals the sum of the ranks of the involved tensors. Note that within the used notation, vectors (or 1-st order tensors) are symbolized by bold, small Latin characters, whereas tensors of n -th order ($n > 1$) are defined by bold, capital Latin characters. Furthermore, the rank of a n -th order tensor is clarified by a superscripted rank for $n > 2$.

Scalar product

The result of a scalar product is a scalar value, whereby the single basis vectors are combined scalarly:

$$\begin{aligned}\alpha &= \mathbf{a} \cdot \mathbf{b} = a_i b_i, \\ \alpha &= \mathbf{A} \cdot \mathbf{B} = A_{ij} B_{ij}.\end{aligned}\tag{A.2}$$

Linear mapping and tensor product

The linear mapping as well as the tensor product are operations, in which the rank of the resulting tensor is reduced (contracted) with respect to the sum of the ranks of all involved tensors. In both operations, the resulting tensor is formed by a combination of

both scalar and dyadic products of the basis vectors of the involved tensors:

$$\begin{aligned} \mathbf{c} &= \mathbf{A} \mathbf{b} = A_{ij} b_j \mathbf{e}_i, \\ \mathbf{C} &= \mathbf{A} \mathbf{B} = A_{ij} B_{jk} \mathbf{e}_i \otimes \mathbf{e}_k, \\ \mathbf{C} &= \overset{4}{\mathbf{A}} \mathbf{B} = A_{ijkl} B_{kl} \mathbf{e}_i \otimes \mathbf{e}_j. \end{aligned} \quad (\text{A.3})$$

A.1.2 Symmetric and skew-symmetric part of a tensor

Each arbitrary 2-nd order tensor \mathbf{A} can be uniquely decomposed into a symmetric and a skew-symmetric part:

$$\begin{aligned} \mathbf{A} &= A_{ij} \mathbf{e}_i \otimes \mathbf{e}_j = \text{sym } \mathbf{A} + \text{skw } \mathbf{A}, \\ \text{where: } \text{sym } \mathbf{A} &:= \frac{1}{2}(\mathbf{A} + \mathbf{A}^T), \quad \text{skw } \mathbf{A} := \frac{1}{2}(\mathbf{A} - \mathbf{A}^T). \end{aligned} \quad (\text{A.4})$$

Therein, the transpose of a tensor is given by $\mathbf{A}^T = A_{ji} \mathbf{e}_i \otimes \mathbf{e}_j$. It follows that

$$\text{sym } \mathbf{A} = (\text{sym } \mathbf{A})^T, \quad \text{skw } \mathbf{A} = -(\text{skw } \mathbf{A})^T. \quad (\text{A.5})$$

A.1.3 Fundamental tensors

Fundamental tensors are tensors, which are built by a combination of basis vectors.

2-nd order fundamental tensor

The 2-nd order fundamental tensor (or identity tensor) \mathbf{I} leads to an identical map, if it is applied to an arbitrary vector \mathbf{a} or an arbitrary 2-nd order tensor \mathbf{A} , respectively:

$$\mathbf{a} = \mathbf{I} \mathbf{a}, \quad \mathbf{A} = \mathbf{I} \mathbf{A}, \quad \text{where } \mathbf{I} := \delta_{ij} \mathbf{e}_i \otimes \mathbf{e}_j. \quad (\text{A.6})$$

Therein, δ_{ij} is the so-called *Kronecker* symbol, which takes for $i = j$ the value one and otherwise the zero.

3-rd order fundamental tensor

The 3-rd order fundamental tensor (or *Ricci* permutation tensor) $\overset{3}{\mathbf{E}}$ is defined via the following relation:

$$\overset{3}{\mathbf{E}} := e_{ijk} (\mathbf{e}_i \otimes \mathbf{e}_j \otimes \mathbf{e}_k), \quad (\text{A.7})$$

whereby the so-called permutation symbol e_{ijk} is given by

$$e_{ijk} = \begin{cases} 1 & : \text{even permutation} \\ -1 & : \text{odd permutation} \\ 0 & : \text{double indexing} \end{cases} \longrightarrow \begin{cases} e_{123} = e_{231} = e_{312} = 1 \\ e_{321} = e_{213} = e_{132} = -1 \\ \text{all remaining } e_{ijk} \text{ vanish} \end{cases} \quad (\text{A.8})$$

4-th order fundamental tensors

4-th order fundamental tensors are built by dyadic combinations of the 2-nd order identity tensor \mathbf{I} . By additional transpositions of the respective basis vectors, altogether three different 4-th order fundamental tensors can be defined, which have the following properties:

$$\begin{aligned} \text{identical map:} \quad & (\mathbf{I} \otimes \mathbf{I})^{\underline{23}} \mathbf{A} = \mathbf{A}, \\ \text{“transposing” map:} \quad & (\mathbf{I} \otimes \mathbf{I})^{\underline{24}} \mathbf{A} = \mathbf{A}^T, \\ \text{“tracing” map:} \quad & (\mathbf{I} \otimes \mathbf{I}) \mathbf{A} = (\mathbf{A} \cdot \mathbf{I}) \mathbf{I} = (\text{tr } \mathbf{A}) \mathbf{I}. \end{aligned} \tag{A.9}$$

Therein, the transpositions $(\cdot)^{\underline{ik}}$ indicate an exchange of the i -th and k -th basis systems.

A.1.4 Spherical and deviatoric part of a tensor

Each arbitrary 2-nd order tensor \mathbf{A} can be decomposed into a spherical and a deviatoric part:

$$\begin{aligned} \mathbf{A} &= \mathbf{A}^V + \mathbf{A}^D, \\ \mathbf{A}^V &:= \frac{1}{3} (\mathbf{A} \cdot \mathbf{I}) \mathbf{I}, \\ \mathbf{A}^D &:= \mathbf{A} - \frac{1}{3} (\mathbf{A} \cdot \mathbf{I}) \mathbf{I} = \mathbf{A} - \mathbf{A}^V. \end{aligned} \tag{A.10}$$

By the above definition, the deviatoric part \mathbf{A}^D always results in a traceless tensor, i. e., $\mathbf{A}^D \cdot \mathbf{I} = 0$.

A.1.5 Incomplete mapping

If higher order tensors are applied to other tensors in the sense of an incomplete mapping, one has to know how many of the basis vectors have to be linked by scalar products. Therefore, an underlined superscript $(\cdot)^{\underline{n}}$ indicates the order of the desired result after the tensor operation has been carried out. In this context, an incomplete mapping of two 3-rd order tensors results in the following way in a 2-nd order tensor:

$$\mathbf{C} = (\underline{\mathbf{A} \mathbf{B}})^{\underline{2}} = A_{ijk} B_{jkn} (\mathbf{e}_i \otimes \mathbf{e}_n). \tag{A.11}$$

A.1.6 Outer tensor product of a vector and a tensor

The outer tensor product of a vector \mathbf{a} and a 2-nd order tensor \mathbf{B} is defined via

$$\mathbf{a} \times \mathbf{B} = [\underline{\mathbf{E}} (\mathbf{a} \otimes \mathbf{B})]^{\underline{2}} = e_{ijk} a_j B_{kt} (\mathbf{e}_i \otimes \mathbf{e}_t). \tag{A.12}$$

A.2 Invariants of a 2-nd order tensor

From the solution of the eigenvalue problem, the principal invariants of an arbitrary 2-nd order tensor \mathbf{A} yield:

$$\begin{aligned} \text{I}_A &= \mathbf{A} \cdot \mathbf{I} = \text{tr } \mathbf{A} , \\ \text{II}_A &= \frac{1}{2} (\text{I}_A^2 - \mathbf{A}^T \cdot \mathbf{A}) , \\ \text{III}_A &= \frac{1}{6} \text{I}_A^3 - \frac{1}{2} \text{I}_A^2 (\mathbf{A}^T \cdot \mathbf{A}) + \frac{1}{3} \mathbf{A}^T \mathbf{A}^T \cdot \mathbf{A} = \det \mathbf{A} . \end{aligned} \tag{A.13}$$

According to the above definitions, the specific invariants of the presented single-surface yield criterion by *Ehlers* [41, 42] can be expressed by the following relations:

$$\text{I} = \boldsymbol{\sigma} \cdot \mathbf{I} , \quad \text{II}^D = \frac{1}{2} \boldsymbol{\sigma}^D \cdot \boldsymbol{\sigma}^D , \quad \text{III}^D = \det \boldsymbol{\sigma}^D , \tag{A.14}$$

where $\boldsymbol{\sigma}$ denotes the stress tensor of the solid constituent.

Bibliography

- [1] Abbott, M. M.; van Ness, H. C.: *Schaum's Outline of Theory and Problems of Thermodynamics*. McGraw-Hill, New-York, 2nd ed. 1989.
- [2] Ammann, M.: *Parallel Finite Element Simulations of Localization Phenomena in Porous Media*. Dissertation, Bericht Nr. II-11 aus dem Institut für Mechanik (Bauwesen), Universität Stuttgart 2005.
- [3] Antoine, C.: Tensions des vapeurs; nouvelle relation entre les tensions et les températures. *Comptes Rendus des Séances de l'Académie des Sciences* **107** (1888), 681–684, 778–780, 836–837.
- [4] Avci, O.; Ehlers, W.: Parameteridentification of Hostun-sand and shearband simulation of landsliding. *Proceedings in Applied Mathematics and Mechanics (PAMM)* **6** (2006), 351–352.
- [5] Baehr, H.-D.: *Thermodynamik*. Springer-Verlag, Berlin, 12th ed. 2005.
- [6] Bathe, K.-J.: *Finite-Elemente-Methoden*. Springer-Verlag, Berlin 1990.
- [7] Bear, J.: *Hydraulics of Groundwater*. McGraw-Hill, New-York 1979.
- [8] Bielinski, A.: *Numerical simulation of CO₂ sequestration in geological formations*. Dissertation, Mitteilungsheft Nr. 155 aus dem Institut für Wasserbau, Universität Stuttgart 2007.
- [9] Biot, M. A.: General theory of three-dimensional consolidation. *Journal of Applied Physics* **12** (1941), 155–164.
- [10] Blome, P.: *Ein Mehrphasen-Stoffmodell für Böden mit Übergang auf Interface-Gesetze*. Dissertation, Bericht Nr. II-10 aus dem Institut für Mechanik (Bauwesen), Universität Stuttgart 2003.
- [11] de Boer, R.: *Vektor- und Tensorrechnung für Ingenieure*. Springer-Verlag, Berlin 1982.
- [12] de Boer, R.: *Theory of Porous Media*. Springer-Verlag, Berlin 2000.
- [13] de Boer, R.; Ehlers, W.: *Theorie der Mehrkomponentenkontinua mit Anwendung auf bodenmechanische Probleme*. Forschungsberichte aus dem Fachbereich Bauwesen, Heft 40, Universität-GH-Essen 1986.
- [14] Bolzon, G.; Schrefler, B. A.; Zienkiewicz, O. C.: Elastoplastic soil constitutive laws generalized to partially saturated states. *Géotechnique* **46** (1996), 279–289.
- [15] Bowen, R. M.: Theory of mixtures. In Eringen, A. C., editor, *Continuum Physics*, Vol. III. Academic Press, New York 1976, pp. 1–127.

- [16] Bowen, R. M.: Incompressible porous media models by use of the theory of mixtures. *International Journal of Engineering Sciences* **18** (1980), 1129–1148.
- [17] Bowen, R. M.: Compressible porous media models by use of the theory of mixtures. *International Journal of Engineering Sciences* **20** (1982), 697–735.
- [18] Braess, D.: *Finite Elemente*. Springer-Verlag, Berlin 1997.
- [19] Brezzi, F.; Fortin, M.: *Mixed and Hybrid Finite Element Methods*. Springer-Verlag, New York 1991.
- [20] Brooks, A. N.; Hughes, T. J. R.: Streamline upwind/Petrov-Galerkin formulations for convection dominated flows with particular emphasis on the incompressible Navier-Stokes equations. *Computer Methods in Applied Mechanics and Engineering* **32** (1982), 199–259.
- [21] Brooks, R. H.; Corey, A. T.: Properties of porous media affecting fluid flow. *ASCE: Journal of the Irrigation and Draining Division* **92** (1966), 61–88.
- [22] Buckley, S. E.; Leverett, M. C.: Mechanism of fluid displacement in sands. *Transactions of the AIME* **146** (1942), 107–116.
- [23] Burdine, N. T.: Relative permeability calculations from pore size distribution data. *Journal of American Institute of Mining, Metallurgical, and Petroleum Engineers* **198** (1953), 71–77.
- [24] Cernica, J. N.: *Geotechnical Engineering: Soil Mechanics*. John Wiley & Sons, New York 1995.
- [25] Clapeyron, E.: Mémoire sur la puissance motrice de la chaleur. *Journal de l'École Polytechnique* **14** (1834), 153–190.
- [26] Class, H.: *Theorie und numerische Modellierung nichtisothermer Mehrphasenprozesse in NAPL-kontaminierten porösen Medien*. Dissertation, Mitteilungsheft Nr. 105 aus dem Institut für Wasserbau, Universität Stuttgart 2001.
- [27] Class, H.; Helmig, R.: Numerical simulation of non-isothermal multiphase multi-component processes in porous media. – 2. Applications for the injection of steam and air. *Advances in Water Resources* **25** (2002), 551–564.
- [28] Class, H.; Helmig, R.; Bastian, P.: Numerical simulation of non-isothermal multiphase multicomponent processes in porous media. – 1. An efficient solution technique. *Advances in Water Resources* **25** (2002), 533–550.
- [29] Clausius, R.: Über die bewegende Kraft der Wärme und die Gesetze, die sich daraus für die Wärmelehre selbst ableiten lassen. *Annalen der Physik und Chemie* **79** (1850), 368–397, 500–524.

- [30] Coleman, B. D.; Noll, W.: The thermodynamics of elastic materials with heat conduction and viscosity. *Archive for Rational Mechanics and Analysis* **13** (1963), 167–178.
- [31] Cross, J. J.: Mixtures of fluids and isotropic solids. *Archive of Mechanics* **25** (1973), 1025–1039.
- [32] Dalton, J.: *A New System of Chemical Philosophy*. R. Bickerstaff, Stand, London 1808.
- [33] Darcy, H.: *Les Fontaines Publiques de la Ville de Dijon*. Dalmont, Paris 1856.
- [34] Davis, R. O.; Selvadurai, A. P. S.: *Plasticity and Geomechanics*. Cambridge University Press, Cambridge 2002.
- [35] Diebels, S.: A micropolar theory of porous media: Constitutive modelling. *Transport in Porous Media* **34** (1999), 193–208.
- [36] Diebels, S.; Steeb, H.: Stress and couple stress in foams. *Computational Materials Science* **28** (2003), 714–722.
- [37] Ebinger, T.; Diebels, S.; Steeb, H.: Numerical homogenization techniques applied to growth and remodelling phenomena. *Computational Mechanics* **39** (2007), 815–830.
- [38] Ebinger, T.; Steeb, H.; Diebels, S.: Kinematically extended continuum theories: Correlation between microscopical deformation and macroscopical strain measures. *Technische Mechanik* **28** (2008), 64–86.
- [39] Ehlers, W.: On thermodynamics of elasto-plastic porous media. *Archive of Mechanics* **41** (1989), 73–93.
- [40] Ehlers, W.: *Poröse Medien – ein kontinuumsmechanisches Modell auf der Basis der Mischungstheorie*. Habilitation, Forschungsberichte aus dem Fachbereich Bauwesen, Heft 47, Universität-GH-Essen 1989.
- [41] Ehlers, W.: Constitutive equations for granular materials in geomechanical context. In Hutter, K., editor, *Continuum Mechanics in Environmental Sciences and Geophysics*, CISM Courses and Lectures No. 337. Springer-Verlag, Wien 1993, pp. 313–402.
- [42] Ehlers, W.: A single-surface yield function for geomaterials. *Archive of Applied Mechanics* **65** (1995), 246–259.
- [43] Ehlers, W.: Grundlegende Konzepte in der Theorie Poröser Medien. *Technische Mechanik* **16** (1996), 63–76.
- [44] Ehlers, W.: *Continuum Mechanics of Single- and Multiphase Materials*. COMMAS Courses and Lectures, Universität Stuttgart 2001/2002.

- [45] Ehlers, W.: Continuum and numerical simulation of porous materials in science and technology. In Capriz, G.; Ghionna, V. N.; Giovine, P., editors, *Modeling and Mechanics of Granular and Porous Materials*. Birkhäuser, Boston 2002, pp. 244–292.
- [46] Ehlers, W.: Foundations of multiphasic and porous materials. In Ehlers, W.; Bluhm, J., editors, *Porous Media: Theory, Experiments and Numerical Applications*. Springer-Verlag, Berlin 2002, pp. 3–86.
- [47] Ehlers, W.: *Vector and tensor calculus: An introduction*. Lecture notes, Institute of Applied Mechanics (CE), University of Stuttgart 2007. <http://www.mechbau.uni-stuttgart.de/l2/lehre/uebungen/index.php>.
- [48] Ehlers, W.; Acartürk, A.: The role of weakly imposed Dirichlet boundary conditions for numerically stable computations of swelling phenomena. *Computational Mechanics*, submitted 2007.
- [49] Ehlers, W.; Ammann, M.; Diebels, S.: h -Adaptive FE methods applied to single- and multiphase problems. *International Journal for Numerical Methods in Engineering* **54** (2002), 219–239.
- [50] Ehlers, W.; Blome, P.: A triphasic model for unsaturated soils based on the Theory of Porous Media. *Mathematical and Computer Modelling* **37** (2003), 507–513.
- [51] Ehlers, W.; Diebels, S.; Mahnkopf, D.; Ellsiepen, P.: *Theoretische und numerische Studien zur Lösung von Rand- und Anfangswertproblemen in der Theorie Poröser Medien*. DFG-Bericht, Bericht aus dem Institut für Mechanik (Bauwesen), Nr. 96-II-1, Universität Stuttgart 1996.
- [52] Ehlers, W.; Ellsiepen, P.: PANDAS: Ein FE-System zur Simulation von Sonderproblemen der Bodenmechanik. In Wriggers, P.; Meißner, U.; Stein, E.; Wunderlich, W., editors, *Finite Elemente in der Baupraxis: Modellierung, Berechnung und Konstruktion*. Ernst & Sohn, Berlin 1998, pp. 391–400. Beiträge zur Tagung FEM '98 an der TU Darmstadt am 5. und 6. März 1998.
- [53] Ehlers, W.; Ellsiepen, P.: Theoretical and numerical methods in environmental continuum mechanics based on the Theory of Porous Media. In Schrefler, B. A., editor, *Environmental Geomechanics*, CISM Courses and Lectures No. 417. Springer-Verlag, Wien 2001, pp. 1–81.
- [54] Ehlers, W.; Ellsiepen, P.; Ammann, M.: Time- and space-adaptive methods applied to localization phenomena in empty and saturated micropolar and standard porous materials. *International Journal for Numerical Methods in Engineering* **52** (2001), 503–526.
- [55] Ehlers, W.; Ellsiepen, P.; Blome, P.; Mahnkopf, D.; Markert, B.: *Theoretische und numerische Studien zur Lösung von Rand- und Anfangswertproblemen in der Theorie Poröser Medien*. Abschlußbericht zum DFG-Forschungsvorhaben Eh 107/6-

- 2, Bericht aus dem Institut für Mechanik (Bauwesen), Nr. 99-II-1, Universität Stuttgart 1999.
- [56] Ehlers, W.; Graf, T.; Ammann, M.: Deformation and localization analysis in partially saturated soil. *Computer Methods in Applied Mechanics and Engineering* **193** (2004), 2885–2910.
- [57] Ehlers, W.; Karajan, N.; Markert, B.: A porous media model describing the inhomogeneous behaviour of the human intervertebral disc. *Materialwissenschaft und Werkstofftechnik* **37** (2006), 546–551.
- [58] Ehlers, W.; Markert, B.: On the viscoelastic behaviour of fluid-saturated materials. *Granular Matter* **2** (2000), 153–161.
- [59] Ehlers, W.; Markert, B.: A linear viscoelastic biphasic model for soft tissues based on the Theory of Porous Media. *ASME Journal of Biomechanical Engineering* **123** (2001), 418–424.
- [60] Ehlers, W.; Markert, B.: A macroscopic finite strain model for cellular polymers. *International Journal of Plasticity* **19** (2003), 961–976.
- [61] Ehlers, W.; Markert, B.; Acartürk, A.: Swelling phenomena of hydrated porous materials. In Abousleiman, N.; Cheng, A. H.; Ulm, F. J., editors, *Poromechanics III, Proceedings of the third Biot conference on Poromechanics*. Balkema at Taylor & Francis, Leiden 2005, pp. 781–786.
- [62] Ehlers, W.; Markert, B.; Karajan, N.: On the load bearing mechanism of the human intervertebral disc. In Abousleiman, N.; Cheng, A. H.; Ulm, F. J., editors, *Poromechanics III, Proceedings of the third Biot conference on Poromechanics*. Balkema at Taylor & Francis, Leiden 2005, pp. 51–56.
- [63] Ehlers, W.; Markert, B.; Karajan, N.: A coupled FE analysis of the intervertebral disc based on a multiphasic TPM formulation. In Holzapfel, G. A.; Ogden, R. W., editors, *Mechanics of Biological Tissue*. Springer-Verlag 2006, pp. 373–386.
- [64] Ehlers, W.; Markert, B.; Klar, O.: Biphasic description of viscoelastic foams using an extended Ogden-type formulation. In Ehlers, W.; Bluhm, J., editors, *Porous Media: Theory, Experiments and Numerical Applications*. Springer-Verlag, Berlin 2002, pp. 275–294.
- [65] Ehlers, W.; Müllerschön, H.: Parameter identification of a macroscopic granular soil model applied to dense Berlin sand. *Granular Matter* **2** (2000), 105–112.
- [66] Ehlers, W.; Volk, W.: On theoretical and numerical methods in the theory of porous media based on polar and non-polar elasto-plastic solid materials. *International Journal of Solids and Structures* **35** (1998), 4597–4617.
- [67] Eipper, G.: *Theorie und Numerik finiter elastischer Deformationen in fluidgesättigten porösen Medien*. Dissertation, Bericht Nr. II-1 aus dem Institut für Mechanik (Bauwesen), Universität Stuttgart 1998.

- [68] Ellsiepen, P.: *Zeit- und ortsadaptive Verfahren angewandt auf Mehrphasenprobleme poröser Medien*. Dissertation, Bericht Nr. II-3 aus dem Institut für Mechanik (Bauwesen), Universität Stuttgart 1999.
- [69] Eriksson, K.; Estep, D.; Hansbo, P.; Johnson, C.: *Computational Differential Equations*. Cambridge University Press, Cambridge 1996.
- [70] Fick, A.: Über Diffusion. *Annalen der Physik und Chemie* **94** (1855), 59–86.
- [71] Forsyth, P. A.: A control volume finite element approach to NAPL groundwater contamination. *SIAM Journal on Scientific and Statistical Computing* **12** (1991), 1029–1057.
- [72] Fourier, J.: *Théorie Analytique de la Chaleur*. Firmin Didot, Père et Fils, Paris 1822.
- [73] Franca, L. P.; Frey, S. L.: Stabilized finite element methods: II. The incompressible Navier-Stokes equations. *Computer Methods in Applied Mechanics and Engineering* **99** (1992), 209–233.
- [74] Franca, L. P.; Frey, S. L.; Hughes, T. J. R.: Stabilized finite element methods: I. Application to the advective-diffusive model. *Computer Methods in Applied Mechanics and Engineering* **95** (1992), 253–276.
- [75] Fredlund, D. G.; Rahardjo, H.: *Soil Mechanics for Unsaturated Soils*. Wiley, New York 1993.
- [76] van Genuchten, M. T.: A closed-form equation for predicting the hydraulic conductivity of unsaturated soils. *Soil Science Society of America Journal* **44** (1980), 892–898.
- [77] Ghadiani, S.: *A Multiphasic Continuum Mechanical Model for Design Investigation of an Effusion-Cooled Rocket Thrust Chamber*. Dissertation, Bericht Nr. II-13 aus dem Institut für Mechanik (Bauwesen), Universität Stuttgart 2005.
- [78] Gresho, P. M.; Lee, R. L.: Don't suppress the wiggles – they're telling you something. *Computers and Fluids* **9** (1981), 223–253.
- [79] Grigull, U.: *Wärmeübertragung*. Springer-Verlag, Berlin 1963.
- [80] Hairer, E.; Lubich, C.; Roche, M.: *The Numerical Solution of Differential-Algebraic Equations by Runge-Kutta Methods*. Springer-Verlag 1989.
- [81] Hairer, E.; Nørsett, S.; Wanner, G.: *Solving Ordinary Differential Equations, Vol. 1: Nonstiff Problems*. Springer-Verlag, Berlin 1987.
- [82] Hairer, E.; Wanner, G.: *Solving Ordinary Differential Equations, Vol. 2: Stiff and Differential-Algebraic Problems*. Springer-Verlag, Berlin 1991.

- [83] Hansbo, P.; Szepessy, A.: A velocity-pressure streamline diffusion finite element method for the incompressible Navier-Stokes equations. *Computer Methods in Applied Mechanics and Engineering* **84** (1990), 175–192.
- [84] Hartmann, S.; Lührs, G.; Haupt, P.: An efficient stress algorithm with applications in viscoplasticity and plasticity. *International Journal for Numerical Methods in Engineering* **40** (1997), 991–1013.
- [85] Hassanizadeh, S. M.; Gray, W. G.: General conservation equations for multi-phase systems: 1. Averaging procedure. *Advances in Water Resources* **2** (1979), 131–144.
- [86] Hazen, A.: Water supply. In *American Civil Engineers Handbook*. John Wiley & Sons, New York 1930, pp. 1444–1518.
- [87] Heinrich, G.; Desoyer, K.: Hydromechanische Grundlagen für die Behandlung von stationären und instationären Grundwasserströmungen. *Ingenieur-Archiv* **23** (1955), 182–185.
- [88] Heinrich, G.; Desoyer, K.: Hydromechanische Grundlagen für die Behandlung von stationären und instationären Grundwasserströmungen, II. Mitteilung. *Ingenieur-Archiv* **24** (1956), 81–84.
- [89] Heinrich, G.; Desoyer, K.: Theorie dreidimensionaler Setzungsvorgänge in Ton-schichten. *Ingenieur-Archiv* **30** (1961), 225–253.
- [90] Helmig, R.: *Multiphase Flow and Transport Processes in the Subsurface*. Springer-Verlag, Berlin 1997.
- [91] Helmig, R.; Huber, R.: Comparison of Galerkin-type discretization techniques for two-phase flow in heterogeneous porous media. *Advances in Water Resources* **21** (1998), 697–711.
- [92] Hill, R.: *The Mathematical Theory of Plasticity*. Clarendon, Oxford 1950.
- [93] Hughes, T. J. R.: *The Finite Element Method*. Prentice-Hall, London 1987.
- [94] Hughes, T. J. R.; Franca, L. P.; Balestra, M.: A new finite element formulation for computational fluid dynamics: V. Circumventing the Babuska-Brezzi condition: A stable Petrov-Galerkin formulation of the Stokes problem accommodating equal-order interpolation. *Computer Methods in Applied Mechanics and Engineering* **59** (1986), 85–99.
- [95] Kim, M. K.; Lade, P. V.: Single hardening constitutive model for frictional materials, I. Plastic potential function. *Computers and Geotechnics* **5** (1988), 307–324.
- [96] Klubertanz, G.: *Zur hydromechanischen Kopplung in dreiphasigen porösen Medien: Modellbildung und Anwendung auf die Auslösung von Murgängen*. Dissertation Nr. 2027, Ecole Polytechnique Fédérale de Lausanne 1999.

- [97] Klubertanz, G.; Laloui, L.; Vulliet, L.: Numerical modelling of the hydro-mechanical behaviour of unsaturated porous media. In Creechan, A.; Gillot, M.; Kenny, T.; Owen, D. R.; Ramm, E.; Wood, J., editors, *Proceedings of NAFEMS world congress on design, simulation and optimisation, reliability and applicability of computational methods*. NAFEMS Ltd, Glasgow 1997, pp. 1302–1313.
- [98] Knabner, P.; Angermann, L.: *Numerik partieller Differentialgleichungen*. Springer-Verlag, Berlin 2000.
- [99] Kueper, B. H.; Abbott, W.; Farquhar, G.: Experimental observations of multiphase flow in heterogeneous porous media. *Journal of Contaminant Hydrology* **5** (1989), 83–95.
- [100] Lade, P. V.; Duncan, J. M.: Cubical triaxial tests on cohesionless soil. *ASCE: Journal of Soil Mechanics and Foundations Division* **99** (1973), 793–812.
- [101] Laloui, L.; Cekerevac, C.; François, B.: Constitutive modelling of the thermo-plastic behavior of soils. In Laloui, L.; Charlier, R.; Pijaudier-Cabot, G., editors, *Revue Européenne de Génie Civil: Coupled Multiphysics in Geomechanics*. Lavoisier, Paris 2005, pp. 635–650.
- [102] Laloui, L.; Nuth, M.: An introduction to the constitutive modelling of unsaturated soils. In Laloui, L.; Charlier, R.; Pijaudier-Cabot, G., editors, *Revue Européenne de Génie Civil: Coupled Multiphysics in Geomechanics*. Lavoisier, Paris 2005, pp. 651–669.
- [103] Langtangen, H. P.; Tveito, A., editors: *Advanced Topics in Computational Partial Differential Equations*, Vol. 33 of *Lecture Notes in Computational Science and Engineering*. Springer-Verlag, Berlin 2003.
- [104] Lemaitre, J.; Chaboche, J. L.: *Mechanics of Solid Materials*. Cambridge University Press, Cambridge 1990.
- [105] Lewis, R. W.; Schrefler, B. A.: *The Finite Element Method in the Static and Dynamic Deformation and Consolidation of Porous Media*, 2nd Edition. Wiley, Chichester 1998.
- [106] Lube, G.; Auge, A.: Stabilized mixed finite element approximations of incompressible flow problems. *Zeitschrift für Angewandte Mathematik und Mechanik (ZAMM)* **6** (1992), T483–T486.
- [107] Mahnkopf, D.: *Lokalisierung fluidgesättigter poröser Festkörper bei finiten elastoplastischen Deformationen*. Dissertation, Bericht Nr. II-5 aus dem Institut für Mechanik (Bauwesen), Universität Stuttgart 2000.
- [108] Markert, B.: *Porous Media Viscoelasticity with Application to Polymeric Foams*. Dissertation, Bericht Nr. II-12 aus dem Institut für Mechanik (Bauwesen), Universität Stuttgart 2005.

- [109] Mualem, Y.: A new model for predicting the hydraulic conductivity of unsaturated porous media. *Water Resources Research* **12** (1976), 513–522.
- [110] Müllerschön, H.: *Spannungs-Verzerrungsverhalten granularer Materialien am Beispiel von Berliner Sand*. Dissertation, Bericht Nr. II-6 aus dem Institut für Mechanik (Bauwesen), Universität Stuttgart 2000.
- [111] Niessner, J.; Helmig, R.; Jakobs, H.; Roberts, J. E.: Interface condition and linearization schemes in the Newton iterations for two-phase flow in heterogeneous porous media. *Advances in Water Resources* **28** (2005), 671–687.
- [112] Oden, J. T.; Reddy, J. N.: *An Introduction to the Mathematical Theory of Finite Elements*. John Wiley & Sons, New York 1976.
- [113] Paul, M.: *Simulation of Two-Phase Flow Processes in Heterogeneous Porous Media with Adaptive Methods*. Dissertation, Mitteilungen des Instituts für Wasserbau 120, Universität Stuttgart 2003.
- [114] Perzyna, P.: Fundamental problems in viscoplasticity. *Advances in Applied Mechanics* **9** (1966), 243–377.
- [115] Sanavia, L.; Schrefler, B. A.; Steinmann, P.: Geometrical and material non-linear analysis of fully and partially saturated porous media. In Ehlers, W.; Bluhm, J., editors, *Porous Media: Theory, Experiments and Numerical Applications*. Springer-Verlag, Berlin 2002, pp. 341–381.
- [116] Schöberl, J.: NETGEN – an advancing front 2d/3d-mesh generator based on abstract rules. *Computing and Visualization in Science* **1** (1997), 40–52.
- [117] Scholz, B.: *Application of a Micropolar Model to the Localization Phenomena in Granular Materials*. Dissertation, Bericht Nr. II-15 aus dem Institut für Mechanik (Bauwesen), Universität Stuttgart 2007.
- [118] Schrefler, B. A.: Computer modelling in environmental geomechanics. *Computers and Structures* **79** (2001), 2209–2223.
- [119] Schrefler, B. A.: Multiphase flow in deforming porous material. *International Journal for Numerical Methods in Engineering* **60** (2004), 27–50.
- [120] Schrefler, B. A.; Scotta, R.: A fully coupled model for two-phase flow in deformable porous media. *Computer Methods in Applied Mechanics and Engineering* **190** (2001), 3223–3246.
- [121] Schwarz, H. R.: *Methode der finiten Elemente*. Teubner, Stuttgart 1991.
- [122] Simo, J. C.; Hughes, T. J. R.: *Computational Inelasticity*. Springer-Verlag, New York 1998.

- [123] Simo, J. C.; Taylor, R. L.: Consistent tangent operators for rate-independent elastoplasticity. *Computer Methods in Applied Mechanics and Engineering* **48** (1985), 101–118.
- [124] Somerton, W. H.; Keese, J. A.; Chu, S. L.: Thermal behavior of unconsolidated oil sands. *Society of Petroleum Engineers Journal* **14** (1974), 513–521.
- [125] von Soos, P.; Boháč, J.: Properties of soils and rocks and their laboratory determination. In Smolczyk, U., editor, *Geotechnical Engineering Handbook, Volume 1: Fundamentals*. Ernst & Sohn, Berlin 2002, pp. 119–206.
- [126] Spalding, D.: A novel finite difference formulation for differential expressions involving both first and second derivatives. *International Journal for Numerical Methods in Engineering* **4** (1972), 551–559.
- [127] Steeb, H.; Diebels, S.: A thermodynamic-consistent model describing growth and remodeling phenomena. *Computational Materials Science* **28** (2003), 597–607.
- [128] Steeb, H.; Diebels, S.; Vardoulakis, I.: A multiphase continuum-based model capturing erosion and deposition. In Wang, Y.; Hutter, K., editors, *Trends in Applications of Mathematics to Mechanics*. Shaker Verlag, Aachen 2005, pp. 519–528.
- [129] Strang, G.; Fix, G. J.: *An Analysis of the Finite Element Method*. Prentice-Hall, Englewood Cliffs, New York 1973.
- [130] Strehmel, K.; Weiner, R.: *Numerik gewöhnlicher Differentialgleichungen*. Teubner, Stuttgart 1995.
- [131] Thamm, B. R.: *Berechnung der Anfangssetzungen und der Anfangsporenwasserüberdrücke eines wassergesättigten normalverdichteten Tones*. Mitteilung Nr. 1. Baugrundinstitut Stuttgart 1974.
- [132] Törnig, W.; Spellucci, P.: *Numerische Mathematik für Ingenieure und Physiker – Numerische Methoden der Analysis*, Vol. 2. Springer-Verlag, Berlin 1990.
- [133] Truesdell, C.: The origins of rational thermodynamics. In Truesdell, C., editor, *Rational Thermodynamics*. Springer-Verlag, New York, 2nd ed. 1984, pp. 1–57.
- [134] Truesdell, C.: *Rational Thermodynamics*. Springer-Verlag, New York, 2nd ed. 1984.
- [135] Truesdell, C.: Thermodynamics of diffusion. In Truesdell, C., editor, *Rational Thermodynamics*. Springer-Verlag, New York, 2nd ed. 1984, pp. 219–236.
- [136] Truesdell, C.; Toupin, R. A.: The classical field theories. In Flügge, S., editor, *Handbuch der Physik*, Vol. III/1. Springer-Verlag, Berlin 1960, pp. 226–902.
- [137] Udell, K. S.; Fitch, J. S.: Heat and mass transfer in capillary porous media considering evaporation, condensation and non-condensable gas effects. In Yao, L. S.; Chen, M. M.; Hickox, C. E.; Simpkins, P. G.; Chow, L. C.; Kaviany, M.; Cheng, P.; Davis, L. R., editors, *Heat Transfer in Porous Media and Particulate Flows*. The American Society of Mechanical Engineers, New York 1985, pp. 103–110.

- [138] Wieners, C.: Taylor-Hood elements in 3D. In Wendland, W. L.; Efendiev, M., editors, *Analysis and Simulation of Multifield Problems*. Springer-Verlag, Berlin 2003, pp. 189–196.
- [139] Wieners, C.: Distributed Point Objects. A New Concept for Parallel Finite Elements. <http://www.mathematik.uni-karlsruhe.de/~wieners/> Karlsruhe 2003.
- [140] Wieners, C.; Ammann, M.; Diebels, S.; Ehlers, W.: Parallel 3-d simulations for porous media models in soil mechanics. *Computational Mechanics* **29** (2002), 73–87.
- [141] Wieners, C.; Ammann, M.; Ehlers, W.: Distributed Point Objects: A new concept for parallel finite elements applied to a geomechanical problem. *Future Generation Computer Systems* **22** (2006), 532–545.
- [142] Wieners, C.; Ammann, M.; Graf, T.; Ehlers, W.: Parallel Krylov methods and the application to 3-d simulations of a triphasic porous media model in soil mechanics. *Computational Mechanics* **36** (2005), 409–420.
- [143] Wood, W. L.: *Practical time-stepping schemes*. Clarendon Press, Oxford 1990.
- [144] Wriggers, P.: *Konsistente Linearisierung in der Kontinuumsmechanik und ihre Anwendung auf die Finite-Elemente-Methode*. Dissertation, Forschungs- und Seminarberichte aus dem Bereich der Mechanik der Universität Hannover, Bericht-Nr. F 88/4, Universität Hannover 1988.
- [145] Zienkiewicz, O. C.; Taylor, R. L.: *The Finite Element Method*. McGraw-Hill, London 1989.
- [146] Zienkiewicz, O. C.; Taylor, R. L.: *The Finite Element Method: Solid Mechanics*, Vol. 2. Butterworth-Heinemann, London 2000.
- [147] Zienkiewicz, O. C.; Taylor, R. L.: *The Finite Element Method: The Basis*, Vol. 1. Butterworth-Heinemann, London 2000.

Curriculum Vitae

Name: Tobias Graf

Date of birth: 25th January 1975

Place of birth: Nagold, Germany

Nationality: German

Marital Status: Married, two children

Education: 09/1981 – 07/1985
Elementary School: Nagold-Gündringen

09/1985 – 06/1994
Secondary School: Otto-Hahn-Gymnasium Nagold

Studies: 10/1994 – 07/2001
Studies in Civil Engineering at the University of Stuttgart

Community Service: 09/1995 – 09/1996
Community Service at “Johanniter-Unfall-Hilfe e. V.”, Nagold

Professional Occupation: 09/2001 – 08/2007
Research Associate at the Institute of Applied Mechanics
(Civil Engineering) at the University of Stuttgart

since 09/2007
Computational Engineer at DYNAmore GmbH, Stuttgart

Released Report Series

- II-1 Gernot Eipper: *Theorie und Numerik finiter elastischer Deformationen in fluid-gesättigten porösen Festkörpern*, June 1998.
- II-2 Wolfram Volk: *Untersuchung des Lokalisierungsverhaltens mikropolarer poröser Medien mit Hilfe der Cosserat-Theorie*, May 1999.
- II-3 Peter Ellsiepen: *Zeit- und ortsadaptive Verfahren angewandt auf Mehrphasenprobleme poröser Medien*, July 1999.
- II-4 Stefan Diebels: *Mikropolare Zweiphasenmodelle: Formulierung auf der Basis der Theorie Poröser Medien*, March 2000.
- II-5 Dirk Mahnkopf: *Lokalisierung fluidgesättigter poröser Festkörper bei finiten elasto-plastischen Deformationen*, March 2000.
- II-6 Heiner Müllerschön: *Spannungs-Verformungsverhalten granularer Materialien am Beispiel von Berliner Sand*, August 2000.
- II-7 Stefan Diebels (Ed.): *Zur Beschreibung komplexen Materialverhaltens: Beiträge anlässlich des 50. Geburtstages von Herrn Prof. Dr.-Ing. Wolfgang Ehlers*, August 2001.
- II-8 Jack Widjajakusuma: *Quantitative Prediction of Effective Material Parameters of Heterogeneous Materials*, June 2002.
- II-9 Alexander Droste: *Beschreibung und Anwendung eines elastisch-plastischen Materialmodells mit Schädigung für hochporöse Metallschäume*, October 2002.
- II-10 Peter Blome: *Ein Mehrphasen-Stoffmodell für Böden mit Übergang auf Interface-Gesetze*, October 2003.
- II-11 Martin Ammann: *Parallel Finite Element Simulations of Localization Phenomena in Porous Media*, April 2005.
- II-12 Bernd Markert: *Porous Media Viscoelasticity with Application to Polymeric Foams*, July 2005.
- II-13 Saeed Reza Ghadiani: *A Multiphasic Continuum Mechanical Model for Design Investigations of an Effusion-Cooled Rocket Thrust Chamber*, May 2005.
- II-14 Wolfgang Ehlers & Bernd Markert (Eds.): *Proceedings of the 1st GAMM Seminar on Continuum Biomechanics*, September 2005.
- II-15 Bernd Scholz: *Application of a Micropolar Model to the Localization Phenomena in Granular Materials: General Model, Sensitivity Analysis and Parameter Optimization*, August 2007.

- II-16 Wolfgang Ehlers & Nils Karajan (Eds.): *Proceedings of the 2nd GAMM Seminar on Continuum Biomechanics*, December 2007.
- II-17 Tobias Graf: *Multiphasic Flow Processes in Deformable Porous Media under Consideration of Fluid Phase Transitions*, June 2008.